Role of Nox2 oxidase during the cardiac infiltration of T-cells in a model of hypertension

Emmerson, Amber Chi

Awarding institution:
King's College London

Role of Nox2 oxidase during the cardiac infiltration of T-cells in a model of hypertension

Amber Chi Emmerson

Ph.D. Thesis

Cardiovascular division

BHF Centre of Research Excellence

School of Medicine

King's College London

Submitted for the Degree of Doctor of Philosophy from

King's College London

February 2016

Supervised by

Professor Ajay M. Shah

Professor Giovanna Lombardi

Abstract

Chronic hypertension related to increased activation of the renin-angiotensin system causes cardiac remodelling, which can progress to heart failure. Previous studies indicate that NADPH oxidase-2 (Nox2) activation is involved in angiotensin II (AngII)-induced hypertension and cardiovascular remodelling in mice. Nox2 is expressed in multiple cell types including cardiac myocytes, endothelial cells and inflammatory cells. The aim of this work was to investigate the role of T-cell Nox2 in the pathophysiology of AngII-induced cardiovascular remodelling.

Studies were undertaken in mice subjected to chronic AngII infusion with analysis of cardiac function, blood pressure, histology, and myocardial inflammatory cell infiltration (flow cytometry of single cell suspensions). In wild-type (WT) mice, AngII-induced increase in blood pressure was associated with a time dependant infiltration of T-cells into the myocardium. There was an increase in infiltration of anti-inflammatory regulatory T-cells (Tregs) into the myocardium and an increase in mRNA expression of the Treg transcription factor, FoxP3, as well as Treg cytokines and functional surface makers. In global Nox2 knockout (KO) animals, there was a reduction in immune cell infiltration into the myocardium associated with a blunting of AngII-induced hypertension. A novel CD4-targeted Nox2KO model was generated, in which AngII-induced hypertension was also blunted. These mice exhibited an increase in Tregs in the myocardium at baseline as compared to WT littermates, and showed no AngII-induced increase in Tregs. An adoptive transfer study was performed, in which Tregs from WT or global Nox2KO mice were injected via the tail vein into WT mice subsequently treated with AngII. AngII-induced hypertension was significantly blunted in WT-Treg treated mice and an even greater effect was observed in KO-Treg treated mice. Cardiomyocyte hypertrophy was also blunted in these animals. Flow cytometry revealed lower cardiovascular inflammation in both Treg treated groups, especially in the Nox2KO-Treg treated group. Furthermore, *in vitro* Treg suppression assays revealed that Nox2KO-Tregs were significantly more suppressive than WT-Tregs.

These data reveal that myocardial T-cell, specifically $CD4^+$ T-cell, infiltration is a feature of AngII-induced hypertension and is regulated by Nox2. Moreover, Nox2 modulates Treg suppressive function, with significant impact on the development of hypertension and cardiac remodelling. Taken together, these studies identify an important role for T-cell Nox2 in the pathophysiology of AngII-induced hypertension and cardiovascular remodelling.

Acknowledgements

Firstly, I would like to thank my supervisors, Professor Ajay Shah and Professor Giovanna Lombardi, for giving me the opportunity to work in their laboratory groups. My first supervisor, Prof Ajay Shah, has given a lot of his time and patience to guide me through my PhD. Explaining and discussing scientific ideas with me, as well as sharing technical knowledge and encouraging me to present my data at a variety of scientific events. My second supervisor, Prof Giovanna Lombardi, provided much needed direction on the immunology-side of my PhD. Always keen to help and discuss scientific ideas with me, as well as making sure I had correct guidance in the lab. I would also like to thank the British Heart Foundation (BHF) for their financial support throughout my PhD.

The most important person for me to thank is Dr Héloïse Mongue-Din, for all her help and assistance throughout my PhD. As well as being a very good friend, she has given up copious amounts of time to deal with all of my silly questions and problems. She has taught me everything I know, not only in the lab but also terms of careers, general life advice and emotional support. I definitely could not have completed my PhD without her, and will be forever grateful.

I would also like to thank my colleagues, who have helped either in the laboratory, BSU or to discuss ideas with me – Lesley Smyth, Raul Elgueta, Kulachelvy Ratnasothy, Qi Peng, Xuebin Dong, Greta Sawyer, Dominic Boardman, Dan Richards, Ioannis Smyrnais, Moritz Schnelle and Craig Harrison. Also a big thank-you to the Biomedical Research Centre (BRC) flow cytometry facility at Guys and St Thomas' hospital, funded by the National Institute for Health Research (NIHR). Numerous wonderful people have also helped make my time at King's that extra bit more enjoyable; Trusha Mistry, Shana De Silva, Ruth Austin and Elham Zarrinpashneh.

Finally, I would like to thank my family; my parents, Diana Emmerson and Michael Wallace, for all their support and encouragement over the years; my brother, Simon Emmerson, for teaching me to aim high and reach my dreams and my sister, Kaya Emmerson, for her constant emotional support and giggles that keep me going. Last but not least I would like to thank my lovely other half, Simon Russell, who continues to support and care for me even through the tricky times.

I would like to dedicate my PhD to my late father, Paul Emmerson, who even in his absence encourages me to be the best I can be.

Declaration

I declare that I am the sole author of this Ph.D. thesis and it contains my own work, except where indicated.

Amber Emmerson

Table of Contents

Index of Tables

Index of Figures

Abbreviations

(-SO2H)	Sulfinic acid
(-SO_3H)	Sulfonic acid
$^{\bullet}OH$	Hydroxyl radical
$^1O_2$	Singlet oxygen
AAA	Abdominal aortic aneurysm
Ab	Antibody
ACE	Angiotensin-converting enzyme
ACTH	Adrenocorticotrophic hormone
ADP	Adenine diphosphate
Ag	Antigen
ALK	Activin-linked kinase
AMP	Adenine monophosphate
AngI	Angiotensin I
AngII	Angiotensin II
ANOVA	Analysis of variance between groups
AP-1	Activator protein-1
APC	Antigen presenting cell
ARB	Angiotensin receptor blockers
ASK	Apoptosis signal-regulating kinase
AT_1R	Angiotensin II receptor 1
ATP	Adenosine triphosphate
Bax	B-cell lymphoma 2 associated X protein
B-cell	Bone marrow-derived cell
Bcl2	B-cell lymphoma 2
BCR	B-cell receptor
BHF	British heart foundation
B-mode	Brightness-mode
bpm	Beats per minute
Breg	Regulatory B-cells
BSA	Bovine serum albumin
BW	Body weight

Ca^{2+}	Calcium
CAMKII	Calcium/calmodulin-dependent protein kinase II
CCL	C-C ligand
CCR	C-C chemokine receptor
CD	Cluster of differentiation
cDNA	Complementary deoxyribonucleaic acid
CFSE	Carnboxyfluorescein succinimidyl ester
CGD	Chronic granulomatous disease
CHF	Chronic heart failure
CLP	Common lymphoid progenitor
CMP	Common myeloid progenitor
CNS	Central nervous system
CO_2	Carbon dioxide
Col1α1	Collagen1α1
Col3α1	Collagen3α1
cTGF	Connective tissue growth factor
CTL	Cytotoxic lymphocytes
CTLA-4	Cytotoxic T-lymphocyte associated protein-4
CVD	Cardiovascular disease
DAB	3,3'-Diaminobenzidine
DAMP	Damage-associated molecular patterns
DAPI	4',6-diamidino-2-phenylinodole
DC	Dendritic cell
ddH_2O	Double-distilled water
DHE	Dihydroethidium
DN	Double negative ($CD4^-CD8^-$ T-cells)
DNA	Deoxyribonucleic acid
Dnase	Deoxyribonuclease
dnRAR	Double negative retinoic acid receptor
DOCA	Deoxycorticosterone acetate
DP	Double positive ($CD4^+CD8^+$ T-cells)
DPX	Distyrene, plasticizer and xylene
DRI	Direct renin inhibitor

dTGR	Double transgenic rat
Duox	Dual oxidase
DuoxA	Dual oxidase activators
ECC	Excitation-contraction coupling
ECM	Extracellular matrix
EDTA	Ethylenediaminetetraacetic acid
EF	Ejection fraction
ELISA	Enzyme-linked immunosorbent assay
EPC	Endothelial progenitor cell
ER	Endoplasmic reticulum
ERK	Extracellular-signal regulated kinase
ET-1	Endothelin-1
ETA	Endothelin-A
ETB	Endothelin-B
ETC	Electron transport chain
EtOH	Ethanol
FACS	Fluorescence activated cell sorting
FAD	Flavin adenine dinucleotide
FCS	Foetal calf serum
FITC	Fluorescein isothiocyanate
FMO	Fluorescence minus on
FoxP3	Forkhead box P3
FS	Fractional shortening
Fsc	Forward scatter
Fsc-A	Forward scatter area
Fsc-H	Forward scatter height
Fsc-W	Forward scatter width
GAPDH	Glyceraldehyde-3-phosphate dehydrogenase
G-CSF	Granulocyte colony stimulating factor
GDI	Guanosine diphosphate inhibitor
GDP	Guanosine diphosphate
GITR	Glucocorticoid-induced TNF receptor family related gene
GM-CSF	Granulocyte-monocyte colony stimulating factor

GMP	Granulocyte-monocyte progenitor
GPCR	G-protein coupled receptor
GTP	Guanosine triphosphate
GTPase	Guanosine triphosphatase
H&E	Haematoxylin and eosin
H_2O_2	Hydrogen peroxide
HGF	Hepatocyte growth factor
HGFR	Hepatocyte growth factor receptor
HRP	Horse radish peroxidase
HSC	Haematopoietic stem cell
HW	Heart weight
ICAM	Intercellular adhesion molecule
IFN	Interferon
Ig	Immunoglobins
IL	Interleukin
IRF	Interferon regulatory factor
iTregs	Inducible regulatory T-cells
IVIS	In vivo imaging system
IVS	Interventricular septum
IκB-α	NFκ light polypeptide gene enhanced in B-cells inhibitor, alpha
JG cells	Juxtaglomerular cells
KCl	Potassium chloride
KO	Knockout
LAG3	Lymphocyte-activation gene 3
LN	Lymph node
LV	Left ventricle
LVED	Left ventricle end diastolic
LVEDV	Left ventricular end-diastolic volume
LVES	Left ventricle end systolic
LVESV	Left ventricular end-systolic volume
LVH	Left ventricular hypertrophy
M1	Macrophage type 1 cells
M2	Macrophage type 2 cells

MAPK	Mitogen activated protein kinases
MCP-1	Monocyte chemotactic protein-1
MEP	Megakaryocyte, erythrocyte progenitor
Mg^{2+}	Magnesium
MHC	Major histocompatibility complex
MI	Myocardial infarction
MMO	Microsomal monooxygenase
M-mode	Motion-mode
MMP	Matrix metalloproteinases
MPP	Multipotent progenitor
MPR	Mean pump rate
MRI	Magnetic resonance imaging
mRNA	Messenger ribonucleic acid
Na^{2+}	Sodium
NAC	N-acetylcysteine
NaCl	Sodium chloride
NADPH	Nicotinamide adenine diphosphate
NaOH	Sodium hydroxide
NCF-1	Neutrophil cytosolic factor-1
ND-1000	Nanodrop-1000
NF-κB	Nuclear factor κB
NK cells	Natural killer cells
NMRI	Naval medical research institute
NO	Nitric oxide
NOS	Nitric oxide synthase
Nox	Nicotinamide adenine diphosphate oxide
NoxA	Nox Activator e.g. NoxA1 or NoxA2
NoxO	Nox Organiser e.g. NoxO1 or NoxO2
NTP	Nucleoside trisphosphate
nTregs	Natural regulatory T-cells
$O_2^{\bullet-}$	Superoxide
PAI1	Plasminogen activator inhibitor 1
PAMP	Pathogen-associated molecular patterns

PBS	Phosphate buffered saline
PCR	Polymerase chain reaction
PD-1	Programmed death-1
PDGF	Platelet derived growth factor
PDI	Protein disulphide isomerase
PFA	Paraformaldehyde
PI3K	Phosphatidylinositol 3-kinase
PIZ	Peri-infarct zone
PKC	Protein kinase C
PKD	Protein kinase D
PKG	Protein kinase G
PLAX	Parasternal long axis
PMA	Phorbol 12-myristate 13-acetate
PPR	Pattern recognition receptors
PSAX	Parasternal short axis
PSC	Pluripotent stem cell
PSR	Picrosirius red
pTregs	Peripheral-derived regulatory T-cells
PX domain	Phox homology domain
qPCR	Quantitative polymerase chain reaction
RAAS	Renin-angiotensin-aldosterone system
RAG	Recombination-activating gene
RAR	Retinoic acid receptor
Redox	Reduction-oxidation
RNA	Ribonucleic acid
RNase	Ribonuclease
RNS	Reactive nitrogen species
RORγt	Retinoid-related orphan receptor gamma t
ROS	Reactive oxygen species
RPMI	Roswell Park Memorial Institute
RSK	Ribosomal S6 kinase
RT	Reverse transcription
RyR	Ryanodine receptor

SA	Sinoatrial
SEM	Standard error of the mean
SFO	Subfornical organ
SHR	Spontaneous hypertensive rats
siRNA	Small interfering ribonucleic acid
SLO	Secondary lymphoid organs
SOD	Superoxide dismutase
SOH	Sulfenic acid
Ssc	Side scatter
Ssc-A	Side scatter area
Ssc-H	Side scatter height
Ssc-W	Side scatter width
STAT	Signal transducer and activator of transcription
TAC	Trans aortic constriction
TBS	Tris-buffered saline
T-cell	Thymus-derived cell
TCR	T-cell receptor
Teff	Effector T-cells
TGFβ	Transforming growth factor β
Th	T-helper
TIM-3	T-cell immunoglobulin and mucin-domain containing-3
TIMP	Tissue inhibitors of matrix metalloproteinases
TL	Tibia length
TLR	Toll-like receptor
TNF	Tumour necrosis factor
TNFR	Tumour necrosis factor receptor
Treg	Regulatory T-cell
tTregs	Thymic-derived regulatory T-cells
UV	Ultraviolet
VAT	Visceral adipose tissue
VCAM	Vascular cell adhesion molecule
VEGF	Vascular endothelial growth factor
VPR	Volume-pressure recording

VSMC	Vascular smooth muscle cell
WGA	Wheat germ agglutinin
WT	Wild-type
XO	Xanthine oxidase
YFP	Yellow fluorescent protein
α-SMA	α-smooth muscle actin
β-ME	β-mercaptoethanol

Chapter 1: General Introduction

1.1 Reactive oxygen species

1.1.1 Basics of oxidation and reduction

Reduction-oxidation (redox) reactions include reactions involving molecules with an altered oxidation state due to the transfer or loss of electrons. Both oxidation and reduction occur simultaneously, where oxidation is the loss of electrons (an increase in oxidation state) and reduction is the gain of electrons (a decrease in oxidation state). Many biological processes involve redox reactions, such as respiration and photosynthesis, however there are also negative consequences. Free radicals can be generated as a by-product of these natural reactions; these are atoms or a group of atoms containing at least one unpaired election. They are highly reactive and can be involved in a number of different processes within the cell by beneficially or adversely altering lipids, proteins and deoxyribonucleic acid (DNA)[1].

1.1.2 ROS, sources and scavenging systems

Most reactive oxygen species (ROS) and reactive nitrogen species (RNS) are free radicals derived from oxygen and nitrogen respectively[1], an exception is hydrogen peroxide (H_2O_2), which is a ROS but does not contain unpaired electrons. ROS are involved in numerous signalling pathways in either physiological or pathological conditions, including the development of cardiac remodelling. ROS include molecules such as superoxide ($O_2^{\bullet-}$), H_2O_2, hydroxyl radical ($^{\bullet}OH$), and singlet oxygen ($^1O_2$)[2,3]. $O_2^{\bullet-}$ is the most common ROS within the cell, and is the precursor to H_2O_2[4]. There are a variety of sources of ROS including the mitochondrial electron transport chain (ETC), cytochrome P450 family proteins, uncoupled nitric oxide synthase (NOS), peroxisomes and nicotinamide adenine diphosphate (NADPH) oxidases (Nox)[2,3,5-9].

The mitochondrial ETC is an important source of ROS. During aerobic respiration, electrons are passed along the mitochondrial ETC to facilitate the movement of hydrogen. This generates an electrochemical gradient that allows the synthesis of adenosine triphosphate (ATP). Electron leakage can occur before the electrons reach cytochrome C oxidase, where normally oxygen is reduced to water[5]. Electron leakage leads to a reaction with oxygen, forming $O_2^{\bullet-}$ [5]. Cytochrome P450 also contributes to

cellular ROS levels. Different isoforms of cytochrome P450 contribute to the membrane-bound microsomal monooxygenase (MMO) system within the endoplasmic reticulum (ER). Here, two electrons are transferred from endogenous and exogenous compounds to cytochrome P450, enabling oxidation. This in turn activates oxygen and allows the transfer of one oxygen atom to the substrate[6]. Electron leakage from this system increases generation and cellular levels of ROS. NOS catalyse the synthesis of nitric oxide (NO) by converting L-arginine to L-citrulline[7]. NOS can become 'uncoupled' due to certain cellular conditions, lack of substrates or cofactors. During this time NOS transfers electrons to oxygen, synthesising $O_2^{\bullet-}$ instead of NO, thereby contributing to ROS production[7]. In addition, xanthine oxidase (XO) catalyses the oxidation of hypoxanthine, generating xanthine, that can then further be oxidised to form uric acid[8]. During this process, H_2O_2 and $O_2^{\bullet-}$ are generated[3]. Although the main role of XO is to aid purine degradation it also contributes to the levels of ROS within the cell[8].

In contrast to the above enzymes, Nox are the only enzymes whose sole purpose is to produce $O_2^{\bullet-}$ and H_2O_2, depending on their isoform[3, 9]. The enzyme is membrane-associated and is involved in catalysing the reduction of oxygen via NADPH[9]:

$$NADPH + 2O_2 \rightarrow NADP^+ + H^+ + 2O_2^{\bullet-}$$

In addition to the numerous sources of ROS discussed above, there are also scavenging systems, which aim to maintain redox balance within the cell. These include superoxide dismutase (SOD)[1], catalase[10], glutathione peroxidases, peroxiredoxin and the thioredoxin system, and antioxidants such as ascorbate[11]. SOD catalyses the dismutation of $O_2^{\bullet-}$ into H_2O_2, while catalase, glutathione peroxidase and peroxiredoxin reduce H_2O_2, generating water, thereby maintaining a safe level of ROS within the cell[1,10,11]. Thioredoxins are oxidoreductase enzymes that facilitate the reduction of other proteins such as peroxiredoxin and glutathione by cysteine thiol-disulfide exchange[11].

1.1.3 Concept of oxidative stress

Maintaining redox homeostasis is essential due to its wide involvement in cellular responses and signalling. When ROS production increases or ROS scavenging

decreases, the delicate balance is shifted towards pro-oxidants. This imbalance leads to 'oxidative stress', which has been implicated in a range of different diseases[1]. Exposure to environmental, physiological and pathological agents can increase the levels of ROS within a cell. ROS are highly reactive, and can interact with vital components of the cell such as lipids, carbohydrates, DNA and proteins[1].

1.1.4 ROS as signalling molecules

ROS are capable of reversibly altering protein structure and subsequent function, hence contributing to physiological and pathological signalling pathways. A selection of protein sensors can act as signal transducers, responding to local redox levels by a modification in protein conformation, stability, molecular interactions and hence activity[4,12]. Such proteins include ion transporters, receptors, kinases, phosphatases, transcription factors and even structural proteins[4,12].

Signalling initiated by ROS depends on specific redox-reactive residues such as cysteine thiols. When oxidised, cysteine forms reactive sulfenic acid (-SOH), which can in turn form disulphide bonds with other cysteine residues[4]. This oxidation can impair or enhance the structure of the protein involved, potentially also altering protein function. This level of oxidation remains reversible by scavenging systems, however further oxidation can also occur forming sulfinic acid ($-SO_2H$) or sulfonic acid ($-SO_3H$), which are relatively irreversible[4].

ROS can reversibly modify a number of signalling molecules involved in different pathways, which are essential in physiological and pathological cardiovascular processes[4]. Physiologically, ROS can direct cardiomyocyte differentiation and proliferation, for example by redox activation of the phosphatidylinositol 3-kinase (PI3K)-Akt pathway[13]. In addition ROS can alter proteins involved in excitation-contraction coupling (ECC) such as ryanodine receptor 2- (RyR2) leading to changes in its conductance of calcium (Ca^{2+}) ions[14]. Furthermore, ROS signalling can aid blood pressure regulation, for instance the oxidative activation of protein kinase G1α (PKG1α) is essential for effective vasodilation[15].

During cardiac stress, ROS levels within the heart increase and their signalling here contributes to a variety of pathological processes, such as hypertrophy and fibrosis[16,17]. As an example, redox modulation of extracellular-signal regulated kinases 1/2 (ERK1/2) and nuclear factor-κB (NF-κB) is involved in the development of hypertrophy due to G-protein-coupled receptor (GPCR) stimulation[4]. This can occur by oxidation of cysteine thiols in small guanosine triphosphatases (GTPases) such as Ras and Rac, which act as signal transducers in this setting[18,19]. ROS are also implicated in a number of other signalling cascades that lead to hypertrophy. In the setting of cardiac fibrosis, redox signalling within different cell types such as cardiomyocytes, fibroblasts or even immune cells may be involved[4]. ROS have been found to activate the main mediator of fibrosis, transforming growth factor β (TGFβ) and promote other pro-fibrotic transcription factors[4,20,21].

Further to this, the source of ROS within these settings has been linked to Nox, whose sole purpose is to generate ROS[4].

1.2 NADPH oxidases: structure and function

1.2.1 Nox structure and biochemistry

ROS produced by Nox may contribute to signalling pathways involved in cardiac remodelling[4]. There are seven different Nox enzymes: Nox1-5, dual oxidase (Duox) 1 and Duox2[3,22]. They each contain a different membrane-integrated catalytic subunit and a number of additional associated proteins; however these vary between the different Nox proteins (*Table 1*)[22]. All Nox catalytic subunits comprise a six transmembrane-spanning protein with an N- and C-termini within the cytosol[22]. Nox5 also contains four N-terminal Ca^{2+} binding domains, which regulate activation of the enzyme[22]. Duox1 and 2 contain additional domains. Nox1-4 relies on $p22^{phox}$ for membrane targeting, activity and stabilization of the enzyme[3]. Nox1-3 also require $p47^{phox}$ (Nox organiser 2 (NoxO2)) or NoxO1, and $p67^{phox}$ (Nox activator 2 (NoxA2)) or NoxA1. In addition to this Nox2 also require $p40^{phox}$ [3]. The catalytic activity of Nox1-3 is also dependent upon a small GTPase, Rac[3]. The structures of the Nox isoforms are illustrated in *Figure 1-1*.

The assembly and function of Nox enzymes is relatively similar amongst different isoforms, except for Nox4, which is constitutively active and does not require adaptor proteins. The main principle is that phosphorylation of adaptor proteins brings the specific components of the Nox complex together into an active complex, once NADPH is recruited this enables the transfer of electrons. Two electrons from NADPH transfer to the constitutively bound flavin adenine dinucleotide (FAD) molecule generating $FADH_2$ and $NADP^+$ [3]. One electron at a time is then transferred to one heme group and then to the other, gradually moving across the membrane complex[3]. The electron can then transfer to oxygen on the external membrane generating $O_2^{\bullet-}$, which is produced by Nox1-3 and Nox5[3]. Within Nox4, Duox1 and Duox2, $O_2^{\bullet-}$ is thought to be quickly converted to H_2O_2 via dismutation[3].

Adaptor proteins	Nox family member	Function
$p22^{phox}$	Nox1-4	Targeting complex to the membrane, activity and stabilization of the protein
$p47^{phox}$ (NoxO2)	Nox2 (sometimes Nox1)	Regulatory subunit responsible for translocating adaptor proteins to the membrane complex
$p67^{phox}$ (NoxA2)	Nox2 (sometimes Nox1)	Regulatory subunit responsible for activation of the enzyme
$p40^{phox}$	Nox1-3	Provides further support to activation of the enzyme by aiding recruitment of cytosolic adaptor proteins to the membrane
NoxO1	Nox1 and Nox3	Regulatory subunit responsible for translocating adaptor proteins to the membrane complex
NoxA1	Nox1 and Nox3	Regulatory subunit responsible for activation of the enzyme
Rac1	Nox1 and Nox2 (in some cells)	Rho family GTPase essential for catalytic activity
Rac2	Nox2	Rho family GTPase essential for catalytic activity
DuoxA1	Duox1	Regulatory subunit responsible for activation of the enzyme, traffic from endoplasmic reticulum (ER) to golgi apparatus
DuoxA2	Duox2	Regulatory subunit responsible for activation of the enzyme, traffic from ER to golgi apparatus
Poldip2	Nox4	Polymerase (DNA-directed) Delta-interacting protein 2 increases activity
TKS4/5 ($p47^{phox}$ analogue)	Nox1 and Nox4	Associate to established Nox binding partners, unknown function
PDI	Nox1 an dNox4	Associate to established Nox binding partners, unknown function
Calmodulin	Nox5	Further supports activity of the enzyme
Hsp90	Nox5 and possibly Nox1 and Nox2	Heat shock protein 90. Further supports activity of the enzyme
N-terminal Calcium-binding sites (four)	Nox5	Regulate activity of the enzyme

***Table 1: Adaptor proteins that associate with different Nox isoforms**. Adapted from Ghouleh et al, 2011), Altenhofer et al 2012 and El-Benna et al 2005[3,22,23].*

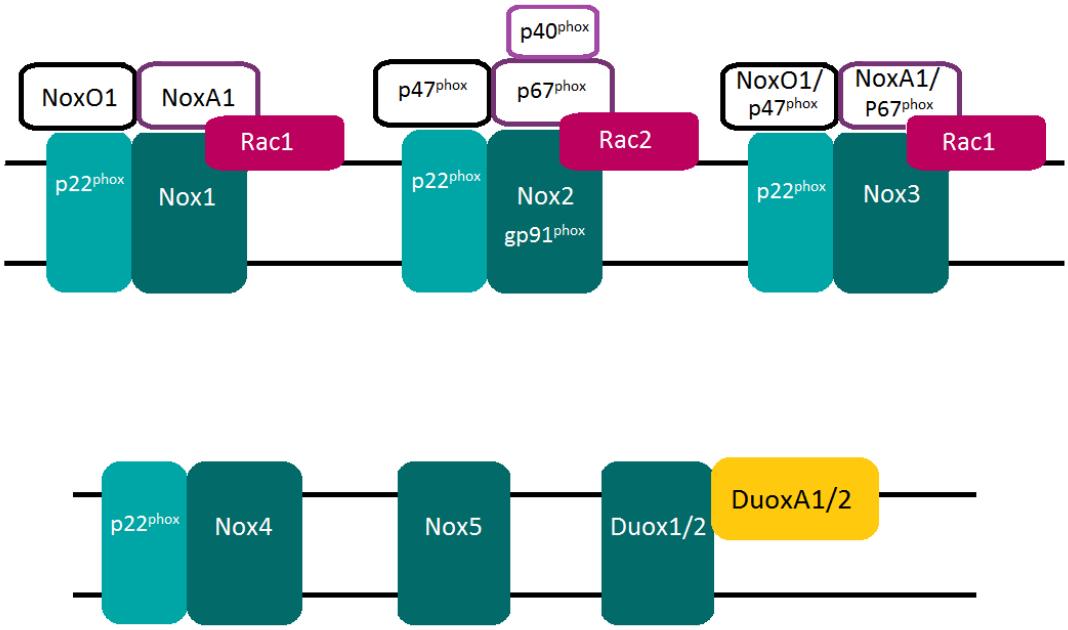

Figure 1-1: Models of the active Nox isoforms. *Adapted from Ghouleh et al, 2011*[3].

1.2.2 Nox isoform tissue-specificity and localisation

The different tissue (*Figure 1-2*) and cellular organisation of Nox isoforms allow their specific roles[3]. Nox1 is predominantly expressed in the colon, but has also been identified in reproductive organs and vasculature[24-26]. Nox1 is expressed in epithelial cells, lymphocytes, vascular smooth muscle cells (VSMCs), endothelial cells and osteoclasts[3,24,25,27]. Nox2, also referred to as gp91^{phox}, was first identified in neutrophils and is also found within the heart, vasculature, liver and immune system[3,28]. The enzyme has been identified within neutrophils, macrophages, VSMCs, fibroblasts, endothelial cells, skeletal muscle cells, cardiomyocytes and hepatocytes[28-31]. Nox3 is highly expressed within the inner ear, and at lower levels in the brain, skull and foetal tissues however its expression within specific cell types requires further clarification[3,32]. Nox4 is more universal, initially identified in the kidney but also discovered in many other organs such as the heart, reproductive organs and pancreas[28,33]. Expression of Nox4 involves VSMCs, fibroblasts, hematopoietic stem cells, osteoclasts, neurons and endothelial cells[25,34-36]. Nox5 is not expressed within the murine model but has been identified within human spleen, stomach, pancreas, reproductive tissues and foetal tissue[3,28,37]. Nox5 is expressed within VSMCs, endothelial cells, bone marrow, and lymph nodes (LNs)[37,38]. Duox1 and 2 are located

within the thyroid, airway and prostate; in addition, Duox2 has also been identified within the digestive system[3,28,39]. Moreover, Nox isoforms also exhibit distinct subcellular localisation, which potentially reflects the different responses of the enzymes to a stimulus[25].

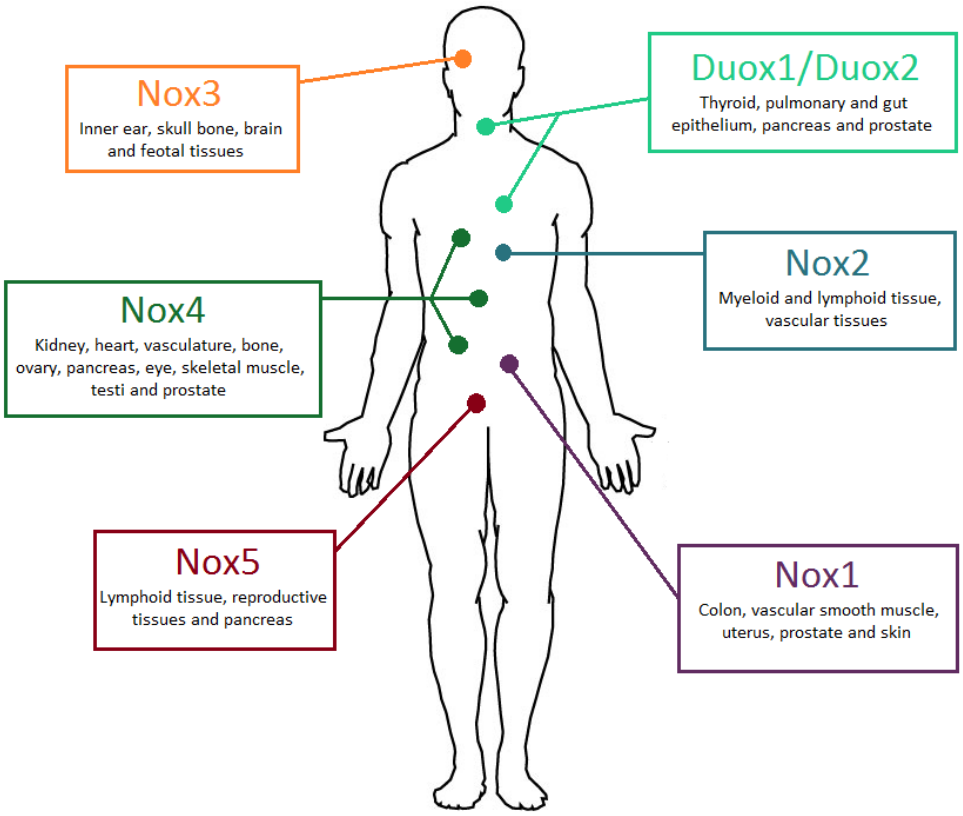

Figure 1-2: Expression of different Nox isoforms within the human body. *Adapted from Quinn et al 2006[28].*

1.2.3 The activation of Nox2

The production of ROS by Nox2 occurs on the external side of the plasma membrane and releases ROS into the phagosome, endosomes or the extracellular space[23]. In comparison, other Nox enzymes release ROS into the intracellular space and tend to produce a smaller quantity.

Assembly of the Nox2 complex (*Figure 1-3*) involves the phosphorylation of the SH3-containing proteins $p47^{phox}$ and $p67^{phox}$ as well as $p40^{phox}$ that naturally accompanies $p67^{phox}$ within the cytoplasm[40]. This induces their translocation to the cell membrane where they all bind the membrane-integrated $gp91^{phox}/p22^{phox}$ heterodimer. This translocation requires a stimulus-induced conformational change within $p47^{phox}$ allowing its two integral SH3-domains to interact with $p22^{phox}$ [40]. Within a resting cell the phox homology (PX) domain of $p47^{phox}$ is bound to its internal SH3-domains and hence these domains are not accessible to bind to $p22^{phox}$ on the membrane[41]. Upon stimulus-dependent activation, $p47^{phox}$ is phosphorylated causing a conformational change that dissociates the PX domain from SH3-domains. This allows the PX domains to be free to bind phophoinositides and the SH3-domains open to bind to $p22^{phox}$, therefore translocation to the membrane occurs[41]. Rac-guanosine diphosphate (GDP) exchanges its GDP with guanosine triphosphate (GTP) and loses its inhibitor, Rho-GDI, before binding between $p67^{phox}$ and Nox2[23]. This induces activation of the complex via an activation domain within $p67^{phox}$. This activation allows cytosolic NADPH to bind to the NADPH binding domain within the cytosolic C-terminus[23]. Two electrons transfer from NADPH to FAD enabling electrons to move across the membrane via heme groups, as described in section 1.2.1. Within Nox2 the electron is then transferred to oxygen, generating superoxide[3].

Many different physiological and pathological signals can trigger the activation and expression of Nox2, such as hypoxia, growth factors, cytokines, and components of the renin-angiotensin-aldosterone system (RAAS)[42].

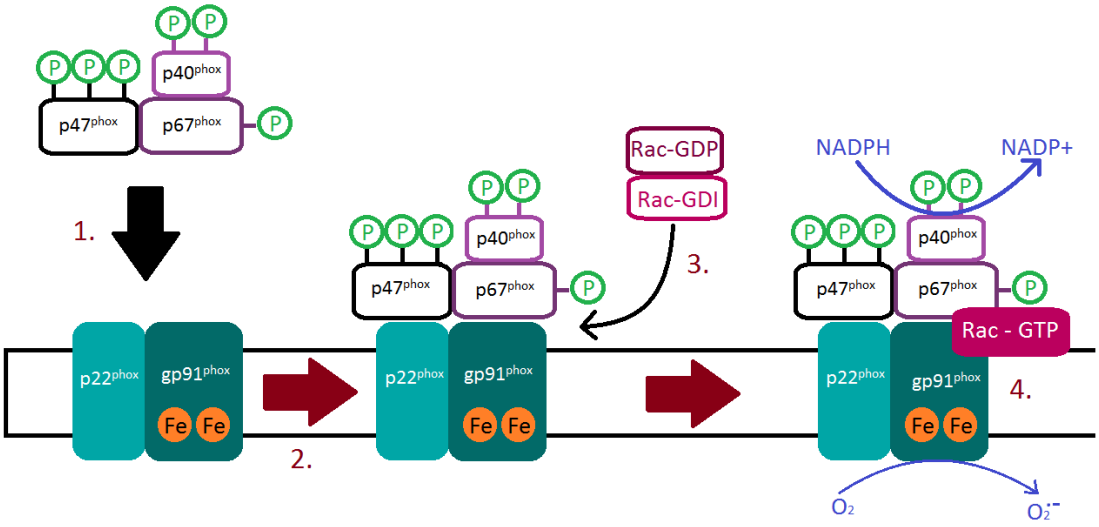

Figure 1-3: Activation of Nox2. *Adapted from El Benna et al 2005*[23].

Nox2 is expressed in a variety of cell types, including immune cells. Endogenous Nox2-derived ROS has the ability to signal in immune cells and potentially play a role in regulating their differentiation, activation, proliferation and overall phenotype. This modulatory function of immune cell Nox2 will be discussed in detail later.

1.3 Immune cell function

All cellular components of the blood, including immune cells, arise from pluripotent haematopoietic stem cells (HSCs) within the bone marrow (*Figure 1-4*). They then differentiate into two separate lineages; the lymphoid lineage (bone marrow-derived (B-), thymus-derived (T-) cells and natural killer (NK) cells) and the myeloid linage (neutrophils, eosinophils, basophils, monocytes and macrophages, dendritic cells (DCs) and mast cells as well as erythrocytes and platelets)[43]. The myeloid lineage of immune cells mainly comprises of cells involved in the innate immune response (section 1.3.1), whereas the lymphoid lineage mainly comprises cells of the adaptive immune response (section 1.3.2).

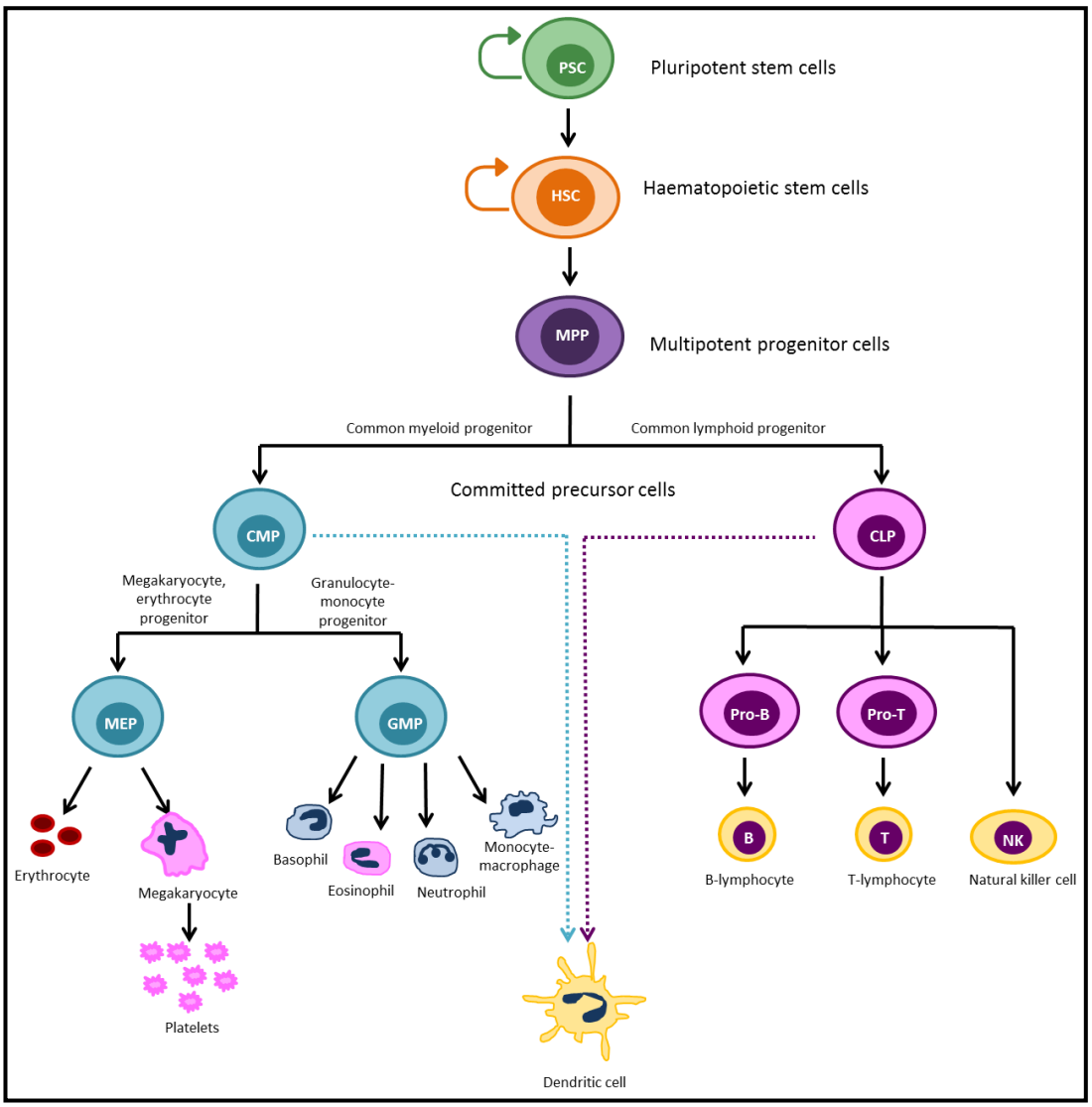

Figure 1-4: Process of haematopoiesis. *Adapted from Ackermann et al 2015*[43].

1.3.1 The innate immune responses

Innate immunity is a non-specific, initial response to invading pathogens[44]. There are a number of different factors that participate in the innate response, including anatomical barriers, complement and immune cell responses. Once an anatomical barrier, such as the skin or mucosal surfaces, is breached by an invading pathogen, an inflammatory response is initiated. Complement can be activated by three different biochemical pathways: the classical, alternative or lectin pathways[45]. The complement system consists of a range of complement regulators, recognition molecules, receptors and enzymes that enable opsonisation, cell lysis or chemotaxis. The cell-mediated response involves NK cells, eosinophils, basophils, macrophages, neutrophils and DCs.

Nox2 is expressed in all immune cells and may modulate specific signalling pathways involved in activation, antigen presentation, cytokine synthesis and cell function. These processes are discussed below; however the impact of Nox2 within these cell types is discussed in section 4.1.1.1.

Eosinophils and basophils are less well understood; they appear to have a role against parasites as well as allergic inflammatory responses. Mast cells are also involved in allergic responses therefore these cells will not be discussed further.

1.3.1.1 Natural killer cells

NK cells are lymphocytes that do not respond to specific antigens, have the ability to recognize and kill abnormal cells[44]. Although recently thought to play a role in adaptive immunity, NK cells are traditionally associated with their cytotoxic mechanisms within the innate immune response. This is mainly due to their ability to directly instigate death of tumour cells and virus-infected cells, without having specific immunity[44]. In terms of cytokines, NK cells produce interferon-γ (IFN-γ), tumour necrosis factor-α (TNF-α), interleukins (IL-) for example IL-10 and IL-3, in addition to an array of C-C chemokine ligands (CCL2, CCL3, CCL4, CCL5, XCL-1 and CXCL8) and growth factors (for example, granulocyte-monocyte colony stimulating factor (GM-CSF) and granulocyte colony stimulating factor (G-CSF))[44]. These enable the modulation of the adaptive immune response in pathological and physiological conditions.

1.3.1.2 Macrophages

Macrophages, neutrophils and DCs are phagocytes, which are implicated in the first line of defence by engulfing, and killing invading pathogens[46-48].

Macrophages are long-lived tissue resident cells, which are thought to differentiate from circulating monocytes. They elicit the first phagocytic response but also have the capacity to orchestrate other immune responses, such as inflammation[48]. Macrophages play an important role in tissue surveillance in order to elicit an

immediate immune response upon discovery of tissue damage or invading organisms[48]. Tissue-resident macrophages also play an important homeostatic role, enabling removal of toxic materials, dead and dying cells[48]. Macrophages can be subdivided into two groups; M1 (classically activated) and M2 (alternatively activated) for which the distinct cytokine profile dictates their functions[48]. M1 is mainly involved in inflammation and therefore express pro-inflammatory cytokines such as TNF-α and IL-12[49]. In comparison M2 produces IL-10 as well as expressing CD163 and CD206, and has a role in regulating the immune response[49]. Hence M2 play a vital role in enabling tissue homeostasis following infection or injury.

Both macrophages and DCs serve as antigen presenting cells (APCs), which process foreign material in order to present antigens to other immune cells within peripheral lymphoid organs. DCs act as mediators between the innate and adaptive responses [47].

1.3.1.3 Dendritic cells

Immature DCs reside within peripheral tissues where they continuously sample the antigenic environment[47,50]. Tissue damage or the presence of a foreign antigen encourages DCs to migrate into the LNs, initiating their maturation[47,50]. The antigen encountered is processed and presented on the major histocompatibility complex (MHC) and co-stimulatory molecules are up-regulated[47]. This allows DCs to effectively activate T-cells within the LN. By interacting with T-cells, DCs are able to modulate the T-cell response (*Figure 1-5*). In the absence of any danger signals, DCs infiltrate the LNs at a low-level maintaining T-cell tolerance to self-antigens. However, in the response to infection, inflammation or tissue damage, DC migration increases enabling a specific T-cell response. DCs are the only immune cells that are able to migrate to the LN and interact between the innate and adaptive immune system[47]. There are thought to be different subtypes of DCs, including a non-migratory subtype that remains in peripheral tissues and acts as an inflammatory mediator[47]. DCs can also interact with other immune cells, such as B-cells and NK cells. In addition, DC associated cytokines include IFN-α, IL-6 and IL-10[47].

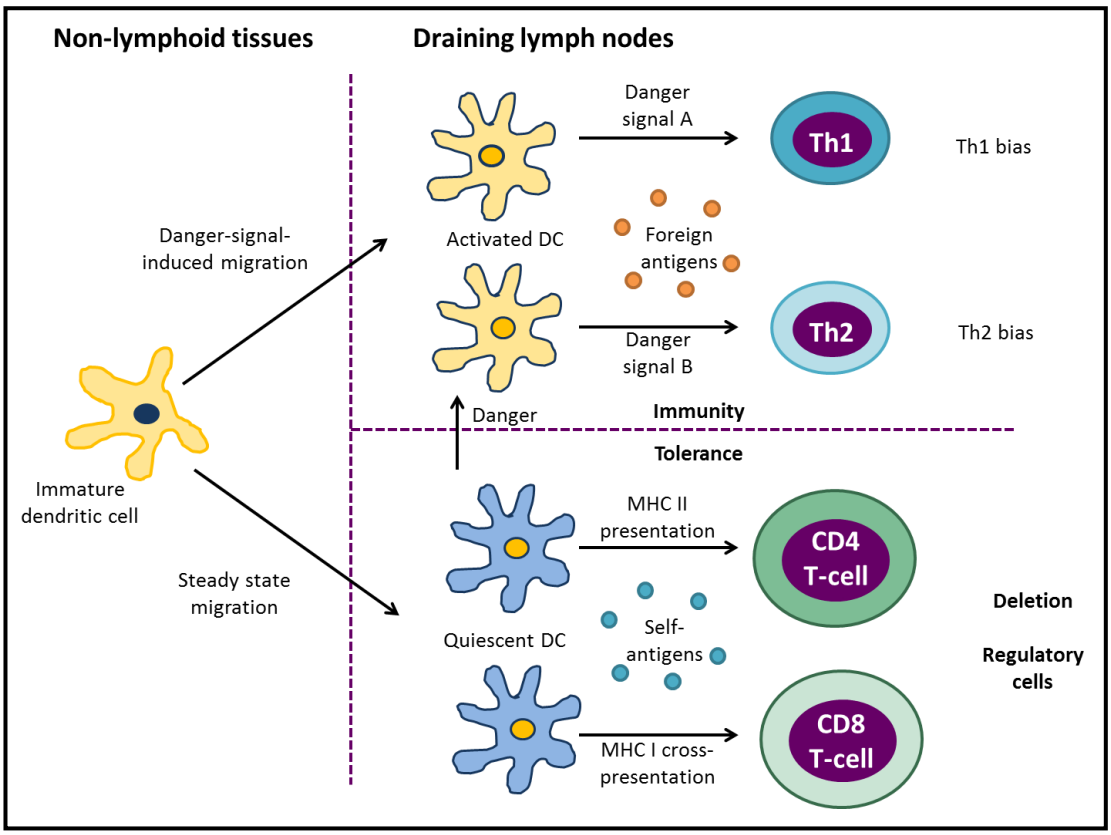

Figure 1-5: Dendritic cell interactions with T-cells. *Adapted from Shortman et al 2002*[47].

1.3.1.4 Neutrophils

Neutrophils are active, phagocytic cells that, in addition to macrophages and DCs, make up the first line of defence within innate immunity[46]. These cells are highly mobile and are mainly located in circulating blood. Upon inflammatory stimuli, neutrophils rapidly migrate to the site of infection or tissue-damage, being drawn by chemo-attractants such as pro-inflammatory cytokines[46,51]. The main function of these cells is to engulf and degrade foreign organisms. One vital component that enables their function is Nox2[46]. Subsequent production of ROS, such as $O_2^{\bullet-}$, enables an oxidative burst within the phagosome, in turn destroying the engulfed material. Furthermore, neutrophils can also influence the inflammatory response by migrating to the LNs, where they can interact with other immune cells such as other APCs and lymphocytes[52,53]. For example, in the case of T-cells, neutrophils have the ability to enhance and direct the T-cell response in addition to suppressing the T-cell response

all together[144]. More recent research has highlighted the potential for distinct subtypes of neutrophils, which may possess unique biological and functional implications[145].

1.3.2 Adaptive immune cells

The adaptive immune system comprises of antigen-specific lymphocyte populations, which bear a wide-variety of distinct antigen receptors in order to elicit a response to any pathogen encountered[44]. There are two types of antigen-specific lymphocytes, T- and B-cells, which play quite distinct roles within the immune system.

1.3.2.1 B-cells

B-cells contain an antigen-specific B-cell receptor (BCR) on their cell membrane. The antigen-binding region of the BCR is highly variable and encoded by variable region-encoding gene segments (V(D)J segments)[54]. During B-cell development, these genes undergo complex rearrangement that enables B-cells to recognise a wide variety of antigens. Due to this, the B-cell development pathway incorporates a number of checkpoints to prevent self-reactive or defective B-cells within the immune system[54]. Immature B-cells migrate to peripheral lymphoid organs where they maturate[55]. When the BCR is activated, this allows proliferation of the antigen-specific B-cell population and differentiation into plasma cells[55]. These effector B-cells are capable of releasing the antigen-specific receptor, known as an antibody or immunoglobulins (Ig), which are capable of binding to pathogens, marking them for destruction. B-cells also have the capacity to act as APCs to T-cells as part of the adaptive response[55]. They can influence T-cell differentiation by cytokine production in addition to regulating DC responses and even anti-inflammatory processes[55]. Further B-cell subsets can be defined by their cytokine production, location and function[55].

B-cell subtypes with a regulatory phenotype (Breg) have also been observed[56]. They may play a role in early regulation of the immune response by secreting anti-inflammatory molecules (*Figure 1-6*). These include IL-10, IL-35, TGFβ and forkhead box P3 (FoxP3), which are thought to be expressed by individual Breg subtypes[56,57, 151].

Hence inhibiting pro-inflammatory cytokines, inflammatory cells and supporting regulatory T-cell (Treg) differentiation[58]. Different subtypes of Bregs are thought to exist, which may arise at different points within the B-cell development[58,59].

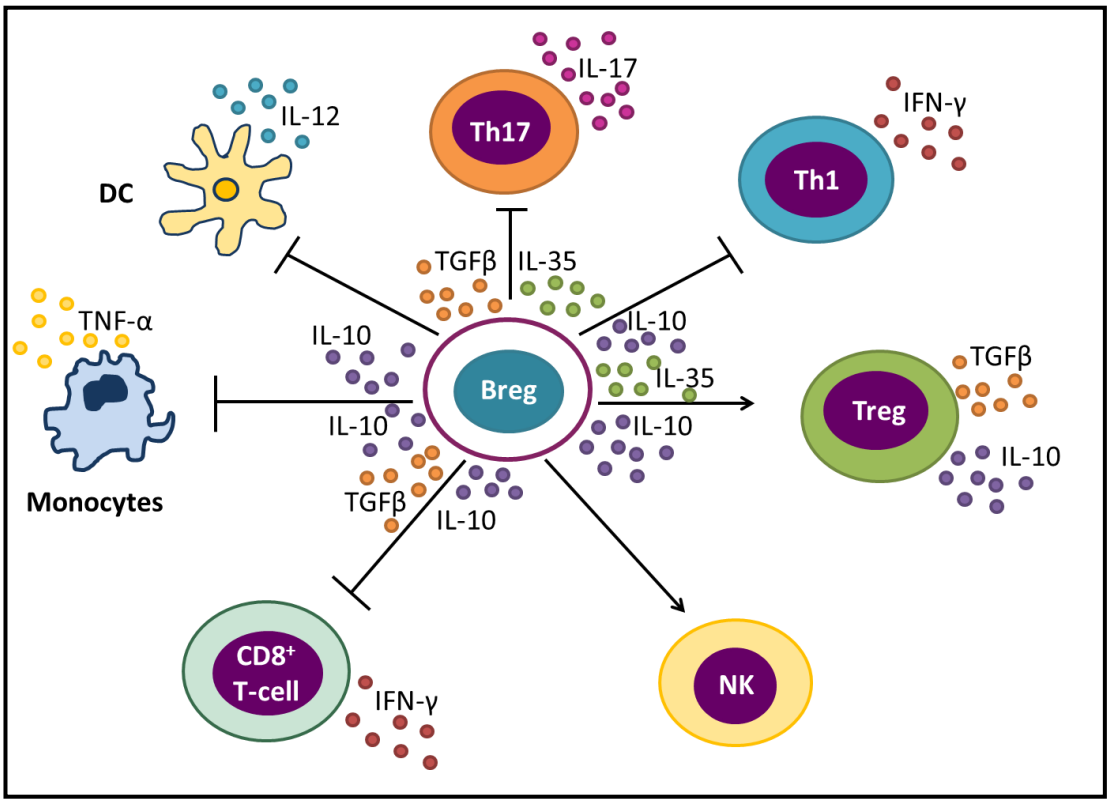

Figure 1-6: Regulatory B-cell functions. *Adapted from Rosser et al 2015 (Immunity)[57].*

1.3.2.2 T-cells

T-cells initially develop in the bone marrow before final maturation within the thymus. Naïve T-cells are double negative ($CD4^-CD8^-$) but can be activated by their T-cell receptor (TCR), which causes the cell to proliferate and differentiate into a number of different effector T-cells (Teffs). Initially, activated T-cells progress through a number of different 'double negative' (DN, $CD4^-CD8^-$) stages before becoming 'double positive' (DP, $CD4^+CD8^+$), *Figure 1-7*[60]. Positive selection then occurs to ensure that the T-cell recognises MHC class I ($CD4^-CD8^+$) or class II ($CD4^+CD8^-$), and negative selection ensures that the T-cells do not respond to self-antigens[60].

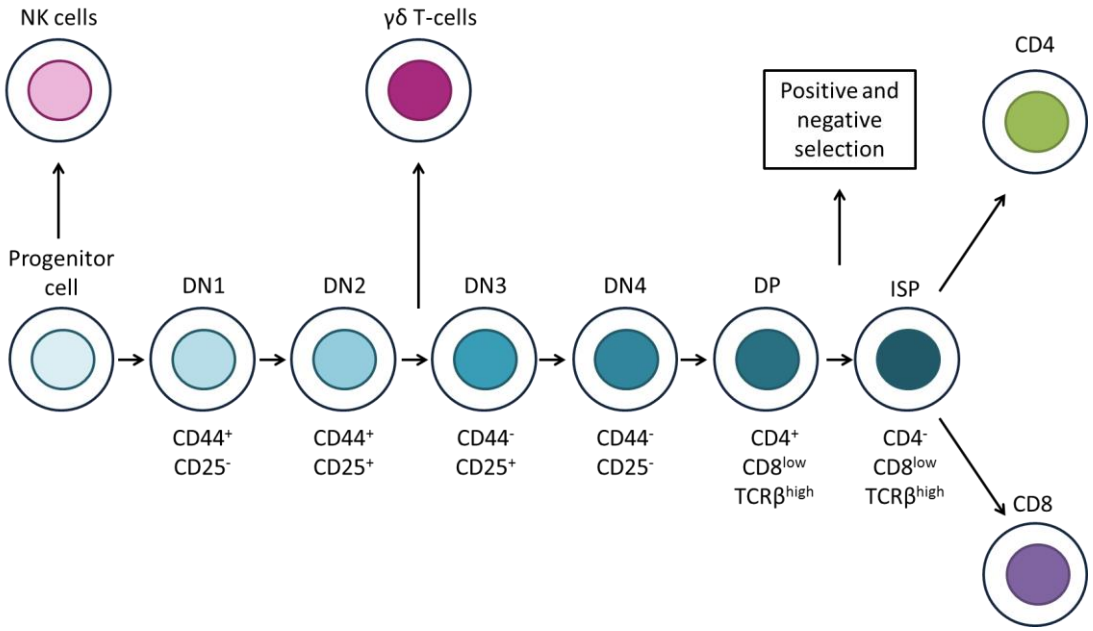

Figure 1-7: T-cell differentiation process. *Adapted from D'Acquisto et al*[60]**.**

In the periphery there are two different subsets of Teff cells; $CD4^+$ T-cells and $CD8^+$ T-cells, which are activated upon recognition of antigen bound to MHC class II or MHC class I respectively. Both subtypes require co-stimulation to enable their activation. This second signal is provided by non-specific molecules on the surface of both cells, for example between CD28 upon T-cells and either CD80 or CD86, on the APCs. These two subtypes of Teff cells have distinct functions within adaptive immunity.

Cytotoxic T-lymphocytes (CTLs) kill cells infected with intracellular pathogens and viruses. They are derived from naïve $CD8^+$ T-cells and proliferate in the presence of IL-2[61]. Compared to other T-cell subtypes, CTLs undergo dramatic clonal expansion due to easy activation by the Ag-MHC class 1 complex, as co-stimulation is not required, and they survive more efficiently within circulation[61]. Cytotoxicity requires contact with the target cell, antigen recognition and release of cytolytic granules. There are two different cytotoxic pathways; Ca^{2+} dependent perforin/granzyme-mediated apoptosis and Ca^{2+} independent Fas ligand/Fas-mediated apoptosis[61].

T-helper (Th) cells are derived from naïve $CD4^+$ T-cells and have a number of different subtypes based on their cytokine expression, producing distinct responses. Th1 cells are mainly driven by the T-bet transcription factor and produce IFN-γ, IL-2, TNF-α and lymphotoxin[61]. Their function is to enhance pro-inflammatory cell-mediated immunity,

for example Th1 cells can induce B-cell production of IgG[61]. Th2 cells are driven by the transcription factor GATA3 (which binds to the GATA DNA sequence) and mainly secrete IL-4, -5, -6, -10 and -13 and play a role in non-inflammatory immediate immune responses such as instigating B-cell production of IgA and IgE[61]. Th17 cells mainly secrete IL-17 and their master transcription factor is the retinoid-related orphan receptor-γt (RORγt)[62]. They are the first subset generated during infection, enabling recruitment of macrophages and neutrophils[61]. They enhance the innate acute inflammatory response but are also implicated in a number of inflammatory diseases[61]. Th9 cells, a recent addition, are distinct due to their production of IL-9 however their implication in the immune response requires further investigation[61].

Finally, Tregs that have anti-inflammatory properties are another $CD4^+$ T-cell subset, which is discussed in more detail in section 5.1.1. Recent research has highlighted the potential plasticity of Th lineages and cytokine production, making Th populations more complicated to define (*Figure 1-8*)[62-64].

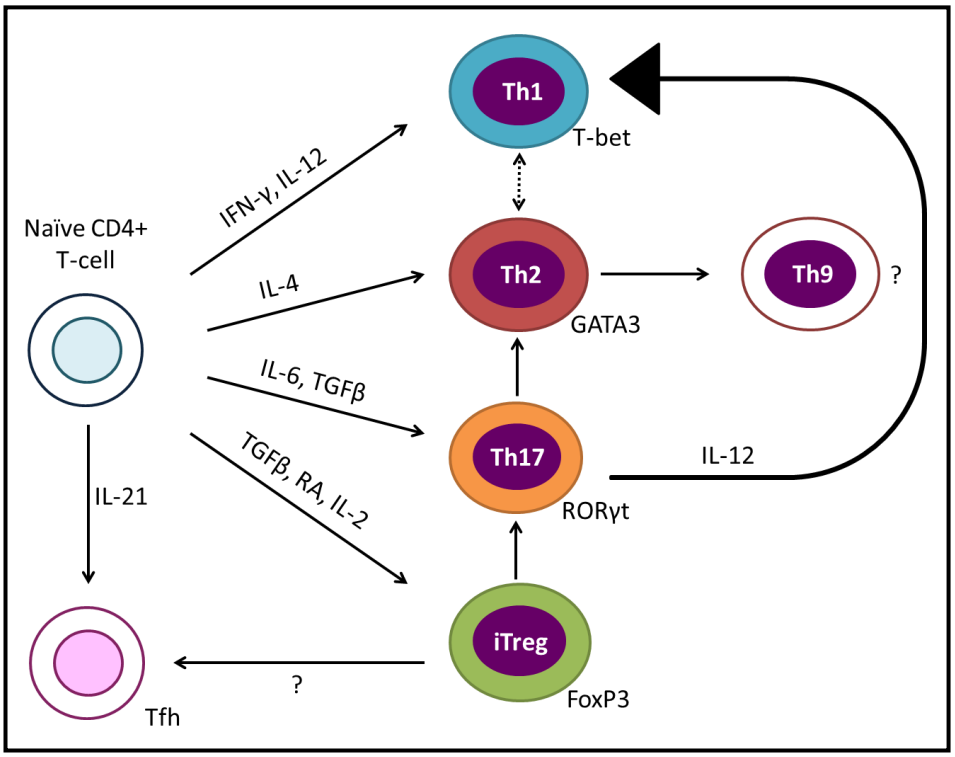

Figure 1-8: T-cell lineage differentiation and plasticity. *Adapted from Zhou et al 2009[63].*

T-cell plasticity describes the ability of T-cells to shift between different lineages rather than obeying a traditional lineage differentiation[62,64]. As described above, unique master transcription factors T-bet, GATA3 and RoRγt were found to be sufficient, and necessary, for the induction of signature cytokines, eliciting differentiation into Teff cells (Th1, Th2 and Th17 respectively)[65]. Cytokines produced by distinct Th subtypes tend to inhibit progression of other lineages. For example Th1 and Th2 cytokines, IFN-γ and IL-4, suppress the expression of each other, and together inhibit production of IL-17[63]. However, commitment to the Th lineages may be compromised, particularly with regard to Th17 and Tregs[63]. TGFβ is required for the differentiation and maintenance of Tregs, however this cytokine was also found to be essential for Th17 differentiation, hence suggesting a link between the two subtypes[63]. Mice deficient in TGFβ showed depletion of Th17 and Tregs in addition to overwhelming autoimmunity due to an enhanced Th1 response[66,67]. In addition, TGFβ can induce upregulation of both RoRγt and FoxP3 in naïve $CD4^+$ T-cells, and cells that co-express both RoRγt and FoxP3 have been identified[63]. These cells may act as a transient population that can differentiate into either lineage depending on environmental cues[68]. Tregs can also co-express a number of other transcription factors, including T-bet, GATA3 and signal transducer and activator of transcription 3 (STAT3), further demonstrating their plasticity[64]. Recent research also suggests the implication of further transcription factors and processes within the Th differentiation pathways[65]. For example STAT3 has also been shown to be important for Th17 differentiation[69]. These addition factors are not lineage-specific and hence understanding their role may elucidate Th differentiation and plasticity[65]. Moreover, evidence suggesting that Th cells can acquire suppressive functions is accumulating[70]. For example, Th1 cells have the capacity to produce IL-10, an anti-inflammatory cytokine in order to modulate their own response[71].

Inflammation has been implicated in the progression of hypertension and associated changes in heart structure and function.

1.4 Hypertension

1.4.1 Clinical basics

Hypertension refers to elevated levels of arterial blood pressure and is defined by a systolic or diastolic blood pressure that is persistently above 140mmHg and 90mmHg respectively[72]. There are two main types of hypertension; primary and secondary. Primary hypertension is the most common type exhibiting high blood pressure as the main symptom, with no underlying conditions found[72]. Genetic variation and a number of environmental factors such as obesity, high salt intake, age and stress all contribute to primary hypertension[72]. In comparison, secondary hypertension occurs due to another defect such as renal failure, renovascular disease, aldosteronism, and other primary causes[72].

Blood pressure is regulated by several different pathways, among which two well-established mechanisms are the RAAS that is a hormone-regulated system[73], and the baroreceptor reflex that elicits responses via the autonomic nervous system[74]. Here, we are interested in the RAAS, which is discussed in more detail in the following sections.

1.4.2 Regulation of blood pressure

The RAAS plays a vital homeostatic role in maintaining blood volume and systemic vascular resistance, thereby influencing cardiac and vascular function, as illustrated in *Figure 1-9*. Activation of this hormone-controlled system initiates the release of renin from the kidneys, allowing the cleavage of angiotensinogen[73]. Secretion of renin from the juxtaglomerular (JG) cells, within the renal glomerulus, is stimulated by a decrease in perfusion pressure, sodium chloride (NaCl) delivery or increases in sympathetic nerve activity[75]. Renin is described as the rate-limiting step of the RAAS cascade[75]. Initial synthesis of renin produces a precursor, which requires proteolytic cleavage of amino acids from the N-terminus of pro-renin, generating mature, activated renin[76]. Mature renin is then stored in granules in JG cells within the kidney, which are released by exocytosis[76].

Meanwhile, the liver constitutively secretes angiotensinogen, so plasma levels remain consistent[73]. Renin regulates the cleavage of circulating liver-derived angiotensinogen, by removing ten amino acids from the N-terminus generating angiotensin I (AngI), an inactive decapeptide that serves solely as a precursor to angiotensin II (AngII) [77 73,76].

Angiotensin-converting enzyme (ACE) then hydrolyses AngI, removing the C-terminal dipeptide to form an active octapeptide, AngII[73]. ACE is a membrane bound enzyme that is highly expressed on the luminal side of the vascular endothelium[73]. AngII is the primary active product of RAAS, however both AngI and AngII are thought to have short half-lives and hence AngII is potentially synthesised very close to its site of action. It is thought that renin may serve as a circulating hormone signal with the ability to initiate RAAS pathway at local sites where AngII is required[73,76,78].

AngII can elicit a number of different responses mediated by the angiotensin II receptor 1 (AT_1R), which provides a negative feedback loop in order to control the system, as shown in *Figure 1-9*[73]**.** AT_1R is responsible for the modulation of a number of processes in the cardiovascular system such as vasoconstriction, increases in blood pressure, cardiac contractility, and cardiovascular hypertrophy[79]. In addition, due to its wide distribution in a range of tissues, AT_1R elicits responses in the kidney, to reabsorb sodium (Na^{2+}) and inhibit renin release, sympathetic nervous system and the adrenal cortex, to stimulate synthesis of aldosterone[73,76,78,79]. Aldosterone is a hormone that binds to the mineralocorticoid receptor to induce ion and water reabsorption into the kidney. This further increases blood volume and hence blood pressure.

Although AT_1R is the main receptor that allows AngII to elicit a response, there are also 3 other reported receptors AT_2R, AT_3R and AT_4R that can be bound by AngII[79]. AT_2R is present in the brain, kidney and other organs during foetal life[73]. Low levels of AT_2R expression are also found in adults and may aid vasodilation, anti-proliferative and apoptotic effects in VSMCs[73]. Upregulation of AT_2R has been observed during injury and once activated may mediate anti-fibrotic and anti-inflammatory effects. Therefore AT_2R is thought to oppose AT_1R responses and act as a protective arm of the RAAS pathway[80]. The importance of any of these AT_2R responses remains uncertain. AT_4R is thought to mediate the release of plasminogen activator inhibitor 1 (PAI1) by AngII, but AT_3R functions remain unknown[73].

The classical RAAS cascade, as described above, is viewed solely as a circulating peptide system involved in blood pressure regulation, salt and fluid homeostasis. However there are a number of recent findings that demonstrate homeostasis by the RAAS cascade that lie outside this traditional view[73,78,80]. For instance, metabolites of AngI and AngII may function biologically in different tissues[81]. Moreover, AngII synthesis can be stimulated by adrenocorticotrophic hormone (ACTH), norepinephrine, endothelin and serotonin, and can be inhibited by atrial natriuretic peptide and NO[73].

In a number of different pathological settings, enhanced activation of the RAAS can lead to hypertension and play an important role in the pathogenesis of cardiovascular disorders. Increasing the level of AngII within the system, a method commonly used within research, can also induce hypertension.

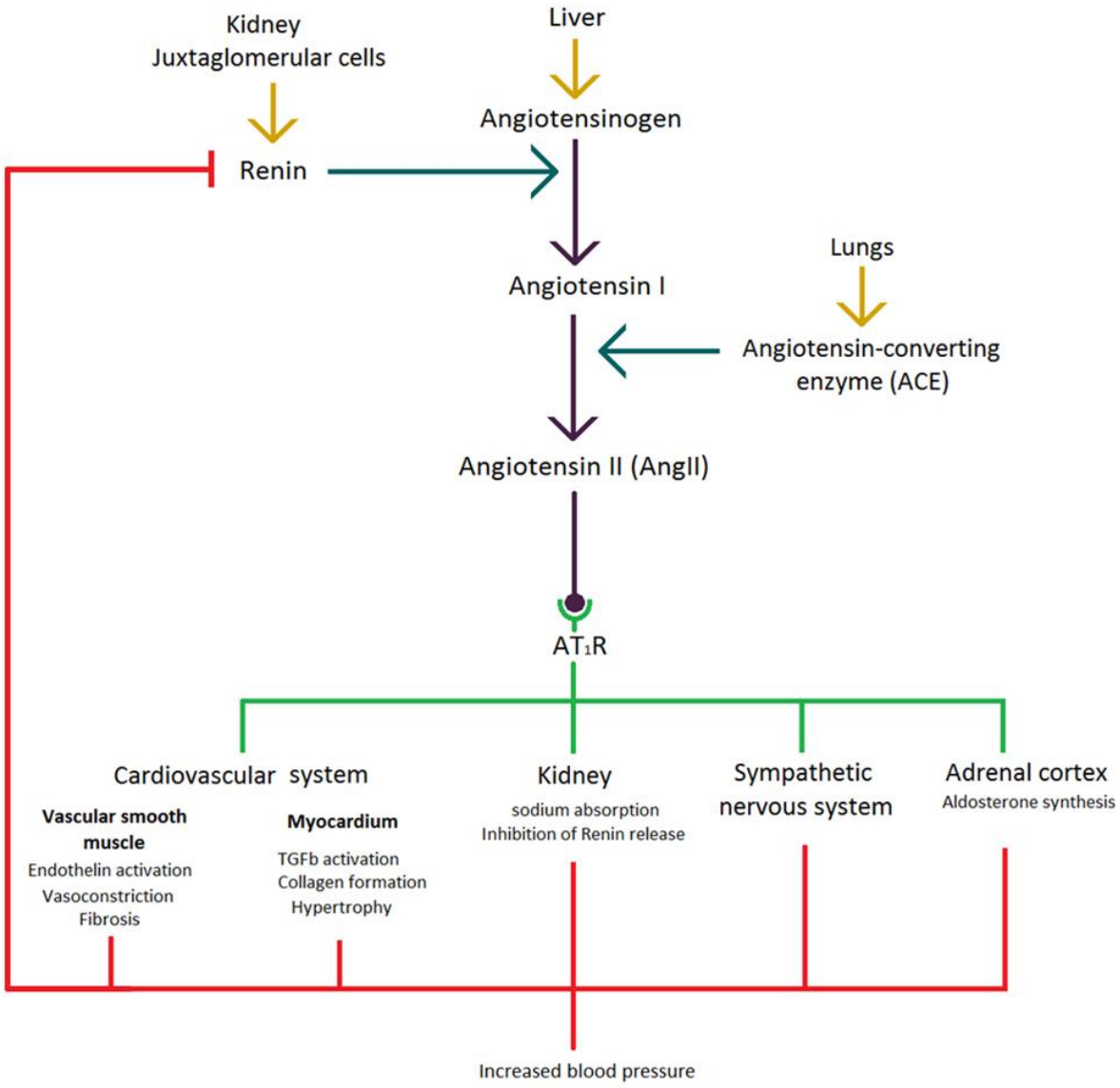

Figure 1-9: Physiological response of the classical renin-angiotensin-aldosterone system (RAAS).

1.4.3 Tissue-specific RAAS

In addition to this classical RAAS pathway, which occurs mainly in the circulatory system, recent evidence has also suggested a tissue-specific RAAS cascade. AngII precursors have been identified in numerous other tissues, including the brain, placenta, adrenal gland, ovary, visceral adipose tissue and even the heart and vascular tissues[73]. However the purpose of these precursors and their generation within these tissues are poorly understood. Accumulating evidence supports the synthesis of RAAS

components in many different tissues, suggesting that tissue-specific AngII levels can be controlled independently from circulating RAAS[76].

Due to the identification of Ang receptor subtypes and signal transduction pathways, truncated Ang peptides and specific cell surface receptors for renin and prorenin, it is thought that the RAAS may also function as a tissue paracrine/autocrine system[82, 13]. Local AngII synthesis may occur by tissue-uptake of circulating renin or angiotensinogen, or independent AngII-generating systems. This is thought to be the case in tissues such as the heart, peripheral blood vessels, kidney, brain, adrenal glands, pituitary, adipose tissue, testes, ovaries and skin.

The cardiac RAAS system is required to maintain cellular balance of inhibiting and inducing cell growth and proliferation in addition to mediating adaptive responses to myocardial stretch. AngII within cardiac tissue is mainly produced by conversion of locally produced AngI into AngII. It has also been postulated that local production of renin and additional proteolytic enzymes may also be involved in this setting. Especially as all the components required for AngII production are present in the heart[76,83]. In addition to this, although ACE is the main enzyme generating AngII, in the heart it has been postulated that this is mainly regulated by chymase. Therefore, new mechanisms allowing local tissue-specific RAAS cascades are coming to light and suggest independent pathways to that of the circulating RAAS components. A similar local generation of AngI and AngII is found in VSMCs, endothelial and endocardial cells. This vascular RAAS exerts an effect on cardiovascular homeostasis by stimulating VSMC and fibroblast proliferation via AT_1R and AT_2R[76].

Collectively, this evidence suggests that AngII can be synthesised locally within tissues, encouraging tissue-specific regulation in addition to circulatory RAAS mechanisms. Within the cardiovascular system AngII is heavily involved in cardiac remodelling processes with are further investigated in section 1.5.

Te Riet et al contradict these ideas in their recent review, suggesting that local AngII generation does occur, but that this is still dependent on renal-renin and hepatic-angiotensinogen[78]. These precursors diffuse into the interstitium where they are locally used to generate AngII via ACE. AngII can then bind directly to local AT_1R to elicit a response, and such binding results in internalisation of AngII, hence explaining

intracellular AngII levels[78]. Therefore the specifics of local tissue-RAAS still remain plausible but yet undetermined.

Further to this, AngII can impact immune cell recruitment, migration and function, which are discussed in later chapters.

1.4.4 RAAS dysregulation and clinical inhibition

Dysregulation of the RAAS cascade has been identified in the pathogenesis of a number of hypertensive disorders. This includes essential hypertension, in addition to the cardiovascular and renal tissue responses to hypertensive and non-hypertensive injury. For example increases in the rate-limiting renin levels can be a cause of primary hypertension by overstimulation of the RAAS, leading to excessive AngII production and hence increased blood pressure. This also causes increased levels of aldosterone production, which further contributes to this problem.

There are many stages within the RAAS that have been identified to target with pharmacological inhibitors to prevent the formation, or block the effects of, AngII and aldosterone. These include renin inhibitors, ACE inhibitors, AT_1R antagonists and mineralocorticoid receptor antagonists[78].

Renin was a clear target, being the rate-limiting step of the RAAS cascade. Inhibition of plasma renin-levels by both renin antibodies and synthetic renin inhibitors showed a significant decrease in plasma renin levels, AngI, AngII and aldosterone. This consequently produced a decrease in systolic blood pressure; however initial renin inhibitors required intra-venous administration. In 2007, an oral direct renin inhibitor (DRI) was developed (named aliskiren), which is an effective anti-hypertensive drug [80].

Beta-blocker therapy (e.g. propranolol) can also be used to block sympathetic (beta1)-mediated renin release by the kidney thereby lowering plasma renin and AngII levels[78]. In addition, this method has also shown a potential to prevent conversion of prorenin into mature renin. All in all, these therapies produced decreased blood pressure and are beneficial for treating hypertension.

ACE inhibitors (e.g. captopril) prevent the conversion of AngI into AngII, therefore reducing circulating and local levels of AngII as well as aldosterone, hence reducing blood pressure[78]. However, by blocking AngI to AngII conversion there is consequently an increase in renin release and AngI, which may progress AngII synthesis via different pathways. They are also thought to exert beneficial effects due to activation of the ACE2-Ang1-7-MAS1 axis. Despite this, ACE inhibitors remain the first-line therapy for patients with hypertension and heart failure, successfully managing blood pressure and left-ventricular hypertrophy (LVH).

Angiotensin receptor blockers (ARBs) prevent the binding of AngII to the AT_1R receptor (e.g. losartan) and hence limit the downstream effects of AngII. ARBs are used in a similar context to ACE inhibitors, to manage hypertension, heart failure and renal protection[84]. However blocking AngII binding to the AT_1R also prevents the negative feedback loop resulting in higher levels of AngII. Similar to ACE inhibitors, ARBs can activate the ACE2-Ang1-7-MAS1 axis potentially giving further beneficial effects[78,80].

These RAAS blockers discussed so far are all related to the traditional RAAS cascade, however as more components of the RAAS pathway are being identified further potential targets emerge[80].

1.5 Cardiac remodelling associated with hypertension

Cardiac remodelling is a process that involves modification of both cardiac structure and function. Processes involved in cardiac remodelling include cardiomyocyte hypertrophy, interstitial fibrosis, ventricular dilation, cell death and contractile dysfunction[42,75]. Although there are a number of causes with different aetiologies, that lead to cardiac remodelling, they all share similar pathways for molecular, biochemical and mechanical events[85]. Cardiac remodelling is thought to initiate as an adaptive mechanism compensating for stress or trauma in order to maintain stroke volume[75]. For instance cardiac hypertrophy allows a greater cardiac contraction per heartbeat, observed by fractional shortening, and hence increased volumes of blood ejected per heartbeat, determined by ejection fraction. Therefore higher blood pressures are managed due to initial cardiac remodelling. However, sustained haemodynamic overload progresses into a transition from compensatory cardiac changes to heart

failure[75,85]. This is characterised by left ventricular dilation, contractile dysfunction and impaired survival.

Ventricular dilation defines a process whereby the chambers of the heart become stretched and thinned, occurring mainly in response to pressure overload[86]. The specific events that lead from compensatory cardiac remodelling into a maladaptive state of ventricular dilation and heart failure require further investigation[86].

1.5.1 Hypertrophy

1.5.1.1 Hypertrophy basics and the cellular response

Cardiac hypertrophy denotes a thickening of the myocardium, which results in an increased chamber mass and wall thickness, often associated with a decreased chamber volume[87,88]. At the cellular level, it involves an increase in the volume of individual cardiomyocytes, enhanced protein synthesis and a higher organisation of the sarcomere[88]. Hypertrophy is regarded as a cardiac remodelling process to compensate for temporary increases in biomechanical stress[75,89].

Hypertrophy occurs in response to chronic exercise training or even pregnancy, and in these instances is described as physiological rather than pathological hypertrophy[89,90]. This type of hypertrophy occurs without interstitial fibrosis, apoptosis or cardiac dysfunction, usually associated with pathological hypertrophy[85,90]. Physiological hypertrophy is thought to be beneficial or even protective, rather than detrimental[85]. Therefore the differences between pathological and physiological hypertrophy are important to study in order to understand how pathological hypertrophy switches to a maladaptive process and progresses to heart failure[90]. Going forward specific processes involved in pathological hypertrophy only will be discussed.

Hypertrophies are further subdivided into concentric or eccentric hypertrophy depending on the initiating stimuli and the effect this has on cell shape[85,91]. Increases in relative wall thickness and cardiac mass but without changes in chamber volume denote concentric hypertrophy[91]. This is usually visualised by a parallel sarcomere addition pattern and hence an increase in cardiomyocyte width[85,91]. For example,

stimuli resulting in pressure overload, such as hypertension and aortic stenosis[90]. In comparison eccentric hypertrophy encompasses increases in cardiac mass with increased chamber volumes[85,91]. For example stimuli resulting in volume overload, such as aortic regurgitation and arteriovenous fistulas[90]. In this setting, sarcomeres are usually added in series leading to increased cardiomyocyte length[7, 90].

At the cellular level, cardiac tissue is composed mainly of cardiomyocytes (muscle cells), non-myocytes that include fibroblasts, endothelial cells, mast cells and VSMCs, and extracellular matrix, which surrounds these cells[90,92]. Proliferation of cardiomyocytes within mammalian hearts occurs up until birth, after this any cardiac growth results from increases in cardiomyocyte size[22]. Cardiomyocytes themselves are composed of myofibril bundles that contain myofilaments. These myofilaments consist of sarcomeres, which are the main contractile unit of the muscle[22]. The left ventricle is composed of cardiomyocytes that are arranged in a circular and spiral orientation[22]. To ensure a normal heart rhythm cardiomyocytes need to contract simultaneously, hence cellular coordination is important. Cell-to-cell adhesion is maintained by intercalated discs at the bipolar ends of cardiomyocytes[22]. This allows the synchronicity of contractile force between adjacent cardiomyocytes.

Hypertrophy involves the activation of a highly complex web of intracellular signalling pathways that activate gene expression, promote protein synthesis and stability, in turn leading to an increase in cardiomyocyte size, as shown in *Figure 1-10*[88,90]. Pathological hypertrophy is associated with elevated levels of AngII, catecholamines and endothelin-1 (ET-1) and their subsequent effects are elicited from GPCR signalling[93,94]. In addition to this, pathological hypertrophy has also been associated with abnormalities leading to enhanced PI3K, mitogen activated protein kinases (MAPKs), protein kinase C (PKC) and D (PKD), and calcineurin[85,93].

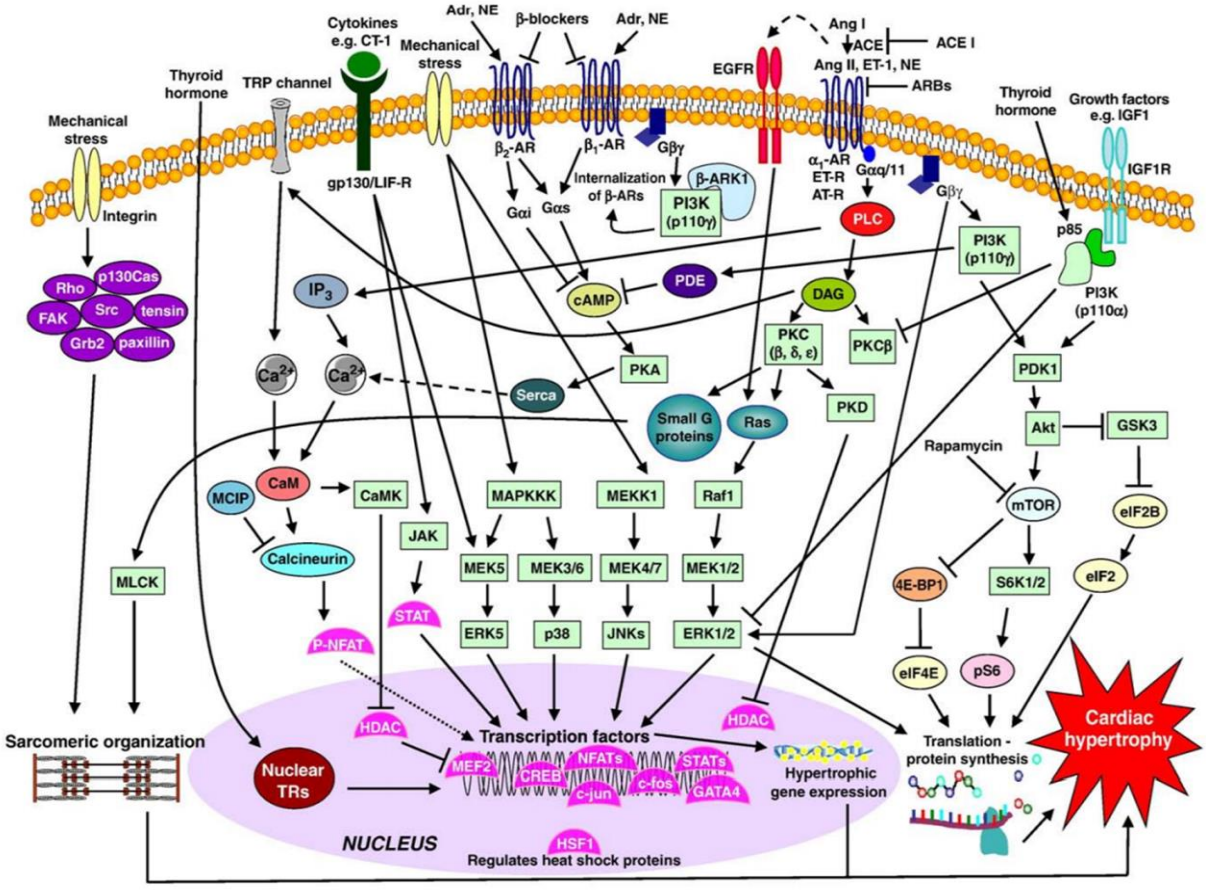

Figure 1-10: Intracellular signal-transduction pathways mediating the cardiac hypertrophic response. *From Bernardo et al, 2010*[90].

1.5.2 Interstitial Fibrosis

Most cardiac diseases are associated with interstitial fibrosis, which contributes to the progression of heart failure. Over-activation of fibroblasts, in response to specific stressors such as hypertension, causes an increase in collagen secretion[42,75]. Secreted collagen occupies the space between cardiomyocytes causing increased myocardial stiffness, impaired cardiac diastolic function and potentiates cardiac arrhythmias. Therefore fibrosis is a key component of cardiac remodelling.

There are two distinct stages of fibrosis, initial reactive interstitial fibrosis and replacement fibrosis[95]. Reactive fibrosis is a mechanism that occurs in response to cardiac stressors, such as hypertension, whereas replacement fibrosis is a response to cardiomyocyte cell death[95]. Here, fibrosis maintains tissue structure by replacing cardiomyocytes, which have undergone apoptosis. Cell types involved in the

development of fibrosis include; fibroblasts, cardiomyocytes, inflammatory cells, endothelial cells and other circulating cells[4,42]. Cardiomyocyte hypertrophy, as described in section 1.5.1, is determined solely by the growth of cardiomyocytes, this can also be accompanied by growth of non-cardiomyocytes and interactions in tissue structure, distorting organ architecture and function[92,95].

1.5.2.1 Basic development and cellular responses resulting in fibrosis

Cardiac fibroblasts play an important role in maintaining normal cardiac function. In healthy cardiac tissue the extracellular matrix (ECM) forms a network that surrounds and interconnects cells providing a 3D structure for myocytes and other cells within the heart[96]. This not only provides a scaffold, maintaining structural integrity of the tissue, but also allows distribution of mechanical forces through the myocardium in a cell-to-cell manner[96]. Fibroblasts, derived from mesenchymal origins, are the main cellular component implicated in synthesis and deposition of the ECM; they also have the ability to interact on a cell-to-cell basis with other fibroblasts, myocytes and endothelial cells[95]. They thereby take a regulatory standing, ensuring the appropriate response is mediated, to changes in chemical, mechanical and electrical signals in the heart[96]. Fibroblasts themselves are flat, spindle-shaped connective tissue cells that lack a basement membrane[96]. They have the ability to produce a variety of ECM components including collagen and fibronectin in addition to cytokine and growth factor secretion, (*Figure 1-11*).

Tissue fibrosis arises when the normal regulation of wound healing fails. Therefore in addition to their tissue-homeostatic function, fibroblasts also contribute to cardiac remodelling. It is the complex interaction of pro-fibrotic and anti-fibrotic cytokines and secreted proteins that regulate the appropriate response. Research has demonstrated phenotypic heterogeneity among fibroblasts. In particular a modified form of the fibroblast, specific to wound-sites, termed myofibroblasts have the ability to express α-smooth muscle actin (α-SMA) and an enhanced ability to contract ECM, which is necessary for wound closure[96]. These cells secrete other specific growth factors and cytokines that are vital for their roles in growth, development, fibrosis and the repair of numerous tissue types. The differentiation from a fibroblast into a myofibroblast is

promoted by TGFβ, cytokines, the surrounding ECM and other growth factors. Other origins for fibroblasts include endothelial cells, by endothelial-mesenchymal transition, or from bone marrow-derived circulating progenitor cells, monocytes and fibrocytes[95,97].

Fibroblasts have the ability to sense changes in the microenvironment and elicit an appropriate response to preserve organ function. After injury, synthesis of new connective tissue involves activated fibroblasts with the ability to proliferate and migrate around the wound[98]. In this setting, synthesis of new ECM proteins such as collagen and fibronectin occurs[98]. One such response occurs due to pathological stimuli, such as hypertension[99]. In addition, matrix metalloproteinases (MMPs), that are required for collagen degradation, are greatly upregulated by fibroblasts[99]. This causes excessive ECM degradation, which has a knock-on effect for cardiac function. During the process of cardiac injury, fibroblasts are influenced by a number of different factors that alter their gene expression. Fibroblast activation and differentiation into a myofibroblast is heavily upregulated within this pathological setting. This in turn is associated with increased secretion of fibronectin and fibrillary type collagens I and III.

As pathological remodelling continues, further increases in cytokines and growth factors stimulate myofibroblast proliferation, migration and remodelling of the cardiac insterstitium[99]. In addition, activated fibroblasts may have a direct influence on cardiomyocyte hypertrophy by paracrine mechanisms, hence further contributing to impaired cardiac function. The abundance of myofibroblasts present during fibrosis contributes heavily to excessive tissue scarring observed in fibrotic disease. At the same time cardiac fibroblasts also secrete increased levels of growth factors and cytokines including IL-1β, IL-6 and TNF-α, which in turn activate MMPs stimulating further cardiac remodelling[99].

Similar to the hypertrophic response, initial stages of fibrosis are beneficial and critical for tissue-repair. As this process continues, it becomes maladaptive leading to interstitial fibrosis, increased mechanical stiffness and hence reduced cardiac function. Although cardiac fibroblasts are non-excitable cells, their coupling to myocytes allows electrical signal transduction, giving a uniform tissue response. However in the setting of fibrosis, excessive levels of collagen provide an insulating layer separating cardiomyocytes. This in turn disrupts their electrical-coupling, preventing synchronicity

of electrical signals and hence increasing the risks of arrhythmias. Cardiac fibroblasts also have the ability to induce or inhibit angiogenesis; however their distinct mechanism here requires further investigation.

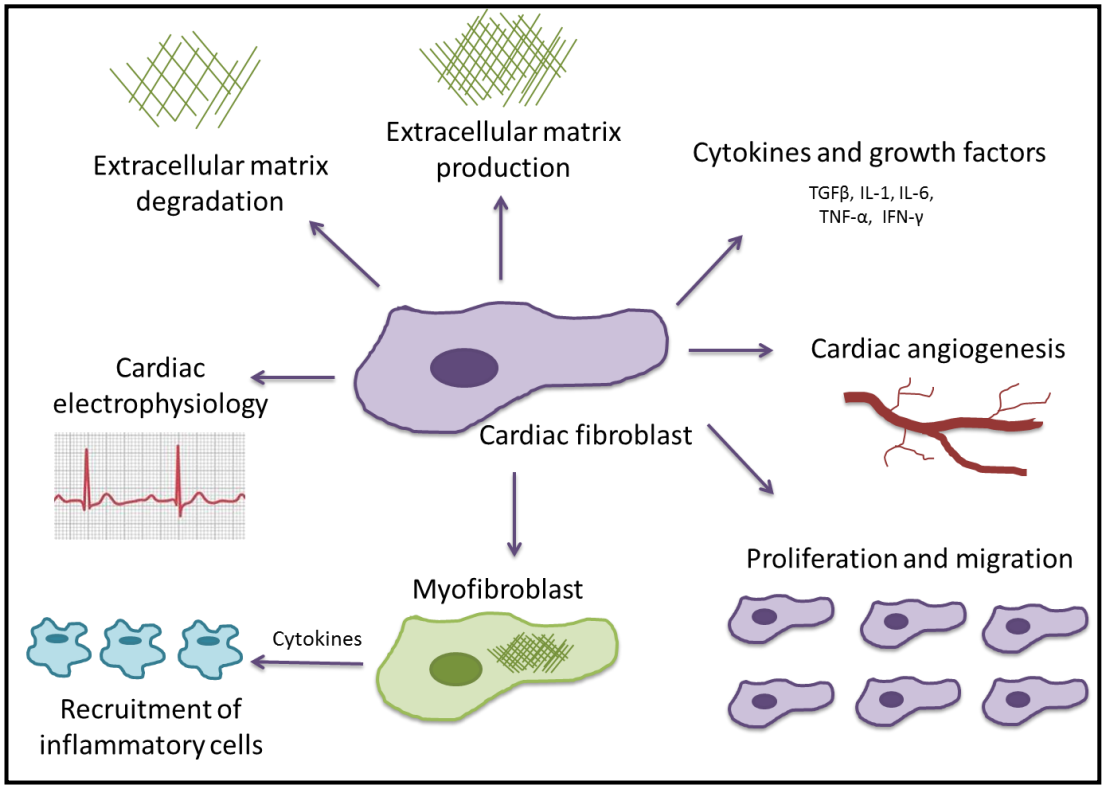

Figure 1-11: Functions of cardiac fibroblasts. *Adapted from Krenning et al 2010 and Souders et al 2009*[95,99].

1.5.2.2 Signalling pathways involved in fibrosis development

Within healthy cardiac tissue the ECM is synthesised and degraded by cardiac fibroblasts in a coordinated, regulatory manner. However during heart failure there is a disruption of these regulatory pathways, which result in an imbalance of ECM synthesis and degradation. This is thought to account for the severity of cardiac remodelling and hence this section is concentrating on understanding these specific signalling processes. A number of different growth factors, cytokines and hormones are responsible for the fibrotic response. These include TGFβ, connective tissue growth factor (CTGF); platelet derived growth factor (PDGF), AngII and ET-1[96].

TGFβ is the main factor promoting the fibrotic response. There are three TGFβ ligands (TGFβ-1, -2 and -3), of which TGFβ-1 mechanisms are the most clarified[96,100]. TGFβ-1 is upregulated in normal tissue repair in addition to the progression of pathological fibrosis. Upon activation, TGFβ binds to a heteromeric receptor consisting of one TGFβ type I, and one TGFβ type II receptor, both of which possess tyrosine kinase activity. TGFβ type I is also known as activin-linked kinase (ALK) -5 within fibroblasts, whose signalling is mediated by the Smad family of transcriptional activators[96]. For instance Smad-3 enables procollagen type III, tenascin-C, collagen lattice contraction and α-SMA expression. ALK-5 inhibitors, developed as a potential anti-fibrotic agent, allow decreased TGFβ activity, reduced fibrosis and collagen messenger ribonucleic acid (mRNA) expression in a model of myocardial fibrosis *in vivo*[96]. However this was associated with an increased inflammatory response and did not have any benefits on myocyte hypertrophy, blood pressure or systolic function.

TGFβ also has the ability to activate other signalling pathways, such as MAPK pathways, which allows modification of gene expression and hence contributes to cardiac fibrosis. In addition this MAPK signalling can link back into the TGFβ/Smad signalling cascade to enable a regulatory feedback mechanism[96]. Upregulation of ECM and the tissue inhibitors of matrix metalloproteinases (TIMP) gene expression by TGFβ promote ECM deposition. This in conjunction with the suppression of MMP gene expression, and promotion of fibroblast to myofibroblast differentiation, allows TGFβ to stimulate fibrosis in response to pathological stimuli. Hence this interplay between MAPK and Smad signalling pathways mediate and control ECM expression[98].

Several proteins downstream of TGFβ are required to enhance the cellular response and hence prolong the wound healing process. These can either prolong the contractile response of fibroblasts, closing wound-sites, or to prolong ECM production. Such proteins include CTGF and the ED-A form of fibronectin[101]. CTGF is a protein that is upregulated in fibroblasts in response to TGFβ, promoting fibroblast proliferation, ECM production (including collagen and fibronectin), adhesion, migration and granulation tissue formation. CTGF is also thought to help TGFβ to bind to its receptors when at lower concentrations. Taken together, CTGF is implicated in the TGFβ-driven fibrotic response however the specific signalling process involved remains to be elucidated. In addition, recent published data has questioned the role of this factor as

a mediator of the pro-fibrotic response. A conditional CTGF-knock out (KO) mouse subjected to transverse aortic constriction (TAC), a model of chronic pressure overload, maintained a normal hypertrophic and fibrotic phenotype[102].

Counteractive responses are also present to dampen down the fibrotic process, mediated by cytokines such as TNF-α and IFN-γ. TNF-α is a pro-inflammatory cytokine that is produced by macrophages during the wound healing process. In addition, TNF-α has an anti-fibrotic phenotype with the ability to suppress ECM expression and the TGFβ induction of collagen and CTGF. Similarly IFN-γ possesses anti-fibrotic responses, it is a cytokine produced mainly by T-cells and NK cells, which orchestrates responses by the Janus kinase (JAK)-STAT pathway.

PDGF encompasses a family of homodimeric or heterodimeric growth factors (e.g. PDGF-A, -B, -C and –D). PDGF-A and –D are increased in endothelial cells, macrophages and fibroblasts after cardiac injury, which is also associated with cardiac responses such as angiogenesis, inflammation and fibrosis. In terms of fibrosis, PDGF is thought to act via elevating TGFβ levels, thereby contributing to the remodelling process.

Hormonal stimuli also have the ability to affect the progression of fibrosis. As described previously, AngII is increased in response to cardiac stress. AngII can be expressed and activated by both macrophages and myofibroblasts in the setting of pathological cardiac remodelling. By binding to the AT_1R, AngII can induce TGFβ-1 expression and in turn TGFβ is required for AngII to induce both cardiac hypertrophy and fibrosis. AngII induces collagen expression by the TGFβ/Smad3 pathway and via IL-6 mechanisms, which potentially involve NF-kB activation. ET-1 can also be stimulated in response to cardiac stress, or even induced by AngII. ET-1 activates the endothelin -A (ETA) and –B (ETB) receptors and is mainly produced by endothelial cells but can also be produced by cardiomyocytes, fibroblasts and macrophages. Responses instigated by the ETA receptor include decreased DNA synthesis and collagen production in fibroblasts.

Another aspect that is vital in the response to cardiac stress and the resultant remodelling process are ROS. A number of signalling pathways involved in cardiac remodelling consist of redox sensitive proteins, suggesting that ROS are implicated in the activation and regulation of theses response cascades[103].

1.5.3 Apoptosis

1.5.3.1 General implications of apoptosis

Another key component in cardiac remodelling is the loss of cardiomyocytes, which is a progressive mechanism leading to the development of heart failure[104]. Cardiomyocyte death can occur by two means; necrosis, the premature death of a cell due to injury or toxicity, or by apoptosis, a programmed cell death mechanism[105,106]. Apoptosis is an evolutionarily conserved suicide process, that occurs when regulated biochemical changes within the cell leads to alterations in cell morphology and eventually cell death[105,106]. Characteristic morphological changes include nucleosomal DNA fragmentation and cell shrinkage, without the loss of membrane integrity[107]. Apoptosis plays critical roles in homeostasis, remodelling, surveillance and host defences[106]. Both internal and external stimuli enable the removal of cells that are damaged, genetically unstable or were inappropriately produced during development[107]. Therefore apoptosis is involved in essential biological processes; however dysregulation of apoptosis has been implicated in cardiac remodelling and heart failure[106]. For instance, as adult cardiomyocytes cannot self-renew after injury the loss of cardiomyocytes due to apoptosis potentially influence cardiac structure and function[107].

1.6 Pathological role of Nox2 in cardiac remodelling

Nox proteins are major sources of ROS within the cardiovascular system and the expression of different Nox isoforms is very complex, not only within different cell types but in different regions of the vascular system. Nox2 is expressed in cardiomyocytes, endothelial cells, VSMCs and adventitial fibroblasts. Nox2-dependent ROS is capable of modulating intracellular signalling pathways, which lead to cardiac hypertrophy, fibrosis, apoptosis and contractile dysfunction (*Figure 1-12*)[42]. The intricate pathways leading to development of these maladaptive changes were previously described in section 1.5, here we look at how these pathways can be altered by Nox2-dependent ROS, hence demonstrating the integral role of Nox2 in the cardiac remodelling process.

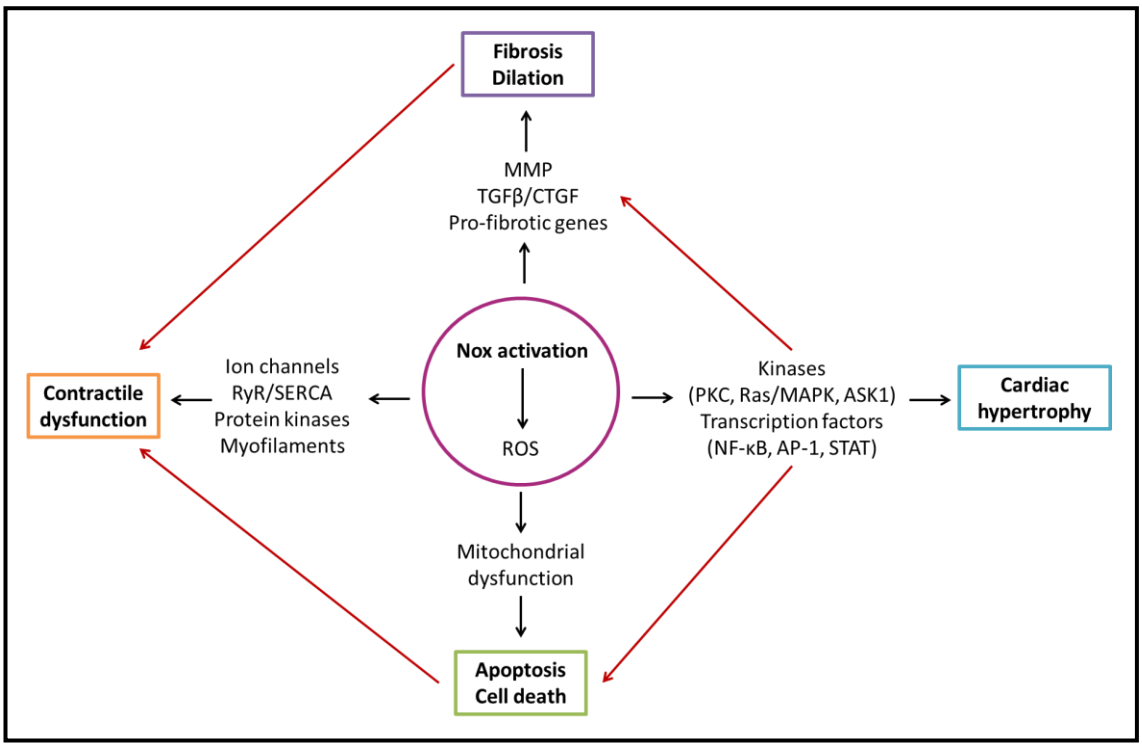

Figure 1-12: Nox2-derived ROS involvement in cardiovascular remodelling. *Adapted from Nabeebaccus et al. 2011, illustrating the main signalling complexes involved in cardiac remodelling*[42].

Nox2 activation is implicated in cardiomyocyte hypertrophy induced by GPCR, such as AngII and α1-adrenoreceptor agonists[4,42]. Nox2KO mice treated with a subpressor dose of AngII show less LVH compared to WT controls, which is confirmed further by a lower increase in molecular markers for hypertrophy[108]. Furthermore, NADPH oxidase activity increases during AngII treatment whereas in the Nox2KO this response is inhibited, suggesting a role for Nox2 within this setting[3]. Mice deficient in ACE2 exhibit exaggerated pressure-overload-induced hypertrophy, however when generated on a $p47^{phox-/-}$ background the level of hypertrophy improves[109]. Nox2 is implicated in a number of different signalling pathways resulting in cardiac hypertrophy (*Figure 1-13*), such as Ca^{2+}, MAPK and protein kinase signalling.

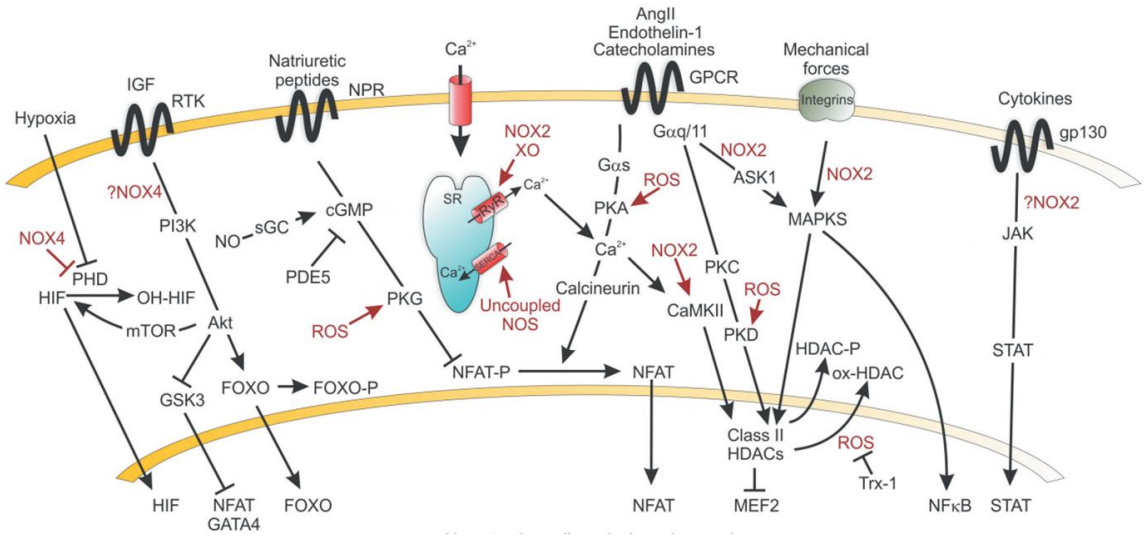

Figure 1-13: Redox -modulated cardiac hypertrophy signalling cascades. *Burgoyne et al 2012*[4].

Most cell types involved in the development of fibrosis express Nox2; fibroblasts, cardiomyocytes, inflammatory cells, endothelial cells and other circulating cells[4,42]. Global Nox2KO mice treated with a sub-pressor/pressor dose of AngII or aldosterone infusion, to induce cardiac remodelling, show a significant decrease in interstitial fibrosis when compared to WT controls[4,42]. Similarly mice globally deficient in proteins tightly linked to Nox2, $Rac^{-/-}$ and apoptosis signal-regulating kinase 1 $(ASK1)^{-/-}$, also show a significant decrease in interstitial fibrosis[4,42,110,111]. In a number of cases where Nox2-dependent ROS production is reduced in mice, interstitial fibrosis is concomitantly reduced. In contrast, the level of hypertrophy remains similar to the WT controls, implying distinct signalling pathways leading to these two processes involved in remodelling[4,42].

Cardiomyocyte apoptosis is an important element in the development of fibrosis, contractile dysfunction and the progression to heart failure. Nox, more specifically Nox2, have been associated with apoptosis in different settings of AngII- and aldosterone-induced cardiomyopathy[4,87]. Potentially, ASK-1 and P38MAPK reduction of B-cell lymphoma 2 (Bcl2), and induction in Blc2 associated X protein (Bax) and caspase-3, plays a role in mediating Nox-dependent apoptosis in the setting of aldosterone and AngII infusion respectively[4,87].

ROS can also modulate proteins involved in ECC, such as RyR2 and Ca^{2+}/Calmodulin-dependent protein kinase II (CAMKII)[87]. It appears that Nox2-dependent CaMKII oxidation causes apoptosis of sinoatrial (SA) cells in a mouse model of AngII infusion. The exact role of Nox2 in AngII-related cardiac dysfunction still needs further clarification.

Nox2 has also been implicated in AngII-specific cardiovascular remodelling, which is discussed in more detail in section 1.8. In addition to Nox2, inflammation has also been linked to cardiovascular disease (CVD) and may play a pertinent role in the associated remodelling process.

1.7 Inflammatory response in cardiovascular remodelling

The inflammatory response plays a major role in the progression of CVD. Within the heart, an immune-mediated response provides a short-term adaptation to stress in an attempt to ultimately restore tissue homeostasis and cardiovascular function. However, if these abnormal conditions are sustained and inflammation progresses this can contribute further to myocardial damage leading to progressive LV dysfunction and remodelling[112].

Immune responses in cardiac tissue are initiated by pathogen-associated molecular patterns (PAMPs) or damage-associated molecular patterns (DAMPs), which are both detected by pattern recognition receptors (PRRs). PAMPs arise from foreign material such as glycolipids from mycobacterium or double-stranded ribonucleic acid (dsRNA) from viruses. In comparison DAMPs arise from endogenous host material that can be released by injured or dying myocardial cells. Upon recognition of PAMPs and DAMPs, PRRs stimulate signalling cascades that in turn activate NF-κB, activator protein-1 (AP-1) and interferon regulatory factor (IRF) transcription factors[112]. These enable the modulation of target genes that encode pro-inflammatory cytokines and interferons within the heart. Hence kick starting an innate immune response, further discussed in section 1.3.

Activation of neurohormonal systems such as the RAAS is sufficient in triggering cardiac inflammation, and the associated pro-inflammatory cytokines have an

extensive role in the pathophysiological response[113]. Inflammatory mediators, which are upregulated in this setting, are instigated in several cardiovascular remodelling processes including hypertrophy, fibrosis and apoptosis[114]. There is a complex, cell-specific response to numerous pro-inflammatory cytokines by cardiomyocytes, fibroblasts and inflammatory cells (*Figure 1-14*); such cytokines include TGFβ, TNF-α, IL-1β and IL-6[115]. The concentration of these cytokines within patients with heart failure has been found to correlate to disease severity, and hence may play a role in disease progression[116]. However the complexity of ascertaining the source and target of these cytokines is increased by the temporal changes in the inflammatory response to cardiovascular injury[115].

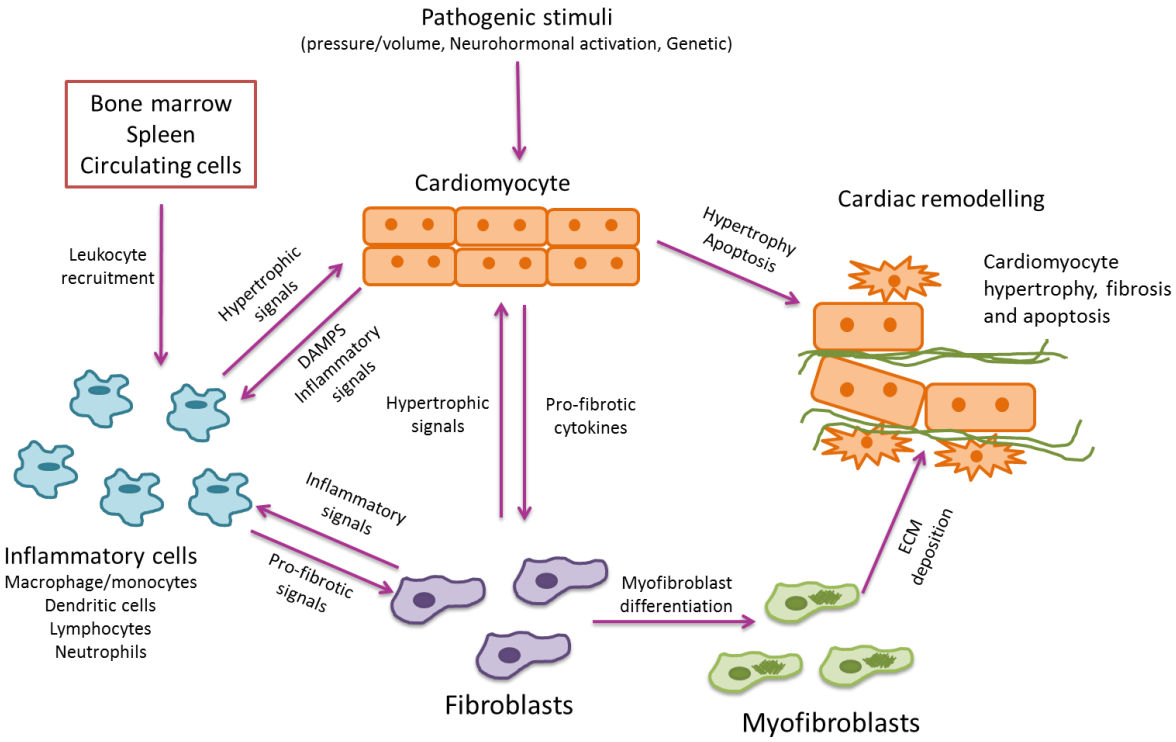

Figure 1-14: Interactions between cardiomyocyte and non-cardiomyocytes during cardiac remodelling. *Adapted from Frieler et al 2015[115].*

TGF-β is a major pro-fibrotic cytokine that is heavily upregulated in hypertrophied and fibrotic hearts resulting from hypertension[115]. With the ability to modulate a range of responses in cardiomyocytes, immune cells and fibroblasts; TGF-β signalling pathways are context dependent[115]. Previous research demonstrates that overexpression of TGF-

β is sufficient to induce cardiac hypertrophy and fibrosis[117]. Similarly inhibition of TGF-β signalling and TGF-β KO models demonstrate reduced levels of fibrosis and prevent cardiac dysfunction[118,119].

Previous studies investigating TNF-α in relation to pressure overload-induced cardiac remodelling have highlighted its importance in this setting[120]. An *in vivo* study increasing the systemic level of TNF-α, to that found during heart failure, showed that this resulted in cardiac dysfunction[121]. Furthermore, the overexpression of cardiac-specific TNF-α leads to the progression of cardiac hypertrophy and fibrosis[122]. This was further confirmed by a TNF-α KO model that prevented cardiac hypertrophy, fibrosis and dysfunction in response to pressure-overload[120].

Pressure-overload induced cardiac hypertrophy and dysfunction is blunted in IL-1β deficient mice, highlighting a role in cardiac remodelling[123]. Furthermore, healthy mice treated with IL-1β induced cardiac dysfunction and reduced exercise tolerance[124]. An IL-1 receptor agonist (anakinra) also confirms the pathological properties of IL-1β, by producing beneficial responses in terms of cardiovascular remodelling and exercise tolerance[125,126].

During hypertension levels of IL-6 tend to increase, however it also has a direct role in associated cardiovascular remodelling[127]. Rats infused with IL-6 for a week displayed cardiac hypertrophy, fibrosis and dysfunction[127]. In addition IL-6 KO models have been shown to prevent AngII-induced cardiac remodelling and associated signalling pathways[128,129]. However, similar studies using pressure overload, show no differences in IL-6KO models in terms of hypertrophy and fibrosis[115]. Therefore the specificity of IL-6 signalling is yet to be ascertained[115].

As described above, the inflammatory response is a key process for the progression of CVD, here we have focused on inflammatory signalling however the immune cell activation and prevalence are also implicated within this setting and are discussed later.

1.8 Nox2 and inflammation in AngII-induced hypertension

The individual impacts of Nox2 and inflammation on CVD have been discussed in sections 1.6 and 1.7. However there are also collaborative effects that aid the progression of cardiovascular remodelling.

There is a key role for Nox in the ROS-dependent increase in blood pressure, suggesting its implication in hypertensive signalling. The RAAS plays a vital homeostatic role in maintaining blood volume and systemic vascular resistance (section 1.4), thereby influencing cardiac and vascular function, as illustrated in *Figure 1-9*. In order to prevent tissue damage and initiate the healing process, in response to stress, the immune system mediates an inflammatory response. Initial inflammation involves activation of tissue resident immune cells, such as macrophages, leading to the release of inflammatory mediators. These in turn cause vasodilation and increased permeability of blood vessels to enable leukocytes, such as T-cells, to migrate into the tissue and aid the inflammatory response[130].

Inflammation is potentially implicated in hypertension as summarised in *Figure 1-15*. A number of different research groups have highlighted the presence of inflammatory immune cells and cytokines within this setting. AngII and other components of RAAS are able to stimulate Nox and the production of ROS. ROS in turn activate pro-inflammatory transcription factors such as Nrf2, NF-κB and AP-1, enabling the expression of adhesion molecules and chemokines[131,132]. In addition, oxidative stress or injury can trigger inflammation by oxidising lipoproteins that can interact with toll-like receptors (TLRs); initiating a number of inflammatory responses[131]. A variety of inflammatory cells also express Nox[133], potentially adding to hypertension by increasing ROS levels further. Moreover, ROS may mediate signalling within immune cells and therefore influence their phenotype within this setting; this is discussed in more detail later. Furthermore, ROS contribute to hypertension directly by inducing vasoconstriction, enhancing water and Na^{2+} retention within kidneys and encouraging sympathetic outflow from the central nervous system (CNS)[131].

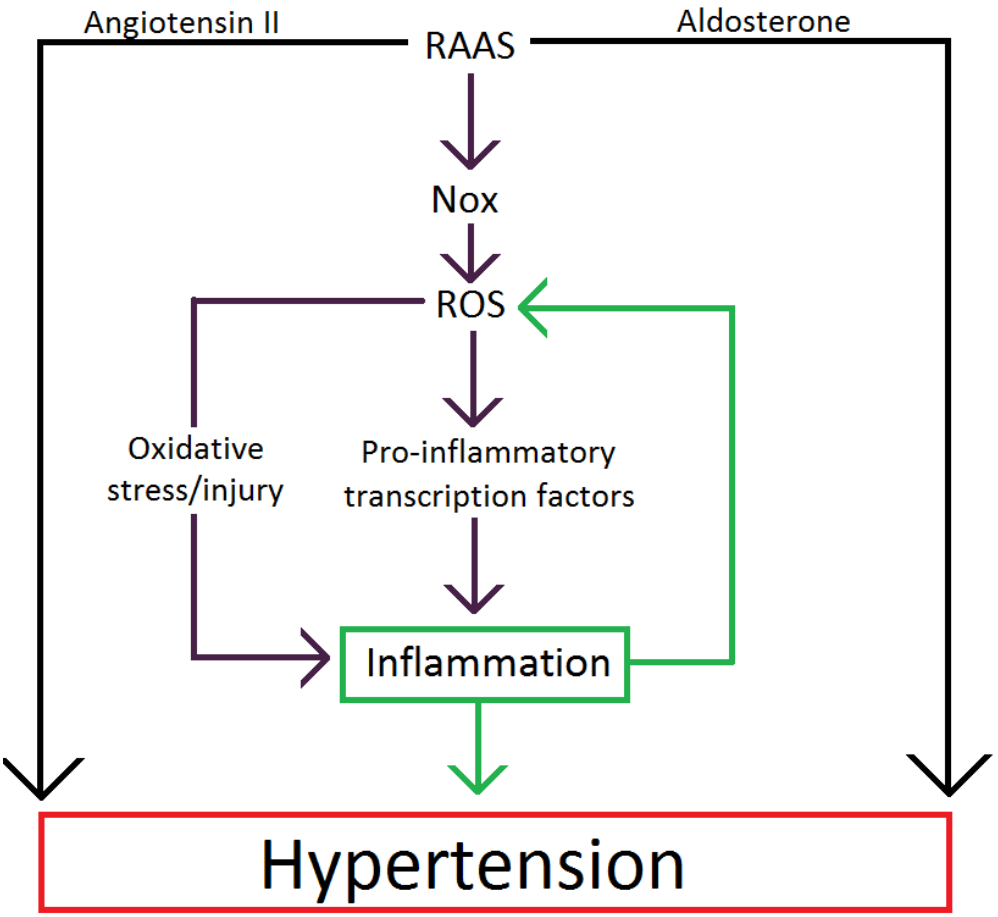

Figure 1-15: Role of Nox-dependent ROS in angiotensin II induced hypertension. *Adapted from Harrison et al*[131].

The involvement of T-cell Nox2 in the setting of AngII-induced hypertension has also been highlighted by Guzik et al[134]. T-cells express Nox2, which is essential for full development of AngII-induced hypertension[133,134]. Recombination-activating gene $(RAG)^{-/-}$ mice, which lack T- and B-cells, showed a blunted response to AngII in terms of hypertension. Furthermore, the adoptive transfer of T- (but not B-) cells was able to restore this response[134]. Adoptive transfer of T-cells lacking $p47^{phox}$, an essential Nox2 subunit were only partially able to restore the expected AngII-induced phenotype. Moreover, mice globally lacking $p47^{phox}$ eliminated the recruitment, activation and infiltration of T-cells within the aorta in response to AngII[134]. Infusion with AngII in C57Bl/6 mice increased expression of T-cell Nox2 subunits whilst enhancing $O_2^{\bullet-}$ production[134]. AngII activation of T-cells was verified *in vitro* where apocynin, an NADPH oxidase inhibitor blunted this effect[134].

Nox2 may therefore have an important endogenous role in T-cells but has also been implicated in the development of blood pressure and inflammation by Lob et al[135]. Specific deletion of $p22^{phox}$, a vital Nox subunit, in the subfornical organ (SFO) in the brain prevented inflammation and decreased accumulation of ROS within this region in AngII treated mice[135]. $p22^{phox}$ is vital for both Nox2 and Nox4 activation, which have been shown to orchestrate opposing responses *in vivo*. Hence this research highlights the general role of Nox in the SFO, but not individual functions and effects in response to AngII infusion.

AngII is primarily involved in the inflammatory response during hypertension by modulating different pro-inflammatory transcription factors and chemokines[132]. AngII-dependent activation of Nox2 is well recognised to be an important contributor to many AngII responses[136].

1.9 Research aim and objectives

As described above, Nox2 and inflammation have separately been identified to have an important role in the pathophysiology of AngII-induced cardiovascular remodelling. Furthermore, T-cell Nox2 within this setting has previously been implicated in the generation of vascular remodelling. However, the specific role of T-cell Nox2 and specific T-cell subtypes in the cardiovascular response to AngII requires further investigation.

Therefore the aim of this thesis was to identify the role of T-cell Nox2 and its capacity to regulate cardiovascular remodelling in the setting of increased RAAS activation.

In order to achieve our aim, our objectives were to:

1. Determine the pattern of T-cell infiltration in the heart during RAAS activation.
2. Investigate the role of Nox2 in AngII-induced infiltration of T-cells into cardiovascular tissues.
3. Analyse the specific role of Nox2 in regulatory T-cell function.
4. Develop a novel *in vivo* mouse model of $CD4^+$ T-cell-specific Nox2 knockout and study the response to chronic RAAS activation.

Chapter 2: General Materials and Methods

2.1 Animal husbandry

All mice were housed and maintained in a designated facility in accordance with the Code of Practice for the Housing and Care of Animals Used in Scientific Procedures issued by the UK Home Office. Up to 6 mice were housed per cage with unlimited access to food and water with 12 hours of light/day. All animal procedures were performed in accordance with the Guidance on the Operation of the Animals (Scientific Procedures) Act, 1986 (UK Home Office) and local institutional guidelines.

2.2 Murine models

Male mice aged 6-8 weeks were used for all experiments. C57Bl/6 mice were purchased from Harlan UK Limited and both global Nox2KO and CD4-Nox2KO mice were bred at our institution as described in sections 4.3 and 6.3 respectively.

2.3 Angiotensin II infusion model

Subcutaneous mini-osmotic pumps (Alzet® Micro-osmotic pump, model 1002) containing a pressor dose (1.1mg/kg/day) of AngII were implanted into mice. Treatment continued up to 14-days, as illustrated in *Figure 2-1*.

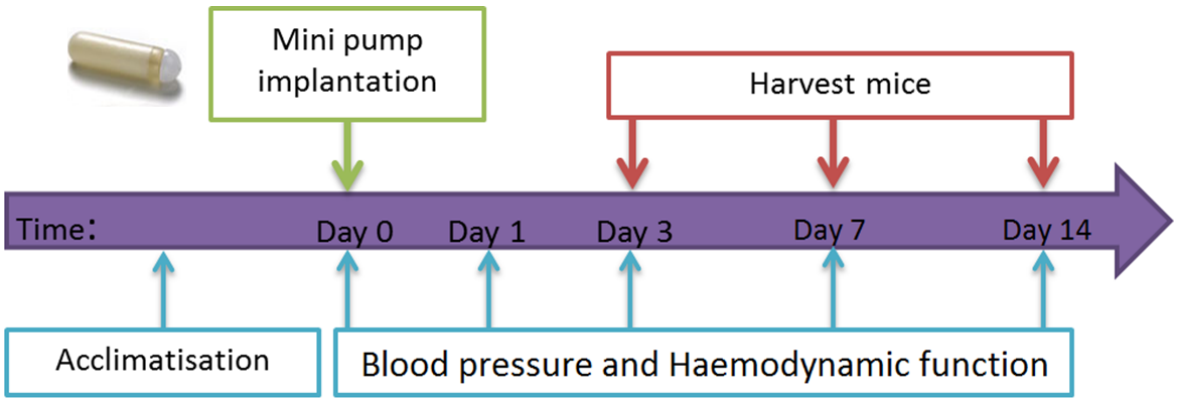

Figure 2-1: Experimental design.

Mini-osmotic pumps were prepared as per the manufacturer's instructions (*Figure 2-2*) and pumps were weighed before and after being filled to ensure correct loading. The concentration of AngII (CAngII) used to fill the mini-osmotic pump was calculated using the following equation:

$$CAngII\ (\mu g/\mu l) = \frac{Desired\ dose\ (\mu g/kg/hr) x\ mW(kg)}{MPR\ (\mu l/hr)}$$

Where the desired dose was 45.83µg/kg/hr (1.1mg/kg/day), the mean pump rate (MPR) was 0.25±0.05µL/hr and the mouse weight (mW) was determined on the day of surgery. The MPR is calculated by the manufacturer during performance tests, using the following calculation:

$$K = Q\ x\ C$$

Here, 'K' is the mass delivery rate (µg/hr), 'Q' is the volume delivery rate (µL/hr) and 'C' is the concentration (µg/µL) of the agent in the vehicle. Finally, the maximum amount of time the drug will defuse for is calculated using:

$$D = \frac{V}{Q}$$

Where 'D' is the duration (hrs), 'V' is the reservoir volume (µL) of the mini-osmotic pump and 'Q' is the pumping rate (µL/hr). Therefore based on the mean fill volume of 110.7µL, and a MPR of 0.25µL/hr, the maximum amount of time the drug will defuse for is 442.8 hours (18.5 days). As shown in *Figure 2-1* mini-osmotic pumps were removed prior to the maximum time limit, after 14-days of infusion.

With the mini-osmotic pump held in an upright position, a 1mL syringe was used to inject the solution into the top of the mini pump, ensuring the pump reservoir was full and all air had been displaced (*Figure 2-2*B). Finally the flow modulator was inserted to displace any remaining trapped air and prevent leakage (*Figure 2-2*C). Mini-osmotic pumps were then kept in sterile saline until surgical implantation. Animals from the sham group were implanted with empty mini-osmotic pumps.

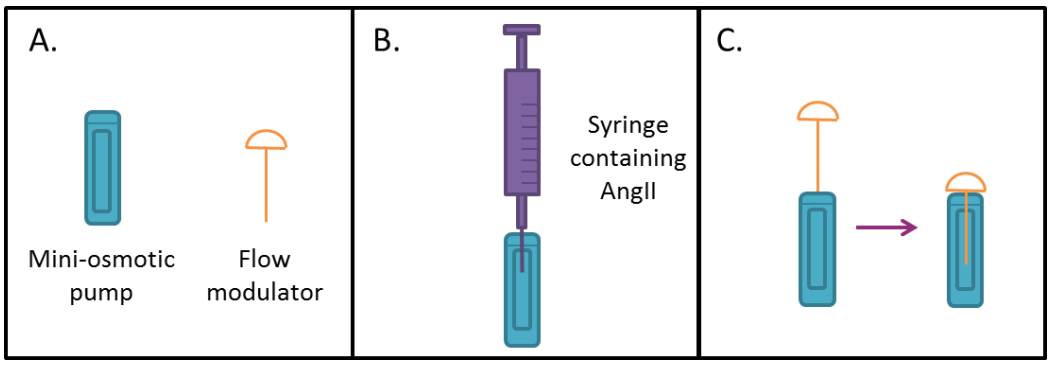

Figure 2-2: Mini-osmotic pump filling procedure.

Mice were anaesthetised using 2% isoflurane in medical O_2 at 2L/minute, and then anaesthesia was maintained at this concentration using a nose cone. Fur was removed from the surgical area using an electric razor (Wella) and the area was cleaned with iodine and chlorhexidine (Vetasept). Abolition of the toe pinch reflex was used to confirm deep anaesthesia, 1U vetergesic (0.03mg/mL, buprenorphine) and 5U finadyne (1mg/mL, flunixin meglumine) were administered, by subcutaneous and intramuscular injections respectively, to provide long-lasting analgesia. An incision was then made at the top of the mouse dorsum in line with the scapula using surgical scissors (*Figure 2-3*). The skin plane and muscle plane were separated by blunt dissection with surgical scissors to create a subcutaneous pocket into which the mini-osmotic pump was inserted. The incision was closed using 5.0 polyglactin coated vicryl sutures (W9442, Ethicon®). Mice were closely monitored for 3-days post-surgery to ensure recovery.

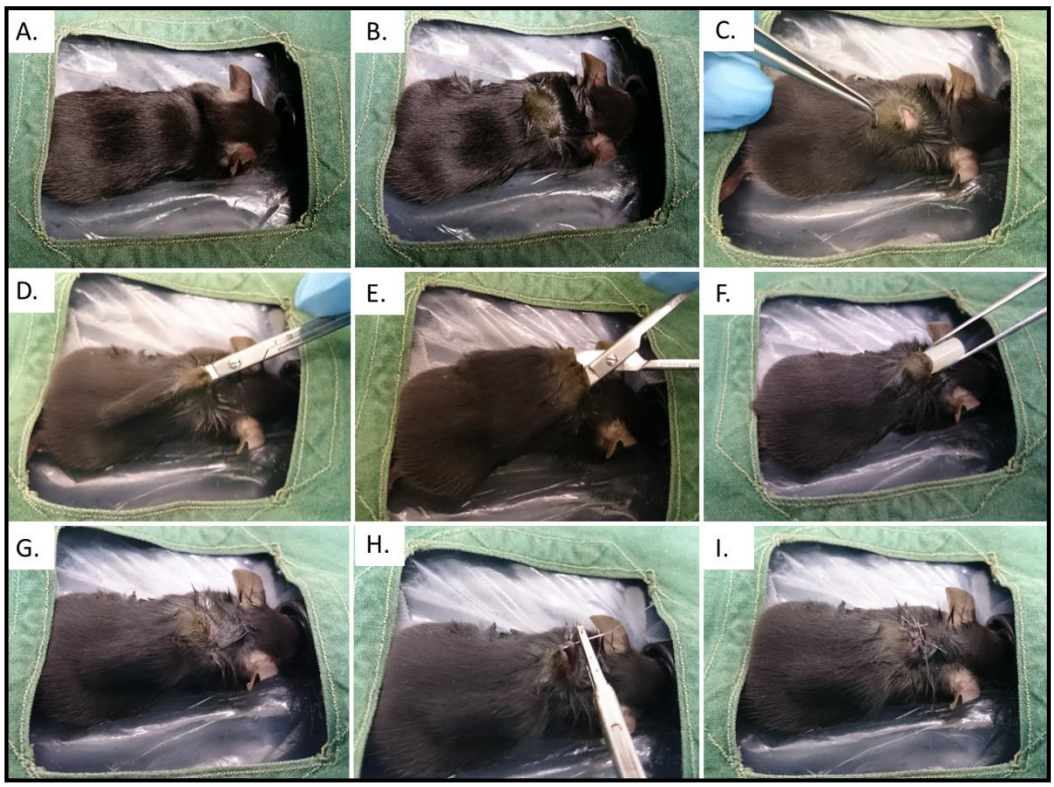

Figure 2-3: Surgical implantation of subcutaneous mini-osmotic pumps. (A) *Maintain anaesthetic using a nose cone,* ***(B)*** *fur is removed and area cleaned and* ***(C)*** *a small incision made at the top of the mouse dorsum.* ***(D&E)*** *A subcutaneous pocket is then made and* ***(F&G)*** *the mini-osmotic pump is inserted. Finally,* ***(H&I)*** *the incision is sutured to close the wound.*

2.4 Harvesting organs

2.4.1 Histology

Animals were submitted to terminal anaesthesia (3% isoflurane in 2L/minute of O_2) and culled by cardiac arrest in diastole induced by injection of 0.5% potassium chloride (KCl) directly in the LV and, followed by excision of the heart. The LV was then dissected as shown in *Figure 2-4* and treated as described in section 2.8 for cryosections and paraffin sections. Heart samples for RNA and protein extraction were snap-frozen in liquid nitrogen and stored at -80°C.

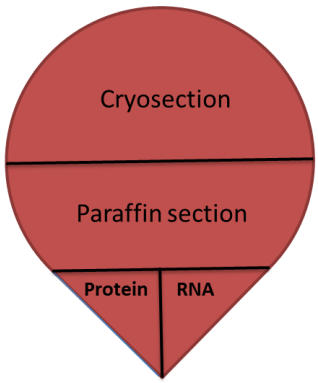

Figure 2-4: Heart dissection for analysis.

2.4.2 Flow Cytometry

All animals were submitted to terminal anaesthesia (3% isoflurane in 2L/minute of O_2) before performing splenectomy. Whole hearts were then perfused with 0.9% NaCl through the LV before harvesting to eliminate residual blood. Both the heart and spleen were stored in isolation buffer (500mL phosphate buffered saline (PBS) w/o Ca^{2+} and Mg^{2+}, 2mL 5M ethylenediaminetetraacetic acid (EDTA), 2mL foetal calf serum (FCS)) on ice before preparation for flow cytometry (section 2.6). In experiments where the kidney was used, the whole left kidney was removed and placed in isolation buffer. For experiments where aorta was required, the aorta was carefully removed after cardiac excision, and placed in isolation buffer as before.

2.4.3 Immune cell isolation

Animals were culled using increasing levels of carbon dioxide (CO_2) prior to removal of LNs and spleen. Peripheral lymph nodes (PLNs) were removed first followed by mesenteric lymph nodes (MLNs) and finally the spleen, as illustrated in *Figure 2-5*. All lymphatic organs were placed in complete media (500ml RPMI with L-Glutamine, 10,000U Penicillin, 10,000µg/ml streptomycin, 10% FCS, 1% HEPES, 500µl β2-mercaptoethanol) on ice until next step. For the initial immune cell characterisation in Chapter 6:, PLNs and MLNs were kept separate in order to analyse individually.

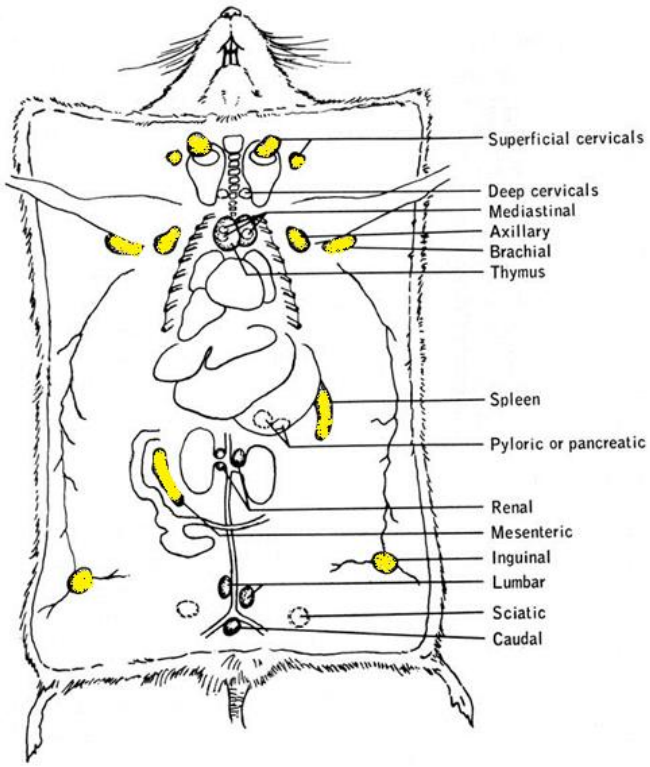

Figure 2-5: Location of lymphoid organs within murine models, adapted from Dunn et al 1954. *Lymphoid organs isolated for our experiments are highlighted in yellow.*

2.5 Physiological measurements

2.5.1 Blood pressure

Blood pressure recordings were measured on conscious mice by tail cuff plethysmography using either CODA™ (Kent Scientific Corporation) or MK-2000ST monitor (Muromachi Kikai, Japan), non-invasive blood pressure systems. Mice were acclimatised for 3-days prior to recordings; this entailed placing the mice into the restraint (*Figure 2-6*) for 10 minutes followed by 6-8 blood pressure measurements. The acclimatisation period reduces animal stress during future recordings, preventing any anomalies. For the CODA™ system, the occlusion and volume-pressure recording (VPR) cuffs determine the blood volume within the tail in order to measure systolic, diastolic and mean blood pressure. For this method an average of 20 blood pressure recordings per mouse were taken. For the MK-2000ST the cuff-pulse sensor is an all-in-one system enabling accurate measurement of systolic, diastolic and mean blood pressure. For this method an average of 8-10 recordings per mouse were taken. Heart

rate was maintained between 600-700 beats per minute (bpm) by allowing mice to rest in-between recordings. Blood pressure recordings were taken at baseline (prior to surgery) and at 3-, 7- and 14-days after surgery. Extra measurements were taken in between recordings to maintain acclimatisation of the mice to the procedure.

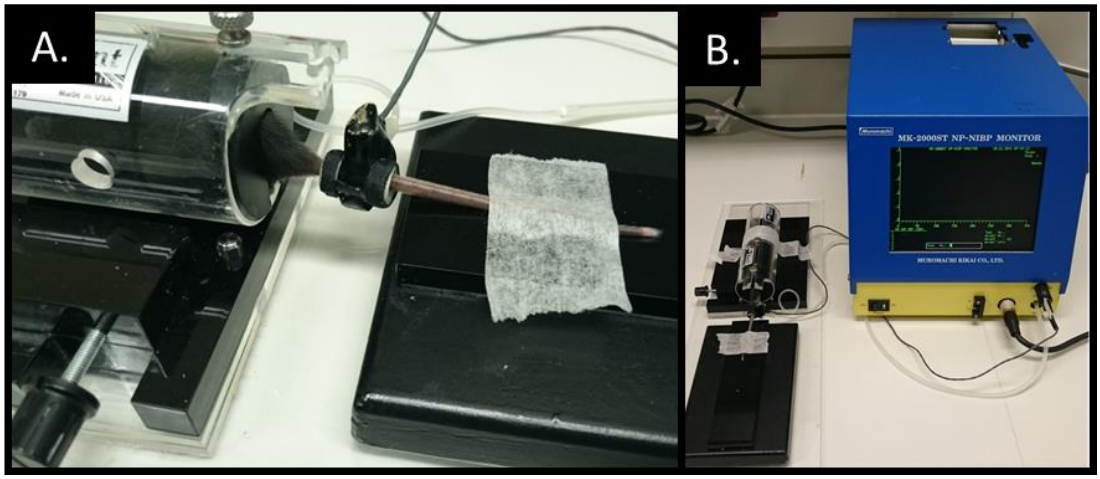

Figure 2-6: Tail cuff plethysmography set up to record blood pressure. (A) *Image showing mouse in a restraint with the cuff-pulse sensor around the tail, which is secured to a weight block.* ***(B)*** *Image showing overall set up with MK-2000ST blood pressure monitor.*

2.5.2 Echocardiography

Echocardiography was performed at baseline (prior to surgery) and at 3-, 7- and 14-days after surgery using the Visualsonics Vevo® 2100 imaging system (FUJIFILM, Canada). Mice were initially weighed and anaesthetised with 5% isoflurane (IsoFlo®) in medical O_2 at 1L/minute, then maintained on a nose cone at 1.25-1.5% isoflurane on a heated platform in the supine position. Fur was removed from the abdomen using a topical depilatory agent (Veet) and residual cream was thoroughly removed using water. Limbs were taped to copper tabs on the heating platform that act as the electrocardiogram gating (*Figure 2-7*). Body temperature was measured using a rectal temperature probe, which was maintained between 36°C and 37°C using the heating platform and a heating lamp to further increase body temperature. In addition, heart rate was maintained above 400bpm by maintaining body temperature and adjusting isoflurane levels appropriately. Ultrasound transmission gel (Skintact ultrasonic gel)

was then applied to the abdomen before lowering the transducer into position using a mechanical arm to maintain stability during recording.

A linear transducer of 32-56MHz (Visualsonics MS550) was used to obtain parasternal long axis (PLAX) and parasternal short axis (PSAX) views (*Figure 2-7*). Both motion-mode (M-mode) and brightness-mode (B-mode) images in PLAX and PSAX were used to measure the left ventricular end diastolic (LVED) and systolic (LVES) diameter (*Figure 2-8*). From these measurements LVED and LVES volume, ejection fraction (EF) and fractional shortening (FS) were automatically determined by Visualsonics Vevo® software. In addition PLAX M-mode was used to measure the interventricular septum (IVS) thickness. These measurements allowed analysis of cardiac structure and function.

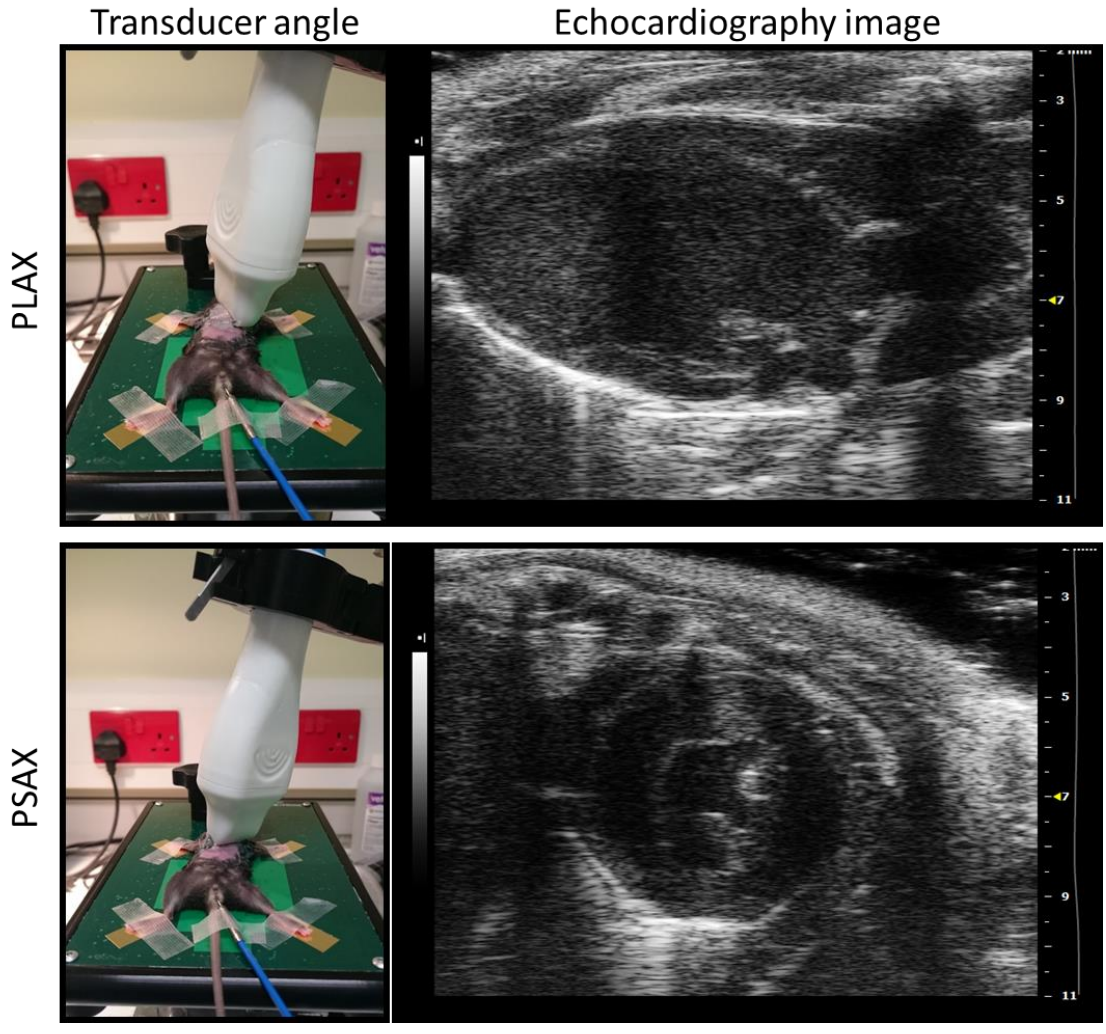

Figure 2-7: Obtaining PLAX and PSAX echocardiography images.

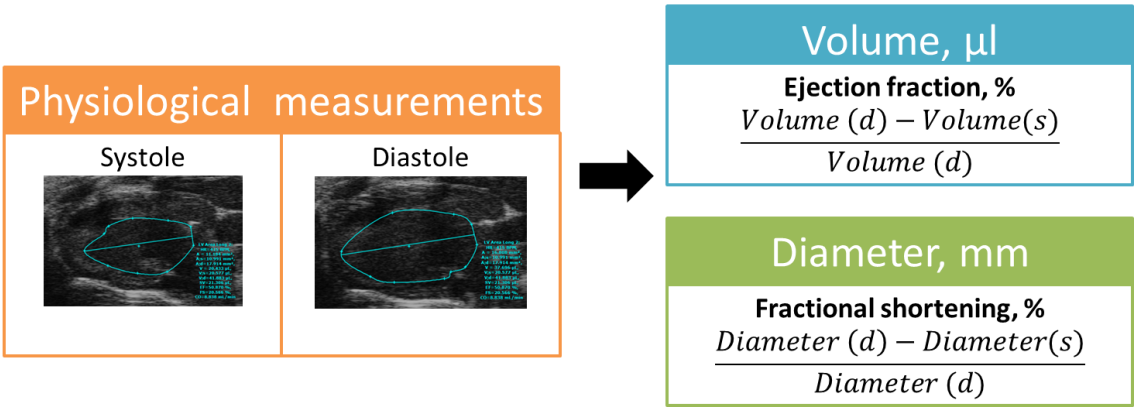

Figure 2-8: Measurements for cardiac structure and function. *Echocardiography provides physiological measurements in both systole and diastole to analyse heart function.*

Echocardiography images were analysed using Visualsonics Vevo® 2100 1.5.0 software. Measurements from B-mode images involved tracing around the LV, as shown in *Figure 2-8*. For M-mode images the posterior and anterior LV walls were traced over at least three contractions and measurements were generated automatically by the software (*Figure 2-9*). Three measurements were recorded per image, for B-mode and M-mode, and the average was calculated between all PLAX and PSAX images.

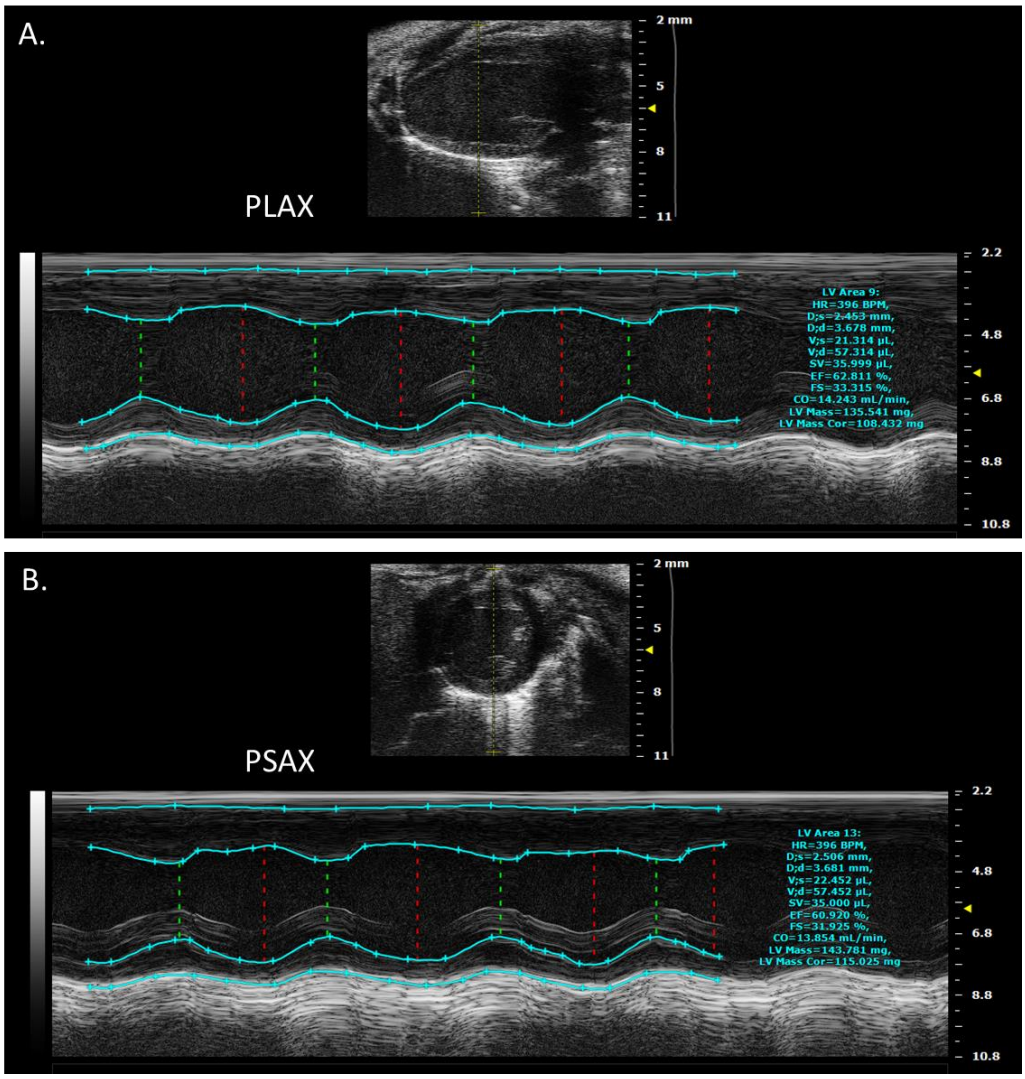

Figure 2-9: Echocardiography analysis of M-mode images. *Images to show analysis of* ***(A)*** *parasternal long axis (PLAX) and* ***(B)*** *parasternal short axis (PSAX).*

2.6 Flow cytometry

2.6.1 Principles of flow cytometry

Flow cytometry uses fluorophore-bound antibodies in order to analyse the different cell types within a single cell suspension. The cell suspension is hydro-dynamically focused to intersect an argon-ion laser (*Figure 2-10*), with a specific wavelength, and scattered light is detected in terms of forward scatter (Fsc) and side scatter (Ssc) indicating cell surface area and granularity respectively. There are three parameters to detect scattered light; height (H), width (W) and area (A). Detectors are also present for fluorescent light emitted from fluorophores bound to specific antibodies. These allow detection of specific cells dependent on their distinct cell surface markers.

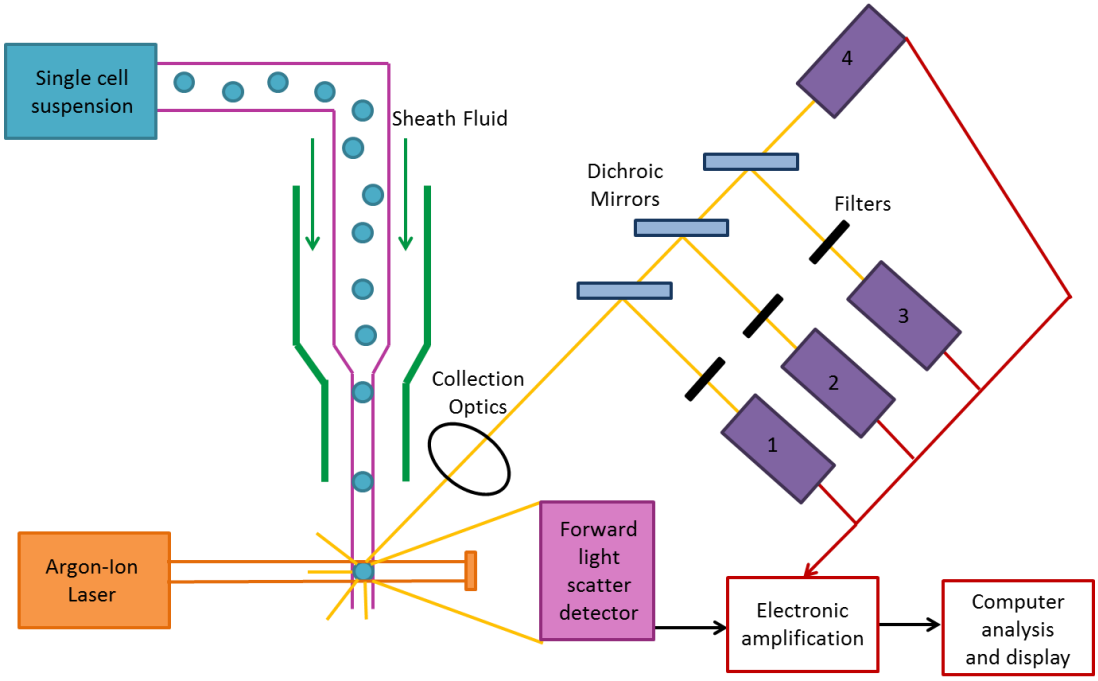

Figure 2-10: Schematic of a flow cytometer. *Single cell suspensions are focused hydro-dynamically with sheath fluid to intersect a laser. Emitted signals are detected by a forward light scatter detector, side light scatter detector (1) and multiple fluorescence emission detectors (1-4). Detected signals are then amplified and converted into a digital signal for analysis. Adapted from Brown et al 2000 (clinical chemistry)*[137].

Within this thesis three flow cytometry machines are used, BD FACS Calibur™, BD FACS Canto II™, and BD LSRFortessa™. All of these machines are multi-parameter systems. The Calibur™ is a basic flow cytometry machine that utilises two lasers to enable detection of up to 4 fluorophores whereas the Canto II™ contains three lasers and allows detection of up to 8 fluorophores at once (*Table 2*). Finally the Fortessa™ utilises five lasers and detects up to 18 fluorophores at once (*Table 3*). All machines analyse Fsc and Ssc, however the Calibur™ measures only Fsc-H and Ssc-H whereas the Canto II™ and Fortessa™ can measure all Fsc and Ssc parameters (H, W and A) enabling elimination of doublets. Doublets occur when two cells become physically attached to each other or when two cells pass through the laser beam close together, so that they are recorded as a single event. The Calibur™ was initially used to carry out preliminary experiments that are shown in section 2.6.3.1, these were then repeated on the Canto II™ instrument, fully analysed and are discussed in section 3.3. The Fortessa™ was used only for the immune composition analysis of lymphoid organs of the CD4-Nox2KO model at baseline in section 6.4.3.

Flow cytometer	Laser	BP filters	Intended fluorophore
BD FACS Calibur™	488nm	488/10	Ssc
		530/30	FITC
		585/42	PE
		670	PerCP
	633nm	661/16	APC
BD FACS CantoII™	488nm	780/60nm	PE-Cy7
		670nm LP	PerCP-Cy5.5
		585/42nm	PE
		530/30	FITC
		488/10	Ssc
		616/23	PE-TexasRed
	633nm	780/60	APC-Cy7
		660/20	APC
		712/21	Alexa700
	405nm	510/50	AmCyan
		450/50	Pacific Blue

Table 2: BD FACS Calibur™ and Canto II™ laser specifications.

Flow cytometer	Laser (nm)	BP filters (nm)	Intended fluorophore
BD FACS Fortessa™	488	575/26	PE
		530/30	FITC
		488/10	Ssc
		525/50	FITC
		515/20	EGFP
		545/35	YFP
		670 LP	PerCP, PerCP-Cy5.5
	561	780/60	PE-Cy7
		710/50	PE-Cy5.5
		660/20	PE-Cy5
		610/20	PE-TexasRed
		585/15	PE
		780/60	PE-Cy7
		670/30	PE-Cy5
	633	780/60	APC-Cy7
		710/50	Alexa700
		670/14	APC
		780/60	APC-Cy7
		730/45	Alexa700
		670/30	APC
	405	780/60	QDot 800
		710/50	QDot 700
		610/20	QDot 605
		585/42	QDot 585
		525/50	AmCyan
		450/50	Pacific blue
	351	530/30	Indo1
		450/50	DAPI

Table 3: BD LSR Fortessa™ laser specifications.

2.6.2 Preparation of samples

Single cell suspensions were prepared from whole organs. Fibrous tissues, such as heart and aorta, were digested for 30 minutes at 37°C in digestion solution (Ca^{2+}/Mg^{2+}

free PBS, 0.5% bovine serum albumin (BSA), 1mg/mL collagenase, 1mM EDTA, 100U/mL deoxyribonuclease I (DNase I) 500U/mL hyaluronidase IV-S). All samples were then triturated and filtered separately through a 70µm nylon mesh, followed by a second filtration through a 30µm nylon mesh. Cell suspensions were then washed in isolation buffer (200mM EDTA, 0.4% FCS in Ca^{2+}/Mg^{2+} free PBS) and centrifuged at 1800rpm for 5 minutes at 4°C. Spleen samples were treated for 3 minutes with 1x red cell lysis buffer (Biolegend) at room temperature followed by a final wash in isolation buffer. Samples were re-suspended in 500µL of isolation buffer and 30-40µL of each sample was used for 'fluorescence-minus one' (FMO) controls for each antibody used. The FMOs are prepared in the same way as the samples and contain all but one antibody, in *Table 4* and *Table 5*, therefore allowing clear identification between positively and negatively stained cells.

Cell suspensions and FMOs were FcRγ-blocked for 15 minutes on ice, using anti-mouse CD16/CD32 antibody (BD pharmingen, 10µg/mL, 1:50) followed by staining (30 min, on ice) with a combination of antibodies in *Table 4* and *Table 5*, depending on the flow cytometry machine being used. The samples were then washed in 2mL isolation buffer, centrifuged (5 mins, 1800rpm, 4°C) and the pellet was re-suspended in 500µL isolation buffer.

Samples that included anti-FoxP3 antibody staining required a further fixation and permeabilisation step before incubation with this antibody. All other antibodies were incubated as previously stated, however prior to re-suspending the cell pellet in 500µL isolation buffer; cells are incubated with 200µL fixation buffer (Biolegend) for 20 minutes at 4°C before being washed twice in 1mL 1x permeabilisation washing buffer (Biolegend). Samples were then incubated with anti-FoxP3 antibody, at concentrations shown in *Table 4***,** for 15 minutes before a final wash in permeabilisation buffer.

Before running samples through the BD FACS Canto II™ machine they were filtered through a 30µm nylon mesh. For fixed samples a Zombie aqua™ dead cell stain (1:100, ebioscience) is incorporated into the initial antibody staining step before fixation, however unfixed samples were incubated for 3-5 minutes with Sytox®Blue Dead Cell Stain (Invitrogen, 2µM, pacific blue) instead.

Antibody	Fluorophore	Concentration (mg/mL)	Concentration for heart samples (µg/mL)	Concentration for spleen samples (µg/mL)	Source
anti-CD45	FITC	0.5	0.5	0.25	Biolegend
anti-TCRb	PE	0.2	0.15	0.075	BD Pharmingen
anti-CD4	PerCP	0.2	0.1	0.05	BD Pharmingen
anti-CD3	PerCP	0.2	4.4	4.4	Biolegend
anti-CD4	APC	0.2	1.1	1.1	Ebioscience
anti-CD8	PE	0.2	0.73	0.73	Ebioscience
anti-CD8	APC	0.2	0.06	0.03	BD Pharmingen
anti-CD25	PE	0.2	0.05	0.025	BD Pharmingen
anti-FoxP3	APC	0.2	0.05	0.025	Ebioscience
anti-CD19	PE	0.2	0.56	0.45	BD Pharmingen
anti-B220	APC	0.2	0.83	0.6	Ebioscience
anti-F4/80	PE	0.2	0.28	0.22	Ebioscience
anti-CD11b	APC	0.2	0.28	0.22	Ebioscience

Table 4: Antibodies used for flow cytometry with the Calibur™.

Antibody	Fluorophore	Concentration (mg/mL)	Concentration for Samples (µg/mL)	Concentration for controls (µg/mL)		Source
				FMO	Beads	
anti-CD45	FITC	0.5	10	2	4.2	Biolegend
anti-TCRb	PE-Cy7	0.2	3	0.6	1.25	BD Pharmingen
anti-CD8a	APC	0.2	2	0.4	0.83	BD Pharmingen
anti-CD4	PerCP-Cy5.5	0.2	2	0.4	0.83	BD Pharmingen
anti-CD25	PE	0.2	2	0.4	0.83	BD Pharmingen
anti-CD8a	APC-Cy7	0.2	2	0.4	0.83	BD Pharmingen
anti-FoxP3	APC	0.2	4	0.8	1.67	Ebioscience
anti-IgM	APC	0.2	2	0.4	0.83	Ebioscience
anti-CD21/CD35	FITC	0.5	2	0.4	0.83	Ebioscience
anti-B220	APC-Cy7	0.2	2	0.4	0.83	Biolegend

Table 5: Antibodies used for flow cytometry with the Canto II™ and Fortessa.

2.6.3 Compensation

When using multiple fluorophores in an experiment, spectral overlap can occur. This is where the fluorescence emitted from one fluorophore is detected within the specific wavelength channel designed to measure the signal from a different fluorophore[138]. Compensation is a process that enables the spectral overlap between different fluorophores to be mathematically eliminated, so that acquired data are accurate[139].

BD FACS Calibur™

Compensation for the BD FACS Calibur™ was performed manually on the flow cytometer, comparing single stained samples and removing spectral overlap between the channels being used.

BD FACS Canto II™ and BD LSR Fortessa™

The BD FACS Canto II™ and BD LSR Fortessa**™** automatically perform compensation on single stained samples; for this compensation beads (BD™ CompBeads, BD biosciences) were used. To prepare the beads, 1 drop of the anti-Rat and anti-hamster Ig κ solution and 1 drop of the negative control solution were added to 120µL isolation buffer for each antibody being used, in addition to an unstained beads control. Beads were then incubated for 30 minutes at room temperature with individual antibodies, shown in *Table 4* and *Table 5*. Finally, the beads were washed in 2mL isolation buffer and centrifuged (1800rpm, 5mins). Supernatants were removed and beads were re-suspended in 500µL isolation buffer. Beads stained individually for each antibody and unstained beads were run through the machine before automatic compensation.

2.6.3.1 *Flow cytometry protocol development*

Figure 2-11 shows the gating strategy used for flow cytometry on the Calibur™ in order to identify T-cells and different T-cell subpopulations. Initially this method was also used to identify a number of other inflammatory cells such as macrophages and B-cells. Preliminary experiments showed an increase in total leukocytes ($CD45^+$ cells), macrophages, B-cells and T-cells after 3-days of AngII treatment, as demonstrated in *Figure 2-12*. T-cell subpopulations also tended to increase with AngII, with a peak after 3-days of treatment as shown in *Figure 2-13*. In addition, a similar trend was observed in isolated spleens from these animals (*Figure 2-14*). However these results showed a lot of variation and false positives, therefore we investigated the best way to analyse our samples using flow cytometry.

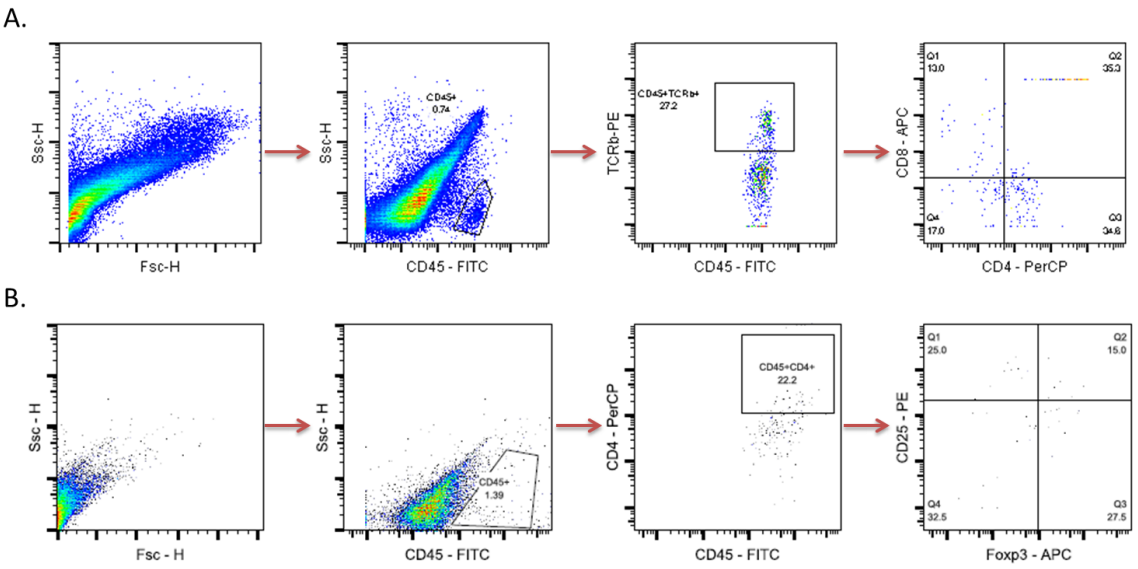

Figure 2-11: Single cell suspensions prepared from whole hearts and analysed using the Calibur™. (A) *T-cells were identified at $CD45^+TCR\beta^+$ and further T-cell subsets analysed using CD4 and CD8.* ***(B)*** *Tregs ($CD25^+FoxP3^+$) were identified from $CD4^+$ T-cells ($CD45^+CD4^+$).*

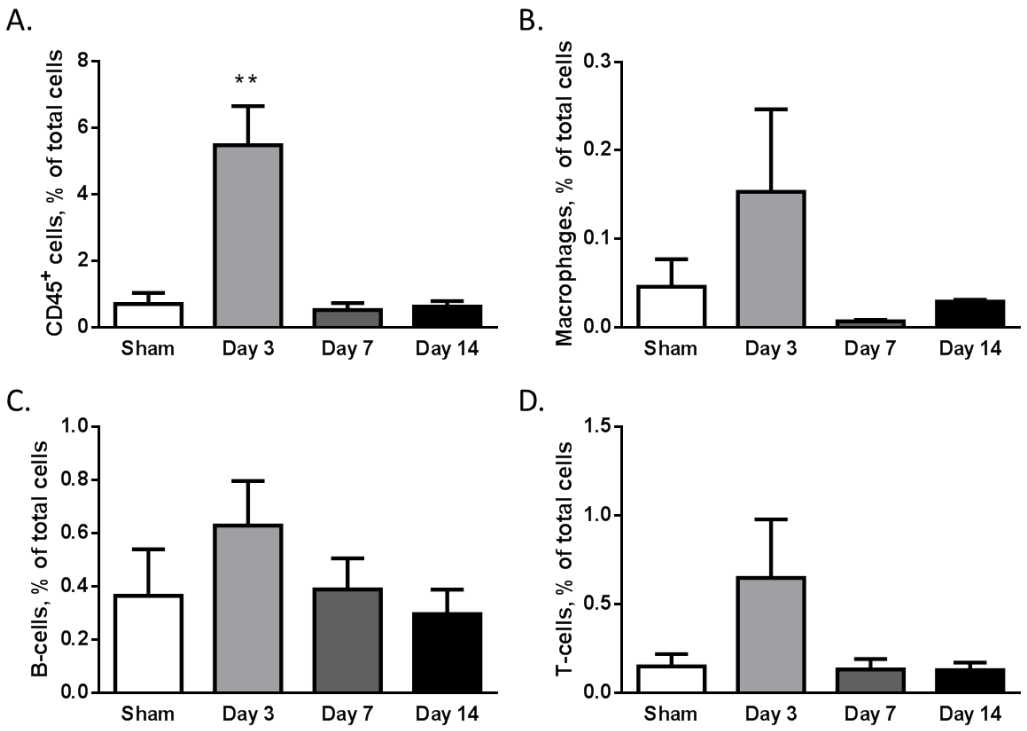

Figure 2-12: Preliminary results showing an altered immune cell infiltration into the heart during AngII treatment. *The effect of AngII treatment on* ***(A)*** *$CD45^+$ cells, and more specifically* ***(B)*** *macrophages ($CD11b^+F4/80^+$),* ***(C)*** *B-cells ($B220^+CD19^+$) and* ***(D)*** *T-cells ($TCR\beta^+$). All cells are represented as a percentage of total cells acquired using the Calibur™.**p <0.01, N=3 per group.*

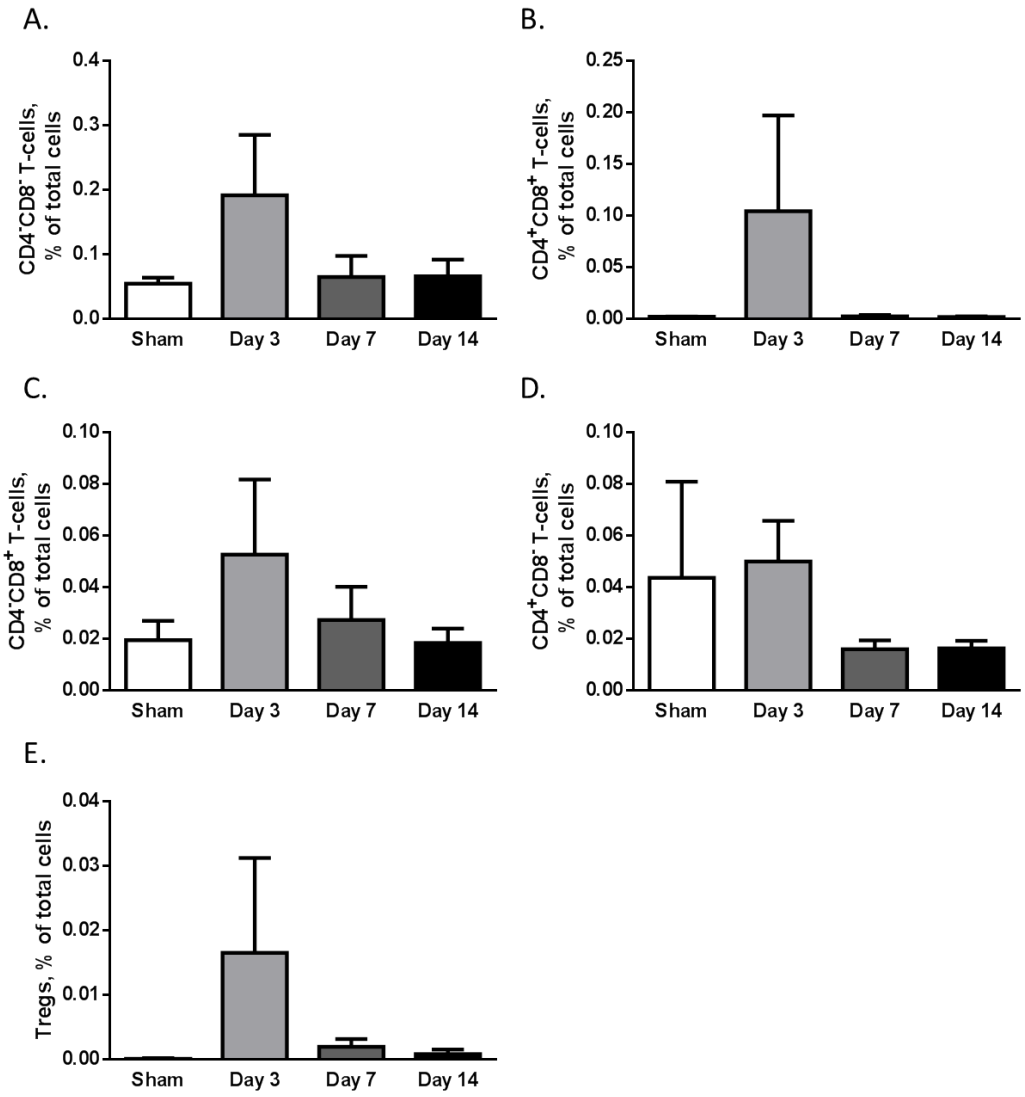

Figure 2-13: Preliminary results showing altered T-cell subtype profile infiltrating the heart during AngII treatment. (A) *Double negative T-cells ($CD4^-CD8^-$)* ***(B)*** *$CD8^+$ T-cells ($CD4^-CD8^+$),* ***(C)*** *Double positive T-cells ($CD4^+CD8^+$),* ***(D)*** *$CD4^+$ T-cells ($CD4^+CD8^-$) and* ***(E)*** *regulatory T-cells ($CD4^+CD25^+FoxP3^+$). All data is represented as a percentage of total cells acquired on the Calibur™. N=3 per group.*

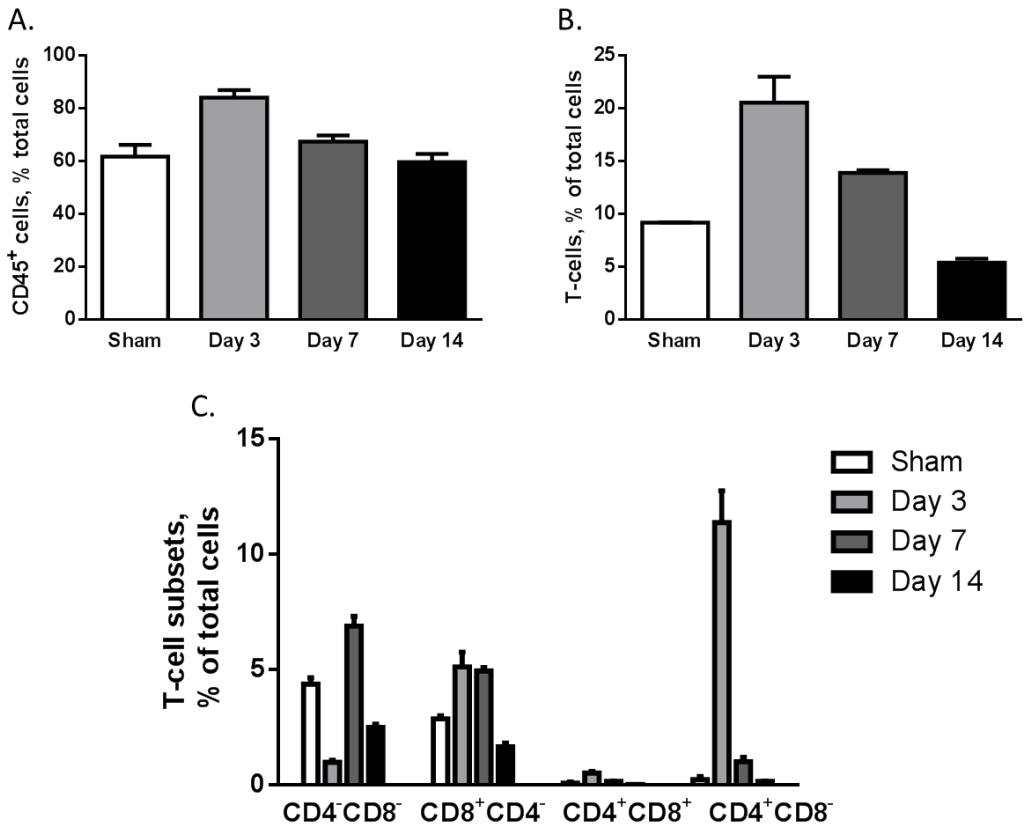

Figure 2-14: Preliminary results showing an altered infiltration of immune cells within the spleen during AngII treatment. *The percentage of* ***(A)*** *$CD45^+$ cells,* ***(B)*** *T-cells ($CD45^+TCR\beta^+$) and* ***(C)*** *T-cell subtypes, identified by expression of CD4 and CD8, in response to AngII treatment up to 14-days. All data is represented as a percentage of total cells acquired on the Calibur™. N=3 per group.*

Results using the Calibur™ looked promising, especially concerning T-cells, however one can argue the accuracy of the T-cell subsets in the spleen in the sham treated mice. Here the $CD8^+$ T-cells were three times more numerous than their $CD4^+$ counterparts whereas a lower ratio is found in the literature, of 1:2 ($CD4^+$:$CD8^+$ T-cells)[140,141].

FMO controls were introduced later, which enable accurate positive and negative gates to be placed for flow cytometry analysis as described in section 2.6.1 however this highlighted further limitations with the method. *Figure 2-15* illustrates a specific gating strategy for a heart sample from a mouse treated for 3-days with AngII. When identifying T-cells ($CD45^+TCR\beta^+$) there is a high amount of background staining due to auto-fluorescent dead cells and doublets, which are visualised as a bright diagonal line, panel 3 of *Figure 2-15*. Using the Calibur™ method, this background material needs to

be gated out of the results; however there are also correctly stained cells that fall amongst this group, making analysis difficult and unreliable. *Figure 2-15*B further highlights this point; this is an FMO control for CD8-APC in which there should not be any $CD8^+$ cells. This figure shows background staining making it impossible to place a reliable CD8-APC positive/negative boundary.

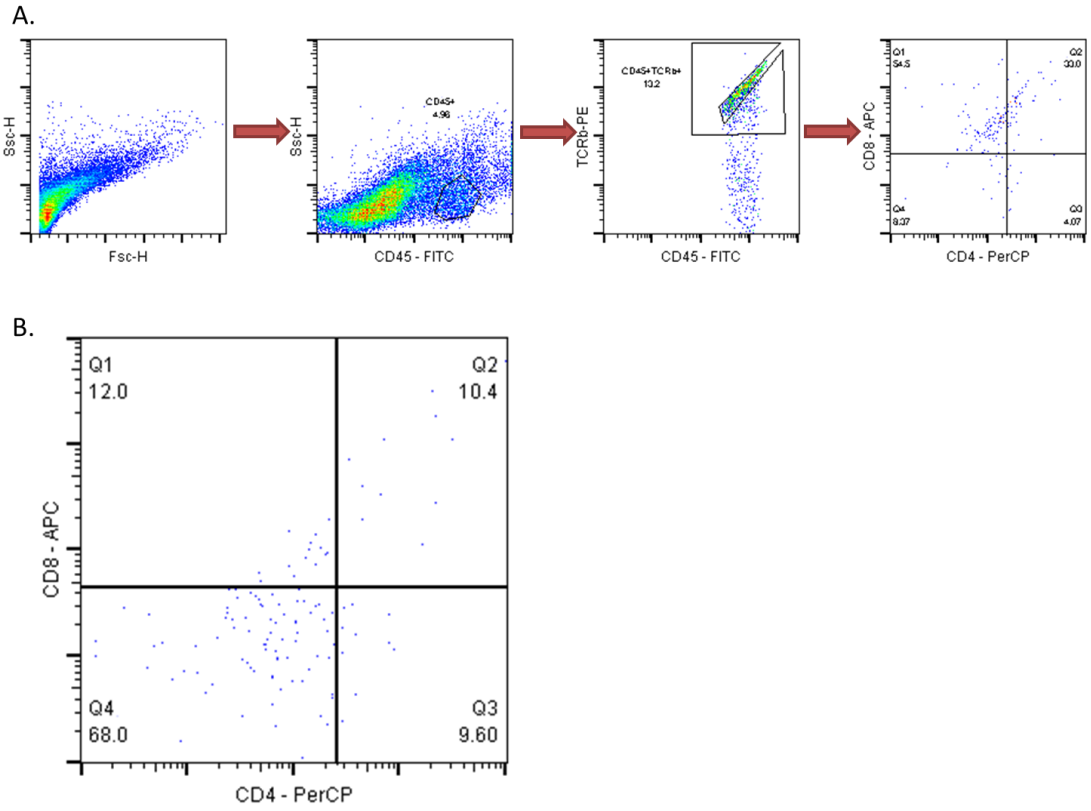

Figure 2-15: Limitations of the Calibur™ method. *The* ***(A)*** *gating strategy for a WT heart sample treated with AngII for 3-days shows significant background staining clearly seen in CD45/TCRβ and CD4/CD8 panels. The* ***(B)*** *CD8-APC FMO shows significant background staining above the boundary between positive and negatively stained cells.*

Due to the low amount of immune cells in the heart this method, which lacked sufficient specificity, was inadequate to confidently identify specific immune cells infiltrating the heart. In order to verify these preliminary results the Canto II™ was used, enabling dead cell and doublet exclusion, as shown in *Figure 2-16*. This method also allows a higher number of events to be acquired as the heart sample can be stained for all antibodies at once whereas the Calibur™ method required samples to be

split in order to analyse each cell type. This is important when analysing more specific, rare cells such as Tregs.

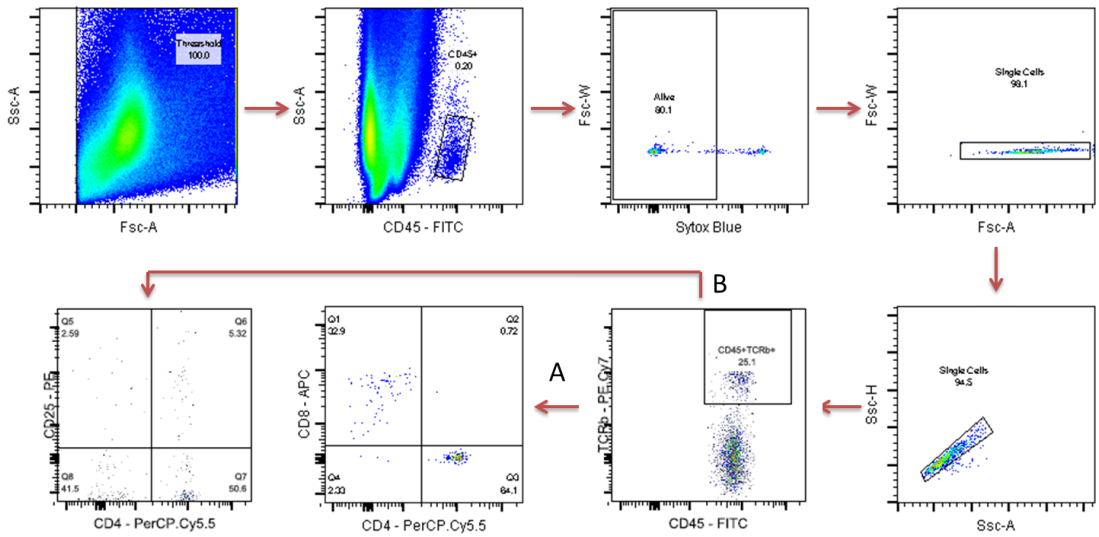

Figure 2-16: Single cell suspensions prepared from whole hearts and analysed using the Canto II™. (A) *T-cells were identified at $CD45^{+}TCR\beta^{+}$ and further T-cell subsets analysed using CD4 and CD8.* ***(B)*** *Tregs ($CD4^{+}CD25^{+}$) were identified from T-cells ($CD45^{+}TCR\beta^{+}$).*

Figure 2-17 shows the CD8-APC FMO where one can clearly distinguish the negative cells below the horizontal line. There are no cells that occur across the positive-negative boundary showing a clearer and more reliable analysis method for both heart and spleen samples. As results with the CantoII™ proved more reliable, we carried out our main flow cytometry experiments using this method, in addition to using controls such as FMOs and compensation beads to ensure correct compensation of fluorescence spill over. These preliminary flow cytometry results are repeated and analysed in more detail in chapter 3.

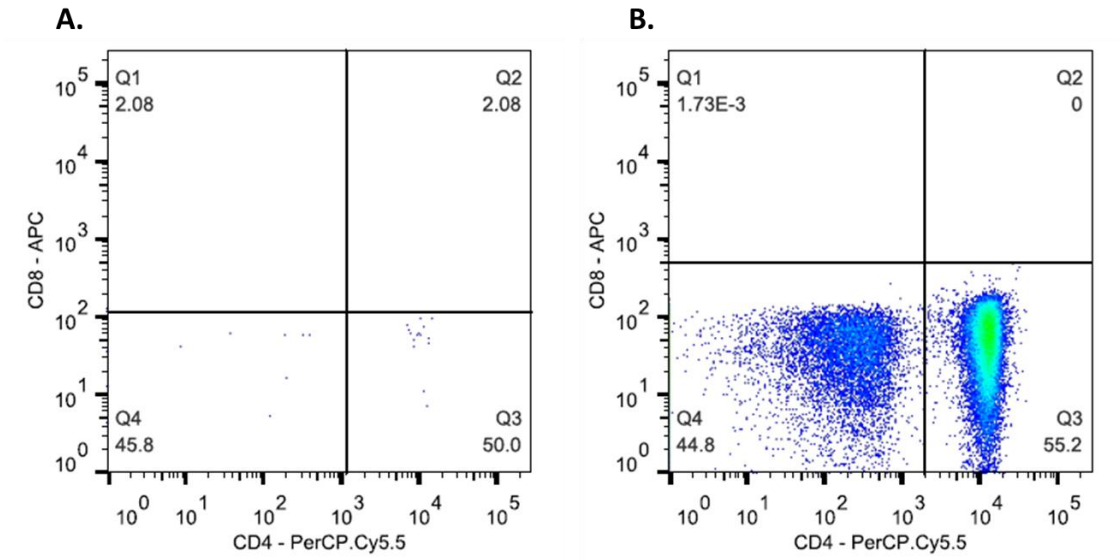

Figure 2-17: Improvement with the Canto II™ when analysing CD8-APC FMO. *CD8-APC FMO for* ***(A)*** *heart samples and* ***(B)*** *spleen samples are clearer using the Canto II™.*

2.7 RNA extraction and qPCR

2.7.1 RNA extraction

RNA was extracted according to the manufacturer's technical datasheet from whole tissues (RNasy® fibrous mini kit, Qiagen) or isolated cells (RNeasy® mini kit, Qiagen). Tissues were disrupted and homogenised using 300µL buffer RLT (Qiagen, with addition of 10µL β-mercaptoethanol (β-ME) per 990µL of RLT) by pipetting repetitively. Ribonuclease (RNase)-free water (590µL) and proteinase k (10µL, Qiagen) were then added and samples were incubated at 55˚C for 15 minutes. Tissue samples were then centrifuged for 3 minutes at 11,000rpm and transferred to a new tube. Half the total volume of 96% ethanol (EtOH) was then added to the sample and mixed. Isolated cells were disrupted by adding 350µL (for <5 x 10^6 cells) or 600µL (for <1 x 10^7 cells) buffer RLT. The lysate is then pipetted directly into a QIAshredder™ spin column (Qiagen) placed above a 2mL collection tube and centrifuged for 2 minutes at full speed. One volume of 70% EtOH was then added to each sample and mixed well by pipetting.

Lysates from both methods above were then treated as follows. 700µL of the sample was then transferred to the RNeasy mini column (placed in a 2mL collection tube) and centrifuged at 11,000rpm for 15 seconds. The flow-through was discarded and this

step repeated until the entire sample was used. Then, 350µL of buffer RW1 (Qiagen) was added to the RNeasy mini column and centrifuged for 15 seconds at 11,000rpm. Once again, the flow-through was discarded before adding 80µL of DNase, diluted in buffer RDD (Qiagen), (10µL DNase mg/mL + 70µL buffer RDD) directly to the membrane for each sample. After incubating for 15 minutes, 350µL of buffer RW1 was added to the RNeasy mini column and the sample was centrifuged for 15 seconds at 11,000rpm. The flow-through was discarded and this process was repeated with 500µL of buffer RPE (Qiagen) twice, discarding flow-through in between washes, and the second centrifuge was extended to 2 minutes at 11,000rpm. The RNeasy column was then placed into a new 2mL collection tube and centrifuged at full speed for 1 minute to remove any excess EtOH and then placed into a new 1.5mL Eppendorf. 30µL of RNase-free water was then added directly to the membrane and left for 2 minutes at room temperature to allow release of RNA from the membrane. Samples were then centrifuged for 1 minute at full speed and this elution step was repeated using the RNA eluate collected in the 1.5mL Eppendorf.

2.7.1.1 Measuring RNA concentration

RNA concentration was then measured for all samples by using a NanoDrop-1000 (ND-1000). The sample type, nucleic acid, was selected on the ND-1000 software and the pedestal cleaned with water in preparation. 1µL of RNase-free water was then loaded onto the pedestal of the ND-1000 to set and blank the machine. Then, 1µL of each sample was loaded individually onto the pedestal and the absorbance detected at 260nm (for nucleic acid). The following calculation is used by the ND-1000 software to determine the concentration ('C') of RNA:

$$C\left(\frac{ng}{\mu L}\right) = A260 \times Constant(40\ for\ RNA)$$

2.7.2 Reverse transcription

A thousand nanograms (1000ng) of RNA were used for reverse transcription (RT) and added to 7µL of the super-mix (Omniscript® reverse transcription kit, Qiagen), components of which are shown in *Table 6*, and the volume was rounded up to a total of 20µL with RNase-free water. Samples were incubated at 37˚C for 60 minutes using a thermocycler. After the polymerase chain reaction (PCR) cycle is complete, complementary DNA (cDNA) samples are diluted with 50µL of RNase-free water.

Super-mix components	Initial stock concentration	Volume per sample (µL)
Buffer RT	10x stock	2
dNTP Mix	5mM each dNTP	2
Random decamers	2µg/µL	2
Rnase-in	10units/µL	0.5
Reverse transcriptase	8units/µL	0.5

Table 6: Reverse transcription super-mix components.

2.7.3 Quantitative PCR

DNA generated from the RT-step was then used for a quantitative PCR (qPCR). All primers used are shown in *Table 7* and are reconstituted with RNase-free water to generate 100mM stock solutions. 1mM aliquots were then made by diluting these stocks with RNase-free water as a "working" stock to be used for experiments. A master mix was made up for each PCR primer being used with the components in *Table 8*. 18µL of the master mix was then added into the correct wells of a 96-well plate in addition to 2µL of the cDNA generated from the RT-PCR in the previous step.

Gene product of interest	Forward primer sequence	Reverse primer sequence
Collagen1α1	CCTCAGGGTATTGCTGGACAAC	TTGATCCAGAAGGACCTTGTTTG
Collagen3α1	CCTGGTGGAAAGGGTGAAAT	CGTGTTCCGGGTATACCATTAG
CTGF	TGACCCCTGCGACCCACA	TACACCGACCCACCGAAGACACAG
Fibronectin	CCGGTGGCTGTCAGTCAGA	CCGTTCCCACTGCTGATTTATC
TGFβ	CCCTGGACACCAATTACTGC	TCAATATAAAGGGGGCGTACA
B-actin	CTGTCGAGTCGCGTCCACCC	ATGCCGGAGCCGTTGTCGAC

Table 7: Fibrosis-related primer sequences used for qPCR. *All sequences are shown as 5'-3'.*

Component	Per well
Sybr Green	10µL
H_2O	4µL
Primer aliquot (F&R)	4µL

Table 8: Super mix for qPCR.

2.8 Sample preparation and tissue staining

Tissue samples for paraffin sections were fixed for 2-4 hours in 2% paraformaldehyde (PFA), washed and stored in 70% EtOH. Tissues were then embedded in paraffin wax and 6µm thick sections were cut using a microtome. Paraffin sections were mounted onto glass slides (Superfrost® plus, Thermo scientific) with at least 4 sections per slide and stored at room temperature. Before tissue staining, paraffin sections were rehydrated in xylene followed by a series of EtOH dilutions (100%, 100%, 95%, 75%, 50%, 25%) and double-distilled water (ddH_2O) for 1 minute each.

Tissue samples for cryosections were mounted on cork with tragacanth gum (4% tragacanth gum, 1% thymol m/v in ddH_2O) and frozen in liquid nitrogen-cooled isopentane. Samples were stored at -80°C. Transverse sections (6µm thick) were cut using a cryostat and 3 sections were mounted onto each glass slide (Superfrost® plus, Thermo scientific) and air-dried before being stored at -80°C. Prior to tissue staining,

cryosections were thawed at room temperature for 30 minutes and fixed using 4% PFA in PBS for 5 minutes.

2.8.1 Haemotoxylin and eosin Staining

Haemotoxylin and eosin (H&E) staining was performed after rehydration of paraffin sections, the tissues were incubated in 1% aqueous eosin for 10 seconds and then rinsed for 5 minutes under running tap water. Samples were then treated in Harris haematoxylin for 30 seconds before a further 5 minute rinse under running tap water. Stained tissue sections were then dehydrated in successive baths of EtOH and xylene (25%, 50%, 75%, 95%, 100%, 100% EtOH, Xylene) for 1 minute each before mounting with DPX (distyrene, a plasticizer and xylene, Sigma Aldrich) and a coverslip.

2.8.2 Wheat germ agglutinin staining

Wheat germ agglutinin (WGA) is a lectin that binds to residues of N-acetyl-D-glucosamine and sialic acid, which are highly expressed on cell surface membranes[142]. When conjugated with rhodamine, a fluorescence dye, cell membranes can be visualised as red fluorescence.

Rehydrated paraffin transverse sections were treated steamed in antigen unmasking solution (Vector H3300) for a total of 30 minutes to retrieve antigens. Sections were then washed three times for 5 minutes in 1x PBS with agitation before individual sections were isolated with a water repelling marker (Dako, DakoPen). Samples were blocked for 45 minutes with 10% goat serum in PBS (Vector) at room temperature in a humidity chamber. Sections were then incubated for 2 hours at room temperature, in a humidity chamber, with avidin-FITC (1:100) and WGA-rhodamine (1:50) both diluted together in 10% goat serum. Samples were then washed 3x 5 minutes in PBS with agitation. Sections were then stained for 5 minutes with DAPI (1:10,000) and washed as before. Finally slides were mounted using mowiol (10% mowiol 4-88, 25% glycerol and 100mM Tris, pH 8.5).

2.8.3 Picrosirius red

Picrosirius red (PSR) is a strong, linear anionic dye that contains six sulfonate groups that can associate to collagen fibres, which are cationic[143]. This staining therefore identifies fibrillary collagen, such as collagen I and III fibres, and can be visualised as red staining under brightfield microscopy[143].

Following rehydration the paraffin slides were incubated in 0.2% phosphomolybdic acid (Fluka) for 2 minutes. Sections were then washed in ddH_2O before 2-hour incubation in 0.1% PSR (Fluka). Samples were then washed in two changes of acidified water (10% acetic acid) for 10 seconds each, before being dehydrated through a series of 25%, 50%, 75% and 100% EtOH for 1 minute each followed by two immersions in xylene. Slides were then mounted using DPX (Sigma Aldrich) and covered with a coverslip.

2.8.4 Microscopy

H&E and PSR slides were analysed by light microscopy using a Leica DM2000 LED brightfield microscope (Leica). Immunohistochemistry (chapter 3) and WGA slides were analysed using bright-field or wide-field fluorescence on an IX81-2 microscope (Olympus).

Three images were taken for each of the heart sections on the slide. Images were acquired using velocity software (PerkinElmer) and analysed using either velocity or ImageJ (MacBiophotonics). For WGA staining, images were taken at 40x magnification and analysed using velocity software (PerkinElmer). The average of 10 cardiomyocytes were calculated per image taken by tracing the cardiomyocyte membrane of cells where DAPI stain (nucleus) was central and the cell appeared full and rounded. PSR images were taken at 20x magnification and were analysed using ImageJ software by estimating the area containing red picrosirius stain. For immunohistochemistry and H&E staining, three images were taken at 20x magnifications per section and representative images displayed to show the level of immune cell infiltration.

2.9 Statistical analysis

All values were expressed as means± the standard error of the mean (SEM) and significance was accepted when p≤0.05. Level of significance was stated as follows in figures: * P <0.05, **P <0.01, ***P <0.001, ****P <0.0001. Graphpad Prism (Version 6) was used for all graphs and statistical analysis.

Unpaired two-tailed *t*-tests were used for data comparing two distinct groups such as qPCR results showing different mRNA levels of a particular target gene between AngII and Sham animals. Where a *f*-test revealed significant difference in variances between groups, an unpaired *t*-test with Welch's corrections was used.

Data containing multiple groups where one variable is being analysed were statistically examined using a one-way analysis of variance between groups (ANOVA) test for differences between groups. This was followed by Bonferroni's multiple comparison tests to compare individual groups. For example, data comparing cardiomyocyte surface area over different time points were analysed using this method.

A two-way ANOVA, followed by a Bonferroni multiple comparison tests, was used for data where more than one variable was being analysed such as systolic blood pressure, where the WT and sham groups were being compared over a time-course.

Chapter 3: Wild-type response to angiotensin II

3.1 Introduction

Chronic AngII infusion in animals is extensively used as a model of RAAS-dependent hypertension. Pressor doses of AngII significantly increase systolic blood pressure and lead to changes in vascular and cardiac function and morphology[83, 134].

3.1.1 Pathophysiological response to AngII

AngII is the main effector peptide within the RAAS, which facilitates blood pressure homeostasis as described in section 1.4. AngII and related RAAS components circulate in the blood to act on different organs and cell types involved in blood pressure regulation. For instance, AngII can target the brain to increase sympathetic nerve activity, allowing blood pressure maintenance[144]. In addition, AngII stimulates aldosterone production from adrenal glands, promoting water retention within the kidneys, hence increasing blood volume. Moreover, AngII can directly act on VSMCs that express AT_1R, to induce vasoconstriction and remodelling, hence increasing blood pressure[145].

During treatment with AngII, the haemodynamic load increases therefore the heart morphology changes in order to maintain cardiac function[89,90]. These remodelling processes include cardiac hypertrophy, interstitial fibrosis and apoptosis that are discussed in detail in section 1.5. Direct effects of AngII on the heart also contribute to these effects. Briefly, increased cardiomyocyte size, and hence heart size, allows increased heart function and efficiency in order to maintain the increase in blood pressure[89,90]. Interstitial fibrosis enables maintenance of tissue structure and required rigidity to withstand higher pressures[95]. Finally, apoptosis is a homeostatic process enabling removal of injured cells[106]. These changes in cardiac structure prove beneficial to compensate for short-term increases in haemodynamic load. In contrast, as the pathological stimulus remains, cardiac remodelling develops a maladaptive stance contributing to cardiac dysfunction and progressing towards heart failure[86].

3.1.2 Angiotensin II and inflammation

In addition to being a major mediator of cardiovascular remodelling, AngII is also implicated in the inflammatory response (section 1.7 & 1.8). Recent studies have described AngII as a pro-inflammatory molecule with the ability to orchestrate an immune response[146]. Initially, AngII increases vascular permeability, by prostaglandins and vascular endothelial growth factor (VEGF), which initiates the immune infiltration[147]. In addition to this, within organs such as the kidney, heart and vasculature, AngII has been found to stimulate inflammation by mechanisms involving pro-inflammatory cytokines and chemokines[148]. This leads to the accumulation of immune cells within these tissues. Furthermore, many immune cells contain the components required to synthesise AngII, hence potentially contributing to and amplifying the pathophysiological response. During initial stages of cardiac remodelling, inflammation is beneficial as a mechanism that enables damaged or dying cells to be cleared away with the aim to restore tissue homeostasis after injury. As the pathological stimulus remains the inflammatory response progresses and contributes to further cardiac damage.

The underlying mechanism enabling immune-cell recruitment by AngII involves the induction of NF-κB and AP-1 transcription factors (in cells such as VSMCs, endothelial cells, fibroblasts and resident or circulating immune cells) that are involved in pro-inflammatory responses[149,150,151-153]. These transcription factors activate genes encoding pro-inflammatory mediators such as IL-1, IL-6, IL-8, IL-12, TNF-α, IFN-γ, monocyte chemotactic protein-1 (MCP-1), C-C chemokine receptor 2 (CCR2), TGF-β, CCL5 and adhesion proteins such as vascular cell adhesion molecule-1 (VCAM-1) and intercellular adhesion molecule-1 (ICAM-1) [149,150]. NF-κB is the main transcription factor enhanced during hypertension[154]. Inactive NF-κB is associated with nuclear factor κ light polypeptide gene enhanced in B-cells inhibitor alpha (IκB-α) in the cytoplasm of a wide range of cells types[155]. Activation involves the phosphorylation and subsequent degradation of IκB-α, thereby permitting NF-κB translocation into the nucleus and allow gene activation[155]. Zhang et al established a new cellular signalling pathway within VSMCs whereby AngII stimulation activates a Ras-MEK1-ERK-ribosomal S6 kinase (RSK) pathway leading to sequential phosphorylation and activation of NF-κB[156]. AngII can also stimulate Nox, and subsequent ROS production may act as a signal

transduction messenger for numerous transcription factors, including NF-κB and AP-1, hence enhancing an inflammatory response[153].

AngII therefore increases the levels of cytokines, chemokines and adhesion molecules in cardiovascular tissues, which all aid the recruitment and infiltration of immune cells. These include macrophages, DCs, B-cells, T-cells and NK cells. Often this recruitment process in turn amplifies cytokine and chemokine production within these specific cell types enabling the inflammatory response to continue and progress. In addition, AT_1R is also expressed on these immune cells, which can therefore be activated directly by AngII[157-159].

3.1.2.1 Innate immune cells implicated in AngII response

Spontaneous hypertensive rats (SHRs), which have elevated levels of AngII, have a significantly higher level of macrophages infiltrating the aorta compared to WT rats[158]. When SHRs were treated with AT_1 antagonists the observed inflammation, associated hypertension and aortic remodelling were attenuated[158]. Similarly, rats treated with AngII directly exhibited an infiltration of immune cells, which included macrophage recruitment[160]. Furthermore, macrophage infiltration is instigated in the setting of increased aldosterone, ET-1, salt and even double transgenic rat (dTGR) models expressing both angiotensinogen and renin genes[151,152,154,161-163]. *In vitro* experiments also confirm these chemotactic properties of AngII in terms of monocyte migration[164].

Increased levels of inflammatory mediators occur concomitantly with cellular infiltration. NF-κB induction of chemokine MCP-1 and its receptor CCR2 are key components that enable the recruitment of macrophages, and elicit an inflammatory response[158,165]. These markers were increased in animals treated with AngII, aldosterone or salt, and accompanied the inflammatory process[158, 160-163,166]. AT_1R antagonists and ACE inhibitors reduced expression of both MCP-1 and CCR2; in addition CCR2 deficient mice displayed a diminished macrophage infiltration in response to AngII[167, 158,168]. Similarly, AngII prompts production of cytokines and chemokines within macrophages and monocytes, such as MCP-1, CCR2, TNFα, IL-1, IL-6, IL-8, IL-12, which further amplifies and progresses the inflammatory response [158,165].

DCs are also implicated in the AngII-inflammatory response. Being major mediators between the innate and adaptive immune responses they potentially play an important role in this setting[169]. In a rat model of chronic kidney fibrosis, AT_1R blockade by valsartan eliminated the marked local increase in DCs and attenuated renal tubulo-interstitial damage[170]. DC activation and stimulation was also confirmed in mice with either AngII- or deoxycorticosterone acetate (DOCA) salt- induced hypertension[169]. The chemotactic properties of AngII in DC recruitment are also confirmed *in vitro*[157]. Human DCs treated with AngII display up-regulation of pro-inflammatory cytokines, which are important in recruiting an adaptive immune response. Similar to macrophages, this involved the activation of NF-κB by AngII treatment, accompanied with higher levels of TNFα and IL-6 production from DCs [171]. Furthermore AngII stimulates upregulation of CD80 and CD86 upon DCs, which enhances antigen-presentation to T-cells via CD28[172]. This process is critical to the development of hypertension, as inhibition of this costimulatory signal prevented T-cell recruitment and the onset of experimental hypertension[172].

Although innate immune cells are important in the initial stages of the inflammatory response and are upregulated with AngII treatment, accumulating evidence implicates the adaptive immune response in the setting of AngII induced hypertension and cardiac remodelling.

3.1.2.2 Adaptive immune cells implicated in response to AngII

Hypertension is prevented in a number of different settings where the adaptive immune response is perturbed. For instance blockade of components involved in instigating the adaptive immune response, such as DCs, reduced hypertension in addition to cardiac and renal damage within SHRs[173,174].

As seen by Vinh et al, T-cells are potentially key components in the progression of hypertension[172]. Preventing T-cell activation by blocking B7/CD28 costimulation prevented T-cell accumulation in the vasculature and the subsequent development of experimental hypertension was attenuated[172]. This was initially highlighted by Guzik et al who demonstrated a key role for T-cells in the progression of AngII-induced hypertension[134]. WT mice treated with AngII had a significant infiltration of T-cells,

specifically $CD4^+$ and DN T-cell subpopulations, within the aorta[134]. Furthermore, RAG deficient mice, which lack T- and B-cells, displayed a blunted hypertensive response to AngII[134]. Adoptive transfer of T-cells restored the pathophysiological responses observed in WT counterparts. Although B-cells also tend to increase during AngII treatment, the adoptive transfer of B-cells into $RAG^{-/-}$ mice did not restore AngII-induced hypertension[134].

Binding of AngII to AT_1 receptors upon T-cells stimulates proliferation and triggers the release of specific cytokines and chemokines by activating transcription factors such as NF-κB and AP-1, including IL-1, IL-2, IL-17, TNF-α, TGFβ, CCR5, CD44[134,146]. These inflammatory mediators further potentiate T-cell recruitment[146]. Human T-cell proliferation assays, in the presence of anti-CD3 antibody, showed that T-cells are more proliferative in the presence of AngII compared to anti-CD3 antibody alone[157]. When NK cells were depleted from isolated T-cells, prior to proliferation, this enhanced proliferative effect by AngII was diminished, suggesting this may be orchestrated by NK cells[157].

Together these results suggest that adaptive immunity, and more specifically T-cells, are implicated in the generation of AngII-induced hypertension. Moreover, increasing baseline levels of Tregs, with the ability to suppress $CD4^+$ T-cell responses, also protects the cardiovascular system from AngII- and aldosterone-induced hypertension and cardiovascular remodelling.

Overall, AngII is implicated in hypertension and cardiovascular remodelling as well as being a key component in the inflammatory response. These processes appear to be intricately entwined in an overactive system, leading to further amplification and hence the progression of organ damage. Published research highlights the importance of inflammation, specifically adaptive immunity, to the development of hypertension. Previous studies have concentrated on T-cell infiltration within the vasculature and shown its importance in the setting of AngII-induced hypertension. As discussed above and in chapter 1, AngII activates Nox2 (which is present in all immune cells) and it seems likely that this would affect the function of immune cells. However the specific role of endogenous Nox2 in T-cells during AngII-induced hypertension and cardiac

remodelling has not been studied. Furthermore, the pattern of T-cell infiltration in the heart during RAAS activation requires further investigation.

3.2 Aims and objectives

The main aims of this chapter were to characterise the pattern and time-course of cardiac T-cell infiltration in the progression of AngII-induced physiopathology in a model of chronic AngII infusion.

3.3 Methods

3.3.1 Experimental model

Male C57Bl/6 mice aged 6-8 weeks (Harlan) were used for all experiments within this chapter. Most methods used are described in the general methods chapter. Briefly, subcutaneous mini-osmotic pumps containing a pressor dose of AngII (1.1mg/kg/day) were surgically implanted into mice for up to 14-days, as described in section 2.3. Blood pressure and haemodynamic function were analysed by tail cuff plethysmography and echocardiography respectively (section 2.5). Another group of C57Bl/6 mice were also treated with a pressor dose of AngII but for 3-days, before organs were harvested for flow cytometry or for immunohistochemistry to analyse immune cells.

3.3.2 Treatment of samples

Harvested hearts were treated as described in section 2.3. RNA was extracted and reverse transcribed to enable analysis by qPCR (section 2.7). Fibrosis-related markers were analysed as described in section 2.7. Histological analysis involved staining of harvested hearts for WGA, H&E and PSR (section 2.8). Further identification of immune cell infiltration was observed using immunohistochemistry for CD45 and CD3, described below (section 3.3.3).

Flow cytometry was performed on whole hearts and spleens using the BD FACS CantoII™ as described in section 2.6. The level of leukocytes, T-cells and T-cell subsets were determined based on expression of CD45, TCRβ, CD4, CD8, CD25 and FoxP3. Further confirmation of immune cell infiltration was determined by qPCR (section 2.7) using primers for CD3, CD25, FoxP3, IL-10, IL-35, CD73, CD37, cytotoxic T-lymphocyte associated protein-4 (CTLA-4), glucocorticoid-induced tumour necrosis factor receptor (TNFR) family related gene (GITR), neuropilin (NRP), CCL1, CCR8, CCL17, CCL22, CCR4, cMet, STAT-3 and CXCR3 (primer sequences shown in *Table 9*).

Gene product of interest	Forward primer sequence	Reverse primer sequence
B-actin	CTGTCGAGTCGCGTCCACCC	ATGCCGGAGCCGTTGTCGAC
CD3	TCCCAACCCAGACTATGAGC	ATGTCCCAGCACTGGCTACT
CD25	TGGTCTATATGCGTTGCTTAGG	TTCTCGATTTGTCATGGGAGT
FoxP3	GAACCCAATGCCCAACCCTAG	TTCTTGGTTTTGAGGTCAAGGG
IL-10	GGGTCTTGGGAAGAGAAACC	CATTCCCAGAGGAATTGCAT
IL-35	CCTGCTGAAGACCACAGATG	CTACCAAGGCACAGGGTCAT
GITR	ATGAGGCCTGGTCTTCCTCT	TTGTGCTAAACGTGGTGCTC
CTLA-4	TGGACCCTGAGCATCTCTCT	CAGGTGTCTGCCTAGCCTTC
CD73	GCCTATGCCTTTGGCAAATA	AGGTTTCCCATGTTGCATTC
CD39	CAAGGGCTGCGAGATAAGAC	GCACCAGGGAACTTGGTAGA
Neuropillin (NRP)	AGCTTCAATGAGCGTCACCT	CAAAAGGGCCCACTGAATAA
CCL-1	CTGCTGCTTGAACACCTTGA	TGGAGGACTGAGGGAAACTG
CCL-17	AAAGGGGCCATTCCTATCAG	CTGGTCACAGGCCGTTTTAT
CCL-22	CAACTTCCACCCCTCTTCAA	TCACTTTGTATGGCCCTTCC
CCR-4	ATCCTGAAGGACTTCAAGCTCCA	AGGTCTGTGCAAGATCGTTTCATGG
CCR-8	GCAGTCTTTGAGGTGGAAGC	TTGAATGGGACCCAGAAGAG
cMet	TCCTGCACTGTGAGCATTTC	ACGATTGGGTTTCAGCAGAC
STAT-3	CTTCCCAGTTTCGCATTCAT	CACACACACACAAGCCATCA
CXCR-3	GTGGCTGCTGTGCTACTGAG	AAGGCCCCTGCATAGAAGTT

Table 9: Immune-related primer sequences used for qPCR. *All sequences are shown as 5'-3'.*

3.3.3 Immunohistochemistry

Samples were treated as described in the general methods (section 2.8) before being stained for either CD45 or CD3, described below, to observe total leukocyte infiltration and T-cell infiltration respectively.

Cryosections were thawed and fixed using 4% PFA in PBS for 5 minutes, then washed for 5 minutes in 1x Tris-buffered saline (TBS)-0.02% Triton (0.05M Tris base, 0.15M NaCl, 0.02% Triton, pH 7.4) with agitation and incubated for 15 minutes in methanol containing hydrogen peroxide (3% H_2O_2, in methanol). Sections were then washed three times for 5 minutes in TBS-0.02% Triton with agitation and each individual section was isolated with DakoPen (Dako). Sections were blocked in normal serum (1:40 diluted in TBS-0.02% Triton, Vectorstain universal quick kit), for 45 minutes at room temperature. Samples were then incubated overnight with an anti-CD45 antibody (1:100 in normal serum, BD Pharmingen) or with anti-CD3 antibody (1:100 in normal serum, BD Pharmingen), both diluted in TBS-0.02% Triton, at 4°C. Slides were washed three times for 5 minutes each in TBS-0.02% Triton with agitation before being incubated with diluted universal biotinylated antibody (1:10 diluted in normal serum, Vectorstain universal quick kit in a humidity chamber at room temperature for 10 minutes. Cryosections were then washed three times for 5 minutes each in TBS-0.02% Triton with agitation and incubated with streptavidin-peroxidase complex (1:40 in normal serum, Vectorstain universal quick kit) for 5 minutes in a humidity chamber before a final set of washes in TBS-0.02% Triton with agitation. Slides were incubated with ImmPACT DAB (3,3'-Diaminobenzidine, Vector) for 2-5 minutes and washed for 1 minute under running tap water. Harris haematoxylin counter staining was then performed for 30-60 seconds and then slides were rinsed for 15 minutes under running tap water. Cryosections were then dehydrated with successive baths of EtOH and xylene as described previously and mounted using DPX and a coverslip. One section per slide was kept as a negative control, which was submitted to secondary antibody but not primary.

3.4 Results

3.4.1 Angiotensin II induces hypertension and cardiac remodelling

3.4.1.1 Haemodynamic response to AngII

C57Bl/6 mice were treated with a pressor dose (1.1mg/kg/day) of AngII over a 14-day period, a well-established model of cardiomyocyte hypertrophy and fibrosis[83,134,175]. Blood pressure was recorded by tail cuff plethysmography and cardiac morphology and function were analysed using echocardiography at time points illustrated in *Figure 2-1*.

With AngII treatment there was a rapid increase in systolic blood pressure by 47% after 3-days ($p=0.007$), which was sustained over the 14 day treatment period, as shown in *Figure 3-1*. Statistical analysis using a 2-way ANOVA revealed a significant difference between the AngII treated group and the sham group ($p=0.010$). In comparison to control mice, AngII treated mice showed no difference in left ventricular end-diastolic and end-systolic volume (LVEDV, LVESV respectively) after 14-days of treatment. LVESV tended to slowly decrease over the 14-day treatment period; however this did not reach significance at day 14. These results consequently lead to a gradual increase in ejection fraction with AngII treatment without reaching significance after 14-days.

This demonstrates that AngII infusion for 2 weeks in this model induced hypertension and that cardiac function remained well compensated over this period.

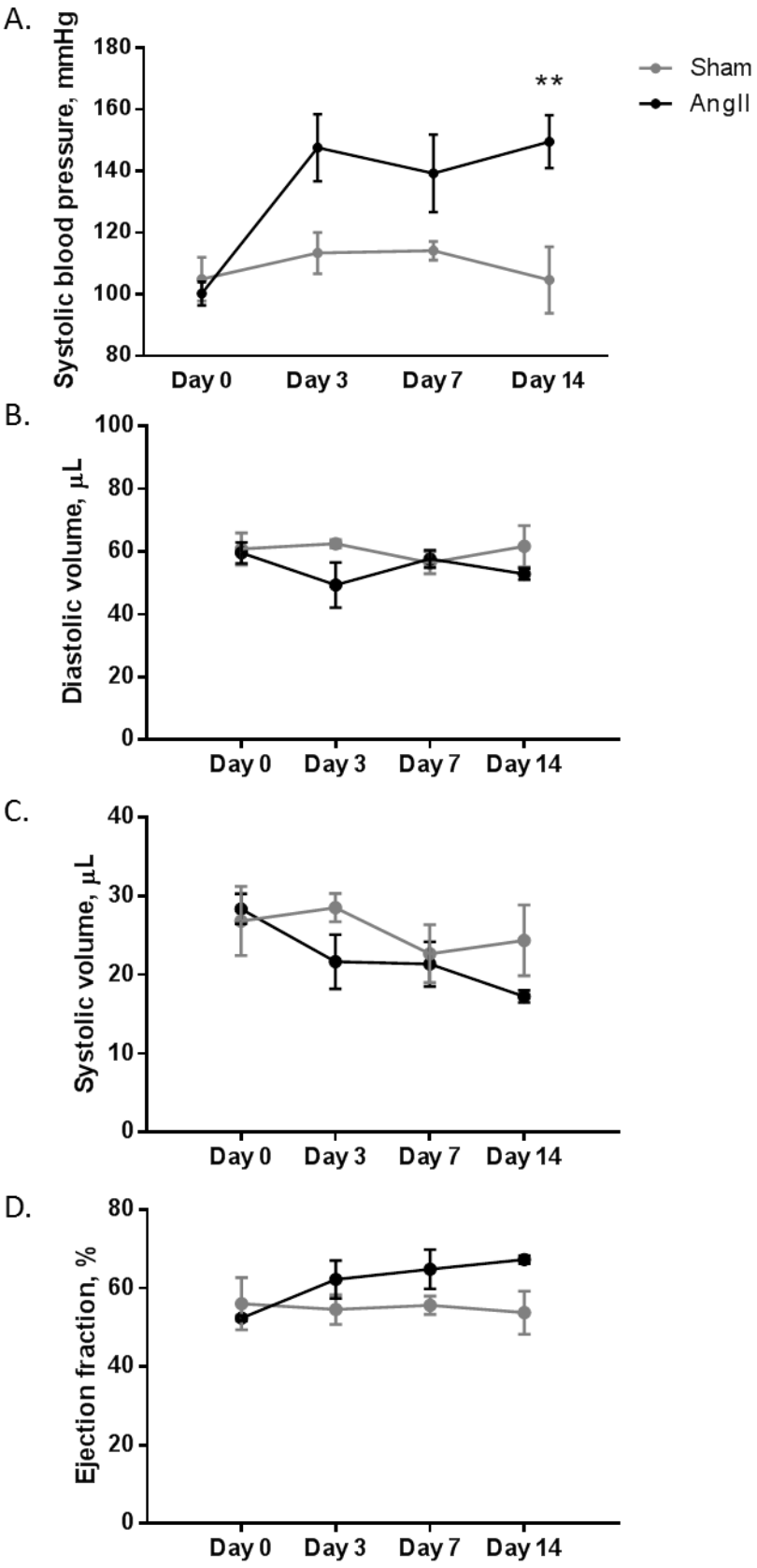

Figure 3-1: Physiological response to AngII after 14-days of treatment. *Increased* ***(A)*** *systolic blood pressure, accompanied by similar levels of* ***(B)*** *end-diastolic and* ***(C)*** *end-systolic volume and hence* ***(D)*** *ejection fraction. **p<0.01, N=3 per group.*

3.4.1.1 AngII induced cardiac remodelling: hypertrophy and fibrosis

Body weight (BW), heart weights (HW) and tibia length (TL) were recorded upon culling and the heart weight-to-body weight (HW/BW) and heart weight-to-tibia length (HW/TL) ratios were calculated for each animal (*Figure 3-2*). As expected, HW/BW ratio gradually increased over the treatment period, reaching significance after 7 days ($p=0.003$), which is maintained after 14-days ($p<0.001$). HW/TL also significantly increased after 7 days, reaching 9.98±0.49 ($p=0.005$), which is preserved up to 14-days ($p=0.004$). This increase in heart size was also accompanied by an increase in IVS thickness that gradually progressed from 0.68±0.03mm to 1.05±0.04mm, suggesting organ-level hypertrophy.

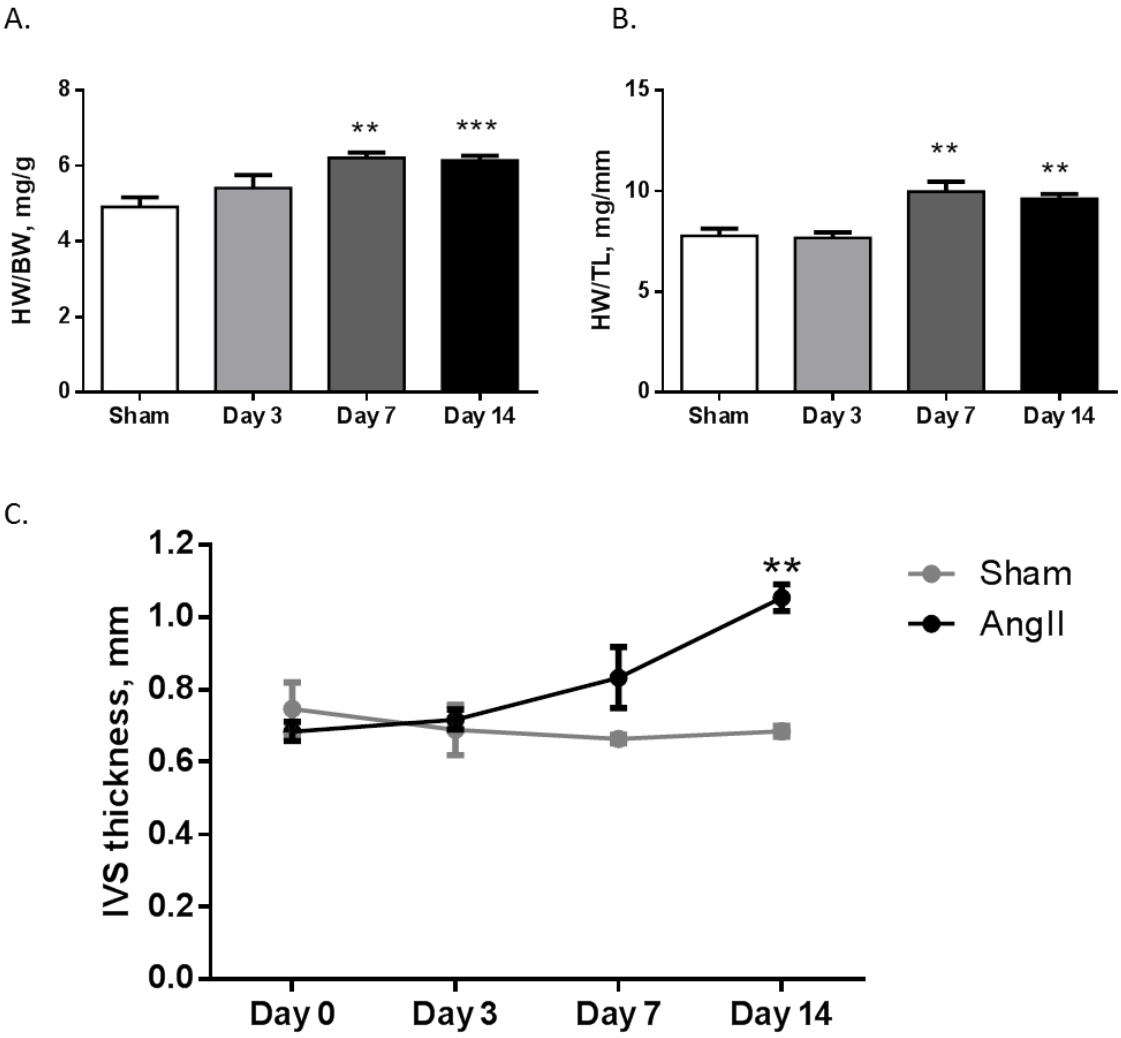

Figure 3-2: Development of organ-level hypertrophy after AngII treatment. *After 14-days AngII treatment* ***(A)*** *heart weight-to-body weight (HW/BW) and* ***(B)*** *heart weight-to-tibia length (HW/TL) significantly increased, accompanied by an increase in* ***(C)*** *IVS thickness.**p<0.01, ***p<0.001, N=3 per group.*

Remodelling was then studied at the tissue level. In order to verify the documented effect of AngII on cardiomyocyte hypertrophy, heart cryosections prepared from AngII and sham treated mice were stained with WGA in order to identify cell membranes (*Figure 3-3*). AngII treated mice showed a significant increase in the cardiomyocyte surface area, rising from an average of 434±14.8µm^2 in the sham group to 518±12.3µm^2 after 14-days treatment (P=0.001).

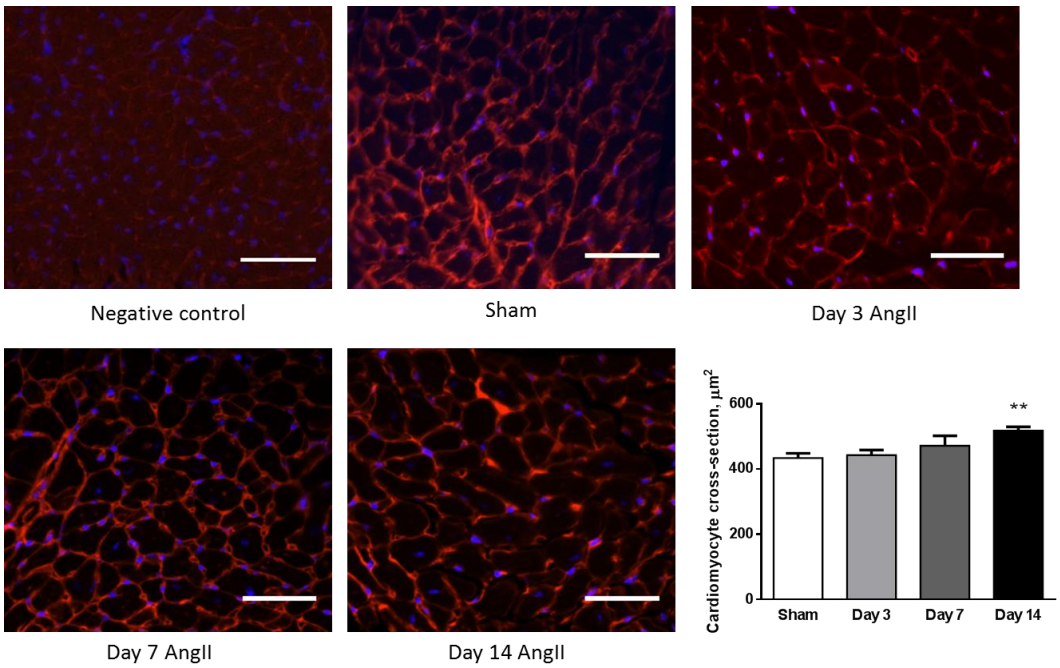

Figure 3-3: Onset of tissue-level hypertrophy with AngII treatment. *WGA staining observed in negative control, sham, day 3 AngII, day 7 AngII and day 14 AngII confirms enlarged cardiomyocyte cross-section. Scale bar represents 25µm, **p<0.01, N=3-7 per group.*

Cardiac cryosections were also stained with PSR in order to identify collagen. The percentage of collagen increased slowly over the treatment period from 0.12% in sham mice to 6.2% after 14-days of AngII treatment (p<0.0001), as highlighted in *Figure 3-4*. Collagen was located in the interstitium, suggesting interstitial fibrosis. This was verified by significant increases in mRNA levels of fibrotic markers identified by qPCR from sham and day 14 tissue samples. Both collagen1α1 (col1α1, p=0.005) and collagen3α1 (col3α1, p=0.022) mRNA levels significantly increased after 14-days of treatment (*Figure 3-5*). However, fibronectin, CTGF and TGFβ mRNA levels remained

unchanged. These findings confirm the development of interstitial fibrosis after 14-days of systemic treatment with AngII.

Taken together these results indicate that, in line with previous results using this model, AngII induces significant cardiac remodelling marked by organ-level and cardiomyocyte hypertrophy, and development of interstitial fibrosis, with well compensated cardiac function.

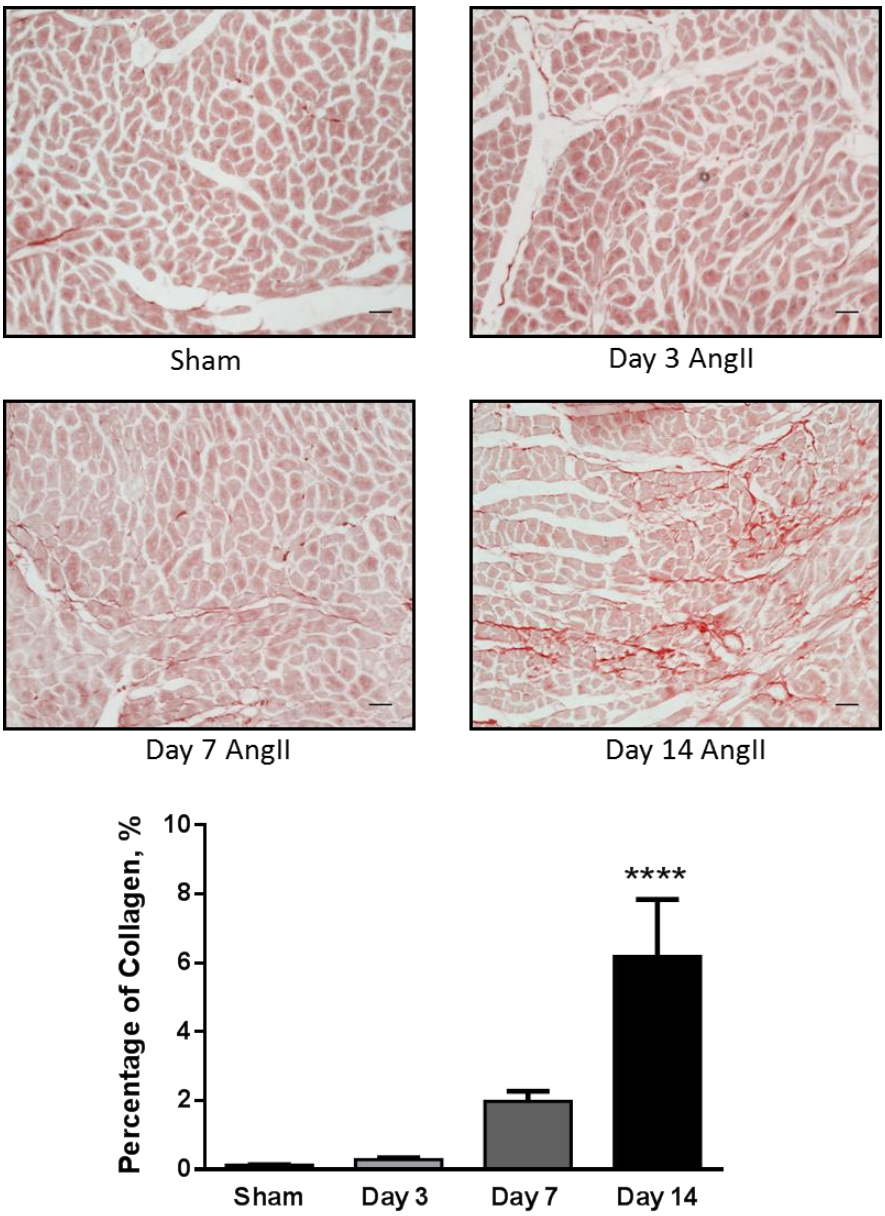

Figure 3-4: Progression of interstitial fibrosis within the heart in response to AngII treatment. Picrosirius red staining highlights increased collagen from sham to day 14 AngII treatment. *Scale bar represents 25µm, ****p<0.0001,* N=6-7 per group.

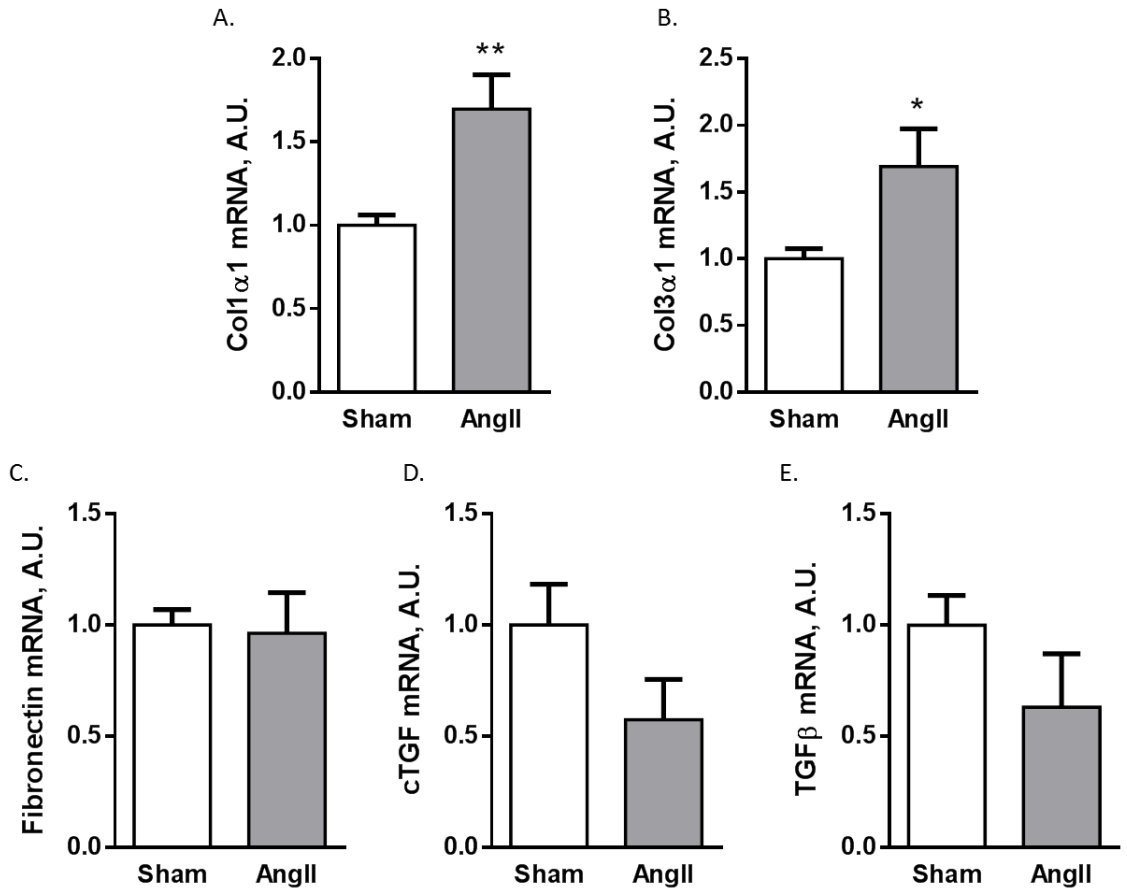

Figure 3-5: Increase in collagen-related mRNA levels with AngII. *A marked increase of* ***(A)*** *collagen1α1 and* ***(B)*** *collagen3α1 further corroborates these findings.* ***(C)*** *Fibronectin,* ***(D)*** *CTGF and* ***(E)*** *TGFβ mRNA levels are unchanged.*p<0.05, **p<0.01, N=5-6 per group.*

3.4.2 Infiltration of immune cells in response to AngII

3.4.2.1 Visualising cardiac inflammation

General tissue structure and cellular infiltration was observed by H&E staining in heart cryosections prepared from sham or AngII treated animals up to 14-days. Infiltration of small cells was observed after 3-days of AngII treatment and these tended to reside up until day 14 (*Figure 3-6*). Cryosections were also stained for CD45 and CD3 to analyse changes in total leukocytes and T-cells respectively. *Figure 3-6* illustrates an increase in both $CD45^+$ and $CD3^+$ cells, observed by brown DAB staining, in response to AngII treatment; this appears to be maintained up to 14-days. After 14-days, leukocytes mainly reside within the interstitium, rather than forming clear peri-vascular clusters as observed at day 3 and 7.

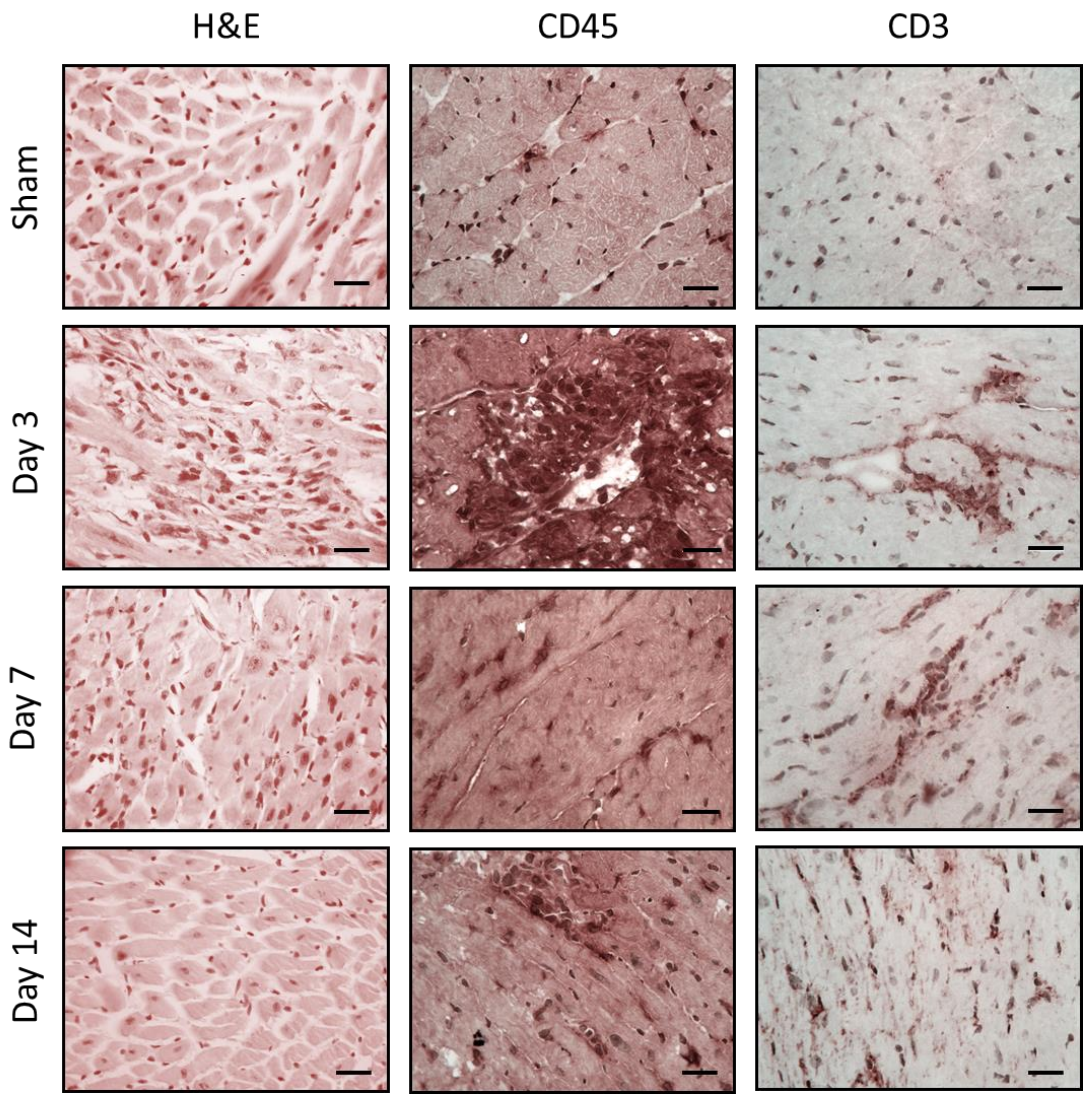

Figure 3-6: Inflammation within the heart of AngII treated mice. *General tissue structure and cellular infiltration observed by H&E staining. Leukocyte ($CD45^+$) and T-cell ($CD3^+$) infiltration was visualised using brown DAB staining performed on cryosections from sham, 3-, 7- and 14-days after AngII treatment. Scale bar represents 25µm.*

3.4.2.2 Quantifying AngII-induced inflammation

Flow cytometry was used in order to better quantify the infiltrating T-cells, identify specific subsets involved in the cardiac response to AngII and to define the time-course of infiltration. Single cell suspensions were prepared from whole hearts obtained from mice treated with AngII for up to 3-days (*Figure 3-7*). Spleens were also isolated from respective animals and used to analyse the general immune status. All samples were analysed using the BD FACS CantoII™. Representative flow cytometry dot plots for

heart samples (*Figure 3-7*) display a higher level of total leukocytes ($CD45^+$ cells), T-cells ($CD45^+TCR\beta^+$ cells) and T-cell subpopulations with AngII treatment after 3-days.

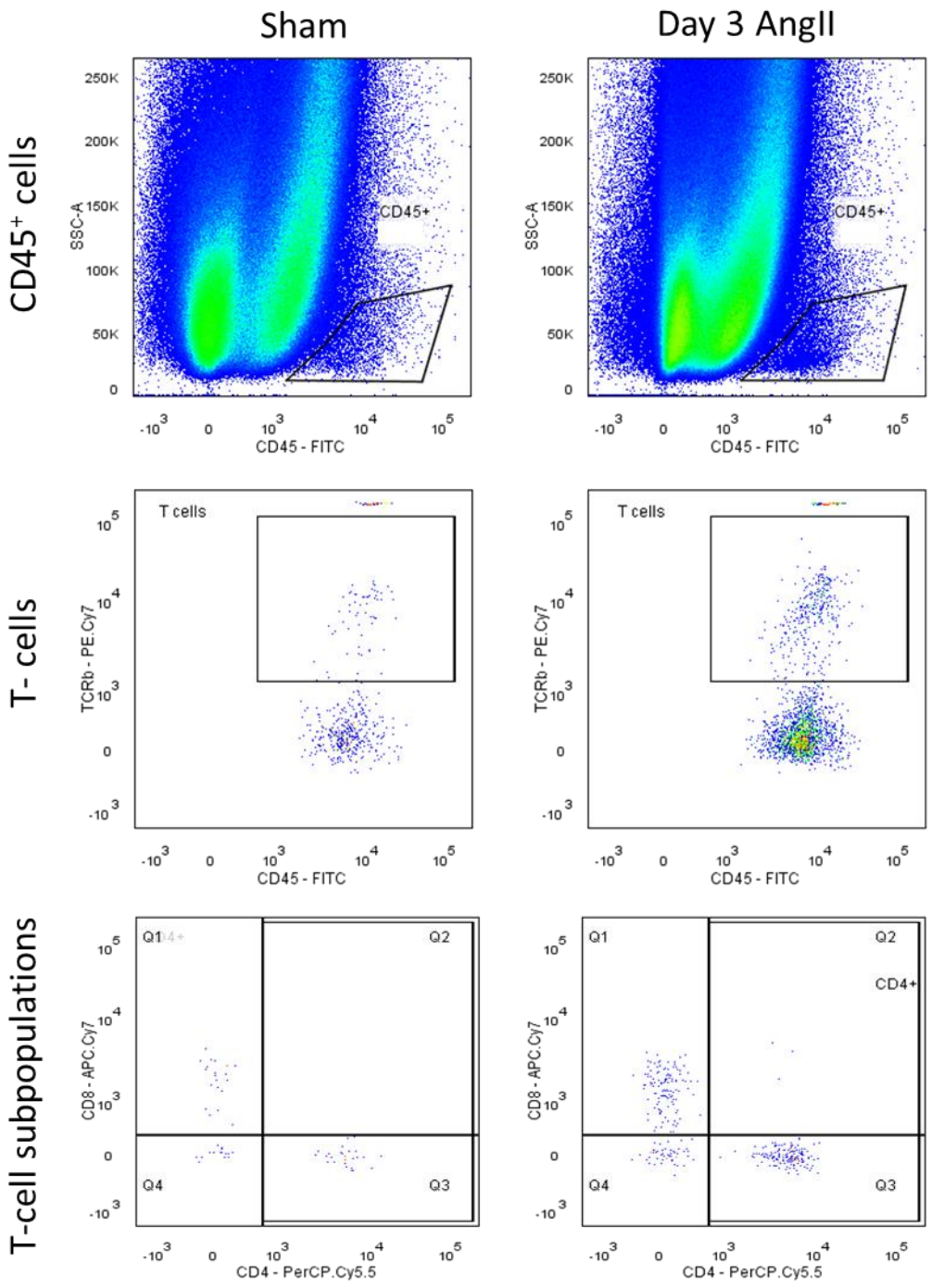

Figure 3-7: Representative dot plots showing cardiac T-cell infiltration. *The effect of AngII treatment on infiltrating leukocytes and T-cells represented as visual flow cytometry dot plots. Acquired on BD FACS CantoII™.*

Upon quantitative analysis, a marked increase in leukocytes ($CD45^+$ cells) from 40.6±5.11 cells/mg to 166±38.5 cells/mg of cardiac tissue (p=0.007) was observed after 3-days of AngII treatment (*Figure 3-8*). However, this reduced back to sham-levels after 7-14-days of AngII treatment. A similar effect was observed with T-cell infiltration ($CD45^+TCR\beta^+$ cells) increasing to 80.4±24.1 cells/mg after 3-days of AngII compared to sham (p=0.005) before reducing back to baseline after 7-14-days.

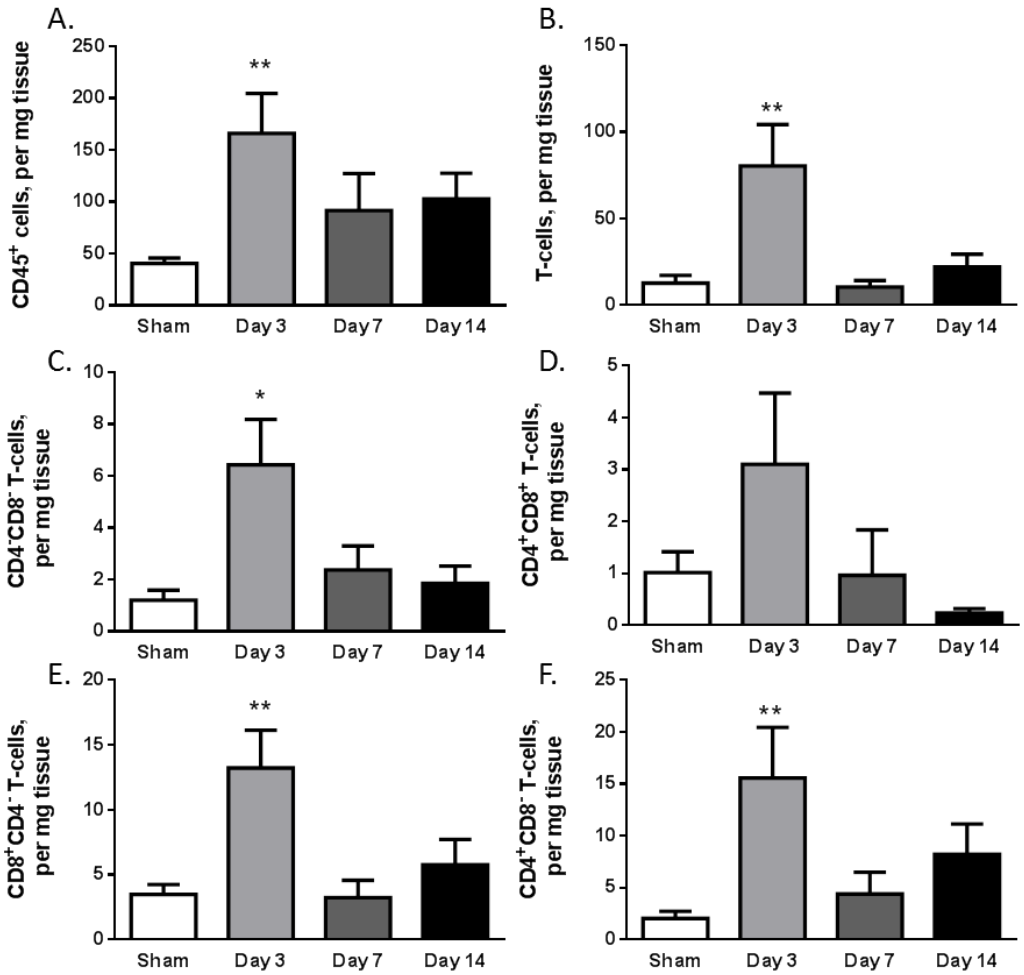

Figure 3-8: Altered cardiac T-cell infiltration during AngII treatment. *Individual analysis of* ***(A)*** *$CD45^+$ cells and* ***(B)*** *T-cells ($CD45^+TCR\beta^+$) infiltration. Individual T-cell subpopulations,* ***(C)*** *double negative ($CD4^-CD8^-$),* ***(D)*** *double positive ($CD4^+CD8^+$),* ***(E)*** *$CD8^+$ and* ***(F)*** *$CD4^+$ T-cells, were also altered by AngII treatment. All data is represented as cells per mg of cardiac tissue acquired on the CantoII™. *p<0.05, **p<0.01, N=5-12 per group.*

T-cell subtypes were also analysed from prepared cardiac samples using the CantoII™, shown in *Figure 3-8***.** After 3-days of treatment with AngII, DP T-cells ($CD4^+CD8^+$) tended to increase, accompanied by a significant increase in DN T-cell ($CD4^-CD8^-$) (p=0.011), $CD8^+$ T-cells ($CD4^-CD8^+$) (p=0.009) and $CD4^+$ T-cells ($CD4^+CD8^-$) (p=0.002) compared to sham. $CD8^+$ T-cells and $CD4^+$ T-cells, after 3-days of AngII, were approximately 4 and 8 times higher than sham levels respectively. As treatment progressed to 7 and 14-days the level of all T-cell subtypes decreased back to baseline.

Due to the systemic nature of the AngII treatment, spleen samples were also analysed to ascertain the general immune status of the mice (*Figure 3-9*). All immune cell subpopulations in the spleen remained unaltered throughout treatment with AngII.

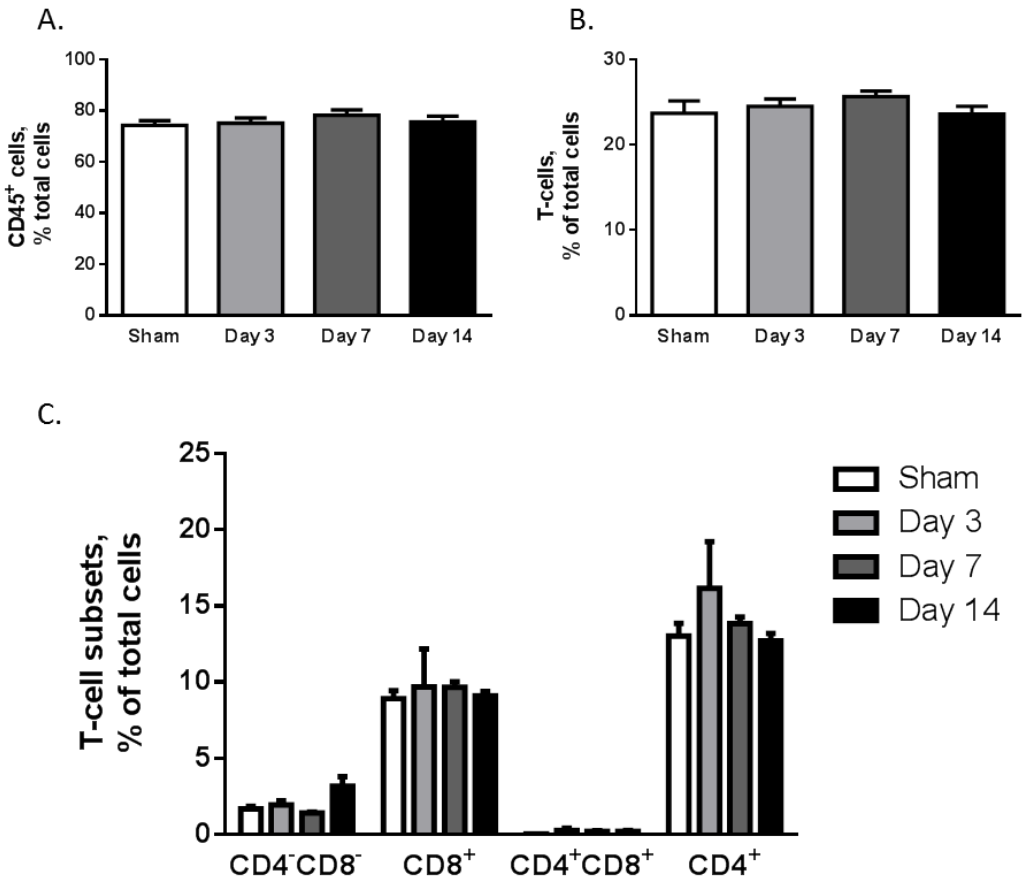

Figure 3-9: Splenic levels of T-cells remain unchanged during AngII infusion. *Splenic levels of* ***(A)*** *$CD45^+$ cells,* ***(B)*** *T-cells and* ***(C)*** *T-cell subpopulations. All data are represented as a percentage of total cells, acquired on the BD FACS CantoII™. N=5-12 per group.*

Tregs were also affected by AngII treatment, as shown in *Figure 3-10*. Initial numbers of $CD4^+CD25^+$ Tregs per mg of heart tissue significantly increased after 3-days (p=0.013) of AngII, before decreasing back to baseline levels after 7 and 14-days of treatment. FoxP3 staining further verified the increase in Tregs after 3-days of AngII by displaying a 2.4 fold increase compared to sham levels (p=0.024). This cardiac peak in Tregs was not seen within treated spleens, where Treg-levels remained unchanged over the treatment period.

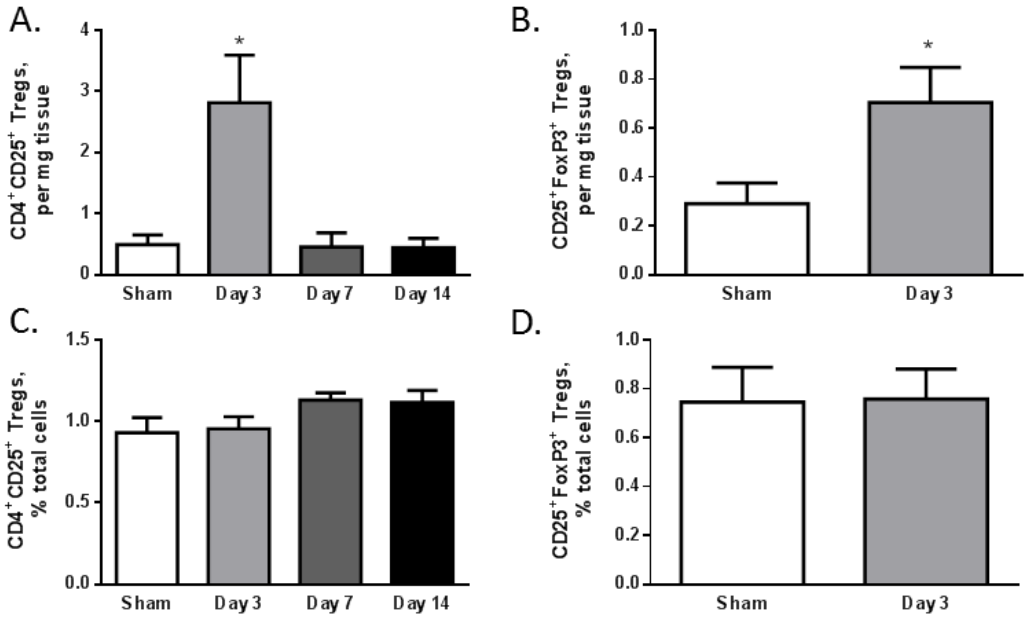

Figure 3-10: Influx of regulatory T-cells in response to AngII treatment. *Increase in cardiac* ***(A)*** *$CD4^+CD25^+$ Tregs and* ***(B)*** *$CD4^+CD25^+FoxP3^+$ Tregs (N=9 per group).* ***(C&D)*** *Splenic levels of Tregs do not differ in response to AngII. Cardiac samples represented as cells per mg of heart tissue; splenic samples represented as a percentage of total cells. All samples acquired on BD FACS CantoII™, *p<0.05, N=5-12 per group.*

Cardiac infiltration of T-cells and Tregs, after 3-days of treatment, was verified by qPCR analysis of mRNA levels (*Figure 3-11*). CD3 (p=0.006), CD25 (p=0.001) and FoxP3 (p <0.001) mRNA levels significantly increased after 3-days of AngII treatment. The Treg-specific cytokine, IL-10 (p=0.025) was also increased after 3-days of AngII. Quantification of Treg-specific surface markers that aid Treg function[176-178], showed a significant increase for CD73 (p=0.032), CD39 (p=0.025) and CTLA-4 (p=0.027) whereas GITR remained the same between sham and AngII treated samples. These data further

corroborate our findings using flow cytometry. NRP, a marker identifying thymus-derived natural Tregs[179,180], was similar between sham and AngII treated samples.

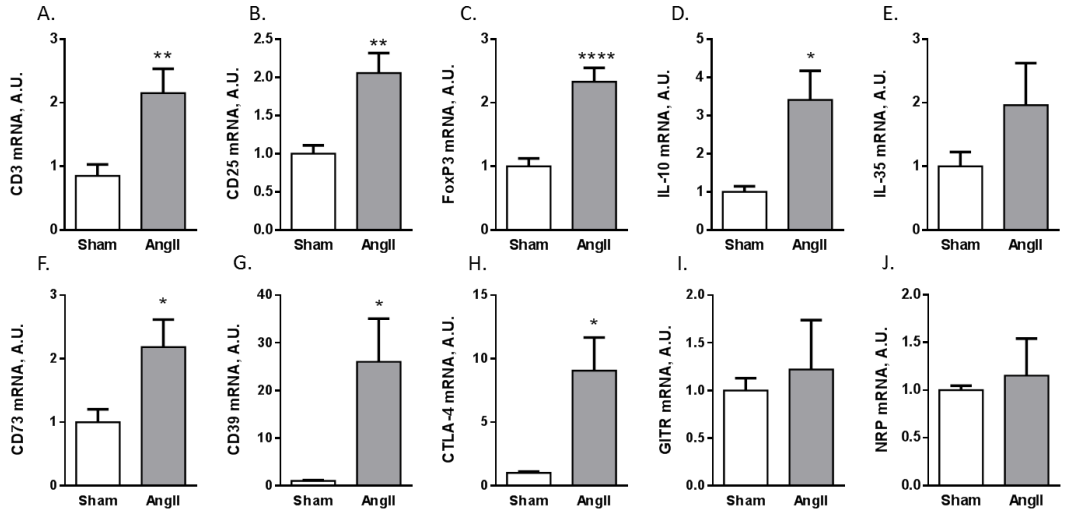

Figure 3-11: AngII increased levels of immune cell mRNA markers. *Quantification of* ***(A)*** *CD3,* ***(B)*** *CD25,* ***(C)*** *FoxP3,* ***(D)*** *IL-10,* ***(E)*** *IL-35,* ***(F)*** *CD73,* ***(G)*** *CD39,* ***(H)*** *CTLA-4,* ***(I)*** *GITR and* ***(J)*** *NRP mRNA levels by qPCR also support Treg infiltration.*p<0.05, **p<0.01, ****p<0.0001, N=8-9 per group.*

Due to increases in total leukocytes, T-cells, $CD4^+$ T-cells and Tregs, analysis of cell populations as a percentage of their parent population was necessary to investigate changes in cell ratios. For example, Tregs as a percentage of $CD4^+$ T-cells were analysed. *Figure 3-12* demonstrates that even though there are increases in each of these individual cell types with AngII treatment, the proportion of cells and balance between subpopulations is unaltered.

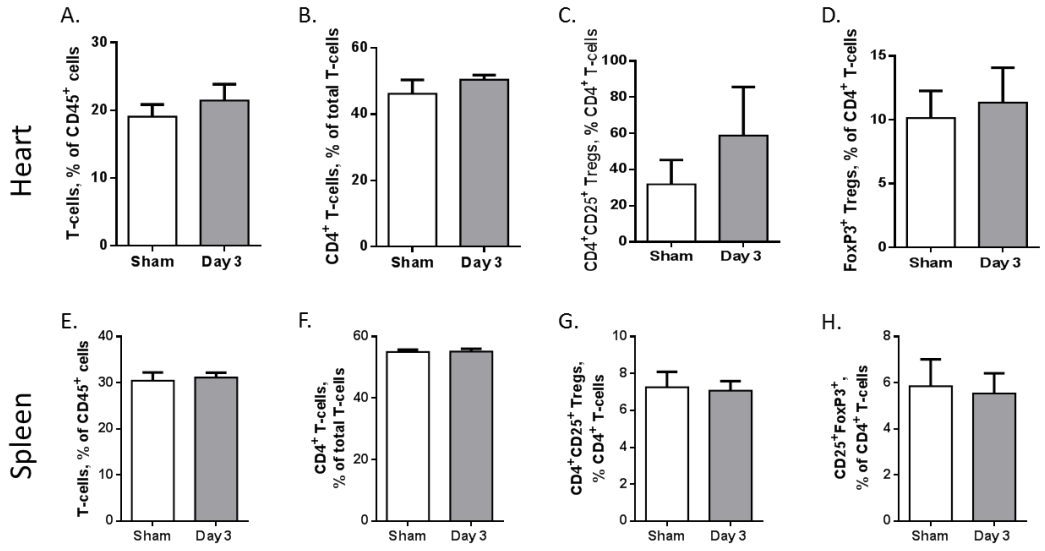

Figure 3-12: AngII effect on immune cell proportions. *For both* ***(A-D)*** *heart and* ***(E-F)*** *spleen samples* ***(A&E)*** *T-cells as a percentage of CD45$^+$ cells,* ***(B&F)*** *CD4+ T-cells as a percentage of total T-cells,* ***(C&G)*** *CD4$^+$CD25$^+$ Tregs as a percentage of CD4$^+$ T-cells and* ***(D&H)*** *CD4$^+$CD25$^+$FoxP3$^+$ Tregs as a percentage of CD4$^+$ T-cells all remain stable with AngII treatment. N=12 per group.*

In order to assess factors that might promote the migration of Tregs to AngII treated hearts after 3-days, mRNA levels of associated chemokines and their receptors were investigated (*Figure 3-13*). After 3-days of AngII treatment, CCL1 tended to increase, with a significant increase in its chemokine receptor CCR8 (p=0.041). A marked rise in CCL17 (p=0.025), CCL22 (p=0.042) and their chemokine receptor CCR4 (p=0.048) also suggests Treg migration to the heart[181,182]. Similarly, significant increases in cMet (p=0.022), STAT-3 (p=0.021) and CXCR3 (p=0.051), recently found to be involved in recruitment of T-cells to the heart[183] (*Figure 3-13*), further support these findings.

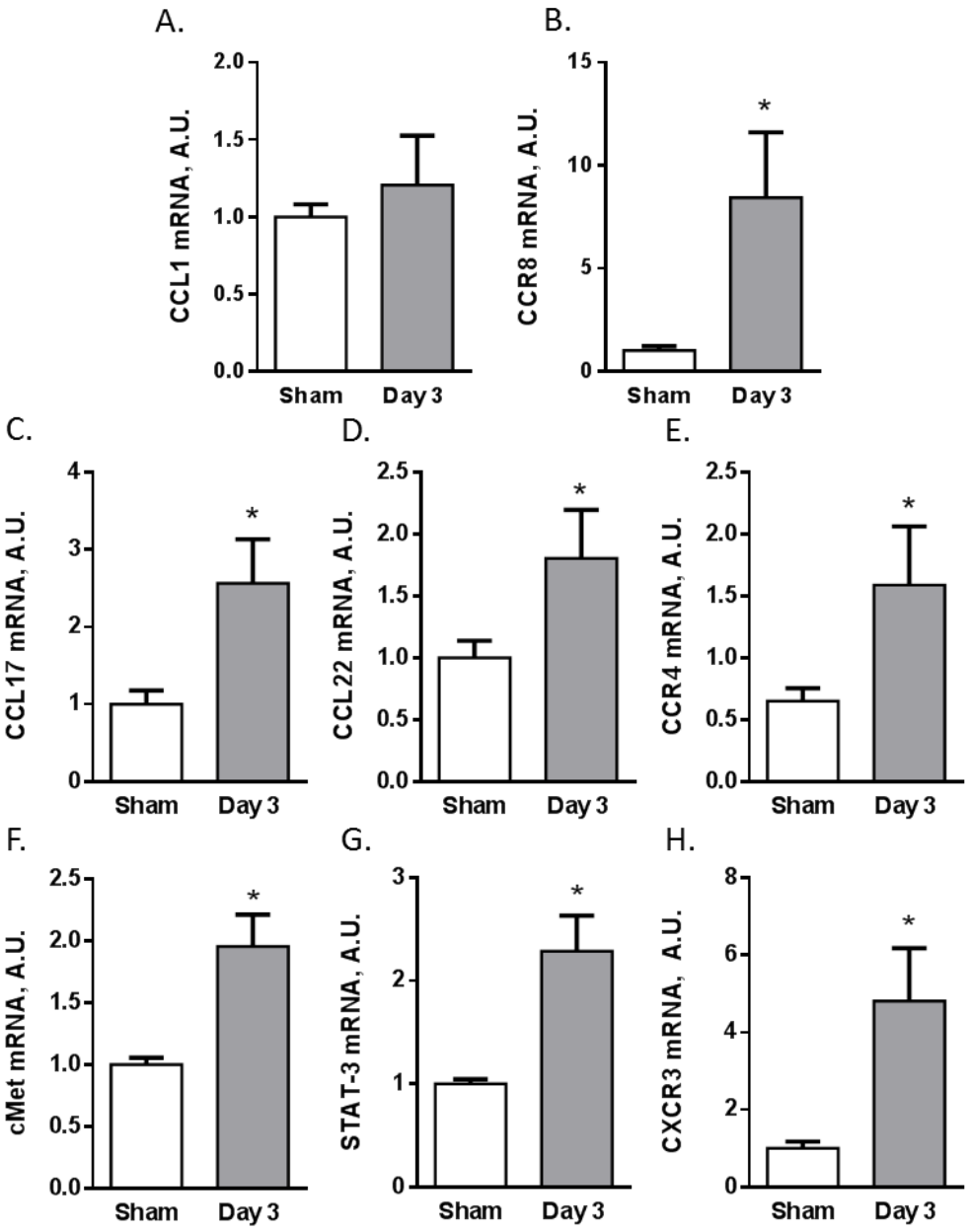

Figure 3-13: AngII treatment increases levels of cardiac-specific chemokines. *After 3-days of AngII treatment* **(A)** *CCL1 tends to increase,* **(B)** *CCR8,* **(C)** *CCL17,* **(D)** *CCL22,* **(E)** *CCR4,* **(F)** *cMet,* **(G)** *STAT-3 and* **(H)** *CXCR3 significantly increase. *p<0.05, N=6-10 per group.*

3.5 Discussion

AngII is extensively used to induce hypertension in murine models. In this study, the efficacy of the agent in initiating both hypertension and subsequent cardiac remodelling in C57Bl/6 mice was verified. In our hands, treatment with AngII led to hypertension as well as cardiomyocyte hypertrophy and interstitial fibrosis, in a time-dependant manner, confirming previous published reports[83, 134].

The novelty of this study was to investigate immune cell infiltration in the heart during treatment with AngII. An important finding within this study is that AngII induces cardiac inflammation in a time-dependent manner. Initial infiltration within the myocardium occurs around the vessels, which is the point of entry, but as treatment continues inflammatory cells are dispersed throughout the tissue. This diffusion of inflammatory cells within the myocardium may be a mechanism that impacts on cardiac remodelling processes, in particular fibrosis. Furthermore the type of immune cells infiltrating the myocardium during AngII treatment was pin pointed towards T-cells.

Until now, other groups have concentrated on the repercussion of hypertension on the vasculature, with a focus on inflammation[134,146,148,167]. Guzik et al observed an infiltration of T-cells within the aorta in response to AngII and carefully characterised the T-cell subsets involved in this particular tissue[134]. Interestingly, the heart seams to respond to AngII in a similar fashion, as highlighted by a major increase in T-cells. The time-course of leukocyte infiltration during AngII treatment was also investigated and revealed a peak after 3-days of AngII infusion. Within the aorta, the same authors identified that all subpopulations were affected by AngII treatment, with a significant increase in DN ($CD4^-CD8^-$) and $CD4^+$ T-cells. This group chose to concentrate on DN T-cells as this cell type increased seven-fold in the aorta during AngII treatment.

Similar to Guzik et al in the vasculature, we showed an increase in all T-cell subtypes, including DN T-cells in the heart. However, the other T-cell subtypes investigated were affected to a greater extent by AngII treatment.

Using specific KO models Laroumanie et al demonstrated that $CD4^+$, but not $CD8^+$, T-cells were associated with cardiovascular remodelling after TAC[184]. This therefore

highlights the impact of $CD4^+$ T-cells within the setting of cardiac remodelling. Here, the profile of both $CD8^+$ and $CD4^+$ T-cells in the heart were affected by AngII, with a significant increase after 3-days of treatment.

$CD4^+$ group encompasses a versatile subpopulation of T-cells. This is composed of pro-inflammatory Th cells, namely Th17, Th1 and Th2, in addition to anti-inflammatory Tregs. Interestingly, Th17 subsets of $CD4^+$ T-cells, which produce IL-17, are markedly increased in the aorta during AngII treatment[185]. $IL17^{-/-}$ mice treated with AngII displayed hypertension, which was not sustained for the duration of AngII treatment, preserved vascular function and decreased T-cell infiltration[185]. Cytokines produced by Th1 (IFN-γ, TNF-α and IL-2) and Th2 (IL-4, 6, 10, 13), have also been implicated in the setting of AngII induced cardiac remodelling. Both IFN-γ receptor and TNF receptor-1 KO mice treated with AngII exhibit reduced levels of cardiac hypertrophy, fibrosis and inflammation[186-188]. In comparison, Th2 cells may arise after the Th1 pro-inflammatory response and produce cytokines involved during the development of fibrosis such as IL-6, acting as a pro-fibrotic mechanism[188].

T-cell subtypes are difficult to analyse within the heart, especially at baseline, due to initial low numbers and further depletion caused by the treatment of tissues required for flow cytometry. Therefore, until more sensitive techniques are established, pooling heart samples or even analysing immune-cells within the LNs draining the heart may provide further detail into immune cell recruitment. This could enable more in-depth analysis of Th subpopulations, associated cytokines and chemokines.

Here, a two-phase response in T-cell infiltration was observed, characterised by an initial increase at day 3, followed by a decrease in cell number on day 7. The observed decrease in T-cells within the heart could be linked to the expression of anti-inflammatory factors. Therefore, by concentrating on anti-inflammatory T-cells, which could be responsible for this phenomenon, potential therapeutic targets may be identified. Within the $CD4^+$ T-cell subset, results show the level of Tregs ($CD4^+CD25^+FoxP3^+$) significantly increased after 3-days of AngII treatment. This was validated by a marked increase in mRNA expression in the Treg transcription factor, FoxP3, in addition to Treg cytokines (IL-10 and IL-35) and functional surface makers (CD25, CD73, CD39, CTLA-4, GITR) 3-days after treatment. These results demonstrate a

clear infiltration of Tregs within the myocardium during AngII treatment, as supported by a number of published papers[189-193].

Tregs have been implicated in the pathophysiology of AngII-induced hypertension and vascular injury. Barhoumi et al highlighted the protective effects of Tregs by performing an adoptive transfer of these cells followed by AngII treatment for 14-days[190]. Treg ($CD4^+CD25^+$) adoptive transfer blunted the pathological effects induced by AngII compared to vehicle or Teff cells ($CD4^+CD25^-$)[190]. This included attenuation of AngII-induced Nox activity[190]. A similar response was observed with the adoptive transfer of Tregs into mice later treated with aldosterone[192].

Komarowska et al studied T-cell migration to cardiac allografts and highlighted specific chemokines that promote recruitment to the heart[183]. The hepatocyte growth factor (HGF) receptor (cMet), CCR4, and CXCR3 were identified as important cardiac-recruitment factors for T-cells[183]. In addition, other studies investigating Treg recruitment to cardiac allografts highlighted CCR4 and CCR8 to be important chemokine receptors involved in this process[182]. Our results fall in line with these findings, as the T-cell and Treg increase observed here was accompanied by increased mRNA expression of cMet, CCR4, CCR8, STAT-3 and CXCR3. In addition to chemokine receptors, increases in associated ligands (CCL1, CCL17 and CCL22) were also observed.

These data suggest that Tregs might be involved in cardiac remodelling associated with experimental hypertension. Hence the infiltration of Tregs during AngII treatment, observed in the present study, may support this further. The initial influx of Tregs observed within the heart may be an attempt to supress inflammation. The percentage of Tregs reduces to baseline after 7-days and hence this may allow the inflammatory response of other T-cell subtypes to resume, aiding the progression of cardiac remodelling. The un-sustained Treg level could potentially lead to the later attenuation of T-cell infiltration in the heart.

Overall, the data presented in this chapter confirm the involvement of AngII in both cardiovascular remodelling and inflammation. T-cells, specifically $CD4^+$ T-cells and Tregs, may potentially play an important role in this setting in a time-dependent manner. ROS have been implicated in the AngII response both within cardiovascular remodelling and inflammation. The role of Nox2 within cardiomyocytes and

endothelial cells has been well established in the setting of AngII-induced cardiac remodelling, but its specific role in infiltrating immune cells in this setting requires further investigation. This is addressed in the next chapter.

Chapter 4: The response of global Nox2KO mice to chronic angiotensin II infusion

4.1 Introduction

Previous research has implicated Nox2 in AngII-induced cardiovascular remodelling[42]. Nox2 is involved in intracellular signalling pathways that modulate cardiac hypertrophy, fibrosis, apoptosis and contractile dysfunction. As discussed in section 1.6, a number of studies where Nox2 levels are depleted demonstrate an attenuated response to RAAS overstimulation. Furthermore, Nox2 has also been identified in the modulation of hypertensive signalling as discussed in section 1.8.

4.1.1 Role of Nox2 in AngII-induced inflammatory response

Nox2 is the main source of ROS within immune cells, and a number of different aspects within the immune system require Nox2[194]. The importance of Nox2 in immunity is clearly highlighted in cases of chronic granulomatous disease (CGD) where patients suffer from severe and recurrent bacterial and fungal infections. This is due to a deficiency in their innate immune response, which is potentially related to a defect in neutrophil phagocytic function[195]. Furthermore, CGD patients with a Nox2 deficiency display an increase in inflammatory genes encoding inflammatory mediators such as CD11b, CD14, CD54, TLR5, CCR1 and many more, which prolong inflammation[196]. In addition, during a phagocytic response, there is a lack of pro-apoptotic proteins such as Bcl-associated X protein synthesis (BAX), leading to defective apoptosis after phagocytosis that may delay resolution during an inflammatory response to infection[196]. Furthermore, CGD patients have an increased prevalence of concurrent autoimmune diseases[194].

Nox2-derived ROS are implicated in different cellular signalling pathways affecting proliferation, differentiation and/or activation of different immune cells. They are also involved in chemotaxis[194], microbicidal activity within phagocytes[17,42] and antigen presentation by DCs[197].

Mice in which $p47^{phox}$ has been knocked-out presented more severe arthritis that is blunted in the presence of Nox2 pharmacological activators[198]. These models also express a higher autoimmune phenotype, suggesting a role for Nox2 in regulating autoimmunity and certain cases of inflammation[194]. Furthermore Nox2KO mice

develop spontaneous age-related arthritis as well as displaying an altered $CD4^+$ T-cell profile, with a tendency towards a Th17 phenotype in the periphery[199].

However, the role of Nox2 within immunity is still not fully understood. The capability of Nox2-derived ROS to enable communication and interaction of different components of the immune system is extensive, and the implication of this in inflammation related to CVD requires further investigation.

4.1.1.1 Nox2 within innate and adaptive immunity

Nox2 was initially identified in immune cells during the phagocytic respiratory burst. This process occurs in the neutrophil phagosome, where ingested pathogens are killed by a rapid increase in Nox2-derived ROS. ROS can directly damage pathogens and produce optimal conditions for neutrophil proteases to function, pH ~6.5-7[200]. ROS have also been implicated in neutrophil chemotaxis; both the direct inhibition of Nox2 or absence of the gene impairs neutrophil chemotaxis[194].

In a similar way to neutrophils, Nox2 provides an oxidative burst to enable digestion of pathogens in the macrophage phagosome. This requires a lower pH (4-5) than neutrophils, which is specific for the activation of the macrophage proteases[200].

Nox2-derived ROS production is implicated in intracellular signalling that can mediate inflammatory responses. Within macrophages, NF-κB activation is critical in the production of cytokines, chemokines and adhesion genes that are essential for the inflammatory response, and ROS have a function in this setting[201]. Recent published data has shown that ROS production is essential for macrophage differentiation (into M1 or M2 cells)[202]. Inhibition of $O_2^{\bullet-}$ production prevents differentiation of monocytes into M2 cells[202]. In this setting, $O_2^{\bullet-}$ was shown to be essential for biphasic ERK activation that is involved in macrophage differentiation[202].

Nox2 has also been implicated in the cellular migration of macrophages in response to CSF-1, a common tissue chemo-attractant[203]. Nox2KO bone-marrow derived macrophages did not display a chemotactic response to a source of CSF-1, and showed a reduced level of ERK1/2 phosphorylation after CSF-1 stimulation[203]. Nox2 regulation

of NF-κB activation also impacts the expression of other chemokines, such as MCP-1 and CCR2, which are key components in macrophage recruitment[158,165,194].

DCs express Nox2 to a lesser extent compared to macrophages; however Nox2-derived ROS still have important roles within this cell type. Human DCs show a requirement for Nox2 activity to aid antigen cross-presentation[204]. Nox2KO mice produce an increased level of acidification within the phagosome of DCs. This causes a higher level of protein degradation, hence impairing antigen cross-presentation to cells of the adaptive immune system[204,205]. Therefore Nox2 is thought to contribute towards alkalinisation in DCs in order to mediate an efficient level of protein degradation for antigen presentation to occur[204,206]. Furthermore, Nox2 in DCs has been linked to cytokine production; Nox2KO DCs express a higher level of cytokines compared to WT controls[207]. Lack of Nox2 also prevents apoptosis so cells have higher viability, enabling a higher production of TNFα in addition to promoting IFNγ production from T-cells and encouraging differentiation into Th1 cells[207]. Moreover, Nox2KO DCs tend to be less mature, expressing lower levels of CD83, the maturation marker and CD86, the DC costimulatory marker[207].

Within B-cells, stimulation of the BCR results in a significant production of ROS, with initial generation being dependent on Nox2[208]. Deletion of Nox2 does not impair BCR signalling or B-cell activation and these cells elicit a normal, if not enhanced response[208]. The later generation of ROS, thought to be of mitochondrial origin, has a more pertinent role. Treatment of B-cells with a ROS scavenger, N-acetylcysteine (NAC), abrogated BCR-dependent PI3K signalling and altered successive activation and proliferation of B-cells[208]. In this case the presence of Nox2-derived ROS does not seem to function to enhance the B-cell response; however other sources of ROS are important in this setting.

Endogenous Nox2 within macrophages and DCs has the ability to alter T-cell activation, proliferation and even orchestrate the type of adaptive immune response. However, intrinsic expression of Nox2 in T-cells may also direct T-cell polarisation and cytokine production, discussed in more detail in section 4.5.

4.2 Aims and objectives

Nox2 has a great impact on a variety of cells within the cardiovascular system that are reflected in its ability to modulate cardiovascular remodelling in response to AngII. The effects of Nox2 on individual immune cells is apparent, however the specific role of T-cell Nox2 in the setting of AngII-induced cardiac pathophysiology has not been studied.

The aim of the studies in this chapter was to define the overall impact of Nox2 on immune cell infiltration into the heart during chronic RAAS activation, using studies in global Nox2KO mice.

4.3 Methods

4.3.1 Maintenance of global Nox2KO line

Male Nox2KO mice were bred on a C57Bl/6 background at our institution[209]. Heterozygous females were crossed with C57Bl/6 (Harlan UK limited) males, or C57Bl/6 females (Harlan UK limited) were crossed with $gp91^{-/-}$ males to generate homozygous $gp91^{-/-}$ (Nox2KO) male mice and WT littermate controls. Nox2KO mice, WT littermates and C57Bl/6 mice were used for experiments between 6-8 weeks of age.

4.3.2 Global Nox2KO genoyping

Ear biopsies were treated with 300µL of 50mM sodium hydroxide (NaOH) at 95°C for 30 minutes. Samples were vortexed to homogenise and 25µL 1M Tris-HCl (pH 8.0) added and incubated at room temperature for 30 minutes. Next, 2µL of sample (~56ng/µL) was added to 23µL of the PCR master mix (*Figure 4-1*), where primers are shown in *Table 10*. All samples were run alongside a no-template sample and known WT and Nox2KO samples on the PCR cycle shown in *Figure 4-1*.

Component	Amount per sample (µl)
RedTaq	12.5
Gp91-F1 (2µM)	0.5
Gp91-F2 (2µM)	0.5
Gp91-R (2µM)	1.0
Dnase-free water	8

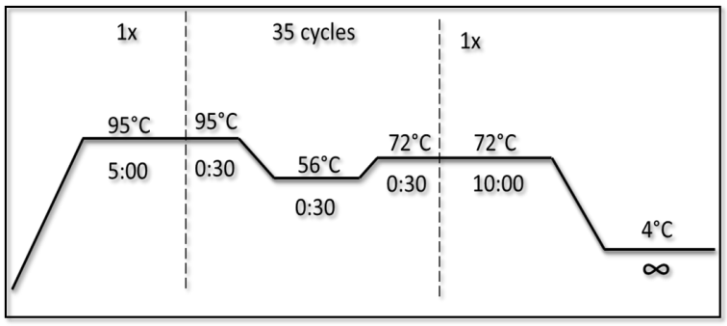

Figure 4-1: Gp91 genotyping PCR Cycle.

Samples (20µL) were then run on a 2% agarose gel (150mL 1 x TAE (Tris base, acetic acid and EDTA) and 3g agarose) infused with ethidium bromide (0.5µL/mL) at 180v for 30 minutes. The gel was then photographed under ultraviolet (UV) light using a transluminator machine. *Figure 4-2* shows the identification of global Nox2KO animals (e.g. 1812-1820) that have a lower band (~200bp) compared to WT littermates (e.g. 1825, 1827-1828), which display a higher band (~300bp) and heterozygotes express a double band (e.g. 1821- 1824).

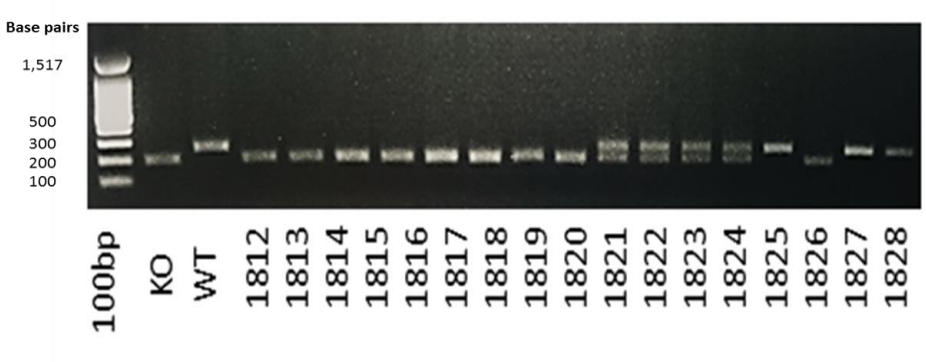

Figure 4-2: Nox2 (Gp91) genotyping example.

Gene of interest	Primer name	Primer sequence
GP91 -F	IMR0517	AAGAGAAACTCCTCTGCTGTGAA
GP91 -F	IMR0518	CGCACTGGAACCCCTGAGAAAGG
GP91 -R	IMR0519	GTTCTAATTCCATCAGAAGCTTATCG

Table 10: Genotyping Primer sequences.

4.3.3 Experimental model

Male Nox2KO mice ages 6-8 weeks were bred at our institution and used for experiments in this chapter along with WT littermate controls. Subcutaneous mini-osmotic pumps containing a pressor dose of AngII (1.1mg/kg/day) were surgically implanted into mice for up to 14-days, as described in section 2.3. Blood pressure and haemodynamic function were analysed by tail cuff plethysmography and echocardiography respectively (section 2.5). A second group of mice were also treated with a pressor dose of AngII for 3-days, before organs were harvested for flow cytometry.

4.3.4 Treatment of samples

Whole hearts were harvested and treated as described in section 2.4.1, RNA extraction and reverse transcription was performed as described in section 2.7 to enable analysis of fibrosis-related markers by qPCR. Histological analysis involved staining of harvested hearts for WGA and PSR (section 2.8).

Immune cell quantification was performed on whole hearts and spleens by flow cytometry using BD FACS CantoII™ as described in section 2.6. The level of leukocytes, T-cells and T-cell subsets were determined based on expression of CD45, TCRβ, CD4, CD8, CD25 and FoxP3.

4.4 Results

4.4.1 Global Nox2KO mice have a blunted response to AngII

4.4.1.1 Physiological responses to AngII

We confirmed the efficacy of AngII in inducing hypertension in both naive C57Bl/6 mice and the C57Bl/6 WT littermates of Nox2KO animals (*Figure 4-3*). Unlike these groups, the Nox2KO animals did not exhibit a significant increase in blood pressure when treated with AngII for 14-days ($p<0.001$). These data confirm results found in previous studies[108,175]. HW/BW and HW/TL tended to be lower in Nox2KO animals

compared to WT littermates and C57Bl/6 mice following AngII treatment for 14-days, however this was not significant.

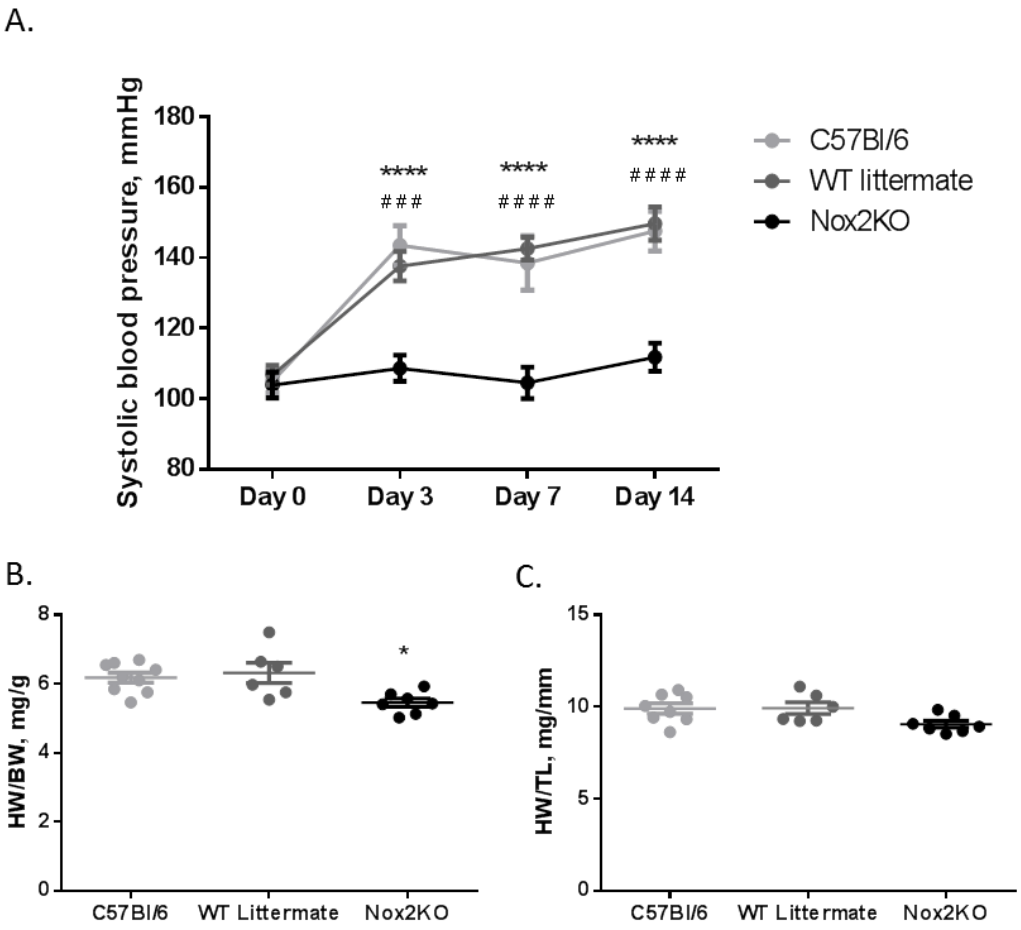

Figure 4-3: Blunted AngII response in Nox2KO model. *Global Nox2KO response to AngII analysed by* ***(A)*** *systolic blood pressure,* ***(B)*** *HW/BW,* ***(C)*** *HW/TL. *Nox2KO vs. C57Bl/6. # Nox2KO vs. WT littermates. *p<0.05, ***p<0.001, ****p<0.0001, N=6-9 per group.*

WGA staining was performed on paraffin sections from Nox2KO mice and WT littermate controls treated for 14-days with AngII. WGA revealed that Nox2KO treated animals had a significantly smaller cardiomyocyte cross-sectional area (p=0.001) compared to WT littermates treated with AngII, consistent with previous data[108]. This can clearly be observed in *Figure 4-4*, where representative images display smaller cardiomyocytes within Nox2KO treated groups with a cross-section of 245±13.8μm^2

compared to 396±13.4μm^2 observed for WT littermate samples. Previous published data report no difference at baseline between WT and Nox2KO mice[108,210].

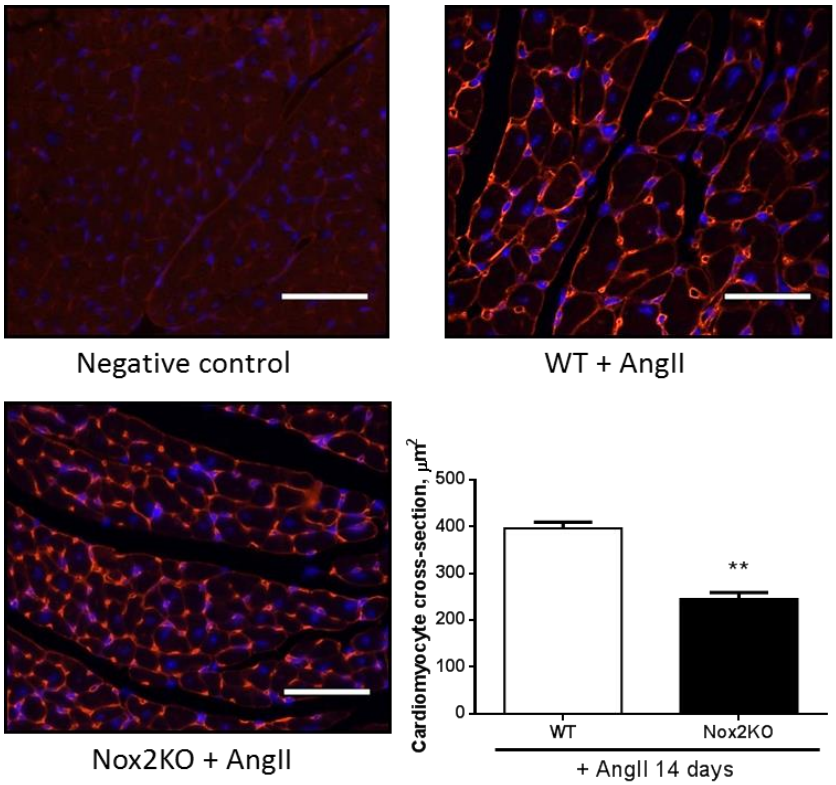

Figure 4-4: Nox2KO prevents AngII-induced cardiomyocyte hypertrophy. *WGA staining to analyse cardiomyocyte cross-section for Nox2KO and WT littermate animals. Scale bar represents 25μm, **p<0.01, N=8 per group.*

Paraffin sections stained with PSR (*Figure 4-5*) highlighted a high percentage of interstitial collagen within WT littermate controls treated with AngII, which was attenuated in Nox2KO treated animals (p <0.0001). The percentage of collagen reduces from 2.64±0.36% in WT littermates to 0.24±0.05% in Nox2KO animals. This was verified by analysis of mRNA levels of fibrotic markers via qPCR, as shown in *Figure 4-6*. After AngII treatment Nox2KO mice had significantly lower mRNA levels of col1α1 (p=0.029), col3α1 (p=0.004) and TGFβ (p=0.023) further confirming blunted levels of interstitial fibrosis, consistent with published reports[175]. Fibronectin and cTGF mRNA levels were similar between Nox2KO and WT animals. No differences were observed in collagen deposition between WT and Nox2KO mice at baseline[175].

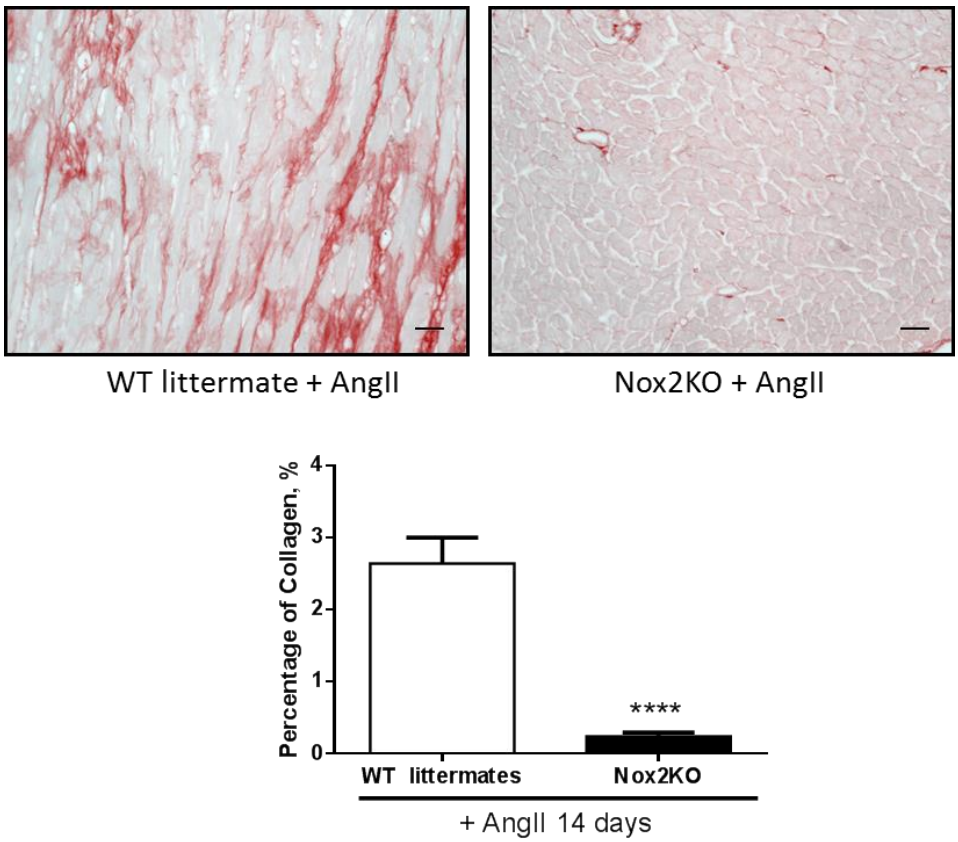

Figure 4-5: ***Global Nox2KO blunts AngII-induced fibrosis.*** *Picrosirus red staining for Nox2KO and WT littermate animals. ****p<0.0001, N=8 per group.*

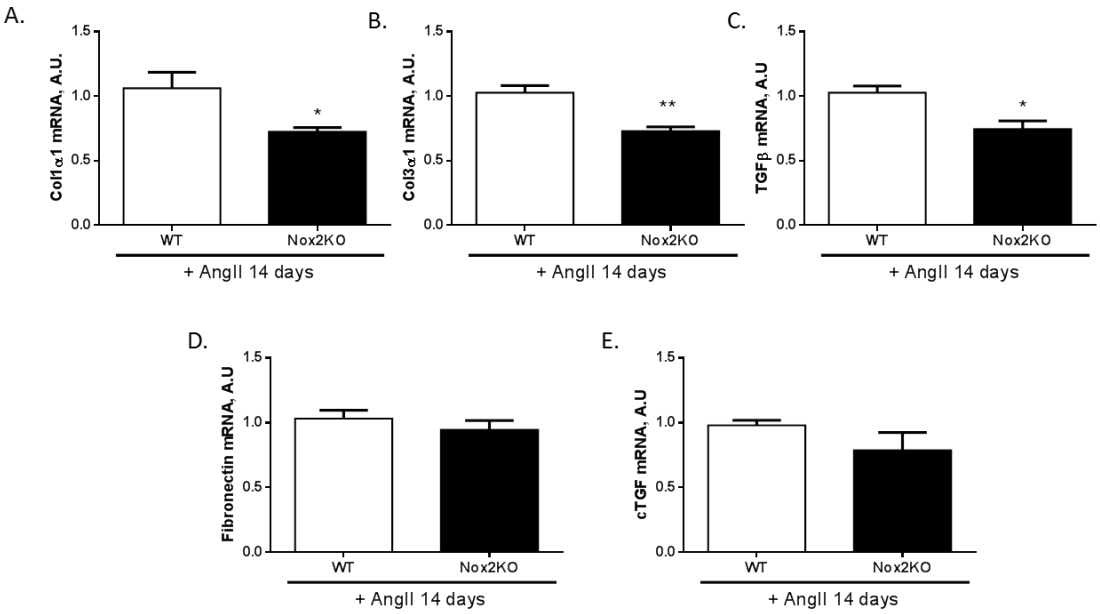

Figure 4-6: Marked decrease in mRNA levels of pro-fibrotic-markers. *Quantitative PCR analysis of pro-fibrotic markers* ***(A)*** *collagen1α1,* ***(B)*** *collagen3α1,* ***(C)*** *TGFβ,* ***(D)*** *fibronectin and* ***(E)*** *cTGF.*p<0.05, **p<0.01, N=8 per group.*

Here, the lack of Nox2 prevents AngII-induced hypertension, cardiomyocyte hypertrophy and interstitial fibrosis, in line with previous published results[25].

4.4.1.2 Altered composition of cardiac-resident T-cells

Global Nox2KO animals at baseline presented no evidence of infection, both clinically and during routine screening for pathogens (appendix), but had enlarged lymphoid organs. *Figure 4-7* shows that the LNs (142% bigger, p=0.025), spleen (21% bigger, p=0.008) and thymus (34% bigger, p=0.043) are larger in Nox2KO, compared to WT littermate mice. This suggests they may also have an altered immune cell composition at baseline and a potentially altered inflammatory response[199]. Hearts were a similar size between the Nox2KO and WT littermates (*Figure 4-8*).

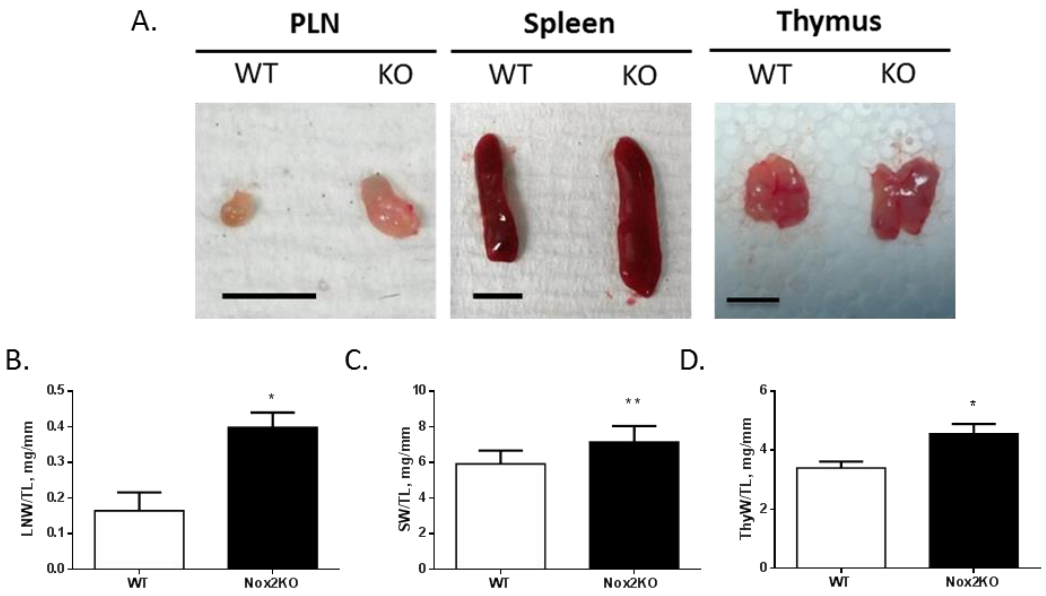

Figure 4-7: Enlarged lymphoid organs in Nox2KO animals at baseline. (A) *Images of freshly harvested lymphoid organs and analysed by* ***(B)*** *lymph node weight-to-tibia length (LNW/TL),* ***(C)*** *spleen weight-to-tibia length (SW/TL) and* ***(D)*** *thymus weight-to-tibia length (ThyW/TL) ratios. Scale bar represents 0.5cm. *p<0.05, **p<0.01, N=6-10 per group.*

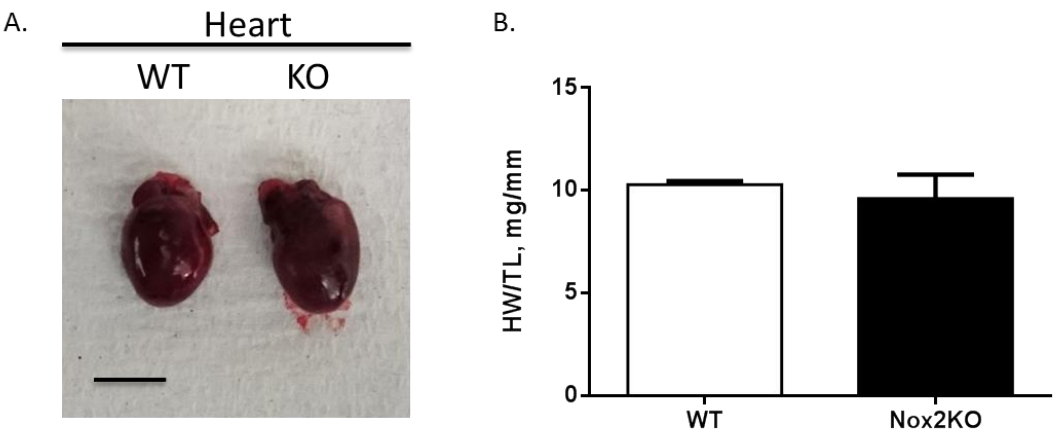

Figure 4-8: Heart weights are the same in Nox2KO compared to WT littermates. (A) *Images of freshly harvested hearts and analysed by* ***(B)*** *heart weight-to-tibia length (HW/TL) ratios. Scale bar represents 0.5cm. N=3 per group.*

Flow cytometry was used to quantify the basal levels of cardiac immune cells, using spleen samples as a control. Within the heart, global Nox2KO mice had a significantly higher level of total leukocytes, T-cells and T-cell subpopulations at baseline as illustrated in *Figure 4-9*, where cells are represented by dots.

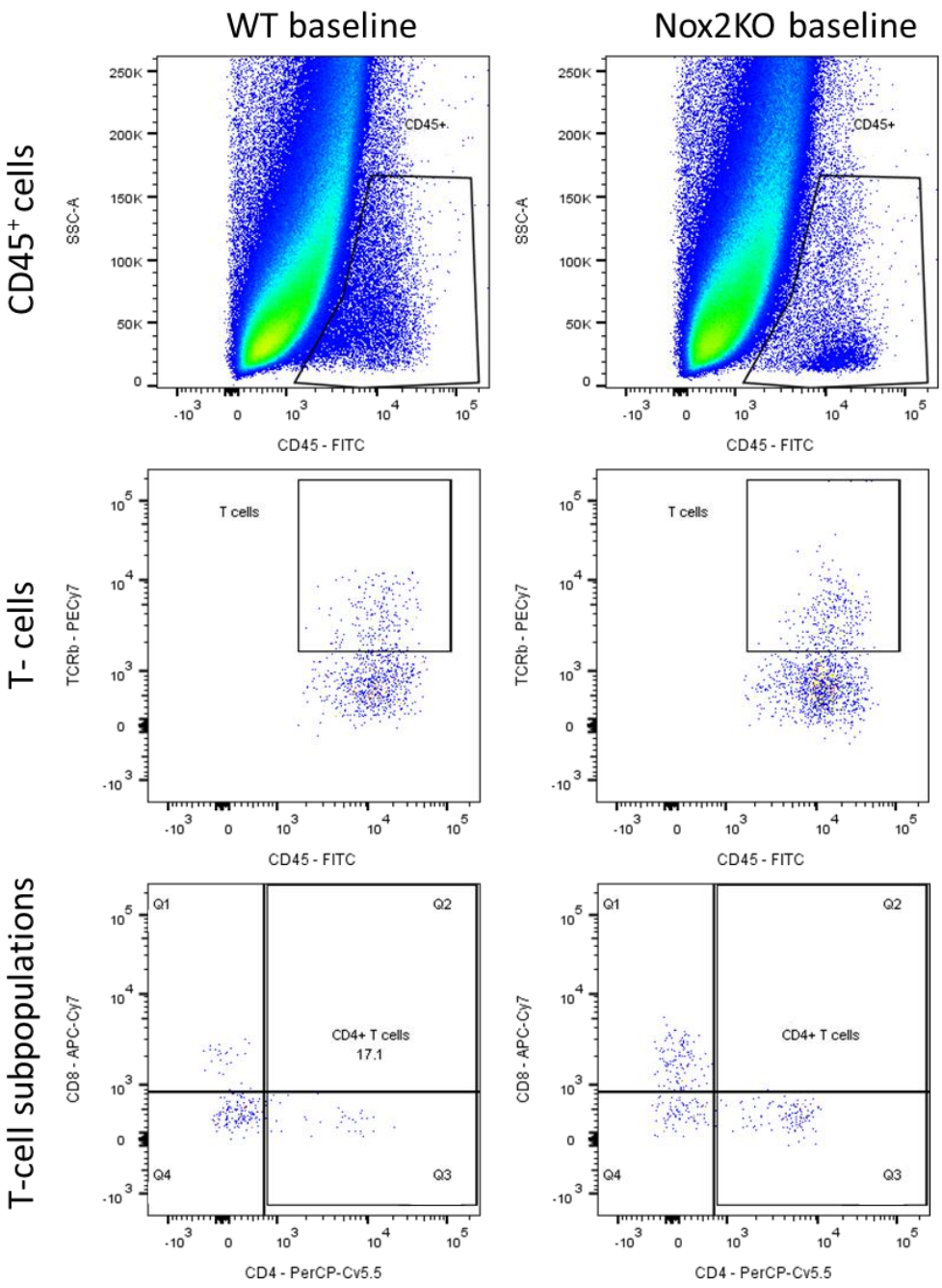

Figure 4-9: Higher levels of cardiac-resident immune cells in Nox2KO mice. *Representative dot plots show an increased level of immune cells in the heart at baseline. Analysed on BD FACS CantoII™.*

Quantitative analysis highlighted an increase of 130% in total leukocytes (p=0.0001, $CD45^+$ cells), of which T-cells (p=0.006, $CD45^+TCR\beta^+$) also showed a marked increase from 10.2±1.67 cells/mg in WT littermates compared to 18.8±1.99 cells/mg in Nox2KO hearts (*Figure 4-10*). T-cell subpopulations were also altered by the lack of Nox2 at

baseline with a significant increase in $CD8^+$ (p=0.003) and $CD4^+$ T-cells (p = 0.005), both being two-fold higher in Nox2KO compared to WT littermate.

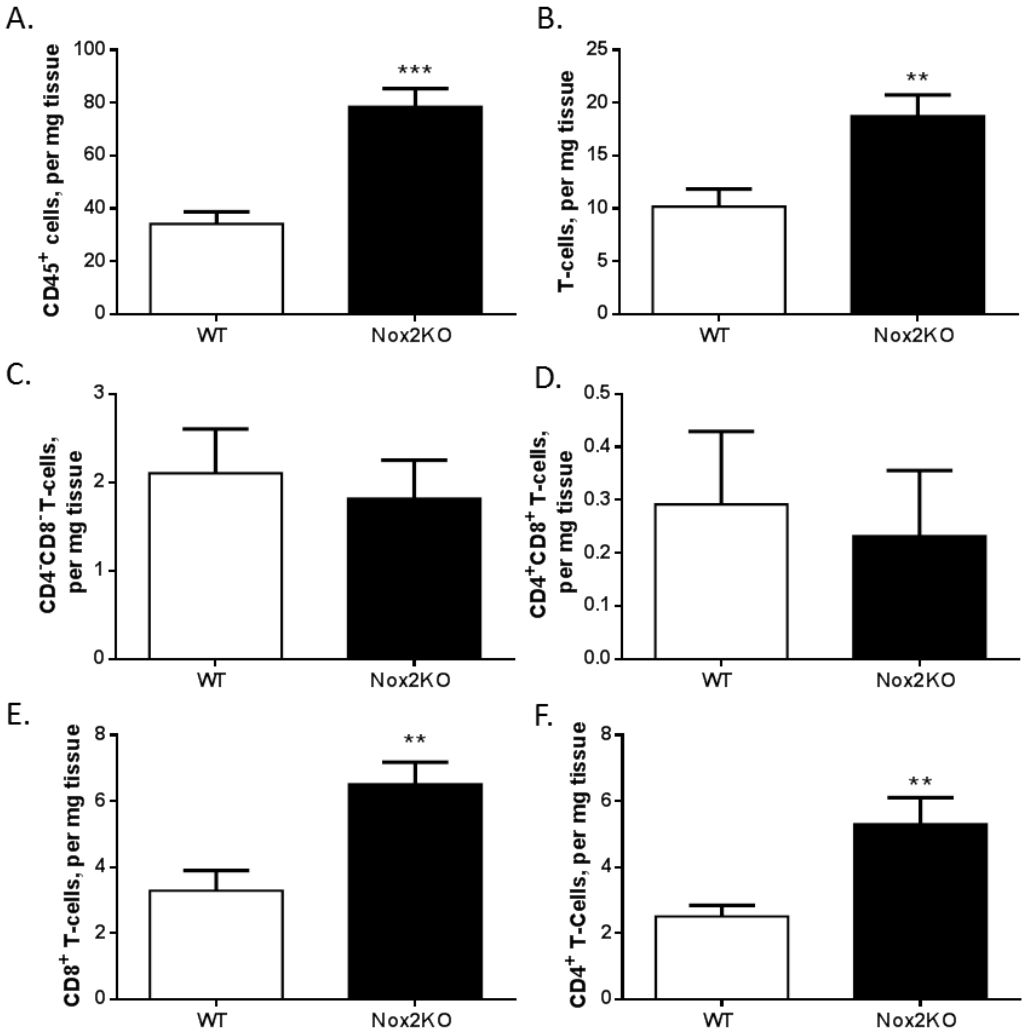

Figure 4-10: Altered levels of cardiac-resident immune cells with Nox2 deficiency. *Baseline immune cell levels of* ***(A)*** *total leukocytes ($CD45^+$ cells),* ***(B)*** *T-cells ($CD45^+TCR\beta^+$ cells) and T-cell subpopulations* ***(C)*** *$CD4^-CD8^-$,* ***(D)*** *$CD4^+CD8^+$,* ***(E)*** *$CD8^+$ and* ***(F)*** *$CD4^+$ T-cells. All data represented as cells per mg of tissue, analysed on BD FACS CantoII™. **p<0.01, ***p<0.001, N=8-11.*

In comparison, the immune cell levels within the spleen remained similar between the WT littermates and Nox2KO mice, as shown in *Figure 4-11*. This was true for total leukocytes ($CD45^+$ cells), T-cells ($CD45^+TCR\beta^+$ cells) and each of the T-cell subpopulations ($CD4^-CD8^-$, $CD4^+CD8^+$, $CD8^+$ and $CD4^+$).

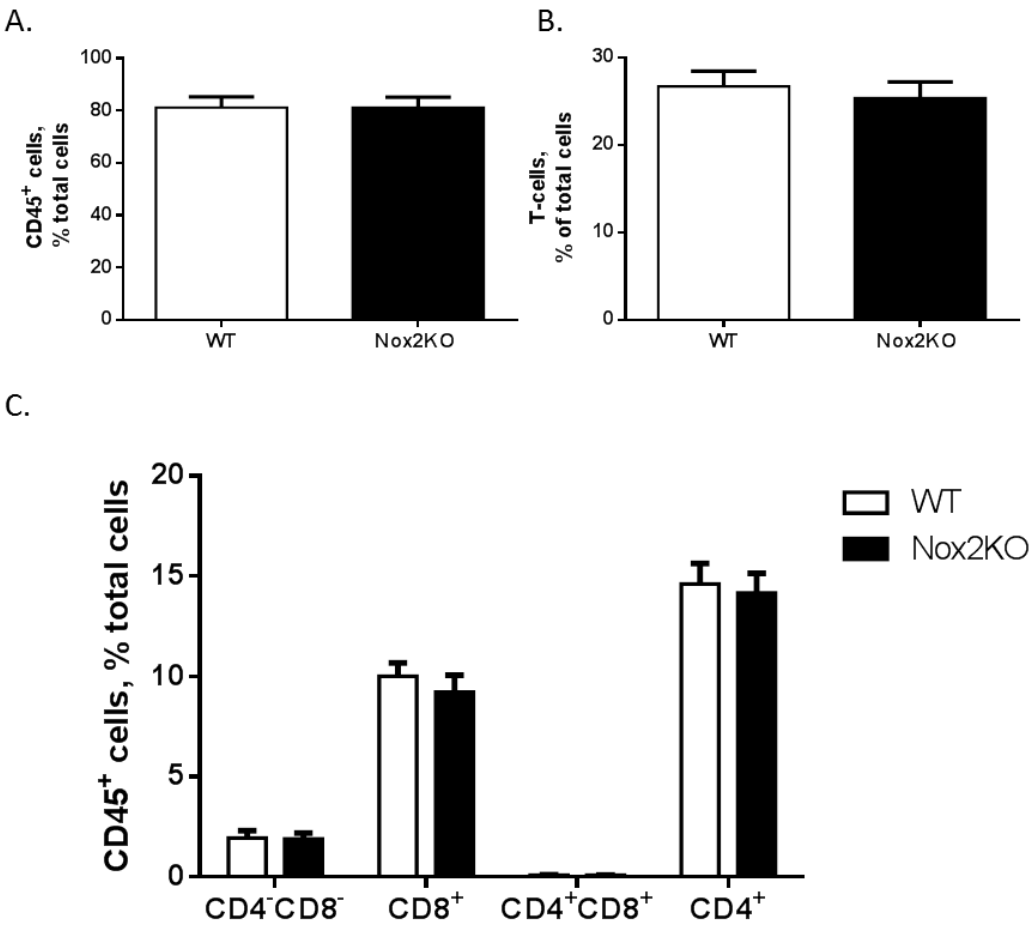

Figure 4-11: Immune cells within the spleen are comparable in Nox2KO. *(A) Total leukocytes (CD45$^+$ cells), (B) T-cells (CD45$^+$TCRβ$^+$ cells) and (C) T-cell subpopulations remain consistent between both genotypes. All data represented as a percentage of total cells, acquired on BD FACS CantoII™. N=8-11.*

Of the CD4$^+$ T-cell population observed within the heart, Tregs (p=0.042) were also significantly higher in the Nox2KO compared to WT littermate controls (*Figure 4-12*). Analysis showed that Nox2KO hearts contain about four times more Tregs compared to WT samples at baseline. However, the opposite was observed within the spleen, with a lower level of CD4$^+$CD25$^+$ Tregs (p=0.021) but similar levels of CD4$^+$CD25$^+$FoxP3$^+$ Tregs.

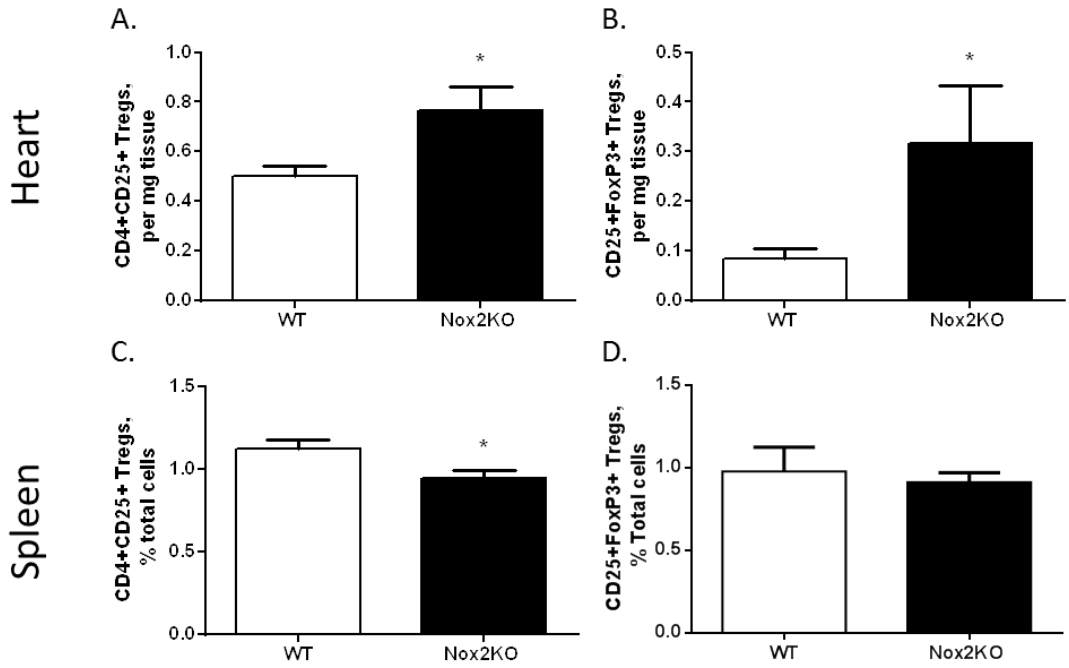

Figure 4-12: Cardiac and splenic Tregs at baseline may alter between WT and Nox2KO mice. *Analysis of cardiac immune cells by* ***(A)*** *$CD4^+CD25^+$ Tregs and* ***(B)*** *$CD25^+FoxP3^+$ Tregs suggest altered levels between the two genotypes. However, spleen levels of* ***(C)*** *$CD4^+CD25^+$ Tregs and* ***(D)*** *$CD25^+FoxP3^+$ Tregs respond differently. Cardiac samples represented as cells per mg of tissue; spleen samples represented as a percentage of total cells acquired. Analysed on BD FACS CantoII™. *p<0.05, N=8-11.*

To determine any differences in T-cell proportions, the percentages of parent populations were calculated (*Figure 4-13*). Looking at the heart samples, T-cells as a percentage of $CD45^+$ cells remained identical between the two groups, as did $CD4^+$ T-cells as a percentage of total T-cells. Meanwhile, $CD4^+CD25^+$ Tregs (p=0.034) and $CD25^+FoxP3^+$ Tregs (p=0.028), represented as a percentage of $CD4^+$ T-cells, were both significantly higher in the Nox2KO heart at baseline. In comparison all T-cell proportions within the spleen were equivalent between the two groups. This suggests that in Nox2KO hearts the ratio of Tregs to T-cells is higher than that in WT littermate controls. This higher ratio could potentially alter the immune-response as Tregs should be able to suppress inflammation.

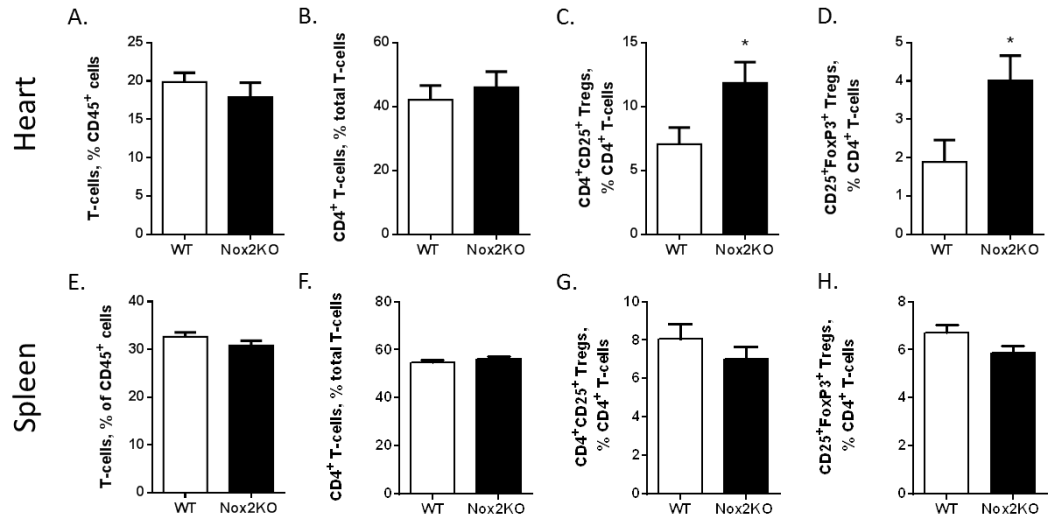

Figure 4-13: T-cell proportions in heart and spleen at baseline. (A&E) *T-cells as % of $CD45^+$ cells,* ***(B&F)*** *$CD4^+$ T-cells as a percentage of total T-cells,* ***(C&G)*** *$CD4^+CD25^+$ Tregs as a percentage of $CD4^+$ T-cells and* ***(D&H)*** *$CD25^+FoxP3^+$ Tregs as a percentage of $CD4^+$ T-cells. Analysed on BD FACS CantoII™.*p<0.05, N=8-11,*

4.4.1.3 Blunted AngII-induced infiltration of cardiac immune cells in Nox2KO mice

Next, the effect of AngII on immune cell infiltration in Nox2KO and WT littermate mice was studied. Single cell suspensions were prepared from hearts of mice that had received AngII by mini-osmotic pump (or a sham mini-osmotic pump) for 3-days, and were analysed using the CantoII™. Representative flow cytometry dot plots highlight lower infiltration of immune cells within Nox2KO animals compared to WT littermates (*Figure 4-14*). This was observed for total leukocytes ($CD45^+$ cells), T-cells ($CD45^+TCR\beta^+$) and each of the T-cell subpopulations ($CD4^-CD8^-$, $CD4^+CD8^+$, $CD8^+$ and $CD4^+$ T-cells).

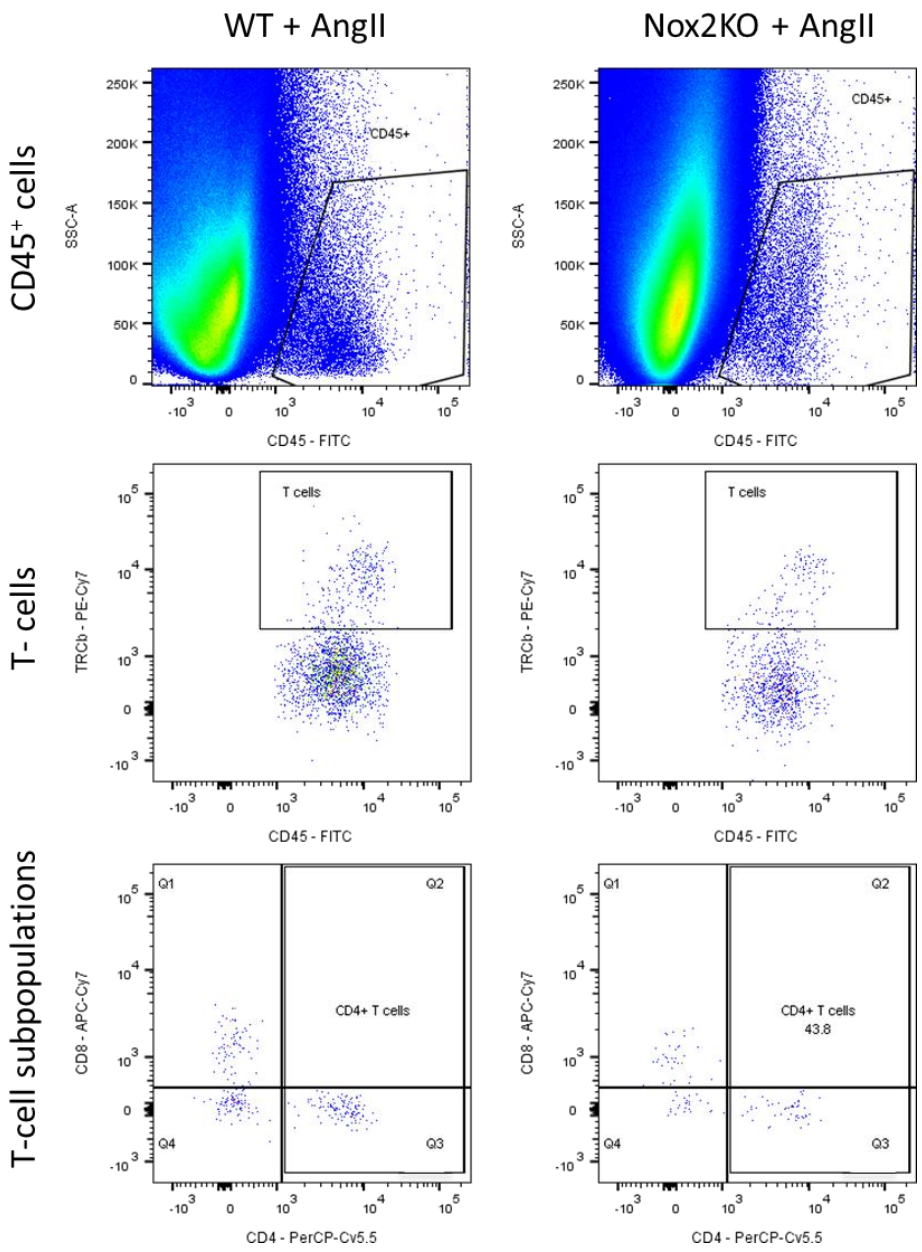

Figure 4-14: Global Nox2KO prevents AngII-induced cardiac inflammation. *Flow cytometry dot plots showing representative examples of WT and Nox2KO both treated with AngII. Analysed by BD FACS CantoII™.*

Analysis, as shown in *Figure 4-15* showed that total leukocyte infiltration significantly increased in WT littermate controls treated with AngII (p=0.0001), as previously observed in chapter 3. This increase was significantly blunted in Nox2KO animals treated with AngII (p=0.005), where leukocytes were twofold lower than their WT counterparts. In addition, no significant increase occurred in Nox2KO animals when treated with AngII. A similar response was observed with T-cell infiltration, where the WT littermate treated hearts contained 37.4±5.69 cells per mg, compared to 12.8±2.16

cells per mg in the Nox2KO treated hearts ($p<0.001$). All T-cell subpopulations tended to be lower in the Nox2KO treated hearts compared to WT littermate hearts treated with AngII, with a significantly lower level of $CD8^+$ T-cells ($p=0.004$) and $CD4^+$ T-cells ($p<0.0001$). Interestingly, no difference was observed between Nox2KO sham and AngII treated mice, demonstrating a blunted response to AngII in the absence of Nox2. The immune-cell differences observed at baseline between Nox2KO and WT littermates is still present in sham groups analysed here, however the 2-way ANOVA with Bonferroni post-test is not suitable to highlight these differences. In comparison, splenic levels of T-cells were not affected by AngII treatment in either Nox2KO or WT littermates (*Figure 4-16*).

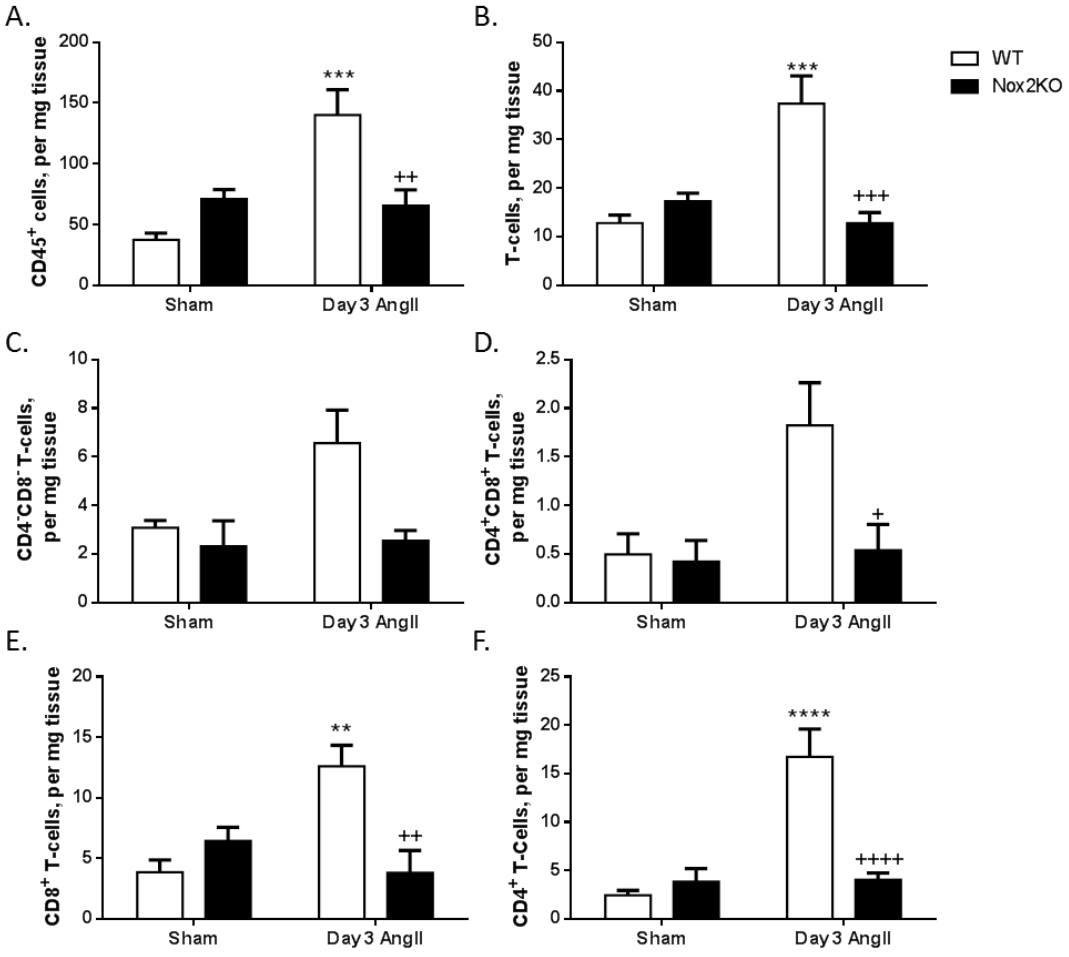

Figure 4-15: Blunted immune cell infiltration in response to AngII with Nox2 deficiency. *Analysis showing* ***(A)*** *total leukocytes ($CD45^+$),* ***(B)*** *T-cells ($CD45^+TCR\beta^+$) and T-cell subpopulatons including* ***(C)*** *$CD4^-CD8^-$,* ***(D)*** *$CD4^+CD8^+$,* ***(E)*** *$CD8^+$ and* ***(F)*** *$CD4^+$ T-cells. *WT AngII vs. WT, +Nox2KO AngII vs WT AngII. Results are represented as cells per mg of heart tissue. Acquired on BD FACS CantoII™, *p<0.05, **p<0.01, ***p<0.001, ****p<0.0001, N=4-8 per group.*

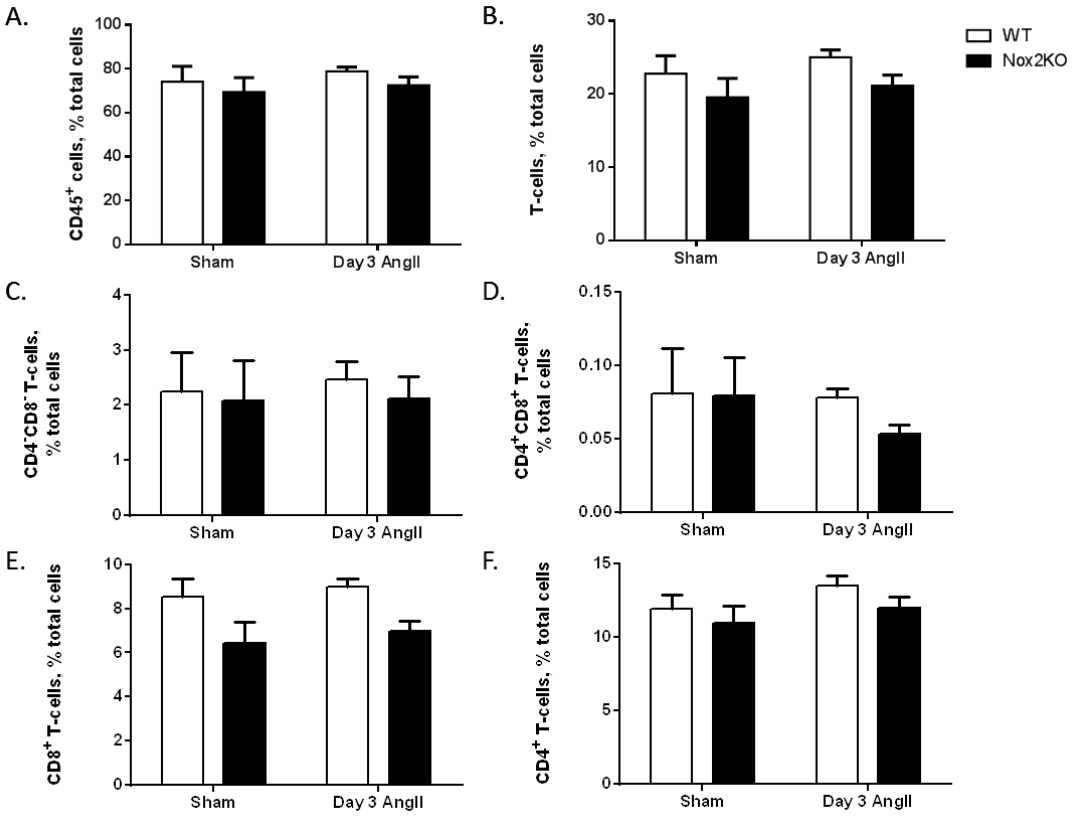

Figure 4-16: Splenic levels of T-cells remain unchanged after AngII infusion. (A) *total leukocytes ($CD45^+$),* ***(B)*** *T-cells ($CD45^+TCR\beta^+$) and T-cell subpopulatons including* ***(C)*** *$CD4^-CD8$,* ***(D)*** *$CD4^+CD8^+$,* ***(E)*** *$CD8^+$ and* ***(F)*** *$CD4^+$ T-cells. Results are represented as a percentage of total cells acquired on BD FACS CantoII™, N=4-8 per group.*

Finally, $CD4^+CD25^+$ Tregs significantly increased in the myocardium of WT animals treated with AngII (p=0.002) compared to sham, as observed previously, however this was significantly blunted in Nox2KO treated animals (p=0.002). Treg levels were then confirmed with a FoxP3 marker showing a significant reduction by 84% ($CD4^+CD25^+FoxP3^+$, p=0.049) in the AngII-treated Nox2KO, compared to the AngII-treated WT littermate (both treated with AngII for 3-days) (*Figure 4-17*). In comparison Treg levels were not affected by AngII treatment within analysed spleen samples.

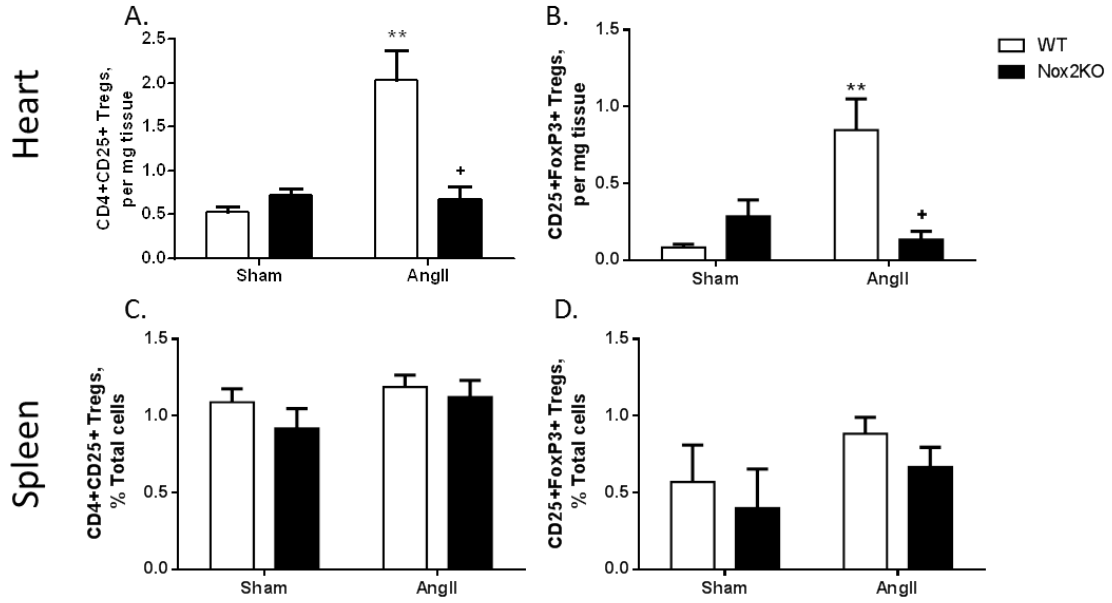

Figure 4-17: Treg infiltration is blunted in Nox2 deficient animals. *Cardiac Treg infiltration was blunted by Nox2 deficiency as by analysis of* ***(A)*** *$CD4^+CD25^+$ Tregs and* ***(B)*** *$CD25^+FoxP3^+$ Tregs. However, Tregs within the spleen remains consistent shown in* ***(C)*** *$CD4^+CD25^+$ Tregs and* ***(D)*** *$CD25^+FoxP3^+$ Tregs. Cardiac data represented as cells per mg of tissue; splenic data represented as a percentage of total cells. Acquired on BD FACS CantoII™. *WT AngII Vs WT sham, +Nox2KO AngII Vs WT AngII. *p<0.05, **p<0.01, N=4-8 per group.*

The proportions of T-cells, $CD4^+$ cells and Tregs were analysed by representing values as a percentage of parent populations (*Figure 4-18*). No significant differences were observed between the four groups by a 2-way ANOVA. Within Nox2KO sham heart samples, there tends to be a higher level of Tregs as a percentage of $CD4^+$ T-cells compared to WT littermates, as observed previously with mice at baseline. This trend was maintained after 3-days of AngII treatment, suggesting a potential protective phenotype against cardiac inflammation.

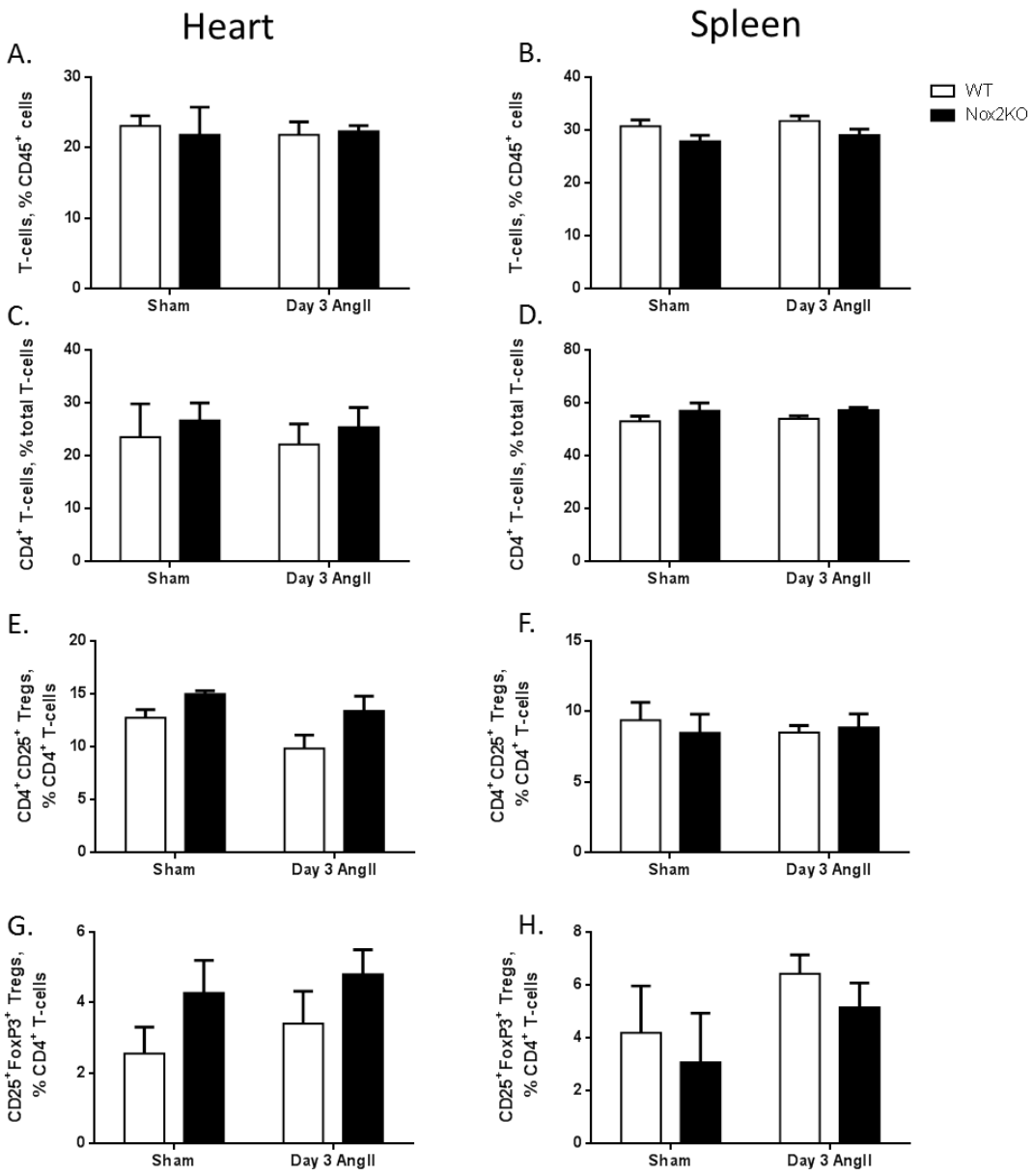

Figure 4-18: Proportion of Tregs to CD4$^+$ T-cells tends to be altered in cardiac samples of Nox2KO mice. (A&B) *T-cells as a percentage of CD45$^+$ cells,* ***(C&D)*** *CD4$^+$ T-cells as a percentage of total T-cells,* ***(E&F)*** *CD4$^+$CD25$^+$ Tregs as a percentage of CD4$^+$ T-cells and* ***(G&H)*** *CD25$^+$FoxP3$^+$ Tregs as a percentage of CD4$^+$ T-cells. Acquired on BD FACS CantoII™. N=4-8 per group.*

Collectively, these data suggest a protective phenotype within the global Nox2KO animals identified by attenuated AngII-induced hypertension, hypertrophy, and interstitial fibrosis and associated cardiac inflammation. The baseline immune phenotype suggests that global Nox2KO animals have a different composition of cardiac immune cells, including an increased level of Tregs and Treg:T-cell ratio.

4.5 Discussion

Previous research has demonstrated the overall role of Nox2 in the development of cardiac remodelling. Nox2KO mice show significantly reduced interstitial fibrosis, compared with WT controls, after AngII or aldosterone infusion, myocardial infarction (MI) or pressure overload induced by aortic banding[4,108,175]. Initial results within this chapter verify these findings as a blunted response to AngII in terms of hypertension, hypertrophy and interstitial fibrosis was observed. Therefore this demonstrated that the global Nox2KO model works efficiently in our hands. However, the novelty of this chapter is in understanding the role of Nox2 in regulating the function of T-cells in this setting.

At baseline, Nox2KO mice displayed LN, thymus and spleen hyperplasia without any signs of infection, which is confirmed in the literature from a study investigating age-induced arthritis in these animals[199]. This may suggest an augmented development of immune cells that may influence the inflammatory response in this murine model[199].

Interestingly, published data suggest increased levels of inflammatory cells within Nox2KO animals[199]; therefore it is important to clarify whether this would alter the level of cardiac-resident immune cells. These results have shown a significantly higher level of total leukocytes, T-cells and more specifically $CD8^+$ and $CD4^+$ T-cells at baseline residing in the heart. In contrast, Lee et al carefully analysed LNs of mice aged 15-18 weeks where they saw higher levels of B-cells, macrophages and monocytes in comparison to a lower level of T-cells. As this is a different tissue and time point from experiments in this chapter, where the mice have high incidence of arthritis, it is unreasonable to determine a trend. However one may suggest a cardio-tropism for T-cells within Nox2KO animals, recruiting more T-cells to the heart and away from LNs at baseline.

Background data using spleen samples showed an equivalent level of T-cells between Nox2KO and WT control mice. In comparison, published results have seen a reduction in splenic T-cell levels, including $CD8^+$ and $CD4^+$ T-cells, from mice aged 15-18 weeks[199]. This difference in results could be attributed to the older age of animals used, where the onset of arthritis is at 60% therefore tissue compositions may alter.

Within $CD8^+$ T-cells, Nox2 is implicated in NF-κB signalling pathways leading to production of TNF-α, IFN-γ and IL-2, pro-inflammatory cytokines[211]. Treatment with apocynin, a Nox2 inhibitor, significantly decreases these inflammatory mediators. Bai et al also demonstrated that inhibition of Nox2 ($gp91^{phox}$) in $CD8^+$ T-cells prevents ROS generation, in turn modulating c-Jun N-terminal kinase (JNK) and NF-κB signalling leading to decreased IFNγ and CD39 expression[212]. Similar investigations have identified a reduction in TNF-α production by $CD8^+$ T-cells lacking Nox2[213]. $CD4^+$ Th differentiation can also be affected by Nox2 levels, where the absence of Nox2 promotes Th1 and Th17 differentiation. Nox2KO mice with spontaneous age-induced arthritis displayed an increase in Th17 cells and a decrease in Tregs (analysed by FoxP3 expression) within LNs[199].

Moreover, the production of Nox2-derived ROS within APCs can also affect T-cell activation and function. During DC antigen presentation to T-cells, bidirectional communication instigates the mediation between innate and adaptive immunity. Both cell types in this setting produce ROS, and ebselen (an antioxidant) is able to inhibit this production[197]. Presence of ebselen in a DC/T-cell coculture inhibits the DC-dependent proliferation by T-cells and has the potential to abrogate sequential adaptive immune responses[197]. The antioxidant also inhibits production of cytokines, suggesting the involvement of ROS within DC and T-cell signalling.

Furthermore, the basal levels of cardiac-resident Tregs in Nox2KO mice were somewhat elevated compared to WT littermate controls and give rise to an increased Treg:T-cell ratio. One could imagine that the higher level of Tregs in the Nox2KO heart provides a local protection to experimental hypertension and its pathological responses. However, one limitation of this model is the absence of Nox2 in all cell types, which makes it difficult to verify this hypothesis. For example, immune infiltration may also be influenced by endothelial cells or by factors released by cardiomyocytes or fibroblasts – all cell types that express Nox2. Results presented here have shown that splenic levels of Tregs remained the same between WT and Nox2KO mice. This was confirmed by a study investigating the effect of Nox2 ($p47^{phox}$) on Treg development, where the baseline levels of Tregs within the spleen were similar between both genotypes[214]. Intriguingly, Lee et al identified a lower level of Tregs within LNs of Nox2KO mice compared to WT in mice aged 12-14 weeks[199].

Nox2 has also been implicated in the direct suppression of $CD4^+$ T-cells by Tregs[214]. Both Tregs from the neutrophil cytosolic factor-1 (Ncf1, $p47^{phox}$)–deficient mice, which lack Nox2 activity, and normal Tregs treated with Nox inhibitors have shown a decreased ability to suppress $CD4^+$ effector T-cells *in vitro*[214]. Hence, suggesting that Nox2 may play a role in regulating the suppressive abilities of Tregs. Further *in vitro* work demonstrated that the suppressive attribute of Tregs is partially dependent on TGFβR signalling within these cells[214]. Within the periphery of Nox2KO mice there are reported to be fewer Tregs compared to WT animals, naïve $CD4^+$ T-cells isolated from the periphery are also less efficient at differentiating into Tregs[199].

Furthermore, production of Nox2-derived ROS upon macrophage activation can stimulate Tregs, and consecutive suppression of T-cells[215]. Co-culture of T-cells and macrophages saw an increase in $CD4^+CD25^+FoxP3^+$ Tregs, which was diminished in the presence of apocynin, a Nox2 inhibitor[215]. This was also confirmed *in vivo*. Dexamethasone, an immunosuppressive drug, also increases ROS levels and T-cell suppressive activity within M2 cells[216]. Nox2 deficient macrophages from CGD patients lacked the ability to produce ROS. The capacity of these Macrophages to suppress T-cell responses was diminished and the levels of Tregs induced were significantly reduced compared to healthy controls[215].

Research investigating human M2 cells indicated the different capacities of ROS production and function between M2 subpopulations. M2 cells appear to produce ROS to a higher capacity, compared to M1, however the different subtypes of M2 cells (M2a, M2b and M2c) also vary in their capacity to produce ROS and ability to induce T-cell activation[49]. M2a has lower ROS production and a better ability at inducing T-cells whereas M2b and M2c are the opposite and also have the ability to induce Tregs[49].

The effect of Nox2 on $CD4^+$ T-cells and Tregs creates an essential balance that can switch between a pro-inflammatory or anti-inflammatory response, which is vital within a variety of diseases outcomes.

In addition, Lee et al examined the differentiation of naïve $CD4^+$ T-cells and reported a skewed phenotype towards Th17 cells and a reduced level of Treg differentiation, suggesting Nox2 alters the Th17/Treg balance[199]. However, cells used were also

isolated from lymphoid organs of mice aged 12-18 weeks; therefore in younger animals, such as those used here, this T-cell skewing and Treg levels may be different.

Madhur et al investigated T-cell infiltration into the aorta of WT mice in response to AngII, and highlighted that IL-17 was a potent cytokine upregulated in this setting[185]. They also identified that IL-17, and hence the Th17 $CD4^+$ T-cell subtype, are critical for the maintenance of AngII-induced hypertension and vascular remodelling[185]. Within the Nox2KO cardiac environment, where a significantly higher level of Tregs were observed at baseline, different modulators such as TGFβ that can promote Treg maintenance and differentiation[217], may alter the Treg:Th17 balance towards Tregs. Previous research has implicated Tregs within cardiac remodelling associated with experimental hypertension. Hence, our findings here may partially explain the blunted response of Nox2KO mice to AngII-induced cardiac remodelling. Therefore Tregs may be a key cellular-modulator within this process.

As global Nox2KO mice display a blunted response to AngII-induced hypertension and cardiac remodelling, in addition to an altered baseline level of immune cells within the heart, this led to the investigation of immune cell infiltration with AngII within these global Nox2KO mice. AngII treatment within WT littermates initiated the typical inflammatory response previously observed; however this was significantly blunted in Nox2KO animals. The cardiac infiltration of total leukocytes, T-cells, $CD8^+$ and $CD4^+$ T-cells were all significantly lower in Nox2KO treated animals compared to their WT counterparts.

One could postulate that as AngII contributes to hypertrophy and fibrosis, the concomitant stimulation of the inflammatory response further aggravates cardiac remodelling and damage. Therefore Tregs may be activated in order to restrain inflammation and hence limit the remodelling process. This supports the idea that the increase in Tregs observed in WT mice after 3-days of AngII treatment could be a transient compensatory mechanism. Thus if AngII treatment persists the inflammatory response may progress. However, as global Nox2KO animals exhibit a higher level of Tregs at baseline, this may keep inflammation at bay as AngII treatment is initiated, and in part protect the heart against AngII-induced pathophysiology.

Overall, data within this chapter have shown that global Nox2KO animals have an increased level of cardiac-resident immune cells at baseline, including an enhanced Treg:T-cell ratio. AngII-induced cardiac immune cell infiltration is obliterated in these Nox2KO animals suggesting a potential protective response of the initial elevated Treg levels in the heart. This in part may contribute to the favourable AngII response of Nox2KO mice. However the impact of $CD4^+$ T-cells, and more specifically Tregs, within this setting requires further investigation.

Chapter 5: Role of Nox2 in the function of Tregs

5.1 Introduction

5.1.1 Regulatory T-cells

Tregs are driven by their master transcriptional regulation, FoxP3[62]. They suppress the activity of other immune cells, such as CTLs, B-cells and Th subsets, in order to control immune responses[218,219]. They play a critical role in peripheral tolerance, to dampen down the amplitude of an immune response, which is pertinent in preventing autoimmune diseases.

Treg differentiation and classification remains controversial, within the literature numerous terms are given to describe Treg subtypes. Tregs that are derived from the thymus are known as natural Tregs (nTregs), or thymic-derived Tregs (tTregs), whereas peripheral-derived Tregs are known as inducible Tregs (iTregs), or peripheral-derived Tregs (pTregs)[220]. iTregs within the secondary lymphoid organs (SLO) are also termed central Tregs that, when activated, differentiate into effector Tregs[178,220]. This differentiation process is initiated by TCR signalling and CD28[178]. Effector Tregs then produce different cytokines and chemokines, depending on the type of inflammatory response, in order to specialise their suppressive function (*Figure 5-1*)[178]. Hence, central Tregs serve as a quiescent pool of Tregs, which recirculate through SLO, differentiating into faster-lived, highly proliferative effector Tregs eliciting an anti-inflammatory response. One must bear in mind that this is one view of the Treg classification, however this still remains controversial and further research is required. In addition, tissue-resident Tregs are also present that possess a unique phenotype specific to their location and homeostatic functions[178,220]. Their origin is not yet defined; however they may propagate from effector Tregs.

$CD4^+CD25^+FoxP3^+$ naturally occurring Tregs, derived from the thymus, represent 10% of the total $CD4^+$ population and have been the focus of recent studies[218].

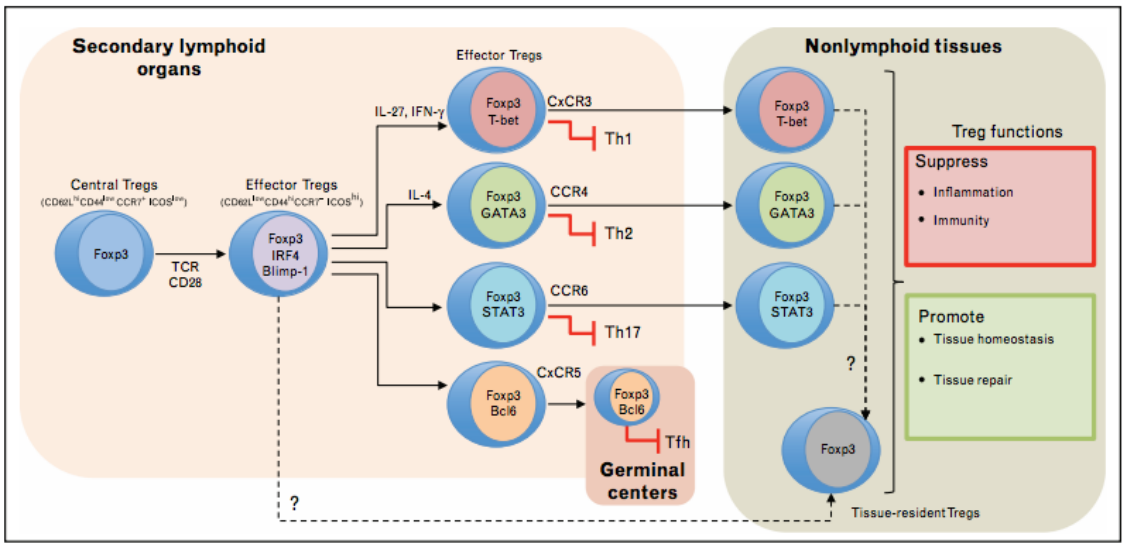

Figure 5-1: Specialisation and diversity of Treg subtypes. *Rothstein et al 2015 (current opinion organ transplantation)*[178].

There are four basic mechanisms thought to be used by Tregs to enable suppression: inhibitory cytokines, cytolysis, metabolic disruption and targeting APCs *(Figure 5-2)*[218]. Firstly, Tregs have the ability to secrete anti-inflammatory cytokines including TGFβ, IL-10 and IL-35, which enable the indirect suppression of immune cells such as Teff cells[221]. These Treg-associated cytokines also have the ability to stimulate development of iTregs, thereby amplifying the anti-inflammatory response[218].

The second mechanism involves cytolysis by the secretion of granzymes that enter target cells via a perforin pore[218]. Perforin is a component of the cytolytic granule that enables permeabilisation of the target cell plasma membrane[218]. Once granzymes have entered the target cell they can elicit an apoptotic response by cleaving and activating intracellular caspases. A number of studies have implicated granzyme A and granzyme B in the Treg-mediated suppression of inflammation[222-224].

Tregs can also mediate metabolic disruption of a target cell by expression of CD25 on Treg membranes[218]. CD25 sequesters IL-2, diminishing local IL-2 levels that are required for T-cell survival[225,226]. In addition, IL-2 has also been found to upregulate FoxP3 expression and hence may be involved in Treg activation and amplification of suppressive mechanisms[221,227]. In addition to this, Tregs express CD39 and CD73 on their cell membranes that produce adenosine, which in turn suppresses the target

cells[221]. Pericellular adenosine binds to and activates adenosine receptor 2 A ($A_{2A}R$), which in turn inhibits Teff cell function[221]. Furthermore $A_{2A}R$ activation can enhance induction of Tregs by inhibiting IL-6 whilst promoting TGFβ secretion[228]. TGFβ enhances Treg differentiation, thereby further amplifying this regulatory response.

Finally, Tregs can modulate the inflammatory response by targeting APCs such as DCs. The binding of CTLA-4 or the lymphocyte-activation gene 3 (LAG3) on Tregs to their DC receptor targets, CD80/86 or MHC class II respectively, inhibits DC maturation and function preventing further inflammation[221,229]. Depletion of CTLA-4 impairs Treg suppressive function both *in vitro* and *in vivo*[177,230].

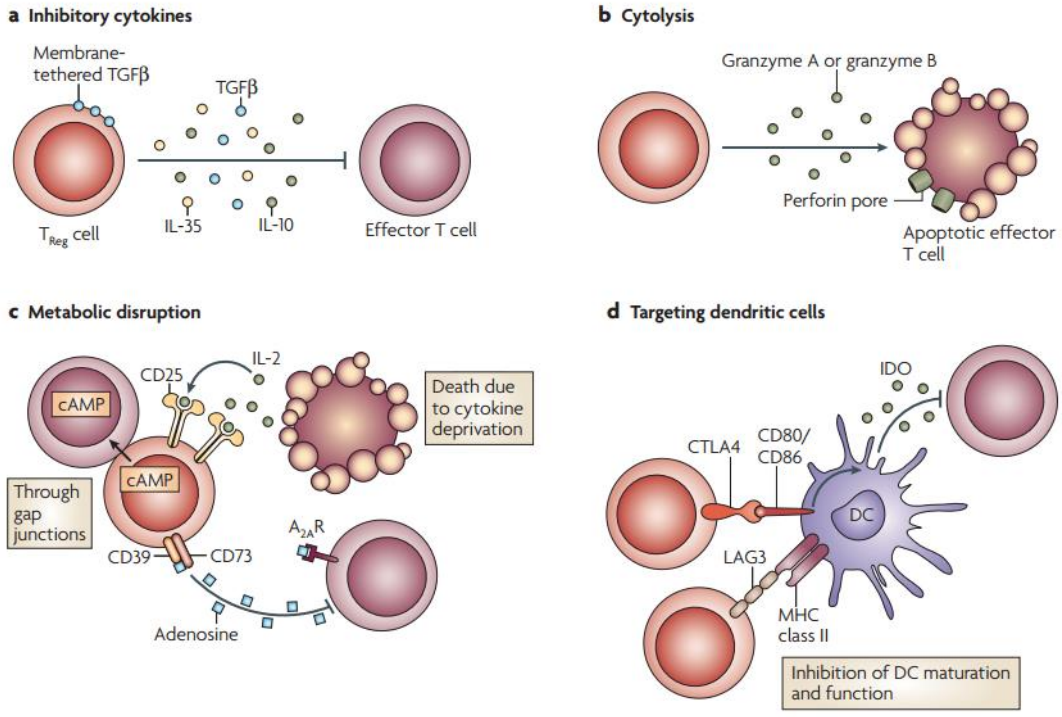

Figure 5-2: Treg suppressive mechanisms. *From Vignali et al 2008*[218].

5.1.2 Role of Nox2 in Treg differentiation, activation and suppressive function

Nox2 has previously been shown to modulate Treg differentiation and function. As briefly discussed in section 4.5, Lee et al demonstrated an integral role for Nox2 in the differentiation of Tregs[199]. They observed a lower level of Tregs within the LNs and

spleens of global Nox2KO mice compared to WT mice, suggesting a role of Nox2 in Treg migration or differentiation[199]. Furthermore, naïve Nox2KO $CD4^+$ T-cells, isolated from LNs, cultured in the presence of anti-IFNγ, anti-IL4, IL-2 and TGFβ were less efficient than their WT counterparts at generating iTregs[199].

In addition, Nox2 was identified as an important component in Treg suppressive function[214]. Tregs isolated from of $p47^{phox-/-}$ mice, which lack the $p47^{phox}$ (Ncf1) adaptor protein of Nox2, show decreased ability to suppress Teff cells[214]. This was also verified by an *in vitro* suppression assay analysing WT Treg suppression of Teffs in the presence of an Nox inhibitor[214].

Activation of Tregs by macrophages may also be modulated by Nox2. ROS have been directly implicated in the activation of Tregs by macrophages[198]. Gelderman et al generated a transgenic (TG) mouse model based on a $p47^{phox-/-}$ background (lacking Nox2), whereby only macrophages contain a functional Nox2 enzyme. Global $p47^{phox-/-}$ mice are highly susceptible to collagen-induced arthritis; however these TG mice were protected to the same extent as WT mice; thereby implicating macrophage Nox2 and associated ROS in anti-inflammatory processes[198]. These findings were validated by *in vitro* analysis of macrophages isolated from CGD patients, lacking Nox2, which were unable to suppress T-cells and induced a significantly lower number of Tregs[215]. Therefore these results demonstrate that macrophage Nox2-derived ROS enable the suppression of T-cells by inducing Tregs[198,215].

5.1.3 Tregs in non-lymphoid tissues

Current research provides substantial evidence of the implication of Tregs in non-lymphoid tissues such as visceral adipose tissues (VAT), skeletal muscle and cardiovascular tissue[231,232]. In this non-lymphoid setting Tregs contribute to tissue homeostasis and repair. This opens a whole new plethora of Treg functions that go beyond the traditional regulation of immune responses. Not only are they vital in modulating immune responses, but also have the ability to control non-immunological processes in a range of tissues[231]. Tissue-resident Tregs exhibit a unique phenotype by expressing certain transcription factors, chemokines receptors or effector molecules[231]. They may also possess a distinct TCR repertoire, migration patterns and

distinct mechanism of action or targets[231]. Local cues within specific tissues may enable this phenotypic and functional specialisation of Tregs in addition to preferential survival within the tissue microenvironment[231].

VAT-specific Tregs are the most well defined tissue-specific Treg population. They overexpress genes that give rise to chemokine receptors (such as CCR1, CCR2 and CCR9), anti-inflammatory cytokines (such as IL-10) and the transcription factor PPAR-γ[233]. PPAR-γ interacts with FoxP3 in order to promote VAT Treg-specific characteristics[233]. Absence of PPAR-γ in mice prevents the accumulation of Tregs within VAT[233]. The specific overexpression of these genes enables VAT Tregs to elicit their unique functional properties (such as impacting on glucose metabolism)[231]. In addition VAT Tregs express a unique TCR repertoire that is distinct from other Treg populations[231].

Skeletal muscle-specific Tregs are upregulated during injury and regeneration of the muscle[231]. They overexpress genes encoding IL-10, growth factors such as amphiregulin and the T-cell immunoglobulin and mucin-domain containing-3 (TIM-3) that regulates macrophage activation[231,234]. These Tregs also have a unique TCR repertoire and phenotypically tend to be more similar to VAT Tregs than splenic Tregs[231]. In this setting, skeletal muscle Tregs have the ability to aid muscle repair by satellite cells due to their overexpression of amphiregulin[231,234].

Tissue-specific Tregs are found, albeit in small numbers, within healthy tissues that can be upregulated in response to injury or infection[231,235]. This increase in Treg numbers may occur due to chemokine-based recruitment, local expansion or by conversion of $CD4^+$ T-cells (*Figure 5-3*)[231]. Tissue resident Tregs express distinct chemokine receptors and adhesion molecules, which may enable their initial recruitment[231]. Treg priming within the LNs is thought to upregulate these tissue-specific chemokine receptors and adhesion molecules in order to direct Treg migration towards the affected tissue and elicit a local response[231].

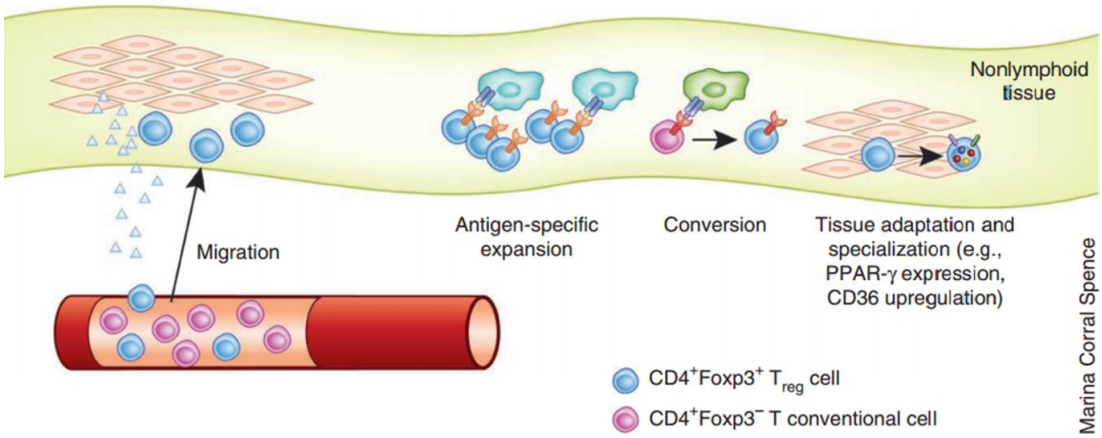

Figure 5-3: Tissue specific Treg accumulation. *Burzyn et al 2013 (nature immunology)*[231].

Research groups investigating Treg recruitment have identified the chemokine receptors CCR4 and CCR8 as important mediators of Treg migration[181,182]. However, very few papers have examined the recruitment of Tregs specifically to the heart. In a model of cardiac allograft tolerance, the recruitment of Tregs is critical for long term graft survival[182]. This recruitment mechanism was reliant on the expression of CCR4 chemokine, as $CCR4^{-/-}$ mice were unable to induce tolerance after receiving a cardiac allograft[182]. In addition, CCR5 may play a role in Treg recruitment during MI, as $CCR5^{-/-}$ mice showed a significantly higher level of inflammation[236].

Taken together, these results identify a novel, local role for Tregs in non-lymphoid tissues, including the myocardium. Local immune responses and Tregs themselves have both been recognised as important elements in tissue homeostasis and repair; however as research continues it becomes apparent that these two areas are more entwined than once thought. Therefore further study into specific cardiac-Tregs may elicit new functions and migration patterns that could be harnessed for potential therapeutic treatment.

5.1.4 Tregs in cardiovascular pathophysiology

Little is known about cardiac-specific Tregs, although Tregs have been implicated in a number of cardiovascular pathologies including atherosclerosis, MI and AngII-induced

abdominal aortic aneurysm[232]. One main limitation in fully understanding cardiac-resident Tregs is the limited number of Tregs at baseline, which makes it difficult to analyse their cardiac-specific phenotype. Tregs are thought to control the development of atherosclerosis, an immune-inflammatory disease characterised by the accumulation of lipids within the artery wall[237]. In this setting Tregs potentially reduce atherosclerotic lesion size, prevent rupture and limit progression of atherosclerosis[238]. Ischemic injury to the myocardium is followed by an enhanced inflammatory response, however a second phase of resolution and repair also occurs that is essential to infarct-healing and prevention of heart failure[239]. Tregs are thought to be involved in this process, and have been shown to expand within the LNs draining the heart[240]. The absence of Tregs in this setting has also been linked to a larger infarct size, increased inflammation and impaired resolution of infarct-associated inflammation[240]. Therefore Tregs enhance cardiac wound healing within the setting of MI. Furthermore, recruited Tregs may modulate fibroblast phenotype and function within the setting of MI by reducing α-SMA and decreasing MMPs[241]. Abdominal aortic aneurysm (AAA) is a chronic inflammatory aortic disease associated with maladaptive vascular remodelling that progress towards aortic rupture[242]. Antibody depletion of Tregs enhances susceptibility of C57Bl/6 mice to AAA and promotes aortic rupture[242]. On the other hand, increased systemic Treg levels provide a protective phenotype against AngII-induced AAA[243,244].

5.2 Aims

Nox2 has been identified as a potential modulator of Treg function and development; however this still requires further examination. In addition, Tregs have been suggested by a number of papers to play an important role in regulating cardiovascular remodelling in response to AngII. However, the specific role of Treg-Nox2 within the setting of AngII-induced hypertension and cardiac remodelling is unknown.

Therefore the aim of the studies in this chapter is to identify the effects of Nox2 on Treg function both *in vitro* and *in vivo* in the setting of AngII-induced cardiac pathophysiology.

5.3 Methods

5.3.1 Immune cell isolation and purification

Immune cells were isolated from fresh spleens and LNs, as described in section 2.4.3, from male C57Bl/6 (Harlan UK Limited) or in-house bred global Nox2KO mice (section 4.3) aged 6-8 weeks. A single cell suspension was created by triturating and passing tissues through a 70µm nylon mesh using the plunger of a 1mL syringe. Cells were then washed in Roswell Park Memorial Institute (RPMI) media (with L-glutamine, Gibco) and centrifuged at 1800rpm for 5 minutes. Spleen samples only were then treated with 1x red blood cell lysis buffer (5mL per spleen) for 3 minutes at room temperature before washing in RPMI as before. Spleen and LN samples were then re-suspended in a suitable volume and pooled together before removing 10µL to count T-cells using a haemocytometer (1:10 dilution with trypan blue (Gibco)).

All immune cell isolations were performed in a laminar flow cabinet (tissue culture hood) to provide a sterile environment for use of sterile buffers, where all added components were filtered.

5.3.1.1 CD4+ T-cells

$CD4^+$ T-cells were isolated using the Invitrogen Dynal® $CD4^+$ T-cell isolation kit, according to the manufacturer's protocol. Briefly, splenic cells were incubated in a solution of 100µL isolation buffer, 20µL FCS and 20µL of the antibody mix for 30 minutes at 4˚C under rotation. Samples were then washed and centrifuged as before using isolation buffer. Dynabeads® (200µL per $10x10^6$ leukocytes, Invitrogen) were prepared by washing twice in 6mL isolation buffer, leaving on a magnet (15mL DynaMag™) for 2 minutes and removing the supernatant using a Pasteur pipette. The supernatant was removed from centrifuged cells and re-suspended in 800µL isolation buffer (per $10x10^6$ leukocytes) and combined with the pre-washed Dynabeads®. The cell-Dynabead® solution was then incubated for 30 minutes at 4˚C under rotation. Cells bound by beads were then removed by adding up to 6mL isolation buffer and placing the solution on a magnet for 2 minutes. The supernatant was then removed and placed into a fresh 15mL tube, which was incubated on the magnet for 2 minutes

before removing the supernatant again to obtain pure $CD4^+$ T-cells. These cells were then washed and centrifuged as before in isolation buffer, the supernatant was discarded and cells were re-suspended in a suitable volume before counting using a haemocytometer. $CD4^+$ cells were then washed and centrifuged for a final time and re-suspended at a concentration of $1x10^6$ cells/mL, in complete media.

5.3.1.2 Antigen presenting cells

Splenic cells were then incubated in a cocktail of CD4 and CD8 depleting antibodies (300µL anti-CD4 antibody (YTS-191.1, Lombardi laboratory) and 300µL anti-CD8 antibody (YTS-169.4, Lombardi laboratory) per spleen) and incubated for 30 minutes at 4˚C under rotation. Cells were then washed and centrifuged as described previously and re-suspended in 1mL isolation buffer per spleen. The cell solution was then incubated with 300µL of pre-washed Dynabead® per spleen for 30 minutes at 4˚C under rotation. Dynabead® bound cells were then removed as before using a magnet and counted using a haemocytometer. APCs were then re-suspended in complete media at a concentration of $2x10^6$ cells/mL.

5.3.1.3 Regulatory T-cells

Spleens and LNs from multiple mice were treated as described above to generate a single cell splenocyte suspension. Tregs were isolated, according to the manufacturer's protocol, using an Invitrogen $CD4^+CD25^+$ Treg Dynabead® kit, as shown in *Figure 5-4*. Initial single cell suspensions were re-suspended at a concentration of $1x10^8$ cells/mL in isolation buffer and incubated with 200µL FCS and 200µL antibody mix (Invitrogen Dynal® $CD4^+CD25^+$ T-cell isolation kit) per 1 x 10^8 cells for 30 minutes at 4˚C under rotation. Cells were washed using isolation buffer and centrifuged at 1800rpm for 5 minutes. Cells were then washed, centrifuged and re-suspended in 2mL cold isolation buffer (per $1x10^8$ cells). Then mixed with 2mL pre-washed Dynabeads® (per $1x10^8$ cells) and incubated for 30 minutes at 4˚C under rotation. Cells bound by beads were then removed using a magnet as described previously and the $CD4^+$ Supernatant was washed and centrifuged before, resuspending in 250µL isolation buffer per $1x10^8$ cells.

25µL FlowComp™ mouse CD25 antibody (Invitrogen) was then added (per $1x10^8$ cells) and the cells were incubated again for 30 minutes at 4˚C under rotation. Cells were then washed, centrifuged and re-suspended in 250µL isolation buffer per $1x10^8$ cells. $CD4^+$ cells were then incubated with 75µL (per $1x10^8$ cells) pre-washed FlowComp™ Dynabeads® for 30 minutes at 4˚C under rotation. Beads were re-suspended by pipetting and placed on a magnet for 2 minutes. The supernatant was removed and kept in a clean 15mL falcon tube; this contains the $CD4^+CD25^-$ T-cells. Remaining beads were washed and reapplied to the magnet twice before resuspending in 0.5mL FlowComp™ release buffer and incubated for 30 minutes at 4˚C under rotation. Cells were then placed on the magnet for 2 minutes and the supernatant removed to a fresh tube, washed and placed back on the magnet for a further 2 minutes and the final $CD4^+CD25^+$ T-cell suspension was removed to a fresh tube and counted. Cells were re-suspended to a final concentration of $2x10^6$ cells/mL for the suppression assay, and 5 x 10^6 for an adoptive transfer experiment.

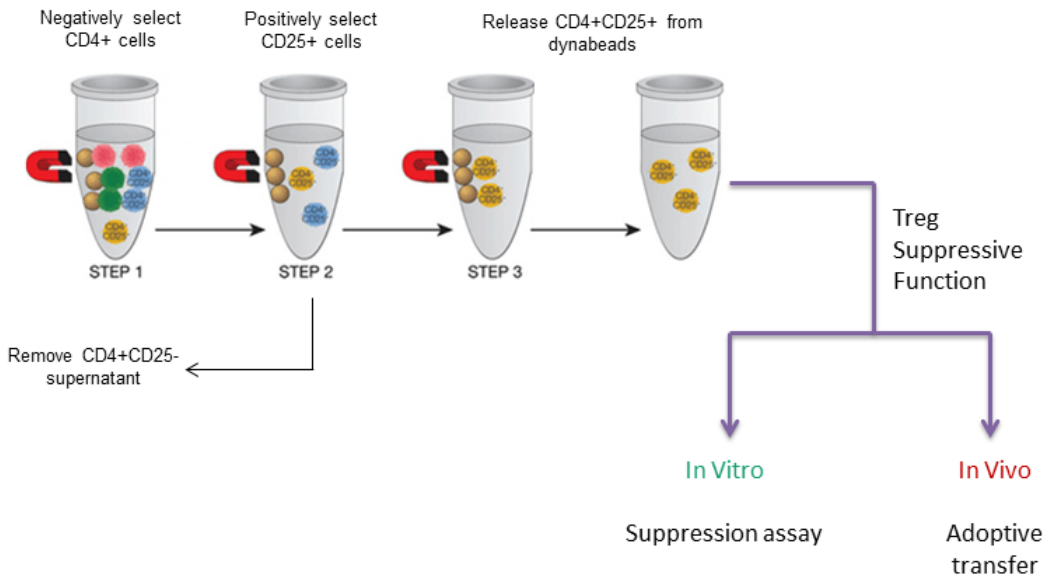

Figure 5-4: Treg isolation method, adapted from Invitrogen Dynal®.

Remaining $CD4^+CD25^-$ T-cells and $CD4^+CD25^+$ Tregs were analysed using flow cytometry to validate efficiency of the isolation process. *Figure 5-5* shows a purity of ~ 90-95% of isolated $CD4^+$ T-cells expressing CD4, with <5% of cells expressing CD25.

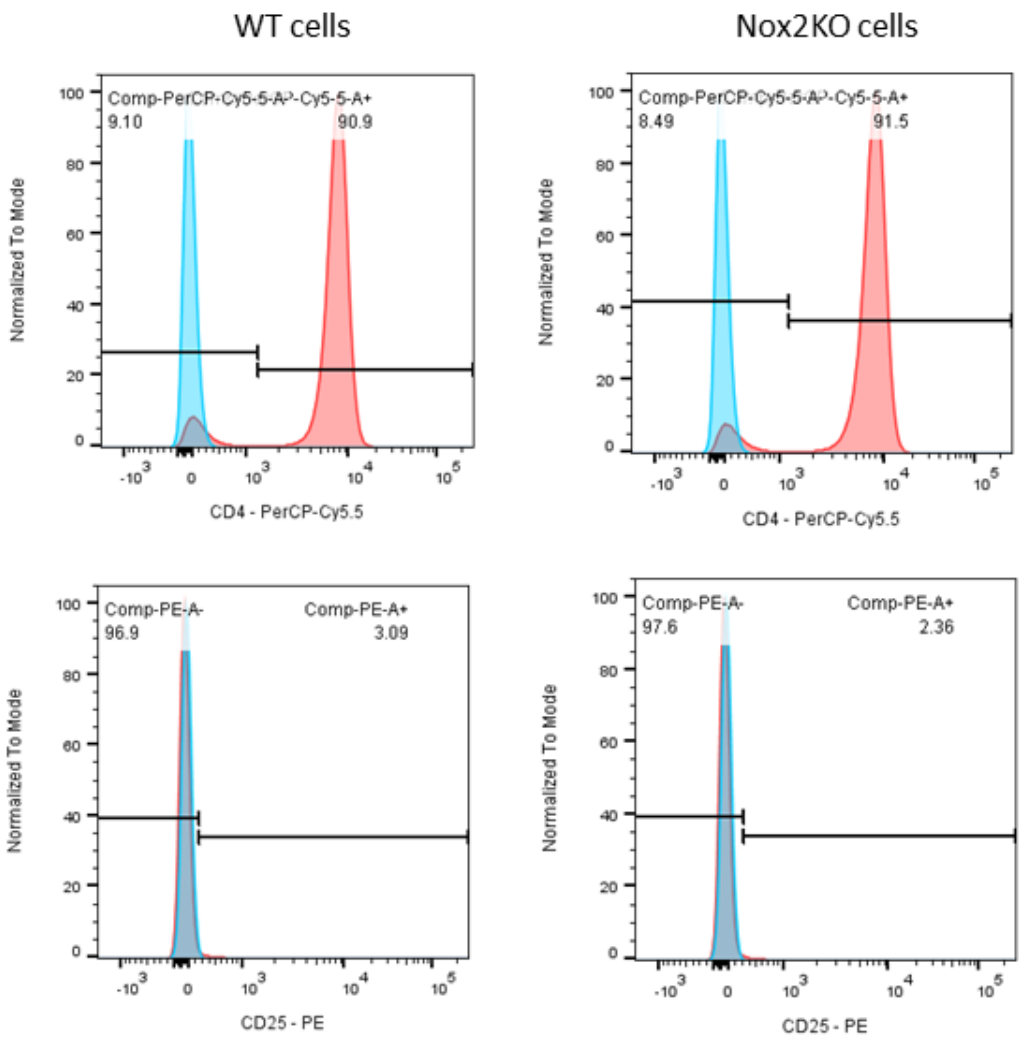

Figure 5-5: Verification of isolated CD4$^+$ T-cells. *Blue peak represents negative control; red peak shows the cell sample.*

Similarly, *Figure 5-6* shows that ~87-90% of isolated CD4$^+$CD25$^+$ Tregs express CD4, where ~93-95% of these CD4$^+$ cells express CD25 and 95-97% express FoxP3. This demonstrates a sufficient purity of isolated cells.

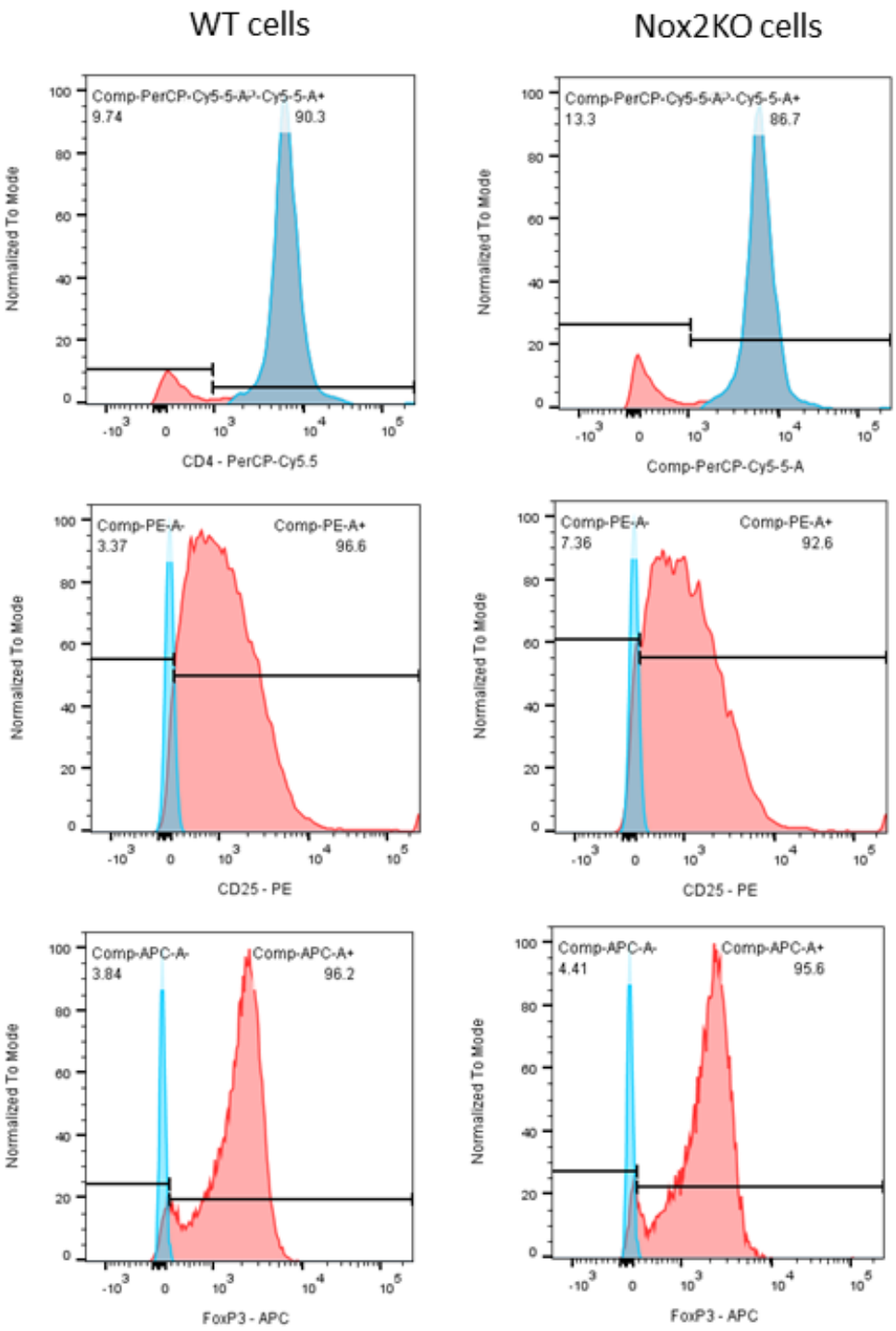

Figure 5-6: Validation of isolated CD4^{+}CD25^{+} Tregs. *Blue peak represents negative control; red peak shows the cell sample.*

5.3.2 Adoptive transfer

$CD4^+CD25^+$ Tregs were isolated from Nox2KO or C57Bl/6 mice, as described above, and re-suspended to a concentration of $5x10^6$ cells/mL in sterile saline and kept on ice. WT mice were warmed in an incubator for 2 hours at 30˚C before injections, and were anaesthetised with 2% isoflurane. Tails were cleaned with 70% EtOH before 200µL of Nox2KO Tregs, WT Tregs or sterile saline were injected into the lateral tail vein to deliver $1x10^6$ cells per injection. Mice were then implanted with a subcutaneous mini-osmotic pump containing a pressor dose of AngII (1.1mg/kg/day) as described in section 2.3. Treatment continued for up to 14-days and both blood pressure and haemodynamic function were recorded at 0-, 3-, 7- and 14-days after treatment, as described in section 2.4.

5.3.3 *In vitro* suppression assays

Teff cells ($CD4^+CD25^-$), APCs and Tregs were isolated from C57Bl/6 or Nox2KO mice (Tregs) as described above and re-suspended in complete media. 50µL of each respective cell suspension was added to each well of a 96 well round-bottom plate with the conditions illustrated in *Figure 5-7***.** Therefore each well contained a combination of 50,000 $CD4^+$ T-cells, 100,000 APCs and 50,000 Tregs. With the ratio of Teff:Treg being altered in certain conditions by diluting Tregs with an equal volume of complete media. Purified anti-CD3 antibody (8µg/µL, final concentration, BD Pharmingen) was also added to certain wells.

Plate 1 (Lanes 1-3)

	CD4	APC	WT Treg	CD3
a	X	X		X
b	XX	X		X
c	X	X	X	X
d	x	X		
e		X	X	X
f		X	X	
g	X			
h			X	

Plate 1 (Lanes 4-6)

	CD4	APC	WT Treg	CD3
a	X	X	1:2	X
b	X	X	1:4	X
c	X	X	1:8	X
d	X	X	1:16	X

Figure 5-7: Suppression assay plate setup. *Different combinations of CD4 T-cells, APCs, Tregs and anti-CD3 antibody are plated in wells, each with three repeats. The same layout is used for WT and Nox2KO Tregs for the thymidine assay.*

5.3.3.1 Thymidine suppression assays

After setting up the assay as described above, the 96-well plate was then incubated at 37˚C, 5% CO_2 for 48 hours. A mixture of 50µL complete media and 1µL ^{3}H-thymidine was then added to each well and the assay was incubated at 37˚C for a further 17 hours. Cells were then transferred to a filter mat using a cell harvester. The filter mat was then dried by microwaving for at least 3 minutes before transferring it to a plastic pouch containing 17mL β-scintillation fluid and sealed. Levels of radioactivity were then detected for each well using a beta plate.

5.3.4 Treg phenotype

Tregs isolated from Nox2KO or WT littermates as described in section 5.3.1.3 were then treated for analysis by flow cytometry (section 2.6.2). These samples were incubated with antibodies shown in *Table 11* and analysed on BD FACS CantoII™.

Antibody	Fluorophore	Concentration (mg/mL)	Concentration for samples (µg/mL)	Concentration for controls (µg/ml)		Source
				FMO	Beads	
anti-CD25	PerCP-Cy5.5	0.2	4	0.8	1.67	Ebioscience
anti-FoxP3	PE-Cy7	0.2	4	0.8	1.67	Ebioscience
anti-CTLA4	APC	0.2	4	0.8	1.67	Ebioscience
anti-GITR	FITC	0.2	4	0.8	1.67	Ebioscience
anti-CD73	PE	0.2	4	0.8	1.67	Ebioscience
anti-CD103	APC	0.2	4	0.8	1.67	Ebioscience
anti-CD62L	FITC	0.2	4	0.8	1.67	Ebioscience
anti-CD39	PE	0.2	4	0.8	1.67	Ebioscience

Table 11: Antibodies used for Treg phenotyping experiments using flow cytometry.

5.3.5 Treatment of samples

After 14-days of treatment, organs were harvested and treated as explained in section 2.4 for histological analysis using WGA and PSR (section 2.8). RNA extraction and reverse transcription were performed as described in section 2.7 to enable analysis of fibrosis-related markers by qPCR. A second group of animals received the same treatment, but were harvested after 3-days of AngII infusion in order to analyse immune cell infiltration. Single cell suspensions were prepared from whole hearts, spleens, aortas and kidneys, and analysed by flow cytometry using the BD FACS CantoII™ as described in section 2.6. The level of leukocytes, T-cells and T-cell subsets were determined based on expression of CD45, TCRβ, CD4, CD8, CD25 and FoxP3.

5.4 Results

The experiments in chapter 4 showed a different response between Nox2KO and WT cardiac T-cell infiltration during AngII treatment, including altered cardiac infiltration of $CD4^+$ T-cell and Treg populations. Therefore, it was important to investigate the effect of Nox2 in Treg function both *in vivo* and *in vitro.*

5.4.1 Adoptive transfer of Nox2KO Tregs blunts AngII-induced cardiovascular changes

Tregs were isolated from global Nox2KO or WT littermate control mice using magnetic beads and the purity was verified using flow cytometry. Isolated Tregs, or sterile saline, were then injected via the tail vein into C57Bl/6 mice, before the implantation of a mini-osmotic pump containing a pressor dose (1.1mg/kg/day) of AngII. These three groups were treated with AngII for up to 14-days, during which time blood pressure and cardiac structure/function were recorded using tail cuff plethysmography and echocardiography respectively.

Typical increases in systolic blood pressure were observed in saline-injected mice treated with AngII, as previously shown in chapter 3. This hypertensive response was attenuated in both WT- and, more efficiently, Nox2KO- Treg injected groups after 3-days of treatment (*Figure 5-8 A*). AngII-treated animals that received a saline injection exhibited an expected increase in systolic blood pressure. Interestingly, all Treg injected animals showed a blunted hypertensive response to AngII after 3- and 7-days, with a more striking effect for KO Tregs. In the early phase of treatment (day 3), animals injected with WT-Tregs displayed systolic blood pressure lower than that observed in the control group ($p=0.0340$), however this difference was attenuated after 7-days. In comparison, the Nox2KO-Treg treated group maintained a blunted systolic blood pressure response during 7-days of AngII infusion (day 3, $p=0.0014$) (day 7, $p=0.0008$). This attenuated response was observed from 3- to 7-days after AngII treatment was initiated, before blood pressure levels increased on par with saline injected animals at day 14. Cardiac function remained similar between all groups over the duration of AngII treatment (*Figure 5-8 B-G*).

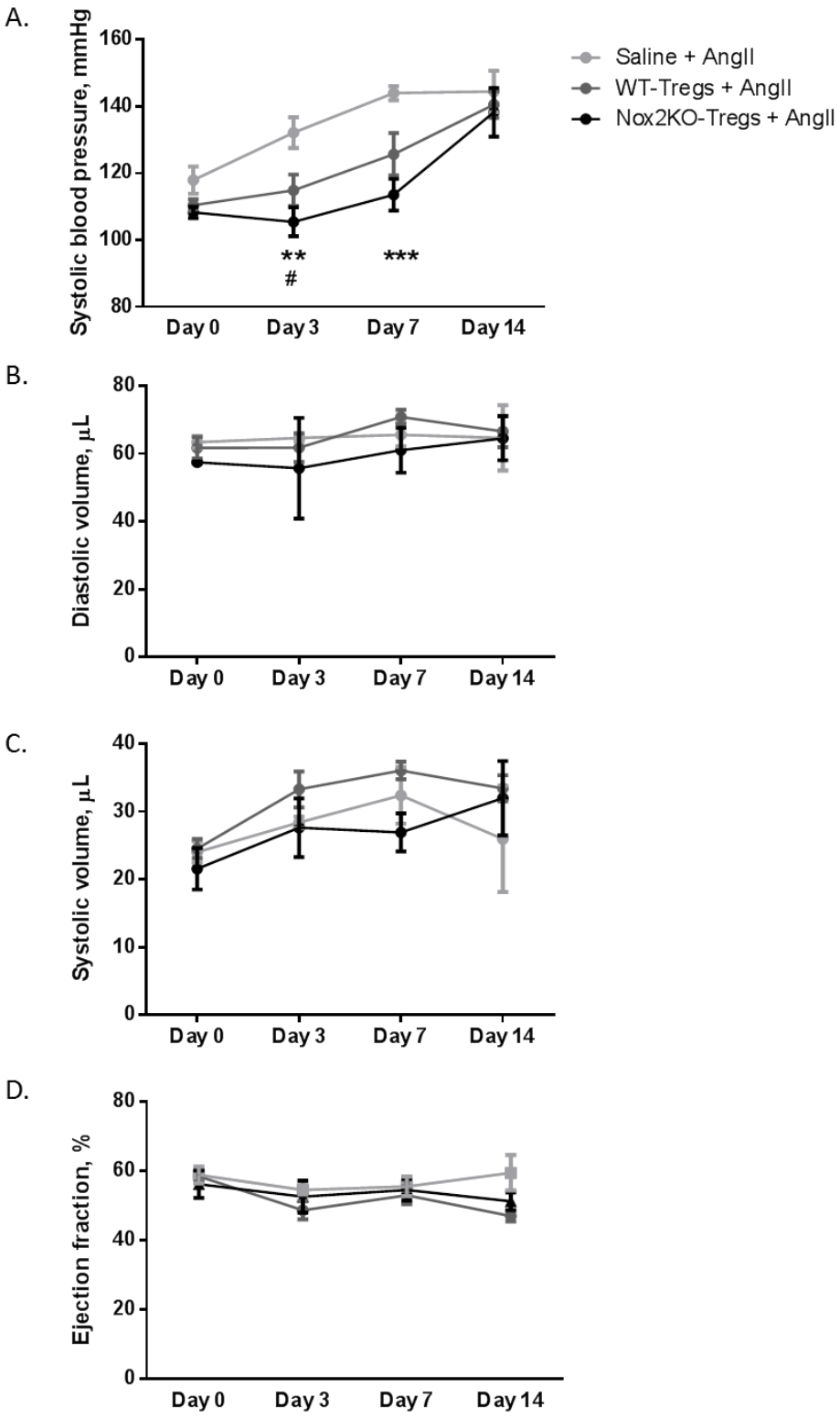

Figure 5-8: Treg adoptive transfer blunts AngII-induced hypertension. *Tail cuffing was used to record and analyse* ***(A)*** *systolic blood pressure. Haemodynamic function was observed using echocardiography looking at* ***(B)*** *LV end-diastolic and* ***(C)*** *LV end-systolic volume, and* ***(D)*** *ejection fraction. *p<0.05, **p<0.01, ***p<0.001. N=6 per group.*

After 14-days of treatment, mice were sacrificed and BW, HW and TL were recorded for all mice to generate HW/BW and HW/TL ratios. These were similar among the three groups (*Figure 5-9*). A gradual increase in IVS thickness was observed in saline injected animals treated with AngII, similar to the WT response to AngII seen in chapter 3. This prominent increase was significantly blunted in both WT- (p=0.001) and more efficiently, Nox2KO- (p<0.0001) Treg injected groups after 14-days of AngII treatment, where the Nox2KO-Treg IVS thickness was 26% lower than that of the control, saline injected AngII treated group.

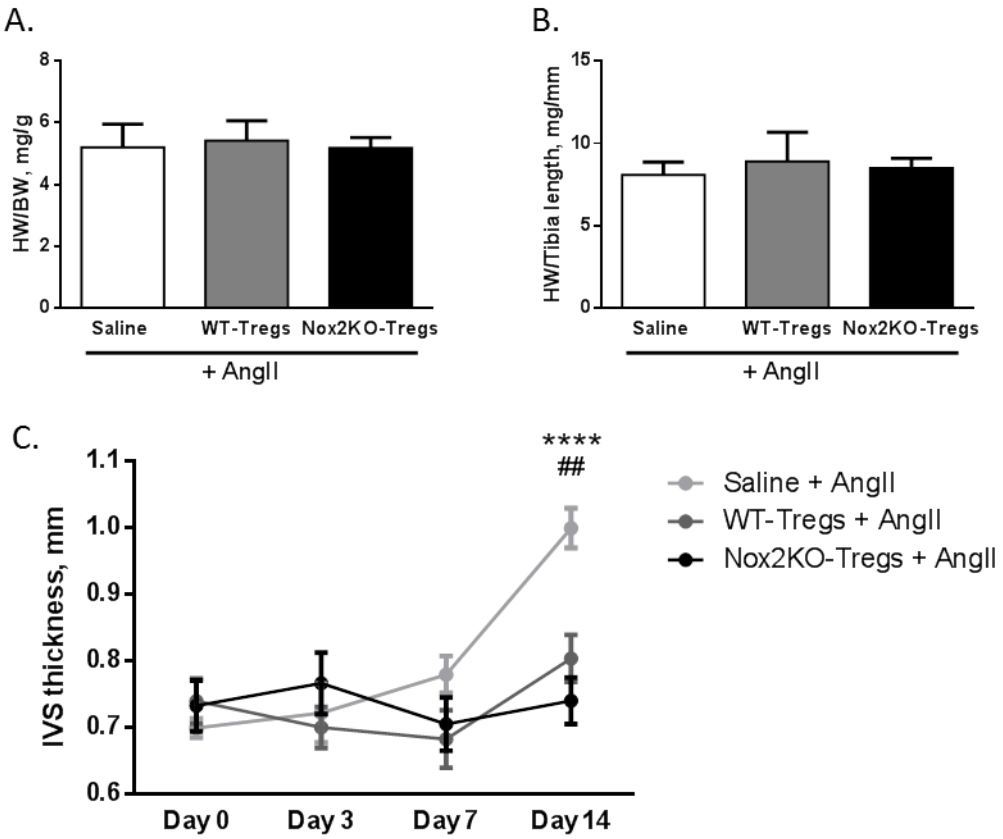

Figure 5-9: Treg adoptive transfer prevents AngII-induced hypertrophy. *Organ-level hypertrophy was analysed by* ***(A)*** *heart weight-to-body weight (HW/BW) ratio,* ***(B)*** *heart weight-to-tibia length (HW/TL) ratio and* ***(C)*** *interventricular septum (IVS) thickness. *Saline AngII vs Nox2KO-Treg AngII. #Saline AngII vs WT-Treg AngII. **p<0.01, ****p<0.0001. N=6 per group.*

Paraffin sections prepared from heart samples were treated with WGA to stain cell membranes of cardiomyocytes. Analysis highlighted significantly smaller cardiomyocyte surface areas in groups treated with both WT- (p=0.003) and Nox2KO-Tregs (p=0.002) compared to saline injected groups, (*Figure 5-10*).

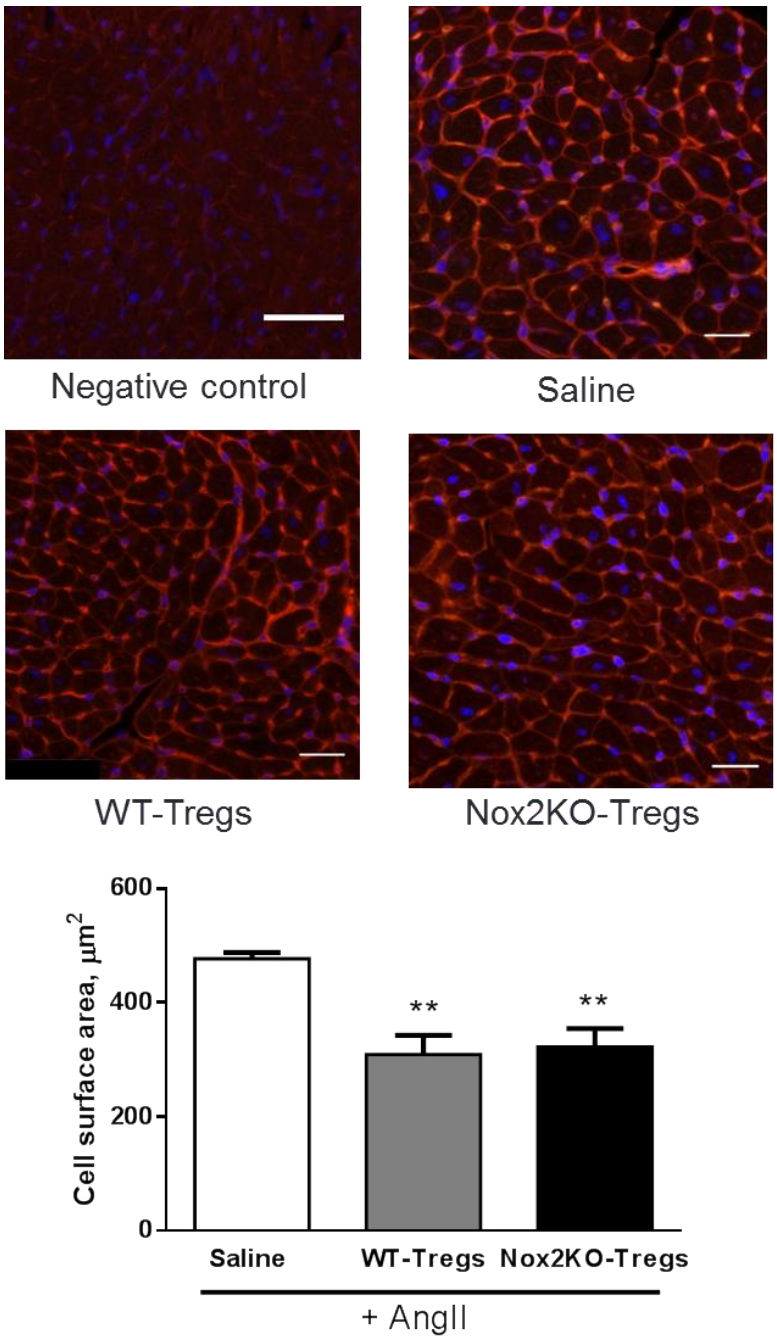

Figure 5-10: Blunted AngII-induced cardiomyocyte hypertrophy observed with Treg adoptive transfer. *WGA staining highlighted smaller cardiomyocyte surface area in both Nox2KO-Treg and WT-Treg injected groups compared to saline, all treated with AngII for 14-days. **p<0.01, N=6 per group.*

PSR staining was performed on cardiac paraffin sections to identify collagen, *Figure 5-11*. The saline injected group, treated with AngII, resulted in interstitial fibrosis to a similar level to that observed in chapter 3. Comparable fibrosis was also observed in WT-Treg injected group treated with AngII after 14-days, however this was blunted in the Nox2KO-Treg compared to both WT-Treg ($p<0.0001$) and saline ($p<0.0001$) injected groups.

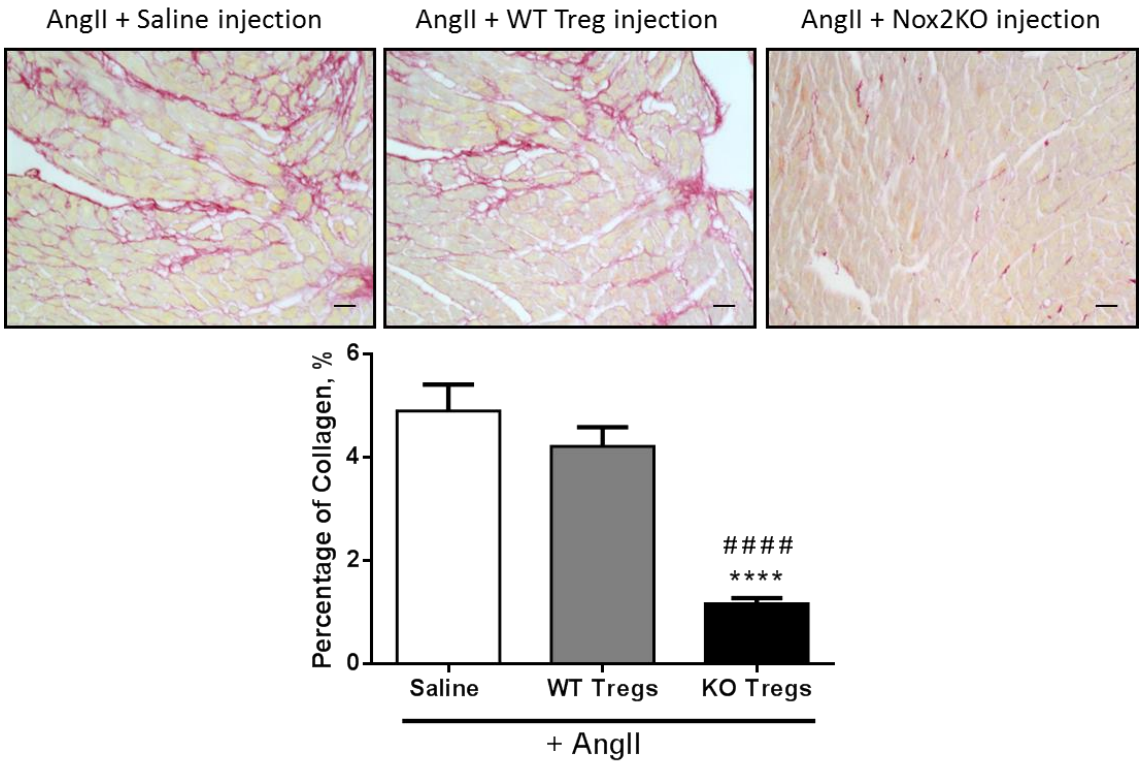

Figure 5-11: Nox2KO-Treg adoptive transfer prevents AngII-induced interstitial fibrosis. *Paraffin sections stained with picrosirius red identify a lower percentage of collagen within Nox2KO-Treg injected hearts treated with AngII for 14-days.*Nox2KO-Tregs vs saline. #Nox2KO-Tregs vs WT-Tregs. ****p<0.0001, N=6 per group.*

Furthermore, col1α1 ($p=0.022$) and col3α1 ($p=0.014$) mRNA levels were considerably lower in Nox2KO-Treg injected animals compared to WT and saline (*Figure 5-12*). However, fibronectin, TGFβ and CTGF were similar among groups.

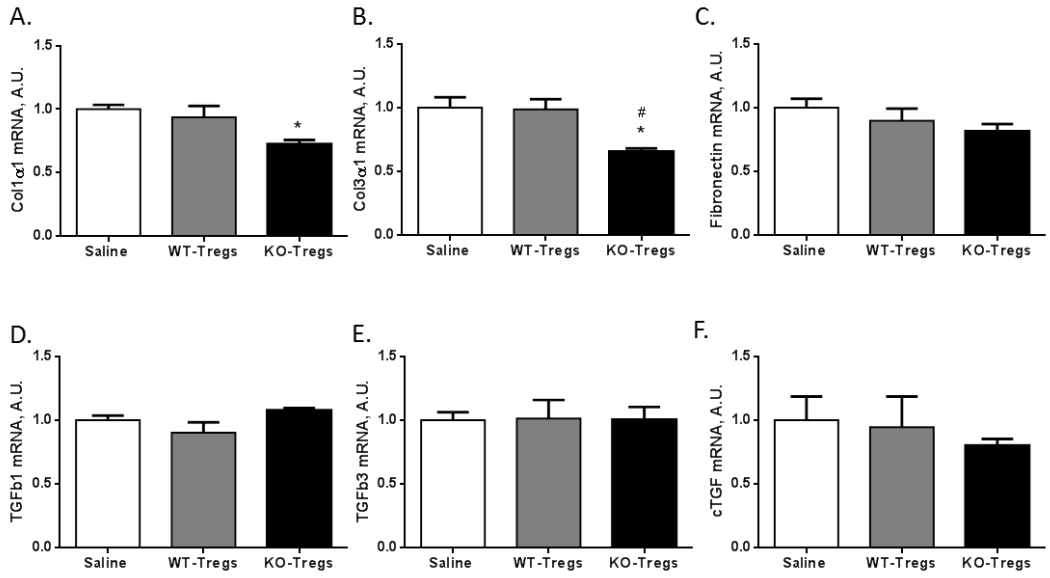

Figure 5-12: Adoptive transfer of Nox2KO-Tregs decreases cardiac fibrotic-related markers. *Analysis by qPCR of mRNA levels for* ***(A)*** *collagen1α1,* ***(B)*** *collagen3α1,* ***(C)*** *fibronectin,* ***(D)*** *TGFβ1,* ***(E)*** *TGFβ3 and* ***(F)*** *CTGF. *Nox2KO-Tregs vs Saline. #Nox2KO-Tregs vs WT-Tregs.*p<0.05, N=5-6 per group.*

5.4.2 Cardiovascular inflammation is altered by Nox2KO-Treg adoptive transfer

Quantification of immune cell infiltration was obtained by flow cytometry using BD FACS CantoII™. Adoptive transfer experiments were performed as described previously, but injected C57Bl/6 mice were treated for 3-days with AngII before analysis. Single cell suspensions were prepared from whole hearts, aortas, kidneys and spleens from all treated animals.

In terms of cardiac infiltration, representative flow cytometry dot plots shown in *Figure 5-13* demonstrate a lower number of leukocytes, T-cells and T-cell subsets in the Nox2KO-Treg injected group compared to saline.

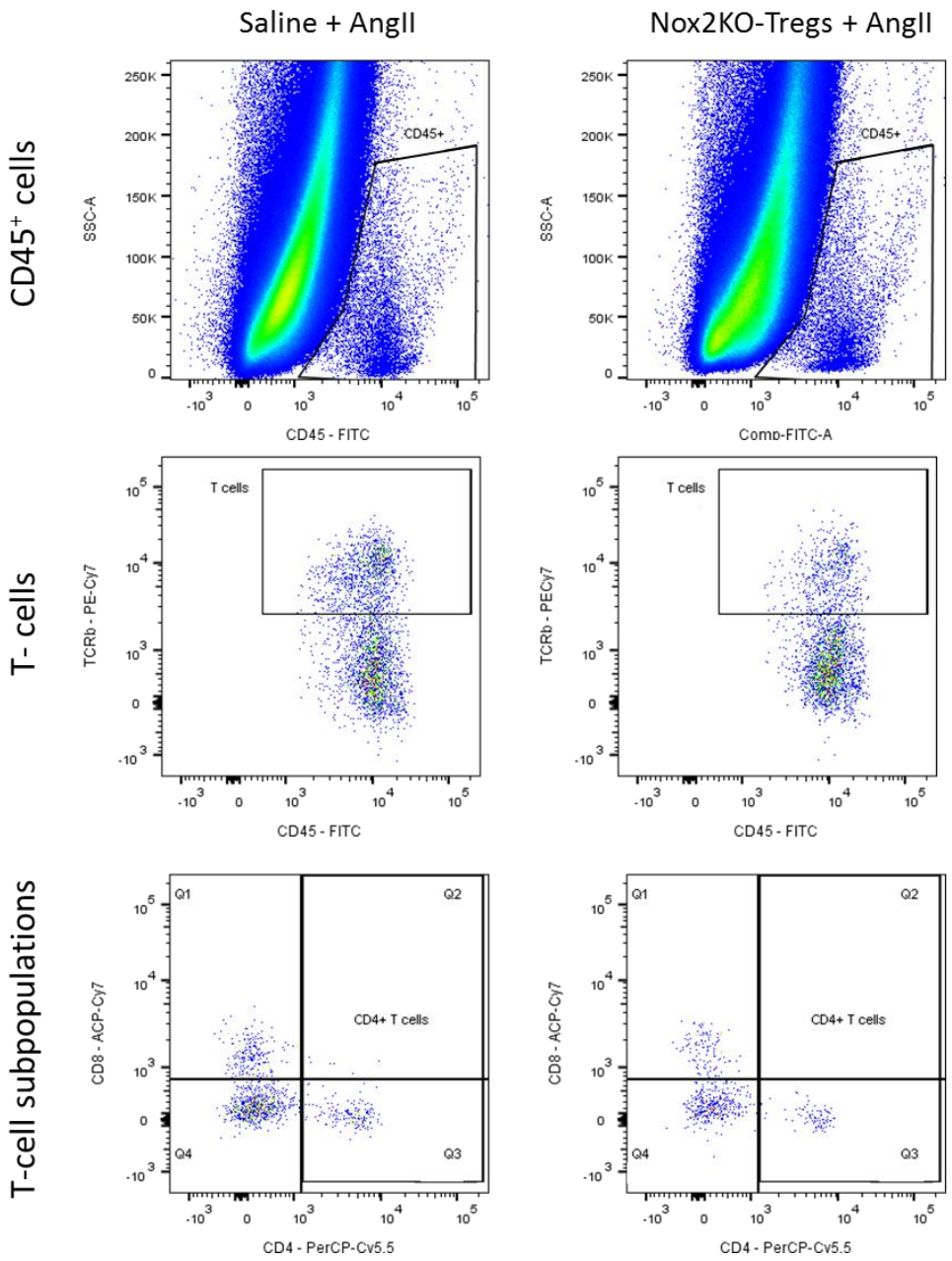

Figure 5-13: Representative flow cytometry dot plots illustrate lower cardiac inflammation with Treg adoptive transfer. *Acquired on BD FACS CantoII™.*

Flow cytometric analysis, *Figure 5-14*, shows that total leukocytes ($CD45^+$ cells) were significantly lower in WT- ($p<0.001$) and in Nox2KO- ($p<0.0001$) Treg injected groups compared to saline. Comparable results were observed with T-cell infiltration with hearts from both WT- ($p=0.003$) and Nox2KO- ($p<0.001$) Treg injected groups containing significantly less T-cells, 76% and 88% respectively, than saline injected animals. Each of the T-cell subpopulations showed a similar response, with DN T-cells ($p_{WT}=0.001$; $p_{Nox2KO}<0.001$), DP T-cells ($p_{WT}<0.001$; $p_{Nox2KO}<0.001$), $CD8^+$ T-cells

(p_{WT}=0.006; p_{Nox2KO}=0.007) and $CD4^+$ T-cells (p_{WT}=0.044; p_{Nox2KO}=0.009) each having a significantly lower infiltration with WT- and Nox2KO-Treg injections compared to saline, all treated with AngII. The Nox2KO-Treg injected group appeared to have a greater reduction in total T-cells and in $CD4^+$ T-cells than the WT-Treg injected group, but this was not statistically significant.

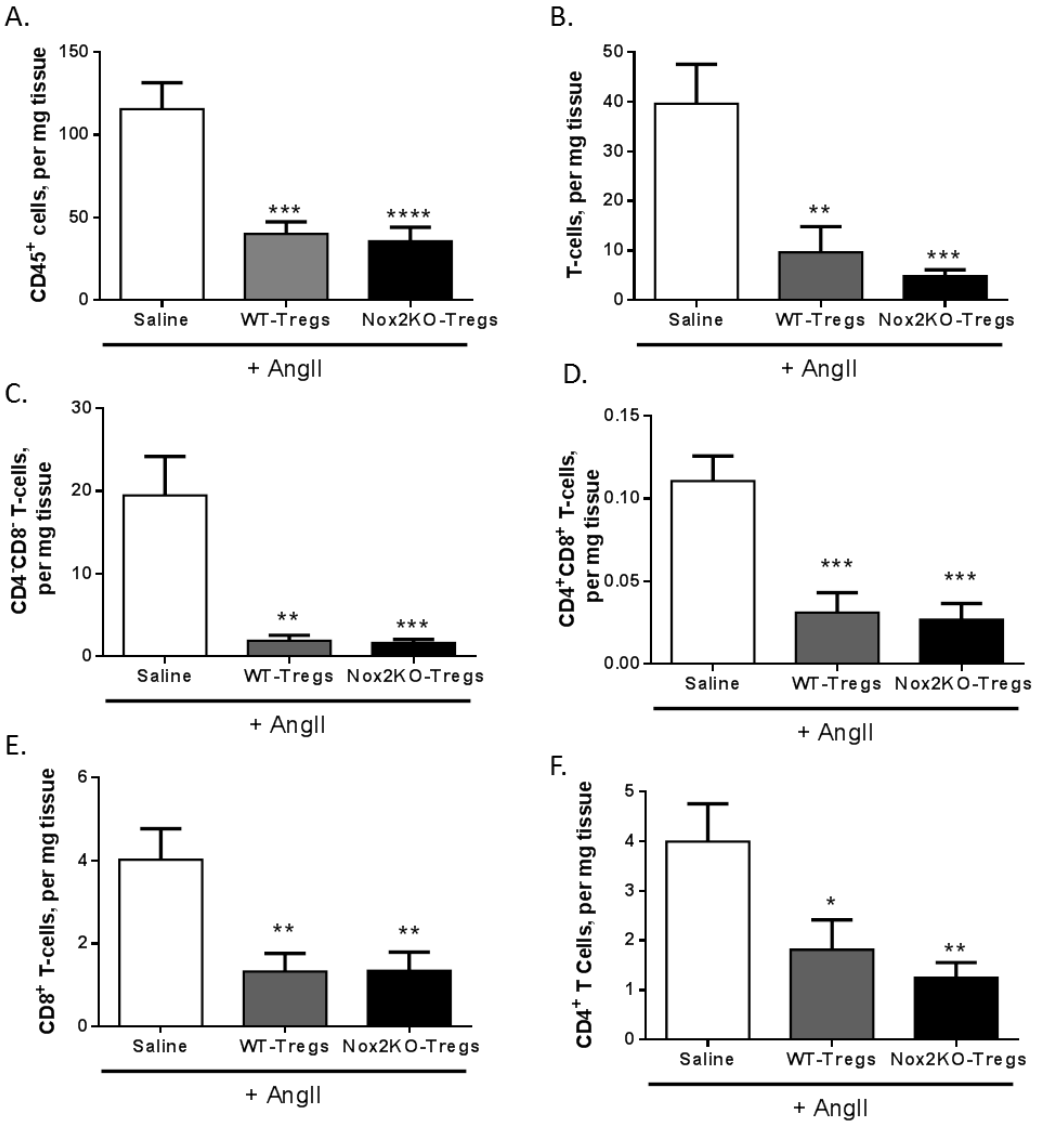

Figure 5-14: Treg adoptive transfer blunts AngII-induced cardiac inflammation. *Analysis of* ***(A)*** *total leukocytes ($CD45^+$),* ***(B)*** *T-cells ($CD45^+TCR\beta^+$),* ***(C)*** *$CD4^-CD8^-$ T-cells,* ***(D)*** *$CD4^+CD8^+$ T-cells,* ***(E)*** *$CD8^+$ T-cells and* ***(F)*** *$CD4^+$ T-cells. Represented as cells per mg of heart tissue, analysed on BD FACS CantoII™.*compared to Saline. *p<0.05, **p<0.01, ***p<0.001, ****p<0.0001. N=8-9 per group.*

Spleen samples, analysed as a background control for the immune system, demonstrated equal proportions of total leukocytes, T-cells and T-cell subpopulations (*Figure 5-15*).

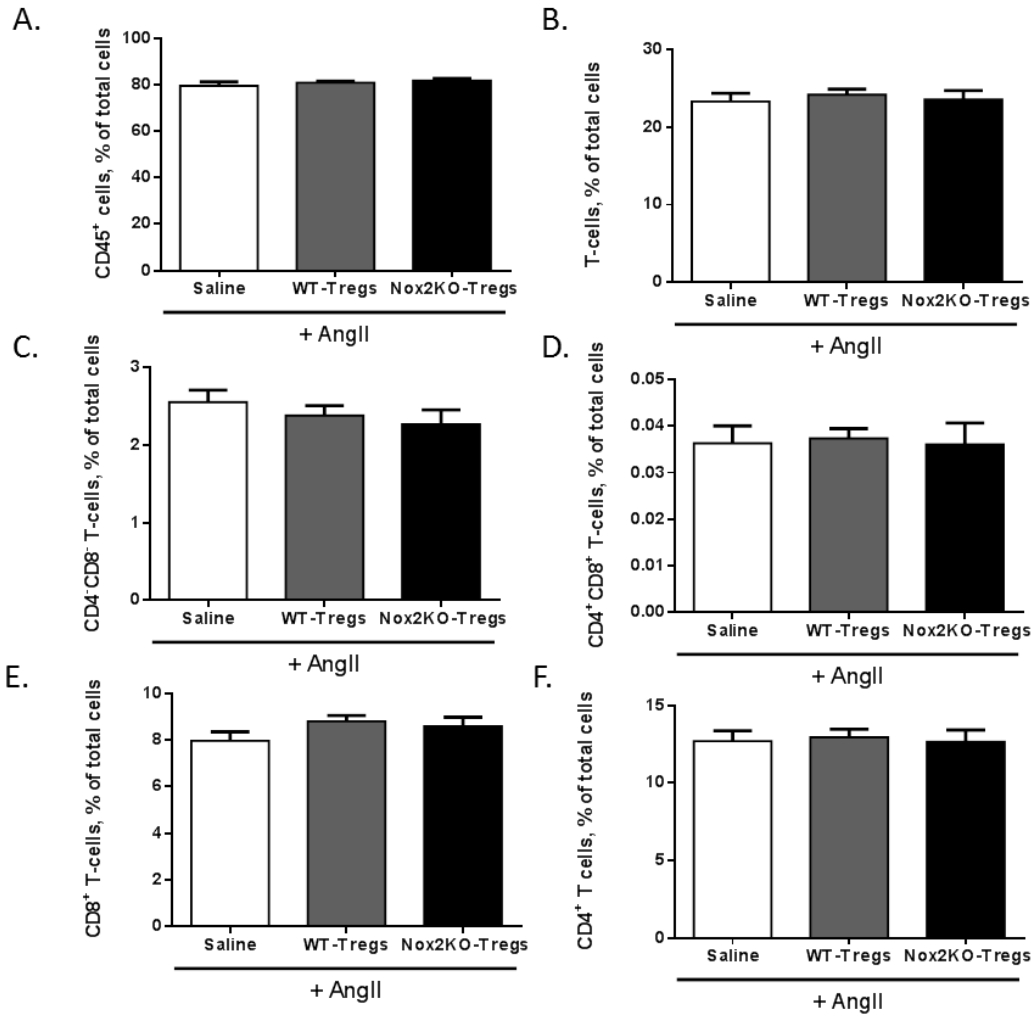

Figure 5-15: Splenic immune cell levels remain unaltered with Treg adoptive transfer. *Analysis of* ***(A)*** *total leukocytes ($CD45^+$),* ***(B)*** *T-cells ($CD45^+TCR\beta^+$),* ***(C)*** *$CD4^-CD8^-$ T-cells,* ***(D)*** *$CD4^+CD8^+$ T-cells,* ***(E)*** *$CD8^+$ T-cells and* ***(F)*** *$CD4^+$ T-cells. Represented as a percentage of total cells, analysed on BD FACS CantoII™. N=8 per group.*

Within the $CD4^+$ T-cell compartment, Tregs ($CD4^+CD25^+$ and $CD25^+FoxP3^+$) remained similar between all three groups (*Figure 5-16*). However, WT-Treg injected animals had a marked decrease in Tregs ($CD25^+FoxP3^+$) within the spleen compared to both Nox2KO-(p=0.019) and saline (p=0.001) injected mice. Highlighting a 34% lower level of Tregs in the spleen of WT-Treg injected animals compared to Nox2KO-Treg injected

animal, all treated with AngII. This may suggest a different Treg recruitment process between these two Treg injected groups.

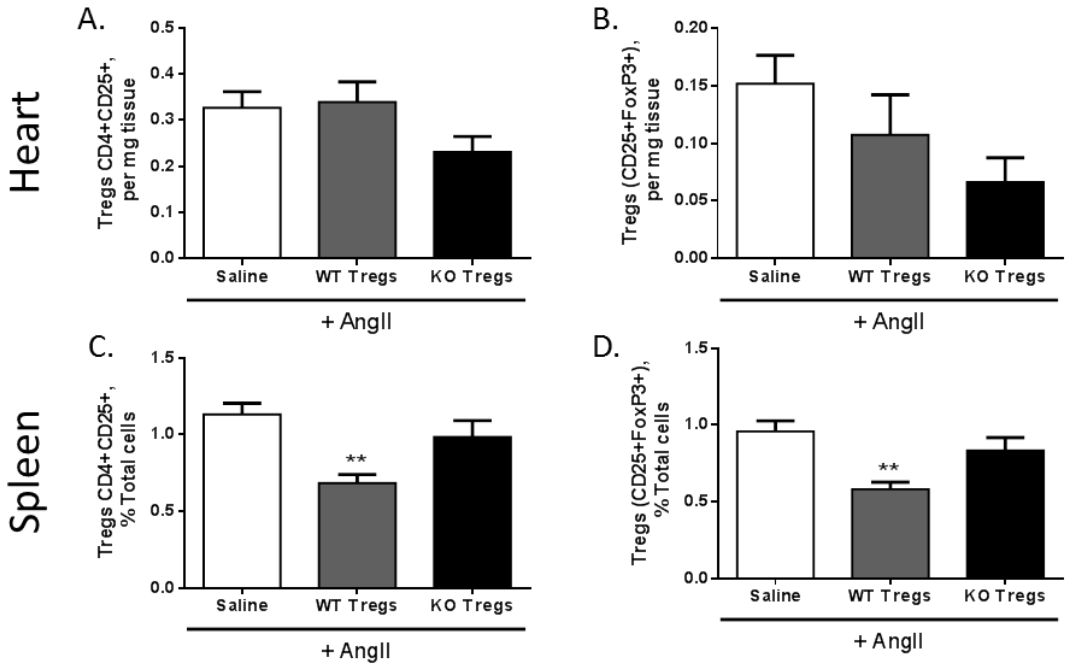

Figure 5-16: Splenic Treg levels are altered by WT-Treg adoptive transfer only. *Cardiac samples analysed by* ***(A)*** *$CD4^+CD25^+$ Tregs and* ***(B)*** *$CD25^+FoxP3^+$ Tregs. Splenic levels of* ***(C)*** *$CD4^+CD25^+$ Tregs and* ***(D)*** *$CD25^+FoxP3^+$ Tregs were also analysed. **p<0.001, analysed by BD FACS CantoII™. N=8-9 per group.*

In order to fully understand immune cell compositions within this setting, the proportions of T-cells required further investigation. Therefore, analysis of cells as a percentage of their parent population was carried out (*Figure 5-17*). Within the heart of AngII-treated WT- ($p<0.001$) and Nox2KO-Treg ($p<0.001$) injected groups, T-cells as a percentage of $CD45^+$ cells were significantly lower by 69% and 66% respectively. This suggests a reduction in T-cells but not necessarily other $CD45^+$ leukocytes; hence T-cells become a lower percentage of total $CD45^+$ cells. In comparison to this, in *Figure 5-17C* , $CD4^+$ T-cells as a percentage of total T-cells show a marked increase in both WT- ($p=0.023$) and Nox2KO-Treg ($p=0.026$) injected groups by a factor of approximately two. This indicates that the reduction in overall T-cells is greater than the reduction in $CD4^+$ T-cells, giving a larger ratio between the two. Interestingly, Tregs ($CD4^+CD25^+$) as a percentage of $CD4^+$ T-cells (*Figure 5-17E*) are significantly higher in

the Nox2KO-Treg injected group compared to saline (p=0.017). This is also confirmed by FoxP3 staining ($CD25^+FoxP3^+$ Tregs, *Figure 5-17G*), which shows an increase from 4.94±2.04% in saline hearts to 8.67±2.01% in Nox2KO-Treg injected hearts (p=0.013). Therefore, even though we do not see an increase in Tregs per mg of heart tissue, the proportion of Tregs to T-cells is significantly higher in the hearts of Treg-injected mice. In comparison WT-Treg injected animals tend to have a higher percentage of Tregs, within the $CD4^+$ T-cell compartment, however this was not significant. Spleen samples showed a similar level of T-cells as a percentage of $CD45^+$ cells and $CD4^+$ T-cells as a percentage of total T-cells (*Figure 5-17B&D*). However $CD4^+CD25^+$ Tregs as a percentage of $CD4^+$ T-cells (*Figure 5-17F*) are greatly decreased in WT-Treg treated animals compared to both saline (p<0.001) and Nox2KO-Treg (p=0.034) injected mice, all treated with AngII for 3-days. This difference was also maintained with more specific FoxP3 staining for Tregs, shown in *Figure 5-17H*, indicating a reduction from 7.46±0.28% in saline injected animals to 4.61±0.54% in WT-Treg injected mice (p<0.001). This suggests a different immune-response mechanism between the WT-Treg injected group and the Nox2KO-Treg injected group.

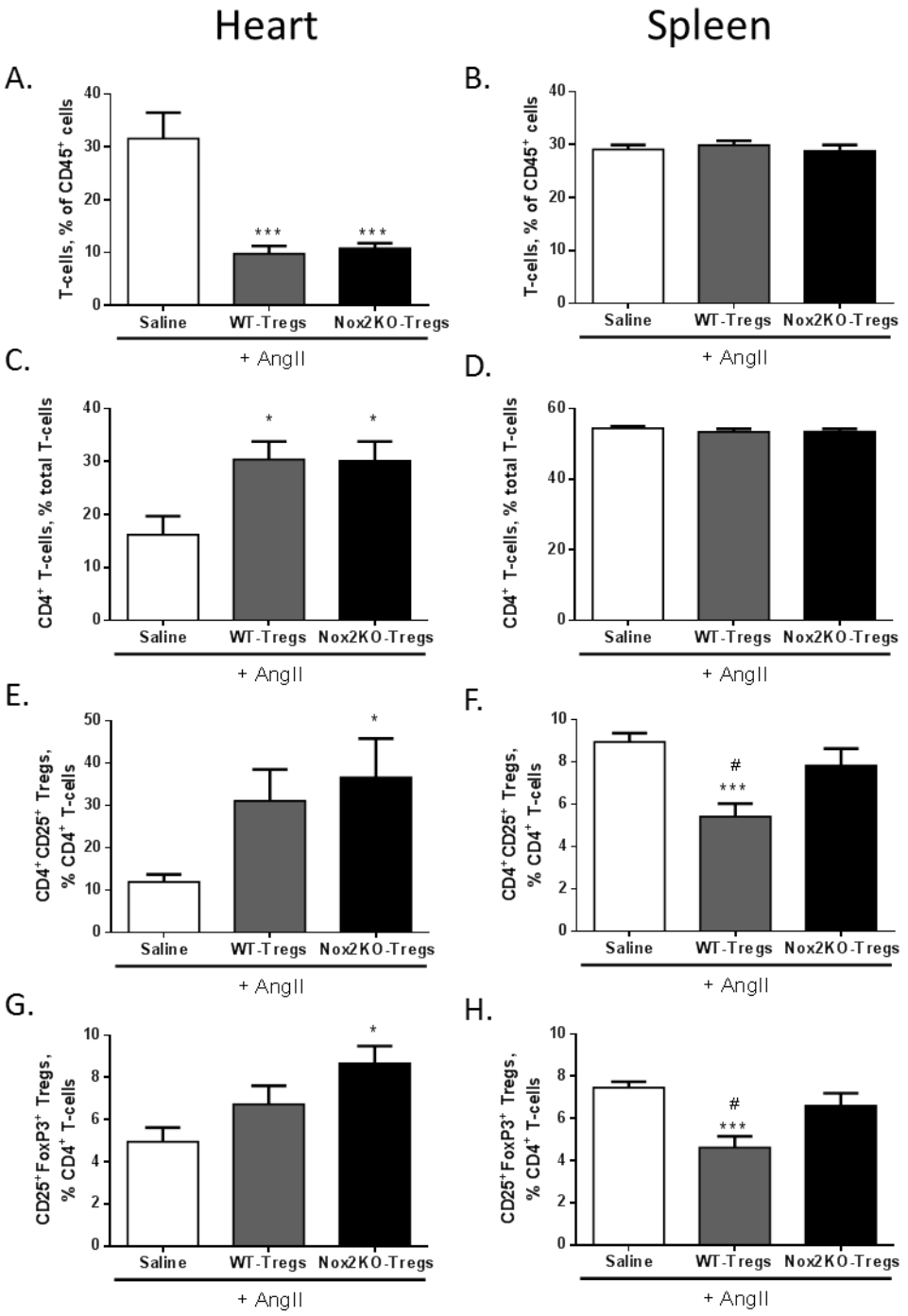

Figure 5-17: Adotive transfer of Tregs alters cardiac proportions of T-cells. *Flow cytometric analysis of* ***(A&B)*** *T-cells as a percentage of CD45$^+$ cells,* ***(C&D)*** *CD4$^+$ T-cells as a percentage of total T-cells,* ***(E&F)*** *CD4$^+$CD25$^+$ Tregs as a percentage of CD4$^+$ T-cells and* ***(G&H)*** *CD25$^+$FoxP3$^+$ Tregs as a percentage of CD4$^+$ T-cells. *WT-Tregs vs Saline; #WT-Tregs vs Nox2KO-Tregs. *p<0.05, ***p<0.001, analysed on BD FACS CantoII™. N=8 per group.*

In order to examine the effect on the vasculature, aortas were also prepared for flow cytometry analysis. All investigated parameters paralleled the previous results observed in heart samples, as shown in *Figure 5-18*. Leukocytes were significantly lower in WT- (p=0.015) and Nox2KO- (p=0.007) Treg treated animals compared to saline. Aortic infiltration of T-cells was blunted in both WT- (p=0.001) and Nox2KO- (p=0.003) Treg injected groups compared to saline, *Figure 5-18B*. This effect was preserved within the T-cell subpopulations, where DN (p_{WT}=0.014; Nox2KOp=0.012), DP, $CD8^+$ (p_{WT}=0.003; p_{Nox2KO}=0.008) and $CD4^+$ (p_{WT}=0.002; p_{Nox2KO}=0.005) all showed a marked reduction compared to saline injected groups (*Figure 5-18*C-F). Aortic infiltration of Tregs was not different among the three groups, shown in *Figure 5-18G-H*.

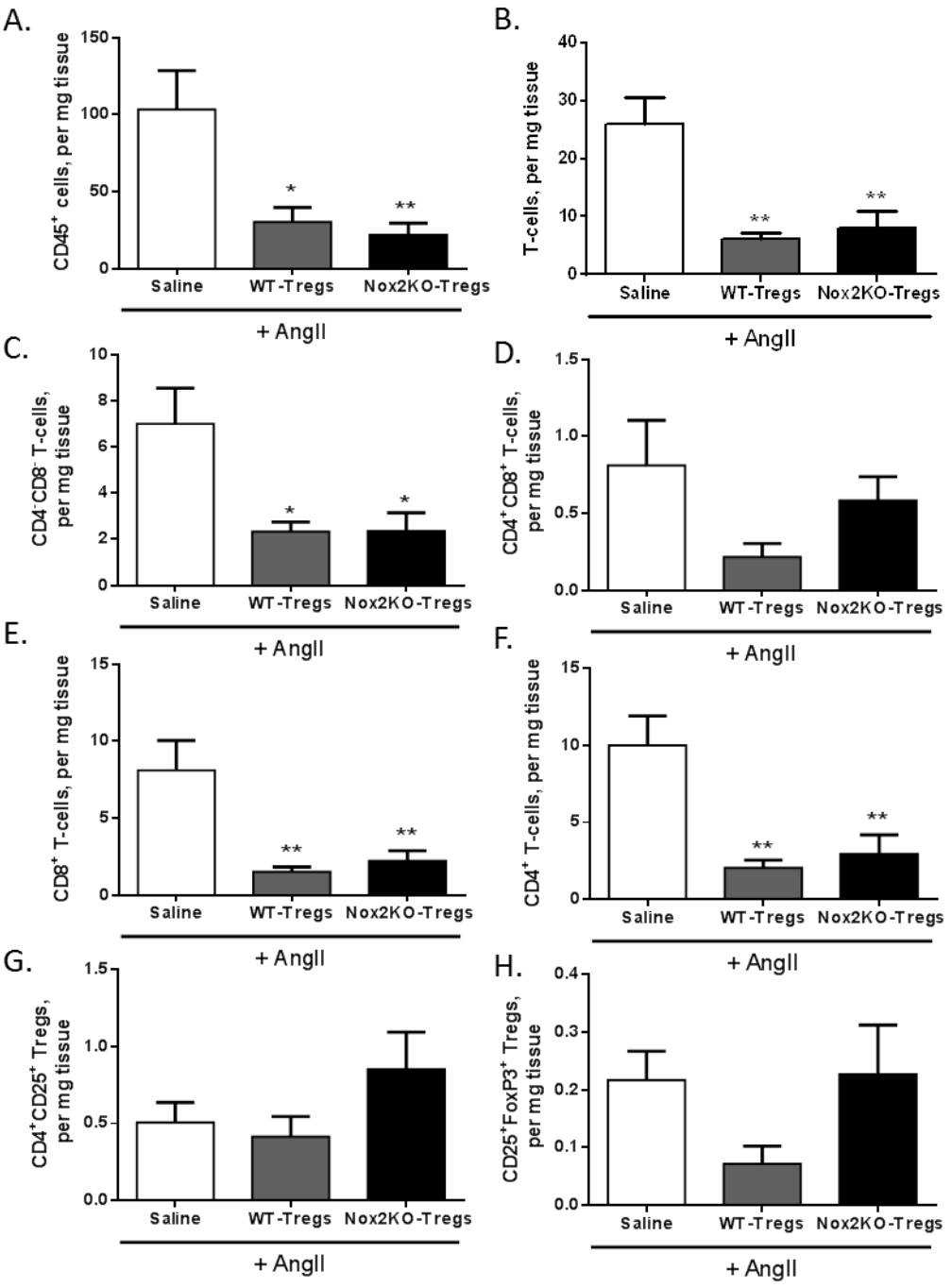

Figure 5-18: Adoptive transfer of Tregs blunted AngII-induced aortic inflammation. *Analysis of* ***(A)*** total leukocytes ($CD45^+$)(WTp=0.015; Nox2KOp=0.007), **(B)** T-cells ($CD45^+TCR\beta^+$) (WTp=0.001; Nox2KOp=0.003), **(C)** $CD4^-CD8^-$ T-cells (WTp=0.014; Nox2KOp=0.012), **(D)** $CD4^+CD8^+$ T-cells, **(E)** $CD8^+$ T-cells (WTp=0.003; Nox2KOp=0.008), **(F)** $CD4^+$ T-cells (WTp= 0.002; Nox2KOp=0.005), **(G)** $CD4^+CD25^+$ Tregs and **(H)** $CD25^+FoxP3^+$ Tregs. All represented as cells per mg of aorta tissue. Analysed on BD FACS CantoII™. N=7-8 per group.

In addition to different immune cell compositions within WT- and Nox2KO-Treg injected groups compared to saline injected groups we also identified altered T-cell proportions. *Figure 5-19A-B* shows consistent levels of T-cells as a percentage of $CD45^+$ cells, and $CD4^+$ T-cells as a percentage of total T-cells. Meanwhile, *Figure 5-19 C* shows a significant increase in $CD4^+CD25^+$ Tregs as a percentage of $CD4^+$ T-cells for both WT- ($p=0.002$) and Nox2KO-Treg ($p<0.001$) injected animals compared to saline. More specific Treg staining with FoxP3 confirms this trend but only shows significance in the Nox2KO-Treg ($p=0.023$) injected group (*Figure 5-19 D*).

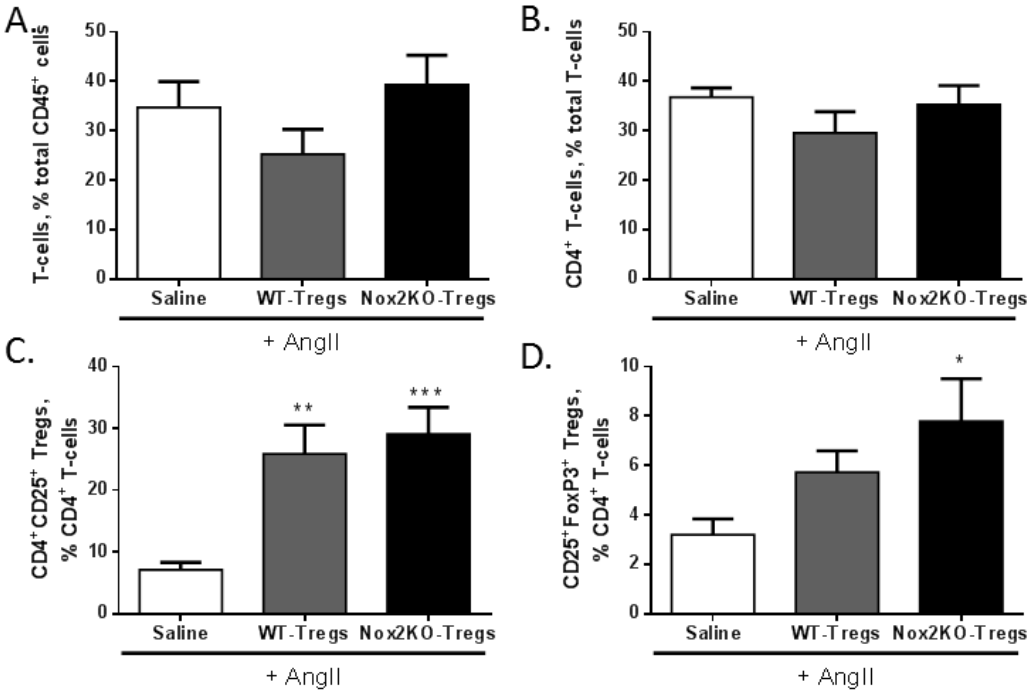

Figure 5-19: Aortic T-cell proportions are altered by adoptive transfer of Tregs with AngII treatment. *Levels of* ***(A)*** *T-cells as a percentage of $CD45^+$ cells,* ***(B)*** *$CD4^+$ T-cells as a percentage of total T-cells,* ***(C)*** *$CD4^+CD25^+$ Tregs and* ***(D)*** *$CD25^+FoxP3^+$ Tregs. *p<0.05, **p<0.01, ***p<0.001, analysed BD FACS CantoII™. N=7-8 per group.*

Due to an impact on systolic blood pressure by the adoptive transfer of Tregs, kidney samples were also analysed for changes in immune cell composition (*Figure 5-20*). This was based on their vital role in blood pressure homeostasis[245]. Total leukocytes, T-cells and each of the T-cell subpopulations remained similar between all three groups, suggesting that the kidneys do not contribute to the differences in blood pressure.

Kidney T-cell proportions, analysed in *Figure 5-21*, also show no differences between the WT-Treg, Nox2KO-Treg and saline injected animals, all treated with AngII for 3-days.

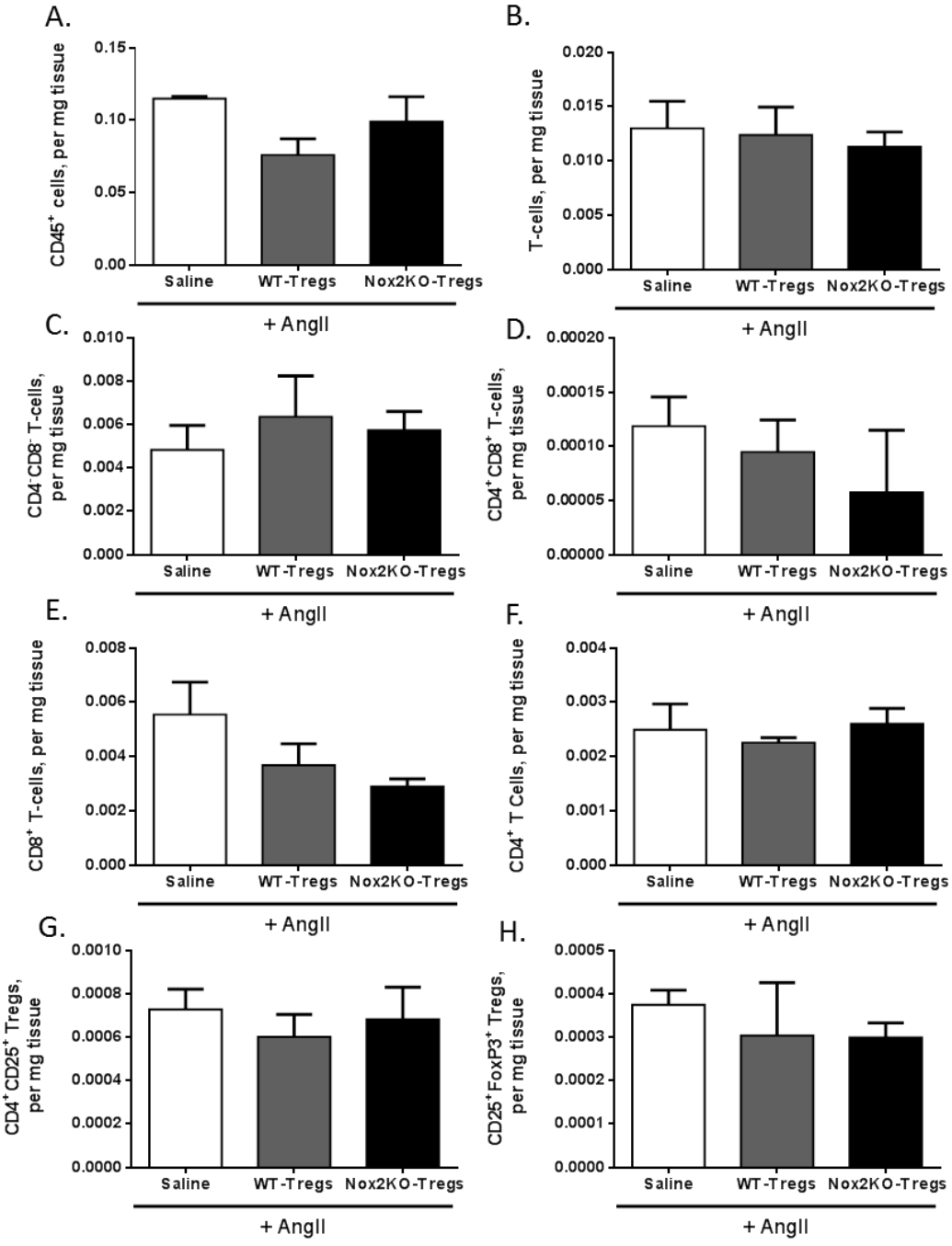

Figure 5-20: Treg adoptive transfer does not alter kidney T-cell compositions. *Analysis of* ***(A)*** *total leukocytes ($CD45^+$),* ***(B)*** *T-cells ($CD45^+TCR\beta^+$),* ***(C)*** *$CD4^-CD8^-$ T-cells,* ***(D)*** *$CD4^+CD8^+$ T-cells,* ***(E)*** *$CD8^+$ T-cells,* ***(F)*** *$CD4^+$ T-cells,* ***(G)*** *$CD4^+CD25^+$ Tregs and* ***(H)*** *$CD25^+FoxP3^+$ Tregs. All represented as cells per mg kidney tissue. Analysed on BD FACS CantoII™. N=3 per group.*

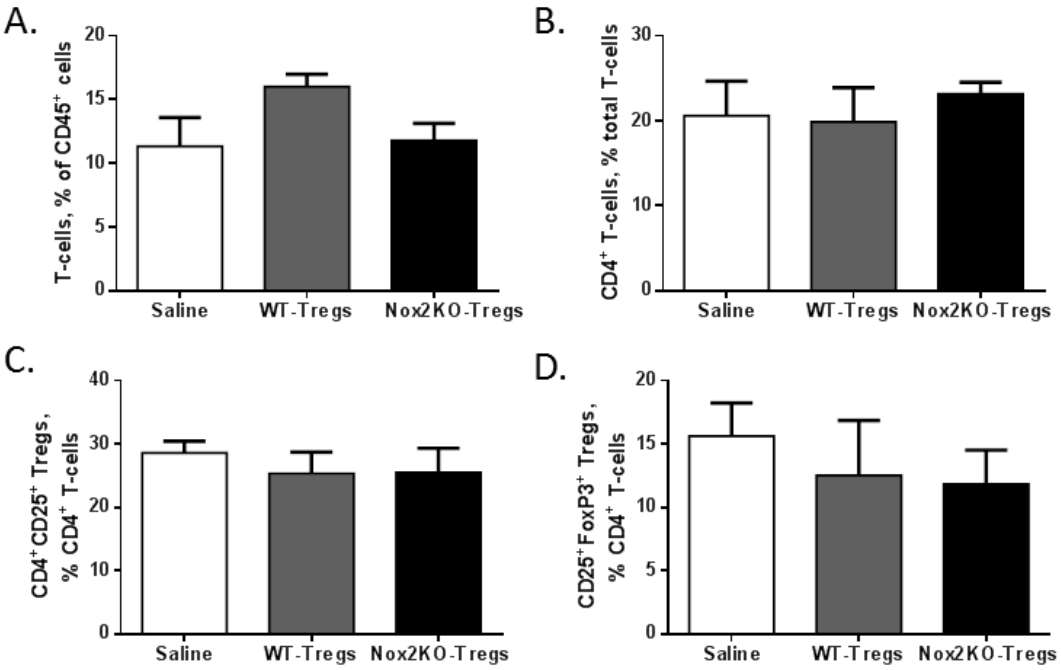

Figure 5-21: Kidney T-cell proportions remain consistent with Treg adoptive transfer and AngII treatment. *Levels of* ***(A)*** *T-cells as a percentage of CD45$^+$ cells,* ***(B)*** *CD4$^+$ T-cells as a percentage of total T-cells,* ***(C)*** *CD4$^+$CD25$^+$ Tregs and* ***(D)*** *CD25$^+$FoxP3$^+$ Tregs. Analysed BD FACS CantoII™, N=3 per group.*

5.4.3 Nox2 regulates Treg suppressive function *in vitro*

Suppression assays were set up using CD4$^+$ T-cells and APCs, isolated from C57Bl/6 mice, in the presence of purified anti-CD3 antibody. Tregs obtained from either WT or Nox2KO mice were then incubated with the CD4:APC (1:2) pool at different Teff:Treg ratios (1:1, 1:2, 1:4, 1:8, 1:16) with WT CD4$^+$ T-cells in the presence of WT APCs and purified anti-CD3 antibody. Thymidine incorporation was used as readout.

CD4$^+$ T-cell proliferation reached approximately 6x10^4 counts per minute (cpm) and in the presence of WT-Tregs this was suppressed by 63% with a 1:1 T-cell to Treg ratio (*Figure 5-22*). In comparison, Nox2KO-Tregs resulted in an 83% suppression of CD4$^+$ T-cell proliferation (2-way ANOVA *Figure 5-22B*, p=0.043). Therefore, Nox2KO-Tregs were significantly more suppressive than WT-Tregs at a 1:1 ratio (p=0.007). This difference in Treg suppressive ability between the two genotypes was maintained at a ratio of 1:2 (p=0.041) before reaching a plateau at a ratio of 1:4 and higher.

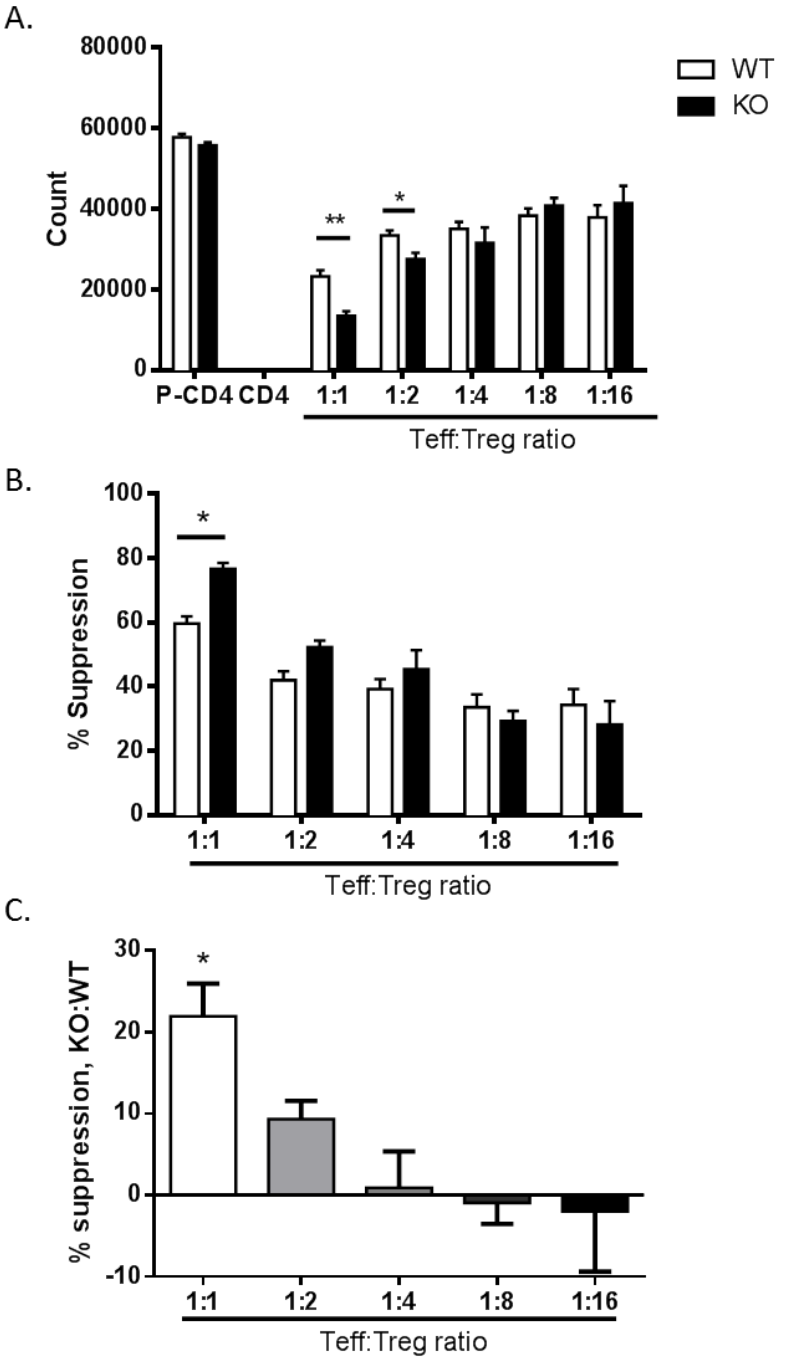

Figure 5-22: Nox2KO-Tregs have a greater suppressive function. *Treg suppression assay was analysed using thymidine to show difference in* ***(A)*** *total cell counts (N=3 per group),* ***(B)*** *percentage of suppression (N=3 per group) and* ***(C)*** *percentage difference between KO- and WT-Tregs (N=6-9 per group). *p<0.05, **p<0.01.*

In order to fully understand the differences in suppression, Treg phenotypes were compared between WT and Nox2KO animals. Specific markers associated with Treg function were analysed on isolated Tregs from both genotypes via BD FACS CantoII™. Nox2KO-Tregs had similar levels of CD25, FoxP3, GITR and CD62L, however they expressed a higher level of CD73 (p=0.001), CD39 (p=0.014), CTLA-4 (p=0.028) in addition to reduced level of CD103 (p=0.004) as compared to WT littermates (*Figure 5-23*).

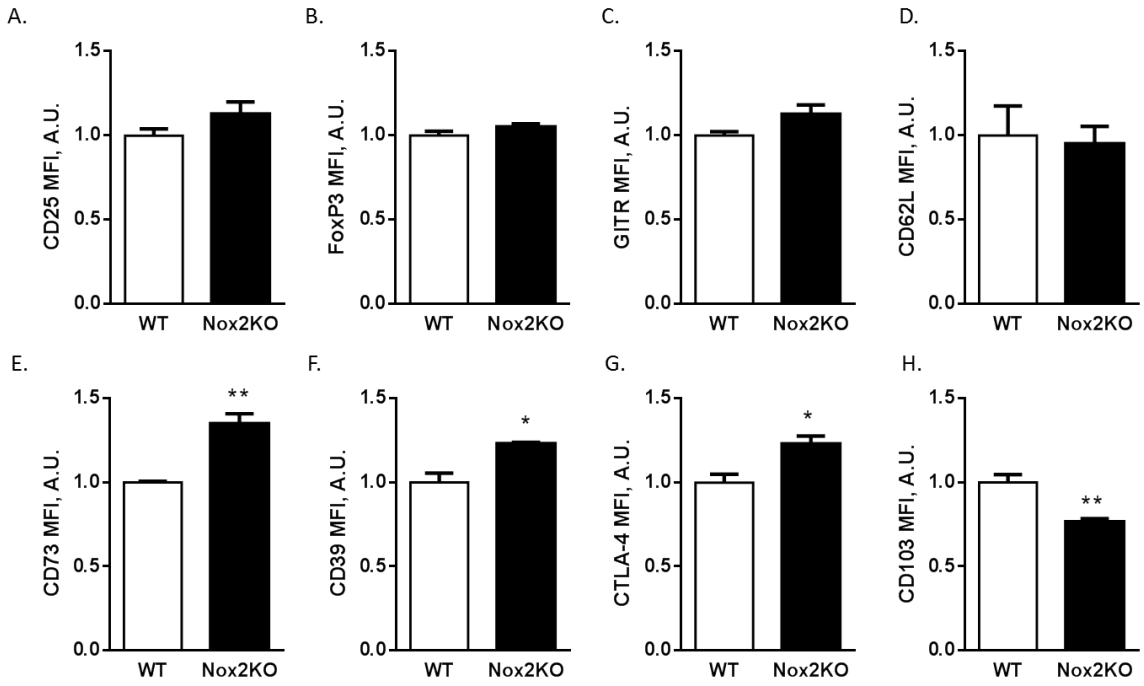

Figure 5-23: Global Nox2KO Tregs express altered levels of phenotypic surface markers. *Flow cytometry revealed similar expression levels of* ***(A)*** *CD25,* ***(B)*** *FoxP3,* ***(C)*** *GITR and* ***(D)*** *CD62L. Whereas expression of* ***(E)*** *CD73,* ***(F)*** *CD39,* ***(G)*** *CTLA-4 and* ***(H)*** *CD103 were altered in Nox2KO-Tregs compared to WT littermates. Analysed on BD FACS CantoII™, *p<0.05, **p<0.01. N=3-4 per group.*

Taken together, our results suggest that an increased baseline-level of Tregs in general, provides a protective response in terms of AngII-induced hypertension and cardiac hypertrophy. Furthermore, the inflammatory response in the heart and aorta of Treg injected mice changed, giving an anti-inflammatory response with greater Treg:T-cell ratios compared to saline. However, the adoptive transfer of Nox2KO-Tregs proved beneficial in the response to AngII-induced interstitial fibrosis and provided a more

efficient protection against AngII-induced inflammation. Hence, both *in vitro* and *in vivo* assays suggested that Nox2KO-Tregs have a greater suppressive function than WT-Tregs.

These findings may reflect a local protective cardiovascular phenotype with higher baseline concentrations of Tregs, which is greater in the setting of Nox2KO-Tregs.

5.5 Discussion

The experiments presented in this chapter show a clear distinction between Nox2KO- and WT-Treg function both *in vivo* and *in vitro*. Adoptive transfer of both Nox2KO- and WT-Tregs did not alter the level of $CD4^+CD25^+FoxP3^+$ Tregs within the heart. One aspect to consider is that Tregs within the myocardium are difficult to obtain and analyse, due to their low numbers. In addition to this, the process of staining for FoxP3 causes further loss of immune cells due to fixation, permeabilisation and extra washing steps involved. The protocol used here involved the injection of $1x10^6$cells per mouse, however not all of these cells would migrate to the heart; therefore our flow cytometry method may not be accurate enough to identify this direct increase in Treg numbers per mg of cardiac tissue. On the other hand, Tregs as a percentage of total $CD4^+$ T-cells tended to be higher in WT-Treg treated group and significantly higher in Nox2KO-Treg injected group. This confirms that after adoptive transfer, the $CD4^+$ T-cell:Treg ratio is altered to that favouring Tregs, and hence an anti-inflammatory processes is in action. Even though an increase in Tregs in the heart (per mg of tissue) cannot clearly be identified, their effect on T-cell numbers, specifically $CD4^+$ T-cells has been observed here.

The adoptive transfer of Nox2KO-Tregs compared to WT-Tregs was more effective at preventing AngII-induced hypertension and associated cardiac remodelling. Interestingly, AngII-induced systolic blood pressure was significantly lower after 3-days of treatment in mice injected with WT-Tregs. Compelling evidence supports these findings with WT-Tregs. For example a similar response was found by Barhoumi et al who performed adoptive transfer of Tregs into C57Bl/6 mice aged 10-12 weeks. This group observed a significantly lower blood pressure in WT-Treg injected mice

compared to PBS- and Teff-injected mice, all treated with a pressor dose of AngII for up to 14-days[190]. This experiment included multiple Treg injections, three times at two week intervals, prior to AngII-infusion, in addition to three Treg injections per week throughout treatment with AngII[190]. Therefore the gradual increase observed in blood pressure after 3-days of AngII treatment, which returns to similar levels as saline-injected mice after 14-days, might be preventable by multiple Treg injections. This attenuated hypertensive response to AngII tended to be greater in mice injected with Nox2KO-Tregs. Until now, Nox2KO- Tregs have not previously been studied in this setting; results here indicate that Nox2KO-Tregs are more suppressive than WT-Tregs. The same research group also demonstrated similar results with aldosterone treatment[192].

The adoptive transfer of both types of Tregs prevented AngII-induced hypertrophy that was observed by IVS thickness and cardiomyocyte cross-sectional area. This confirmed the results of Kvakan et al who carried out a Treg adoptive transfer into Naval Medical Research Institute (NMRI) male mice, which are WT outbred albino mice, one day after initiation of AngII-treatment[191]. Blunted AngII-induced hypertrophy was observed after 2 weeks of treatment as documented by LV wall thickness and LV weight-to-body weight ratio[191]. In this study, HW/BW and HW/TL ratios were analysed but with no differences between all groups. This may be because the hypertrophic response mainly occurs within the LV, so instead of weighing the whole heart, a more accurate method would be to weigh the LV only. Furthermore the IVS measurement is more accurate.

Interestingly injection of Nox2KO-, but not WT-, Tregs inhibited AngII-induced fibrosis, observed by PSR staining. This was also confirmed by qPCR analysis of col1α1 and col3α1, which were both significantly lower in Nox2KO-Treg injected groups. Kvakan et al observed significantly lower cardiac fibrosis, analysed by PSR staining, with NMRI-Treg adoptive transfers compared to AngII treatment alone[191]. This difference in WT results could be due to the specific genotype of mice used, NMRI instead of C57Bl/6, or due to a higher dose of AngII (1.44mg/kg/day instead of 1.1mg/kg/day). Furthermore, Kanellakis et al transferred Tregs, or control vehicle, into mice following TAC and observed that the adoptive transfer of Tregs attenuated cardiac fibrosis and hypertension[189]. Even though these experiments have used a different model or

mouse genotype, both identify a role for Tregs within AngII-induced fibrosis and the results here highlight that Nox2KO-Tregs may be more efficient in this setting.

Furthermore, Tregs have been implicated in cardiac remodelling resulting from MI. Tregs are observed in the peri-infarct zone (PIZ) of hearts from mice that have undergone MI[193]. An increase was observed 3-days after MI with a peak at 7-days and reduction 14-days after surgery, compared to sham animals. The author emphasises on the local recruitment of the cells as no alteration in Treg levels were observed in spleens or LNs[193]. Tang et al further increased the percentage of Tregs within the MI heart by an adoptive transfer, which led to attenuation of post-MI cardiac remodelling[193].

As Tregs have the ability to suppress inflammatory responses, the level of immune cell infiltration, specifically T-cells, within the myocardium was then analysed for saline-injected, WT-Treg injected and Nox2KO-Treg injected mice all treated with AngII. In both Treg-injected groups, AngII-induced inflammation was significantly blunted compared to saline-injected controls. This prevented the accumulation of total leukocytes, T-cells and each of the T-cell subtypes within the myocardium, which was also confirmed in the literature within NMRI-Treg injected mice[191]. Similarly, previous studies have demonstrated a reduced level of cardiac inflammation during the adoptive transfer of Tregs. For instance, Kvakan et al and Barhoumi et al both highlighted that cardiac infiltration of T-cells in response to AngII was prevented by Treg adoptive transfer[190-192]. Adoptive transfer performed by Kanellakis et al also prevented the accumulation of macrophages and T-cells within the LV after TAC[189].

Results here show that Nox2KO-Treg injected groups tended to be more efficient at preventing T-cell, specifically $CD4^+$ T-cell, recruitment. Furthermore, within the heart, T-cells as a percentage of total $CD45^+$ cells were significantly lower in both Treg-treated groups, suggesting that T-cells are specifically targeted and reduced by injected Tregs. In addition, $CD4^+$ T-cells as a percentage of total T-cells were higher in both Treg injected groups, potentially suggesting that Tregs, which are included in the $CD4^+$ T-cell subset, may be recruited to the heart.

These published results and data presented in this chapter have harnessed the beneficial effects of Tregs within the setting of cardiovascular remodelling by

performing a Treg adoptive transfer. This process enables the basal level of Tregs in the animal to be systemically increased, allowing additional control of the inflammatory response.

The increased efficiency of Nox2KO-Tregs observed *in vivo* was also confirmed *in vitro*. Under these experimental conditions, Nox2KO-Tregs are 20% more suppressive than WT-Tregs *in vitro*; however opposing results have been identified by Efimova et al. This research group performed a series of suppression assays by incubating Teff cells in the presence of anti-CD3/CD28 coated beads with varying concentrations of Tregs[214]. These cells were isolated from either $P47^{phox-/-}$ or WT mice[214]. The accuracy of the Treg:Teff ratios was also ensured by adjusting the concentration of Tregs based on the purity of isolated $CD4^{+}CD25^{+}$ Tregs[214]. They observed a lower level of suppressive ability in $p47^{phox-/-}$ Tregs compared to WT Tregs, when both incubated with either $p47^{phox-/-}$ or WT Teff cells[214]. However there are three aspects that vary between their protocol and that used in this study, which may account for the variation in results. Firstly, $p47^{phox-/-}$ mice were used within this paper to analyse the KO-Treg suppressive function, whereas the study presented here used $gp91^{-/-}$ mice. Even though these two genetic models both result in dysfunctional Nox2, the first removes a Nox2 adaptor protein whereas the second model prevents transcription of the main Nox2 catalytic subunit. There have been a handful of studies that suggest differences between these two genotypes[246,247]. For instance, it has previously been reported that deletion of $p47^{phox}$ can worsen vascular endothelial dysfunction whereas the lack of Nox2 is beneficial in terms of cardiovascular remodelling[108,175,246]. Therefore differences in the genetic model used may influence variation in Treg responses. Furthermore, Tregs and Teff cells were isolated from mice aged 6-14 weeks, whereas this study used mice aged 6-8 weeks. As discussed in section 4.5, the age of mice lacking Nox2 is important due to the onset of age-induced arthritis that may alter immune cell composition and function. For example Lee et al demonstrated that Nox2KO $CD4^{+}$ T-cells isolated from mice aged 12-28 weeks were less able to differentiate into Tregs and hence may, at this age, possess a different Treg suppressive ability[199]. Finally, in the study by Efimova et al anti-CD3/CD28 beads were used to stimulate Teff cells, therefore the suppressive ability can only be analysed in terms of mechanisms directly affecting Teff cells. In this study, WT APCS were isolated that were used to stimulate Teff cells; thereby

suppression can also occur via macrophages or DCs. Furthermore, macrophage-derived ROS has also been implicated in Treg-mediated suppression and as isolated macrophages used here were from WT mice, which contain Nox2, this mechanism could occur *in vitro*. There may then be a potential benefit for Tregs lacking Nox2, in the environment of other Nox2-containing immune cells. This could further explain the increased efficacy of Nox2-Tregs *in vivo*.

Moreover, results presented in this chapter indicate that Nox2KO Tregs express higher levels of CD73, CD39 and CTLA-4, whose suppressive activity may not necessarily be instigated in the presence of anti-CD3/CD28 beads. In addition, increased expression of these anti-inflammatory mediators in Nox2KO Tregs further corroborates *in vitro* findings presented in this chapter by demonstrating that Nox2KO-Tregs are more suppressive that WT-Tregs.

Due to the initial impact of the Treg adoptive transfer on the blood pressure response to AngII, immune cells within the aorta and the kidney were also analysed. Within the aorta, a very similar immune cell infiltration was observed as found in the heart, with an overall blunted level of total leukocytes, T-cells and T-cell subtypes with both WT- and Nox2KO-Treg injected mice.

In comparison, no significant differences were observed within the kidney. This suggests that Tregs are not taking effect on this tissue and hence the blood pressure alteration is primarily instigated by cardiovascular responses. Within the literature, Barhoumi et al investigated migration of Tregs within an adoptive transfer experiment during AngII-treatment and identified an increased level of Tregs within the renal cortex of the kidney[190]. From this they postulated that Treg action within this organ may elicit the beneficial responses observed on hypertension[190]. However, this research group performed multiple Treg adoptive transfers prior to, and during, AngII treatment, therefore potentially Tregs may accumulate in the kidney over time. In comparison, one Treg injection does not alter the level of immune cells within the kidney so the benefits observed within this study may not occur due to a kidney-related mechanism.

In comparison, within the spleen, Tregs were significantly lower in WT-Treg injected mice only, even though all other T-cell subtypes remained stable between the groups.

These findings were verified by looking at Tregs as a percentage of $CD4^+$ T-cells, where in the spleens of WT-Treg injected mice only, there was a marked decrease. These results may suggest a different protective mechanism between WT- and Nox2KO-Tregs in this setting; however this would require further investigation to fully clarify.

Further studies to help clarify the role of Tregs, and Treg-specific Nox2, could involve multiple-Treg injections that may provide a prolonged attenuated response to AngII in terms of hypertension and enable a clearer distinction between the benefits of WT- and Nox2KO-Tregs. Furthermore, sub-pressor doses of AngII have the ability to induce cardiac remodelling but without an increase in systolic blood pressure, therefore it would be interesting to observe the effects of adoptively transferred WT- and Nox2KO-Tregs within this setting. One could then distinguish the benefits related directly to cardiac remodelling and those arising as a consequence of reduced blood pressure. In addition, using an anti-CD25 antibody (such as PC61) to deplete Tregs in both Nox2KO and WT mice would allow to investigate whether the lack of Tregs holds any bearing on AngII-induced hypertension, cardiac remodelling and inflammation.

Overall the results presented in this chapter have identified a clear role for Tregs during AngII induced hypertension and cardiac remodelling by reducing $CD4^+$ T-cells within this setting. Furthermore, Nox2KO-Tregs have an increased suppressive function and prove more efficient during the cardiac response to AngII treatment.

Chapter 6: A Novel CD4-Specific Nox2KO mouse

6.1 Introduction

T-cells, specifically $CD4^+$ T-cells, have been identified by a number of research studies to be key mediators during the progression of cardiac remodelling. Separately, Nox2, and its product $O_2^{\bullet-}$, have been extensively shown to be involved in this setting. The global Nox2KO study in chapter 4 demonstrated that the lack of Nox2 prevents AngII-induced hypertension, cardiac remodelling and inflammation. Furthermore, the adoptive transfer of Tregs, which suppress $CD4^+$ T-cell functions, have proven beneficial within the setting of AngII-induced pathophysiology [190,191]. Moreover, the studies with Nox2KO Tregs in chapter 5 demonstrated a different functional response and efficacy as compared to WT Tregs in this setting. Therefore further investigation of the specific role of CD4-Nox2 may provide an insight into the detrimental effects of these cells, in response to AngII treatment.

6.1.1 Specific role of Nox2 in $CD4^+$ T-cells

Nox2-derived ROS has been implicated in a number of different cellular signalling pathways, such as proliferation, differentiation and apoptosis as described in section 1.1.4. Activation of Nox2 has been identified following $CD4^+$ T-cell stimulation by their TCR, and potentially modulates downstream signalling pathways[133]. Therefore, Nox2 may be involved in a number of different responses that could alter $CD4^+$ T-cell differentiation and functions[133,248,249].

As described previously, published research has revealed a role for Nox2 in T-cell differentiation and function. Furthermore, a specific response in Th differentiation was observed by Shatynski et al. T-cells that lack an active Nox2 enzyme demonstrate a decreased level of STAT5 phosphorylation and GATA-3 expression, which are important transcription factors during Th differentiation[249]. This encourages Th differentiation away from the Th2 lineage and towards Th1, resulting in increased secretion of IFN-γ and depletion of IL-4[249]. Similar findings have also been reported by other research groups[248,250,251]. In addition to this, IL-17 was also heavily upregulated in Nox2KO $CD4^+$ T-cells, suggesting Th17 differentiation[207,249]. Further evidence corroborates this potential skewing towards Th17 cells. Lee et al also observed that

activated Nox2KO $CD4^+$ T-cells tend to produce a significantly higher level of IL-17 compared to WT controls[199]. In addition to this, an upregulation of IL-17 *in vivo* during age-induced arthritis was also observed in global Nox2KO mice[199].

Research therefore suggests that endogenous CD4-Nox2 may be involved in pathways leading to Th2 differentiation; hence the lack of Nox2 could potentially enhance Th1 and even Th17 differentiation.

6.1.2 CD4 T-cell role in hypertension and cardiac remodelling

Cardiac infiltration of $CD8^+$ and $CD4^+$ T-cells has been observed in response to a pressure overload model (TAC), where the associated cardiovascular remodelling was diminished in $RAG^{-/-}$ mice[184]. Lack of $CD4^+$ T-cells (MHCIIKO), but not $CD8^+$ T-cells (CD8KO) eliminated the expected cardiovascular response to TAC[184].

Further research showed that mice lacking $CD4^+$ T-cells (CD4KO and MHCIIKO) responded more vigorously to MI with increased LV dilation, increased inflammation and augmented collagen deposition[252]. This highlights a role for $CD4^+$ T-cells to facilitate wound healing of the myocardium. One limitation of this study is that the $CD4^+$ T-cell subpopulation encompasses Tregs, which have been proved beneficial in this setting (chapter 5)[190,191]. Therefore the responses to MI observed here may be due to depletion of Tregs rather than Teff cells.

In comparison, Madhur et al further characterised the $CD4^+$ T-cell response to the level of the Th17 subset and their IL-17 cytokine production[185]. AngII significantly increases IL-17 production from T-cells and $IL\text{-}17^{-/-}$ mice display a protective response to AngII treatment in terms of blood pressure, vascular function, $O_2^{\bullet-}$ production and T-cell infiltration[185].

Th17 cells have also been implicated in the setting of atherosclerosis, but their role here is very controversial. As reviewed by Taleb et al, reducing IL-17 production may not prevent atherosclerotic lesion development, and increasing IL-17 levels may even be beneficial rather than detrimental, which was originally thought[253]. Research suggests that Th17 cells are implicated in CVD but in a context-dependent manner, which may vary according to the tissue microenvironment[253]. In addition, there is

accumulating data that suggests plasticity between Th17 and Treg subtypes of $CD4^+$ T-cells and the potential trans-differentiation between the two[254-258].

Taken together, these research studies highlight a specific role for $CD4^+$ T-cells in the setting of cardiac remodelling and repair. However it is has also been highlighted that the presence of these cell types may also initially be beneficial. Therefore further understanding the endogenous mechanisms of $CD4^+$ T-cells that drive their negative responses in this setting may prove beneficial. Hence, as Nox2 has also been demonstrated to modulate $CD4^+$ T-cell activation and function this is an interesting and potentially beneficial route to investigate.

6.2 Aims

We previously investigated the role of Nox2 in AngII-induced cardiac pathophysiology and inflammation, and highlighted a potential role for $CD4^+$ T-cell Nox2. In addition to this, $CD4^+$ T-cells have also been identified in the literature as an important component during the progression of cardiac remodelling. However the protective responses observed in our global Nox2KO model could be due to the lack of Nox2 in a range of different cell types within this setting. Therefore the aim for this chapter was to generate a CD4-specific Nox2KO model in order to study the endogenous role of Nox2 within $CD4^+$ T-cells in the setting of AngII-induced cardiac pathophysiology.

6.3 Methods

6.3.1 Generation of the novel CD4-specific Nox2KO mouse line

In order to investigate the role of Nox2 in $CD4^+$ T-cells, we generated a specific CD4-Nox2KO mouse line. Novel in-house bred $Nox2^{floxed}$ females (*Figure 6-1*)[259] were crossed with CD4-Cre mice (provided by R. Noelle, KCL Department of Immune Regulation and Intervention). Resulting hemizygous $Nox2^{floxed}$, Cre^+ males were then crossed with $Nox2^{floxed}$ Cre^- females before the second generation, hemizygous $Nox2^{floxed}$ Cre^+ males (CD4-Nox2KO) were used as experimental animals. Specifically within $CD4^+$ cells, cre recombinase excises DNA between the two LoxP sites either side

of exon 1 and 2 of the gp91 gene (Nox2), and recombines remaining DNA, hence preventing transcription of Nox2 (*Figure 6-2*). This therefore generates a CD4-specific Nox2KO model. Male CD4-Nox2KO mice were used for experiments between 6-8 weeks of age. $Nox2^{floxed}$ Cre^{-} mice were used as controls.

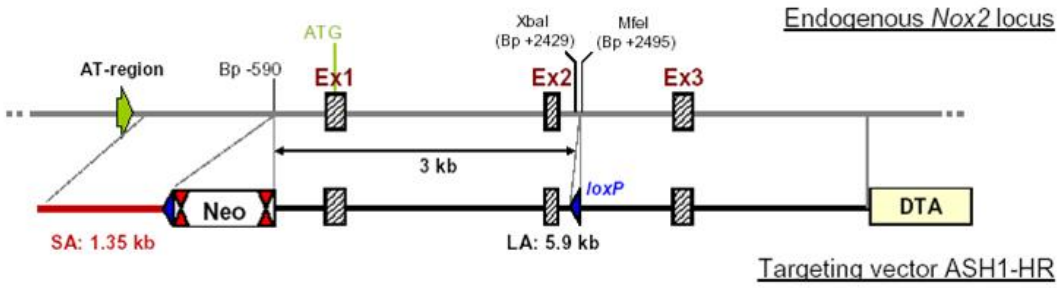

Figure 6-1: Targeting strategy for $Nox2^{floxed}$ mice. *The endogenous Nox2 locus is shown at the top and the targeting vector at the bottom. Blue triangles represent LoxP sites and double red triangles indicate FRT sites. After successful targeting, the Neo cassette was excised using the FRT sites.*

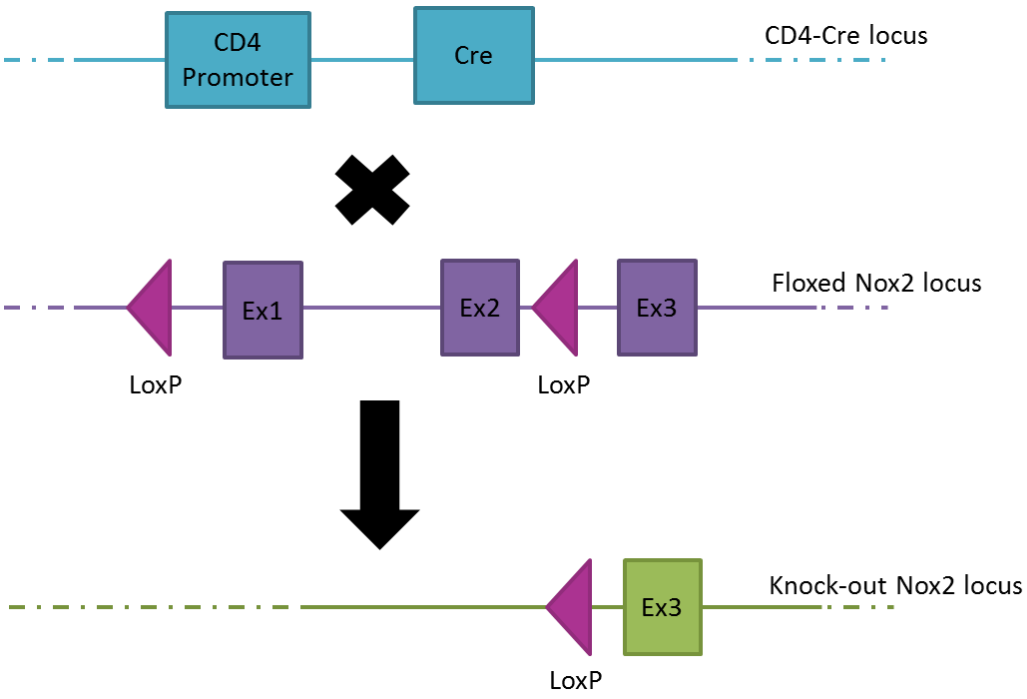

Figure 6-2: CD4-Nox2KO breeding schematic. *CD4-Cre mice were bred with novel, in house bred, Nox2-floxed animals. Cre recombinase cleaves LoxP sites either side of Nox2 exons 1 and 2, preventing its transcription in CD4$^+$ T-cells.*

6.3.2 CD4-Nox2KO genotyping

Ear biopsies were treated with 300µL 50mM NaOH at 95°C for 30 minutes. Samples were vortexed to homogenise and 25µL 1M Tris-Hcl (pH 8.0) added and incubated at RT for 30 minutes. PCR cycles were then carried out to analyse Glyceraldehyde-3-phosphate dehydrogenase (GAPDH)/Cre and Nox2-Flox (ASHL) genes (primers in *Table 12*). For GAPDH/Cre analysis, 3µL of DNA added to 22µL of the PCR master mix, *Figure 6-3*. All samples were run with a no-template sample and known Cre$^-$ and Cre$^+$ samples on the PCR cycle shown in Figure 6-3. Cre$^+$ animals (e.g. 37-38) were identified by the presence of a lower band (200bp), Figure 6-5, whereas Cre- animals only express the upper GAPDH band (300bp, e.g. 39-40).

Component	Amount per sample (µl)
RedTaq	12.5
GAPDH-F (2µM)	0.5
GAPDH-R (2µM)	0.5
Cre-F (2µM)	0.5
Cre-R (2µM)	0.5
Dnase-free water	7.5

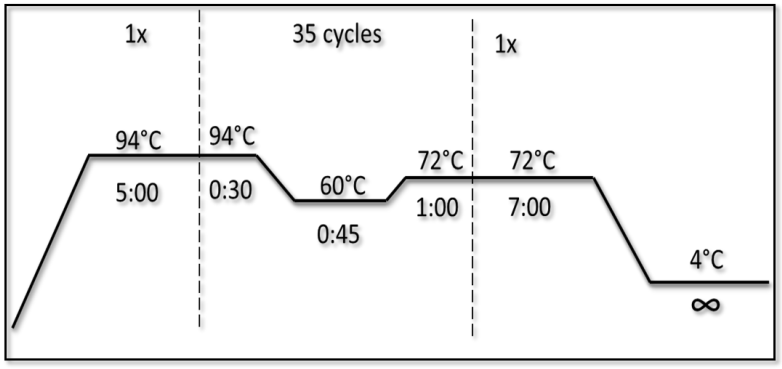

Figure 6-3: GAPDH/Cre PCR cycle.

For Nox2-Flox analysis, 3µL of DNA was added to 22µL of the PCR master mix shown in Figure 6-4. Control samples included a no-transcript sample, homozygous Nox2 Flox and WT samples, all run on the PCR cycle shown in Figure 6-4.

Component	Amount per sample (µl)
RedTaq	12.5
Nox2-Fl - F (2µM)	0.5
Nox2-Fl - R (2µM)	0.5
Dnase-free water	12.5

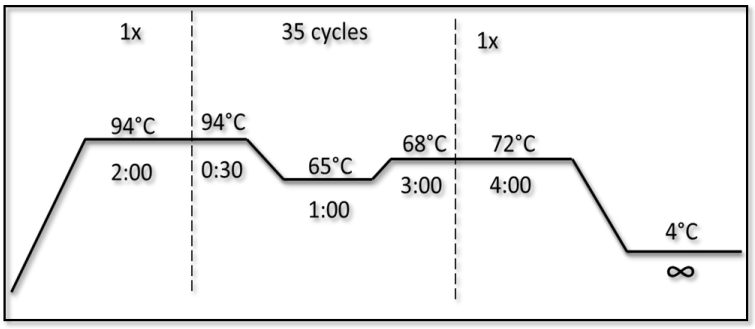

Figure 6-4: Nox2-Flox genotyping PCR cycle.

After the PCR cycles were completed, samples (20µL) were then run on a 2% Agarose gel (150mL 1 x TAE and 3g Agarose) infused with ethidium bromide (0.5µL/mL) at 180v for 30 minutes. The gel was then viewed under UV light using a transilluminator. Nox2 floxed mice (e.g. 40-65) were verified by an upper floxed band (500bp), as shown on Figure 6-5. Whereas WT animals (+/+, e.g. 37-38) have a lower band (200bp) and heterozygotes (e.g. 39) display both bands.

CD4-Nox2KO animals (e.g. 41-65) were then identified by containing the lower Cre^{+} band (200bp) on the first gel (Cre/GAPDH) and the upper Nox2 floxed band (300bp) on the second gel.

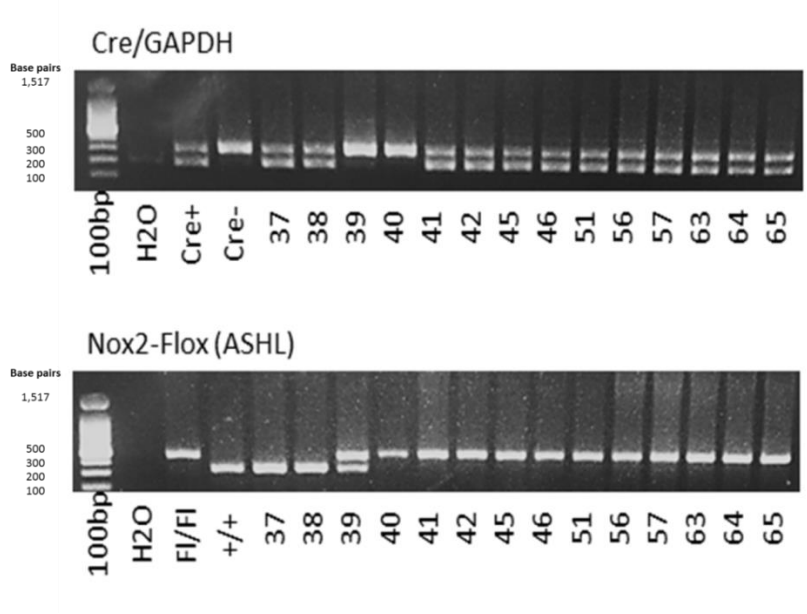

Figure 6-5: CD4-Nox2KO genotyping example.

Gene of interest	Primer name	Primer sequence
GAPDH – F	GAPDH-F	CCTAGACAAAATGGTGAAGG
GAPDH – R	GAPDH-R	GACTCCACGACATACTCAGC
Cre – F	Cre-F	TGCCAGGATCAGGGTTAAAG
Cre – R	Cre-R	CCCGGCAAAACAGGTAGTTA
Nox2-Fl -F	ASHL-1	GTAAATTCACTGTTCTGGGTCTCAGC
Nox2-Fl -R	ASHL-2	ACATGTTCTTCTCACAGGCTCTTCC

Table 12: Genotyping Primer sequences.

6.3.3 Confirmation of the CD4-Nox2KO model

$CD4^+$ T-cells were isolated from whole spleens of CD4-Nox2KO mice and WT littermates. Harvested spleens were triturated and filtered separately through a 70µm nylon mesh. Cell suspensions were then washed in isolation buffer and centrifuged at 1800rpm for 5 minutes at 4°C. Spleen samples were then treated for 3 minutes with 1x red cell lysis buffer (Biolegend) at room temperature followed by a final wash in isolation buffer.

Magnetic beads conjugated to streptavidin (50µL per sample, Dynabeads®M-280 Streptavidin, Invitrogen) were prepared by washing in 1mL PBS and placed on a magnet for 2 minutes before removing the supernatant. Beads were then re-suspended in in 50µL PBS and incubated with anti-CD4 antibody conjugated to biotin (1:200, ebioscience) and incubated for 30 minutes at RT under rotation. Beads were then washed using 1mL PBS as described previously using a magnet.

Harvested splenocytes were then incubated with the dynabead-CD4 complex for 30 minutes at RT under rotation. Cells bound by Dynabeads® were then isolated by placing samples on a magnet for 2 minutes and removing the supernatant, which contains all other immune cells. Beads bound to the magnet, which are $CD4^+$ cells, were then washed in 1mL isolation buffer, incubated on the magnet for a further 2 minutes and then the supernatant discarded. Remaining beads were then re-suspended in 1mL isolation buffer, centrifuged at 13,000rpm, the supernatant discarded and the cell pellet stored at -80˚C. These samples were then treated for RNA extraction as described in section 2.7.

Extracted RNA was reverse transcribed to generate cDNA (section 2.7.2) and used for qPCR analysis of Nox2, its related subunits, Nox4 and eNos (*Table 13*).

Gene product of interest	Forward primer sequence	Reverse primer sequence
Nox2 ($gp91^{phox}$)	ACTCCTTGGGTCAGCACTGG	GTTCCTGTCCAGTTGTCTTCG
$p47^{phox}$	GGACACCTTCATTCGCCATA	CTGCCACTTAACCAGGAAC
$p67^{phox}$	AAGCTGTTTGCCTGTGACGT	CTTCATGTTGGTTGCCAATG
$p22^{phox}$	TGGACGTTTCACACAGTGGTA	TGGACCCCTTTTTCCTCTTTC
Nox4	TGTTGCATGTTTCAGGTGGT	TACTGGCCAGGTCTGCTTT
eNos	GGGAAAGCTGCAGGTATTTGA	CACTGTGATGGCTGAACGAAG
B-actin	CTGTCGAGTCGCGTCCACCC	ATGCCGGAGCCGTTGTCGAC

Table 13: Fibrosis-related primer sequences used for qPCR. *All sequences are shown as 5'-3'.*

6.3.4 Baseline characterisation and observation

Initial experiments involved baseline observations and characterisation of CD4-Nox2KO mice and WT littermates. Blood pressure and haemodynamic function were analysed by tail cuff plethysmography and echocardiography respectively (section 2.5).

Animals were then culled using increasing levels of CO_2 prior to removal of peripheral LNs, spleen, thymus, liver, left kidney, lungs and tibia. All organs were weighed and the tibia length measured and recorded to calculate organ weight-to-tibia length ratios. Representative photographs were taken comparing CD4Nox2KO and WT LNs, spleens, thymuses and hearts. Harvested hearts were treated as described in section 2.8 for WGA and PSR staining.

Baseline T-cell compositions were then analysed by isolating MLNS, PLNs and spleens as described in section 2.4.3 and treated for flow cytometry using the BD FACS Fortessa™ (section 2.6).

6.3.5 Experimental model

Subcutaneous mini-osmotic pumps containing a pressor dose of AngII (1.1mg/kg/day) were surgically implanted into CD4-Nox2KO mice and WT littermates for up to 14-days, as described in section 2.3. Blood pressure and haemodynamic function were analysed by tail cuff plethysmography and echocardiography respectively (section 2.5). A second group of mice were also treated with a pressor dose of AngII for 3-days, before organs were harvested for flow cytometry (section 2.6).

6.3.6 Treatment of samples

Harvested hearts were treated as described in section 2.3. RNA was extracted and reverse transcribed to enable analysis by qPCR (section 2.7). Fibrosis-related markers were analysed as described in section 2.7. Histological analysis involved staining of harvested hearts for WGA and PSR (section 2.8). Flow cytometry was performed on whole hearts and spleens using the BD FACS CantoII™ as described in section 2.6. The

level of leukocytes, T-cells and T-cell subsets were determined based on expression of CD45, TCRβ, CD4, CD8, CD25 and FoxP3.

6.4 Results

6.4.1 Confirmation of CD4-specific Nox2KO model

Initial confirmation of our novel CD4-specific Nox2KO animal model was verified by isolating $CD4^+$ T-cells separately from CD4-Nox2KO animals and WT littermate controls. Extracted RNA was reverse transcribed to generate cDNA and used for qPCR analysis of Nox2 and its related subunits (*Figure 6-6*). Nox2 mRNA levels were significantly lower in $CD4^+$ T-cells isolated from CD4-Nox2KO animals compared to WT littermates (p=0.0001). However, Nox2 mRNA levels in all other immune cells were not altered in either CD4-Nox2KO or WT. All Nox2 subunits ($p67^{phox}$, $p47^{phox}$ and $p22^{phox}$) were unaffected by the absence of CD4-Nox2, as assessed by mRNA expression level.

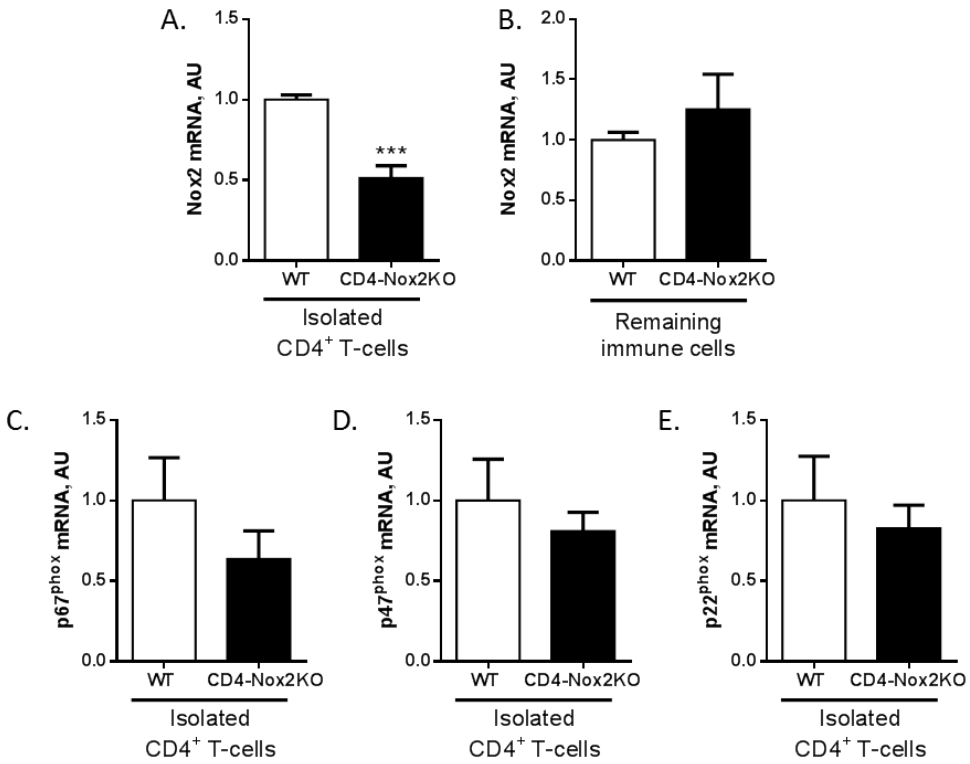

Figure 6-6: CD4-Nox2KO T-cells have significantly lower Nox2 mRNA levels. *Quantitative PCR analysis of* ***(A)*** *Nox2 mRNA in isolated $CD4^+$ T-cells,* ***(B)*** *Nox2 mRNA levels in remaining immune cells and* ***(C)*** *$p67^{phox}$,* ***(D)*** *$p47^{phox}$ and* ***(E)*** *$p22^{phox}$ mRNA levels in isolated $CD4^+$ T-cells. ***p<0.001, N=5-6 per group.*

6.4.2 Baseline characterisation of CD4-Nox2KO mouse model

We initially assessed a number of simple morphometric parameters in the new specific CD4-Nox2KO line to determine whether there were any obvious gross baseline differences between the CD4-Nox2KO and WT littermate controls.

Weights of vital organs were recorded and analysed between the two genotypes and standardised to tibia length. In terms of lymphoid organs at baseline, *Figure 6-7* shows that LNs and the spleen are similar sizes in CD4-Nox2KO animals compared to WT littermates whereas the thymus appears larger in the CD4-Nox2KO. Analysis of organ weights further corroborates these findings where *Figure 6-8* shows similar spleen weights between the two genotypes, however the thymus is 1.5 fold larger ($p<0.001$) in the CD4-Nox2KO compared to WT littermates. Liver weight, lung weight and kidney weight were all similar between the two groups.

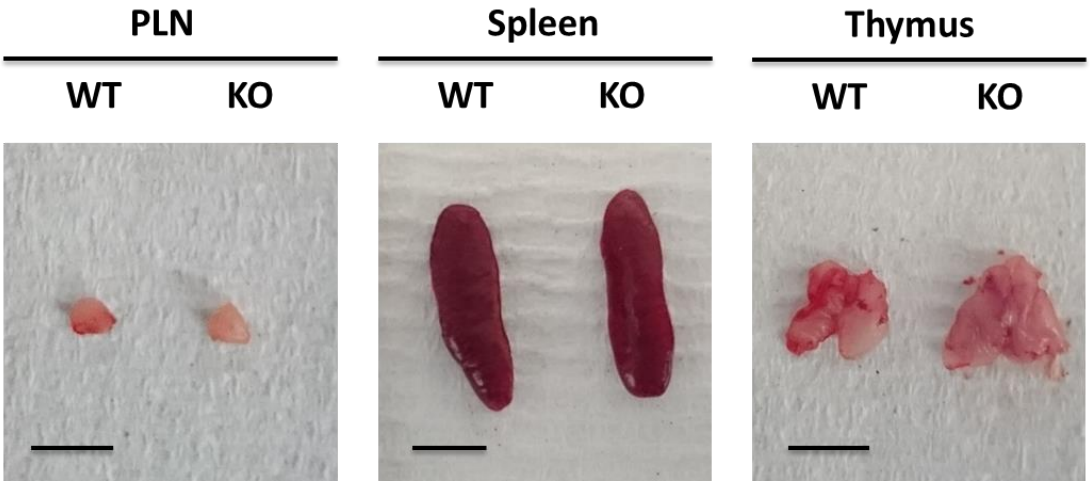

Figure 6-7: CD4-Nox2KO lymphoid organ sizes. *Representative images of CD4-Nox2KO and WT littermate control peripheral LNs, spleens and thymus. Scale bar represents 0.5cm.*

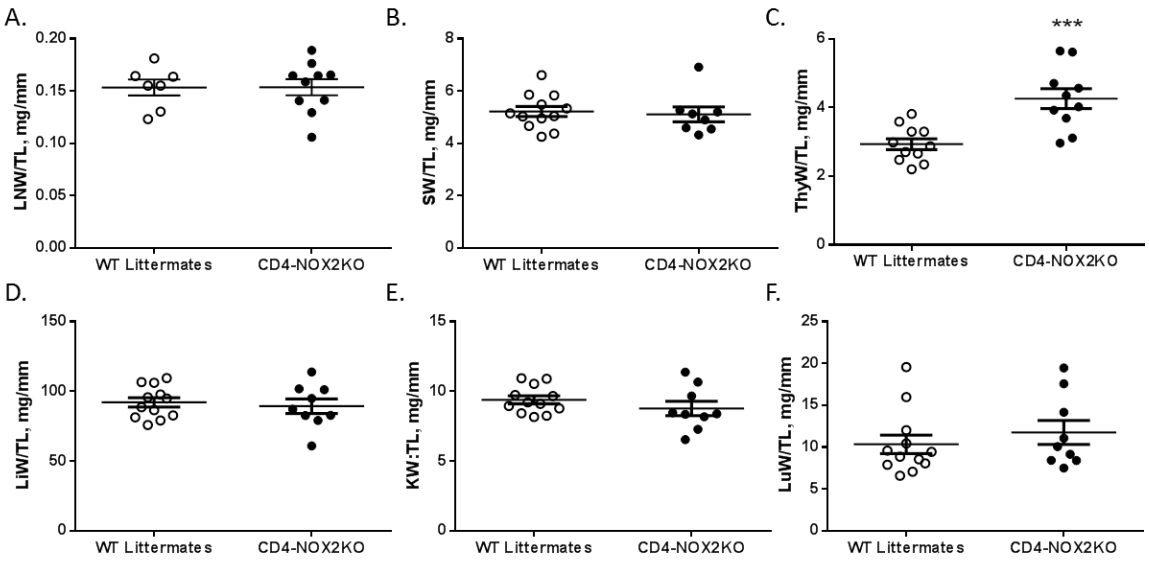

Figure 6-8: CD4-Nox2KO mice display thymus hyperplasia whereas other organs are similar to WT controls. (A) *Lymph node weight (LN/TL)* ***(B)*** *Spleen weight (SW/TL),* ***(C)*** *Thymus weight (ThyW/TL),* ***(D)*** *Liver weight (LiW/TL),* ***(E)*** *Kidney weight (KW/TL) and* ***(F)*** *Lung weight (LuW/TL) all standardised to tibia length (TL). ***p<0.001. N=7-12 per group.*

Baseline cardiac parameters were also investigated in these mice. A smaller heart was observed in CD4-Nox2KO animals, as illustrated in *Figure 6-9*. Analysis of HW/BW (p=0.014) and HW/TL (p=0.033) also showed that these ratios were significantly lower in CD4-Nox2KO animals compared to WT littermates. HW/TL showed an average decrease in heart size by 7% in CD4-Nox2KO animals.

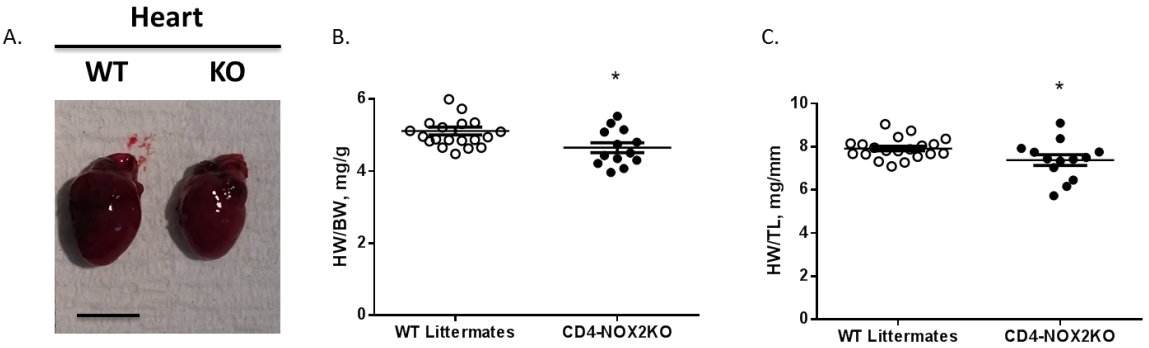

Figure 6-9: Baseline cardiac characterisation of CD4 specific Nox2KO animals. (A) *Representative photographs of excised hearts;* ***(B)*** *heart weight/body weight ratio (HW/BW) and* ***(C)*** *heart weight/tibia length ratio (HW/TL). *p<0.05, N=13-20 per group.*

In addition, WGA staining revealed a significantly lower cardiomyocyte cross-sectional area (-19%; p=0.018) in the CD4-Nox2KO animals compared to WT littermates (*Figure 6-10*). PSR staining showed no difference in the percentage of collagen between the two genotypes at baseline (*Figure 6-11*).

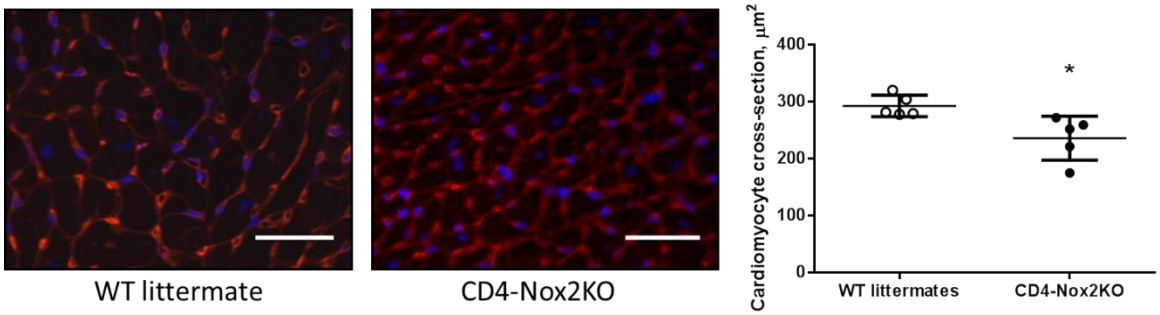

Figure 6-10: Reduced baseline cardiomyocyte cross-sectional area in CD4-Nox2KO mice. *Representative images of WGA staining, and cardiomyocyte cross-section measurement for CD4-Nox2KO and WT littermates, which is smaller in KO animals. Scale bar represents 25µm. *p<0.05. N=5 per group.*

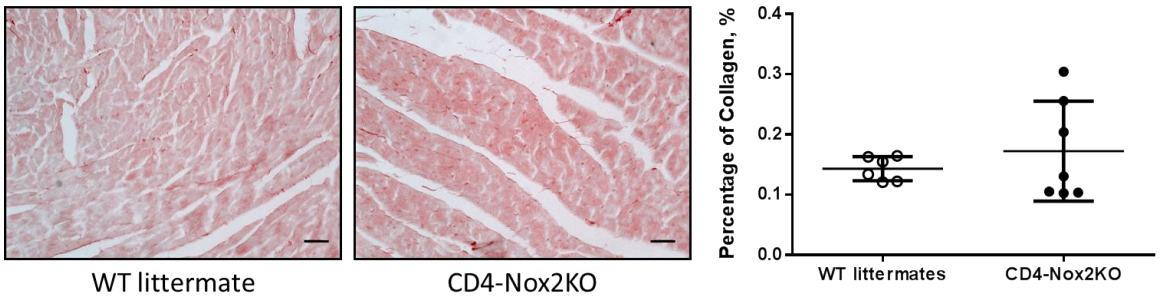

Figure 6-11: CD4-Nox2KO picrosirius red staining at baseline. *Amount of interstitial collagen was similar between the genotypes. Scale bar represents 25µm. N=6-7 per group*

Measurement of systolic blood pressure and cardiac function was carried out at baseline by tail cuff plethysmography and echocardiography, respectively (*Figure 6-12*). Absence of Nox2 in the CD4 T-cells had no consequence on systolic blood pressure, heart rate, LVESV, LVEDV or ejection fraction.

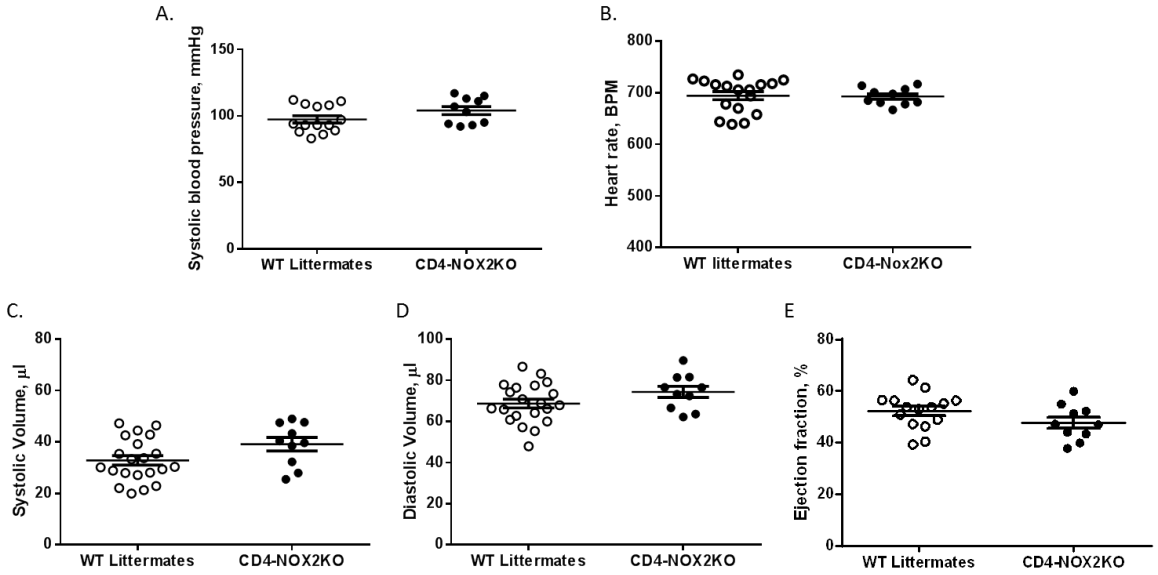

Figure 6-12: Cardiovascular function conserved in CD4-Nox2KO animals. *Baseline cardiovascular function analysed by* ***(A)*** *Systolic blood pressure,* ***(B)*** *heart rate* ***(C)*** *systolic volume,* ***(D)*** *diastolic volume and* ***(E)*** *ejection fractional. N=11-20 per group.*

These results indicate that CD4-Nox2KO animals have a similar baseline contractile function to WT littermates, even with the observed decrease in heart size. The increases in lymphoid organs may suggest an altered inflammatory response in these animals.

6.4.3 Characterising CD4-Nox2KO immune system at baseline

MLN, PLN and spleens were isolated from individual CD4-Nox2KO animals and WT littermate controls in order to verify immune cell composition. Single cell suspensions were prepared and both T- and B-cells were analysed using BD FACS Fortessa™. Total leukocytes were significantly higher in MLNs ($p=0.025$) and PLNs ($p<0.001$) compared to WT littermates, but unchanged within the spleen (*Figure 6-13*). A similar pattern was observed with T-cells ($CD45^+TCR\beta^+$) with an increase in MLNs ($p=0.061$) and a marked increase in PLNs by 47% ($p=0.006$). Analysis of T-cell subpopulations revealed no changes between DN, DP or $CD8^+$ T-cells in the lymphoid organs, however a significant increase in $CD4^+$ ($p=0.014$) T-cells was observed within the PLNs of CD4-Nox2KO animals. Interestingly, $CD4^+$ T-cells increased by 59% in the CD4-Nox2KO mice compared to WT littermates. $CD4^+CD25^+$ Tregs were significantly higher in MLNs and

PLNs of CD4-Nox2KO mice, and this was confirmed with FoxP3 staining. $CD25^+FoxP3^+$ Tregs were 40% higher in MLN's (p=0.010) and 57% higher in PLN's (p=0.0001) of CD4-Nox2KO mice compared to WT littermates. Within the spleen, Treg levels tended to be lower in CD4-Nox2KO mice, however this was not significant. No changes were observed in B-cell numbers within the lymphoid organs (*Figure 6-14*).

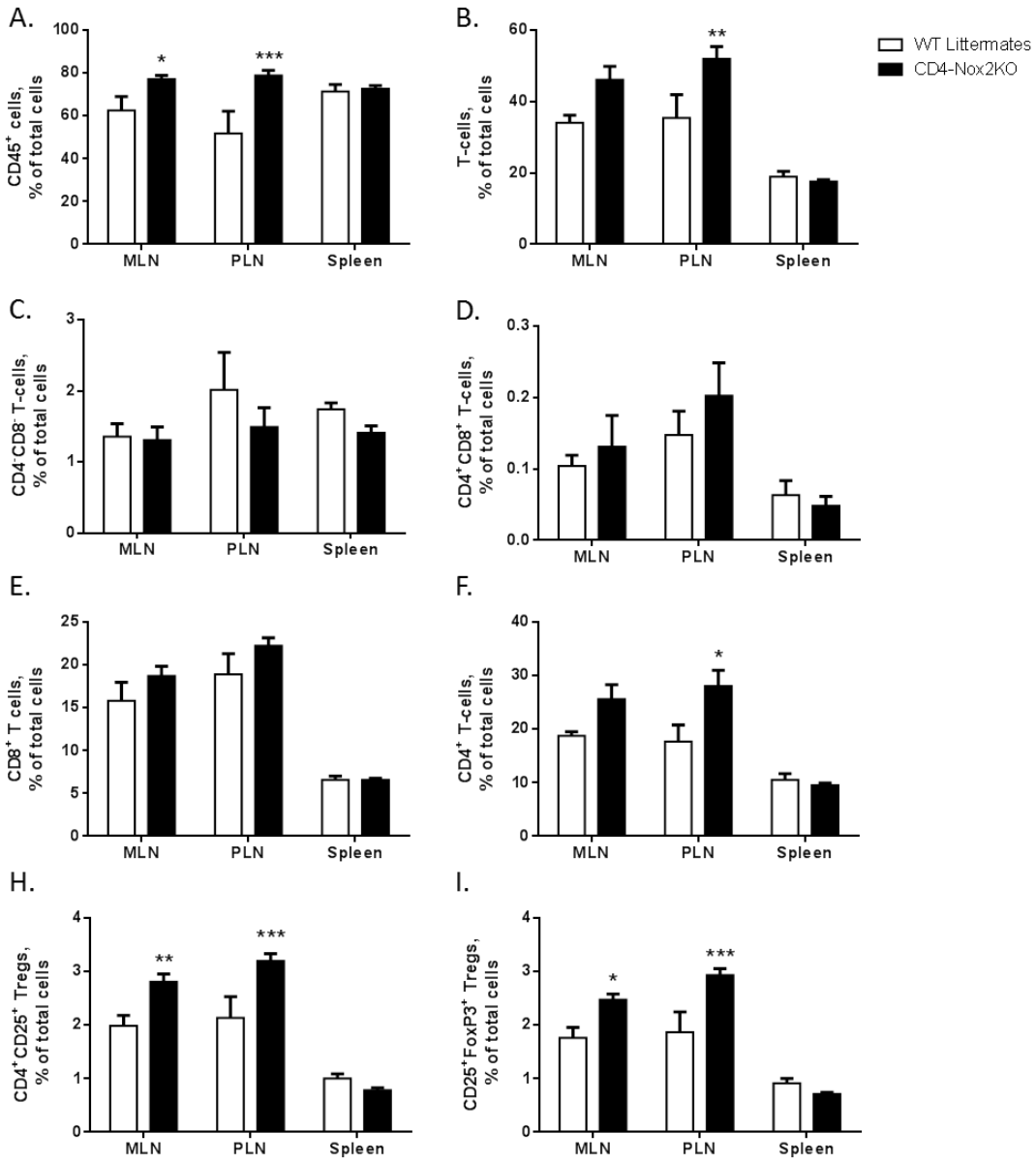

Figure 6-13: Altered T-cell composition in CD4-Nox2KO lymphoid organs at baseline. *Analysis of mesenteric lymph nodes (MLNs), peripheral lymph nodes (PLNs) and spleen of CD4-Nox2KO compared to WT littermate controls. Analysing composition of* ***(A)*** *total leukocytes ($CD45^+$),* ***(B)*** *T-cells ($CD45^+TCR\beta^+$),* ***(C)*** *$CD4^-CD8^-$ T-cells,* ***(D)*** *$CD4^+CD8^+$ T-cells,* ***(E)*** *$CD8^+$ T-cells,* ***(F)*** *$CD4^+$ T-cells,* ***(G)*** *$CD4^+CD25^+$ Tregs and* ***(H)*** *$CD25^+FoxP3^+$ Tregs. *P<0.05, **P<0.01, ***P<0.001, N=5-7 per group, analysed on BD FACS Fortessa™.*

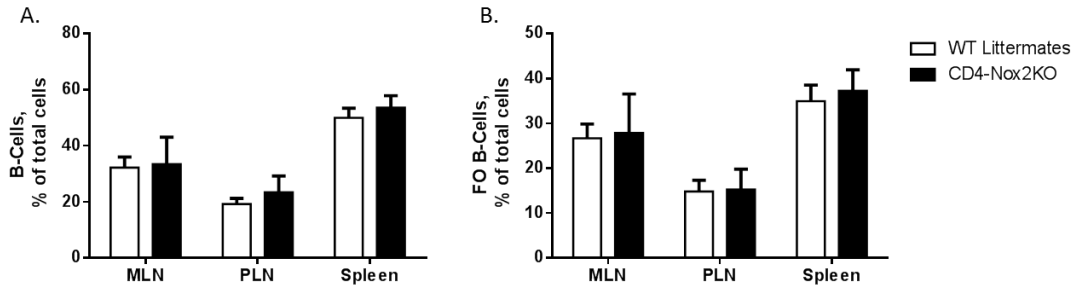

Figure 6-14: Composition of B-cells within CD4-Nox2KO animals. (A) *Total B-cells and* ***(B)*** *follicular B-cells analysed from mesenteric lymph nodes (MLNs), peripheral lymph nodes (PLNs) and spleens of CD4-Nox2KO mice compared to WT littermate controls. Analysed on BD FACS Fortessa™, N=3 per group.*

As the composition of immune cells was different within the lymphoid organs of CD4-Nox2KO animals it was also important to identify whether there was impairment in proportions of immune cells. Therefore we analysed cells as a percentage of their parent population (*Figure 6-15*). T-cells as a percentage of $CD45^+$ cells, $CD4^+$ T-cells as a percentage of total T-cells and Tregs as a percentage of $CD4^+$ T-cells were all similar between the two genotypes in all three tissue samples.

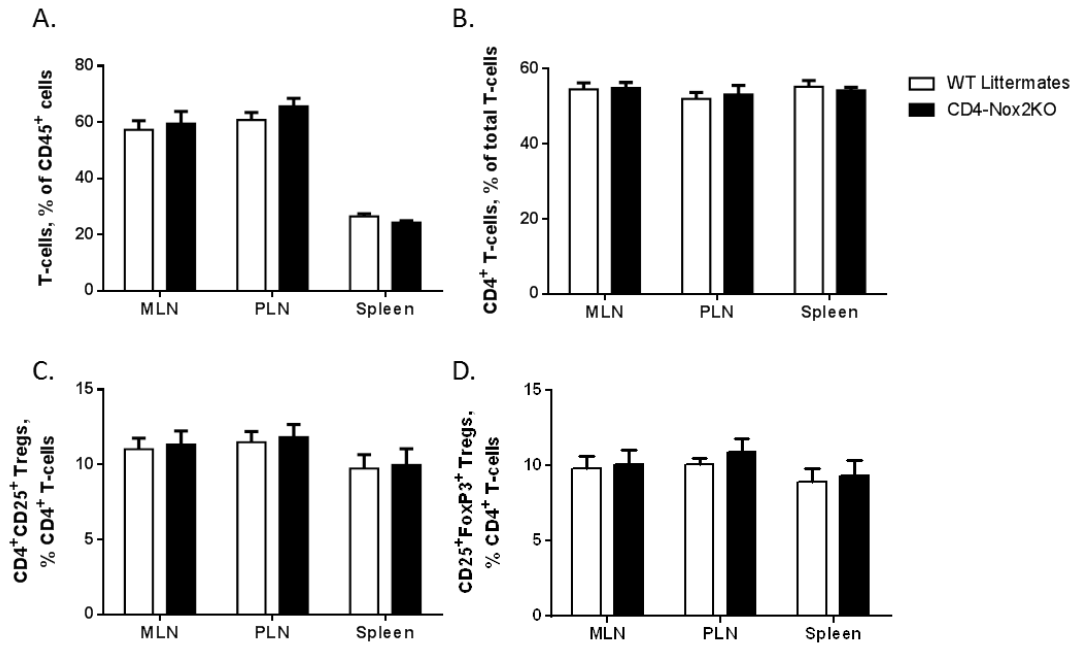

Figure 6-15: Lymphoid T-cell proportions remain unaltered between CD4-Nox2KO and WT littermates. (A) *T-cells as a percentage of $CD45^+$ cells,* ***(B)*** *$CD4^+$ T-cells as a percentage of total T-cells,* ***(C)*** *$CD4^+CD25^+$ Tregs as a percentage of $CD4^+$ T-cells and* ***(D)*** *$CD25^+FoxP3^+$ Tregs as a percentage of $CD4^+$ T-cells. Analysed on BD FACS Fortessa™, N=5-7 per group.*

Flow cytometry dot plots (*Figure 6-16*) suggest an increased basal level of total leukocytes in CD4-Nox2KO heart tissue, including T-cells and T-cell subpopulations. Upon analysis (*Figure 6-17*) it becomes apparent that total leukocytes ($CD45^+$ cells) tend to be amplified in CD4-Nox2KO hearts at baseline compared to WT littermate controls, with a similar response in terms of T-cells. Significantly higher basal level of $CD4^+$ T-cells (p=0.014) was observed in CD4-Nox2KO animals compared to WT littermate controls. Whereas DP ($CD4^+CD8^+$) T-cells remain similar between the two genotypes and DN ($CD4^-CD8^-$) and $CD8^+$ T-cells tend to be higher, however this is not significant. This amplification was also maintained down to the level of Tregs, where there are 4 times more within CD4-Nox2KO heart compared to WT ($CD4^+CD25^+FoxP^+$) (p=0.041).

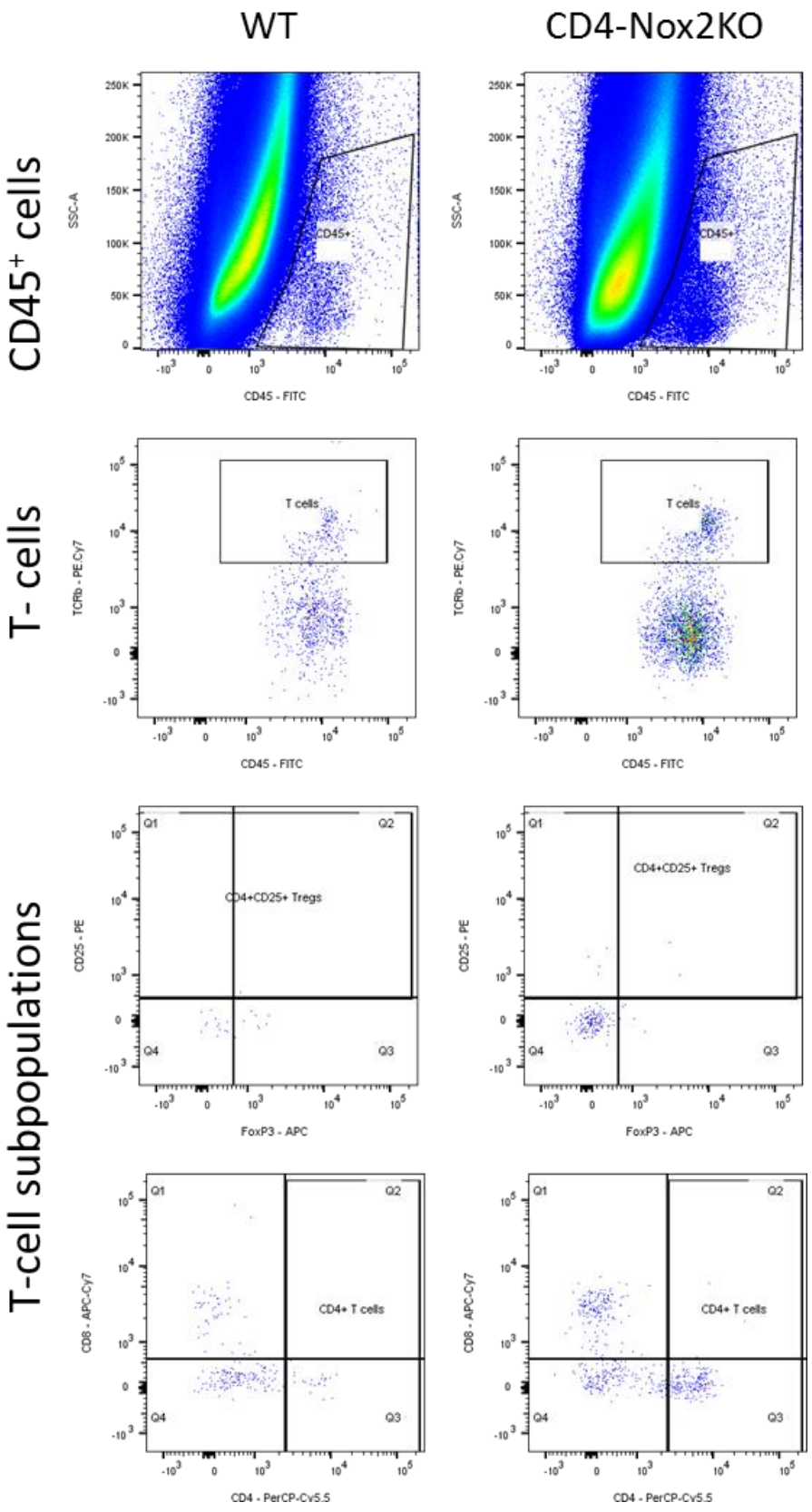

Figure 6-16: Representative dot plots showing baseline cardiac T-cell levels.

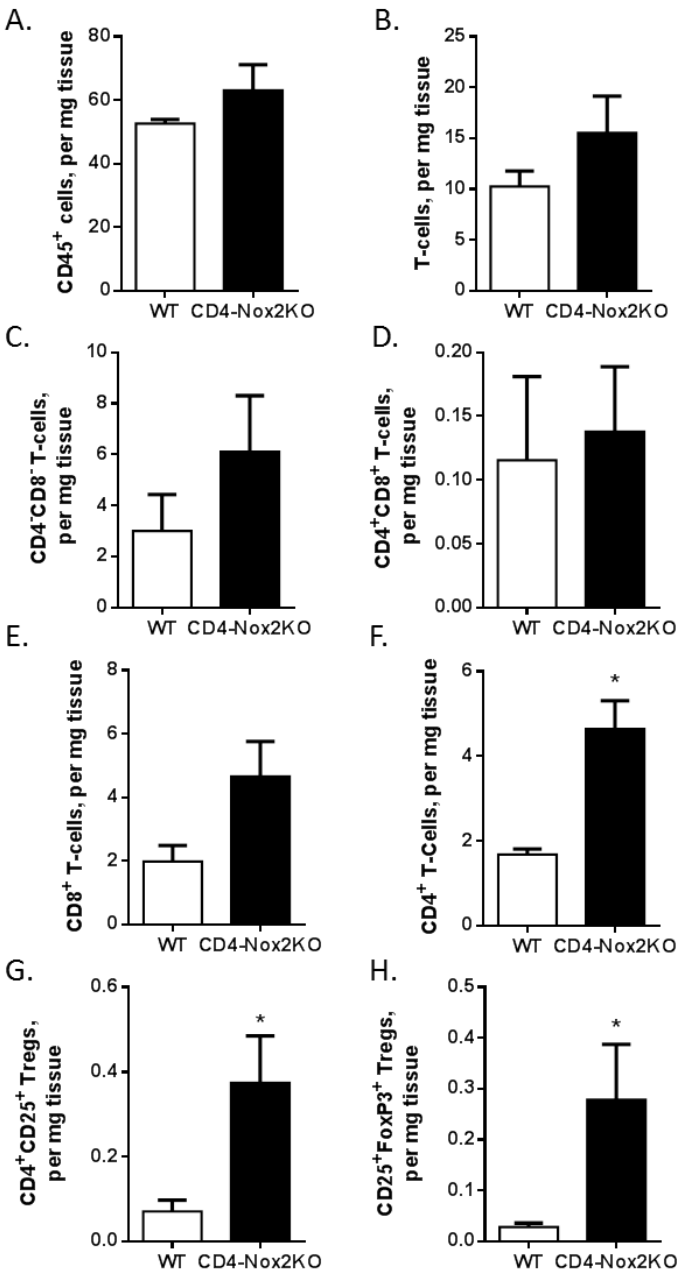

Figure 6-17: Lack of CD4 Nox2 altered baseline level of cardiac T-cell subpopulations. ***(A)*** *Total leukocytes ($CD45^+$),* ***(B)*** *T-cells ($CD45^+TCR\beta^+$) and T-cell subpopulations including* ***(C)*** *$CD4^-CD8^-$,* ***(D)*** *$CD4^+CD8^+$, (**E**) $CD8^+$ and* ***(F)*** *$CD4^+$ T-cells. Tregs are also significantly higher in CD4-Nox2KO show by analysis of* ***(G)*** *$CD4^+CD25^+$ and* ***(H)*** *$CD25^+FoxP3^+$ Tregs. All represented as cells per mg of heart tissue. *p<0.05, analysed on BD FACS CantoII™. N=4 per group.*

Baseline analysis of the spleen showed that total leukocytes ($CD45^+$ cells), T-cells ($CD45^+TCR\beta^+$) and each of the T-cell subpopulations, remain at a similar level in the two genotypes (*Figure 6-18*). However Tregs are significantly lower in CD4-Nox2KO

spleen compared to WT (p=0.014), following a similar pattern to that observed previously in *Figure 6-13*.

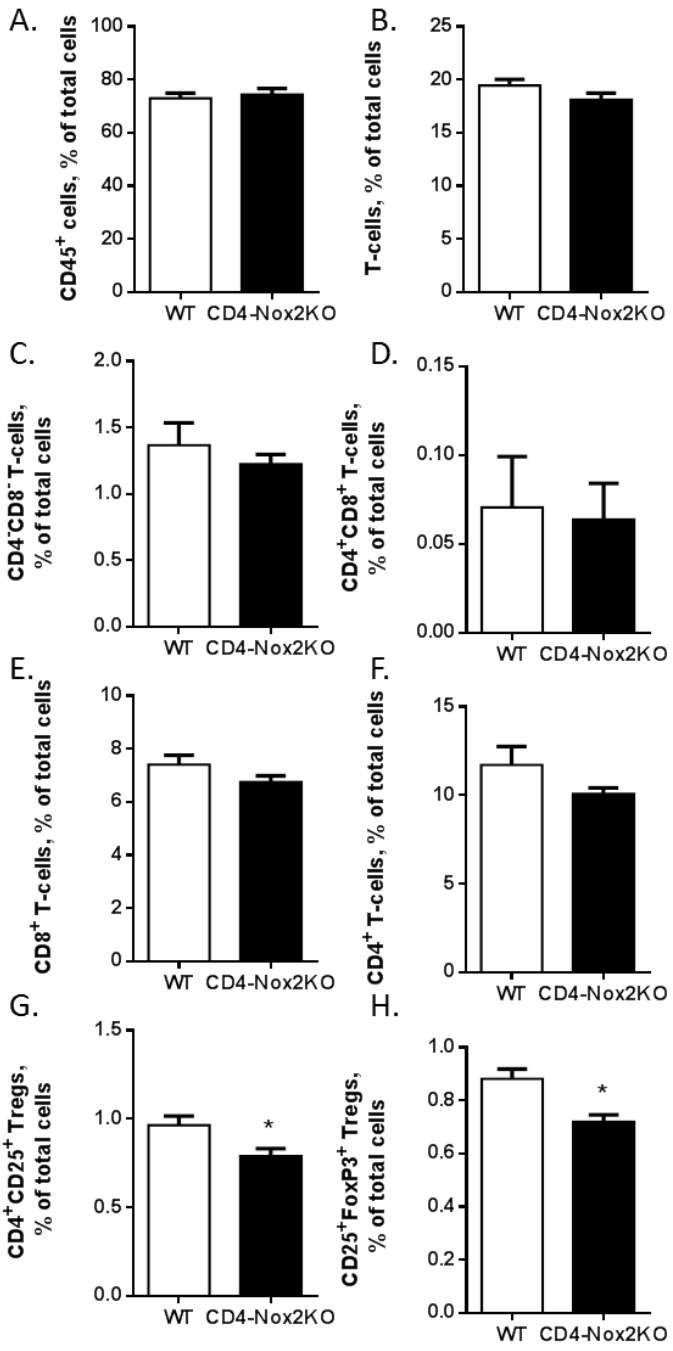

Figure 6-18: Tregs significantly lower in spleens of CD4-Nox2KO animals at baseline. *Comparable levels of* ***(A)*** *total leukocytes ($CD45^+$),* ***(B)*** *T-cells and each of the T-cell subpopulations:* ***(C)*** *CD4-CD8-,* ***(D)*** *$CD4^+CD8^+$,* ***(E)*** *$CD8^+$ and* ***(F)*** *$CD4^+$ T-cells. In addition to alterations in* ***(G)*** *$CD4^+CD25^+$ Tregs and confirmed by (H) $CD25^+FoxP3^+$ Tregs. *p<0.05, analysed on BD FACS CantoII™. N = 3-4 per group.*

As baseline levels of immune cells were altered in the CD4-Nox2KO animal, the proportions of immune cells, as a percentage of their parent population, was analysed for both heart and spleen samples, shown in *Figure 6-19*. Within the heart, T-cells as a percentage of $CD45^+$ cells are the same between WT littermates and CD4-Nox2KO mice. $CD4^+$ T-cells as a percentage of total T-cells tended to be higher in CD4-Nox2KO mice, however this was not significant. $CD4^+CD25^+$ Tregs as a percentage of $CD4^+$ T-cells were significantly higher, by 40%, within the CD4-Nox2KO animals (p=0.012), however the significance was lost when staining for FoxP3. Within the spleen, T-cell sub-population ratios did not alter between the two genotypes analysed. A higher proportion of Tregs within the $CD4^+$ compartment may alter the CD4-Nox2KO immune response to AngII infusion.

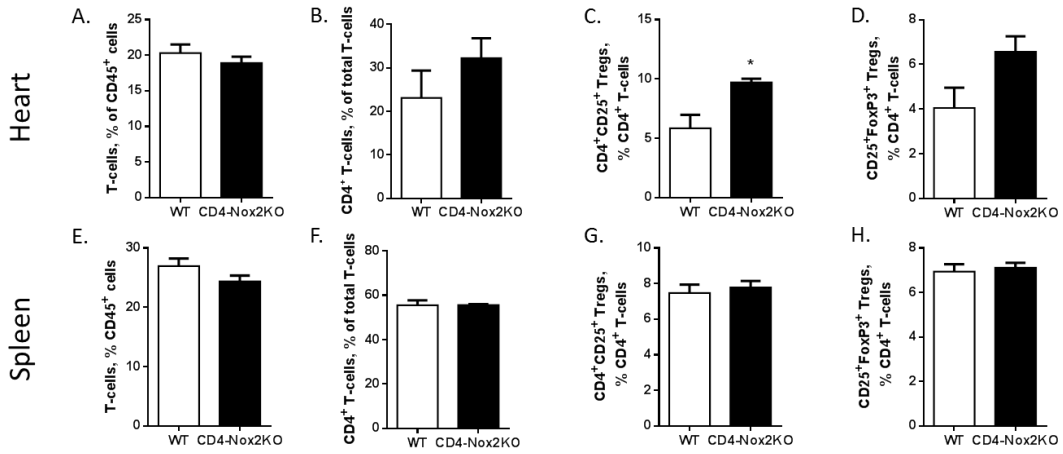

Figure 6-19: Increased cardiac Treg:CD4 T-cell ratio in CD4-Nox2KO at baseline. (A&E) *T-cells as a percentage of $CD45^+$ cells,* ***(B&F)*** *$CD4^+$ T-cells as a percentage of total T-cells,* ***(C&G)*** *$CD4^+CD25^+$ Tregs as a percentage of $CD4^+$ T-cells and* ***(D&H)*** *$CD25^+FoxP3^+$ Tregs as a percentage of $CD4^+$ T-cells.*p<0.05, N=4 per group.*

These results suggest an altered basal organisation of immune cells, both in the lymphoid organs and cardiac tissue, which may reflect an altered inflammatory response, comparable to that seen in the global Nox2KO model.

6.4.4 CD4-Nox2KO physiological response to AngII treatment

CD4-Nox2KO mice and WT littermates were treated with AngII (1.1kg/mg/day) for up to 14-days, and empty mini-osmotic pumps were used for both genotypes as a sham control. Systolic blood pressure and cardiac function and morphology were analysed using tail cuff plethysmography and echocardiography, respectively at time points highlighted in *Figure 6-20*.

WT littermate controls displayed a rapid increase in systolic blood pressure after 3-days of AngII treatment ($p=0.002$), which was maintained after 7 and 14-days of treatment. This increase in systolic blood pressure with AngII was significantly blunted in CD4-Nox2KO animals, reaching only 103±7mmHg, after 3-days ($p<0.001$) and remaining at this low level up until day 14 ($p=0.003$). Analysis of LVESV and LVEDV revealed no changes in terms of cardiac function over the 14-day treatment period. This was also true for ejection fraction and fractional shortening.

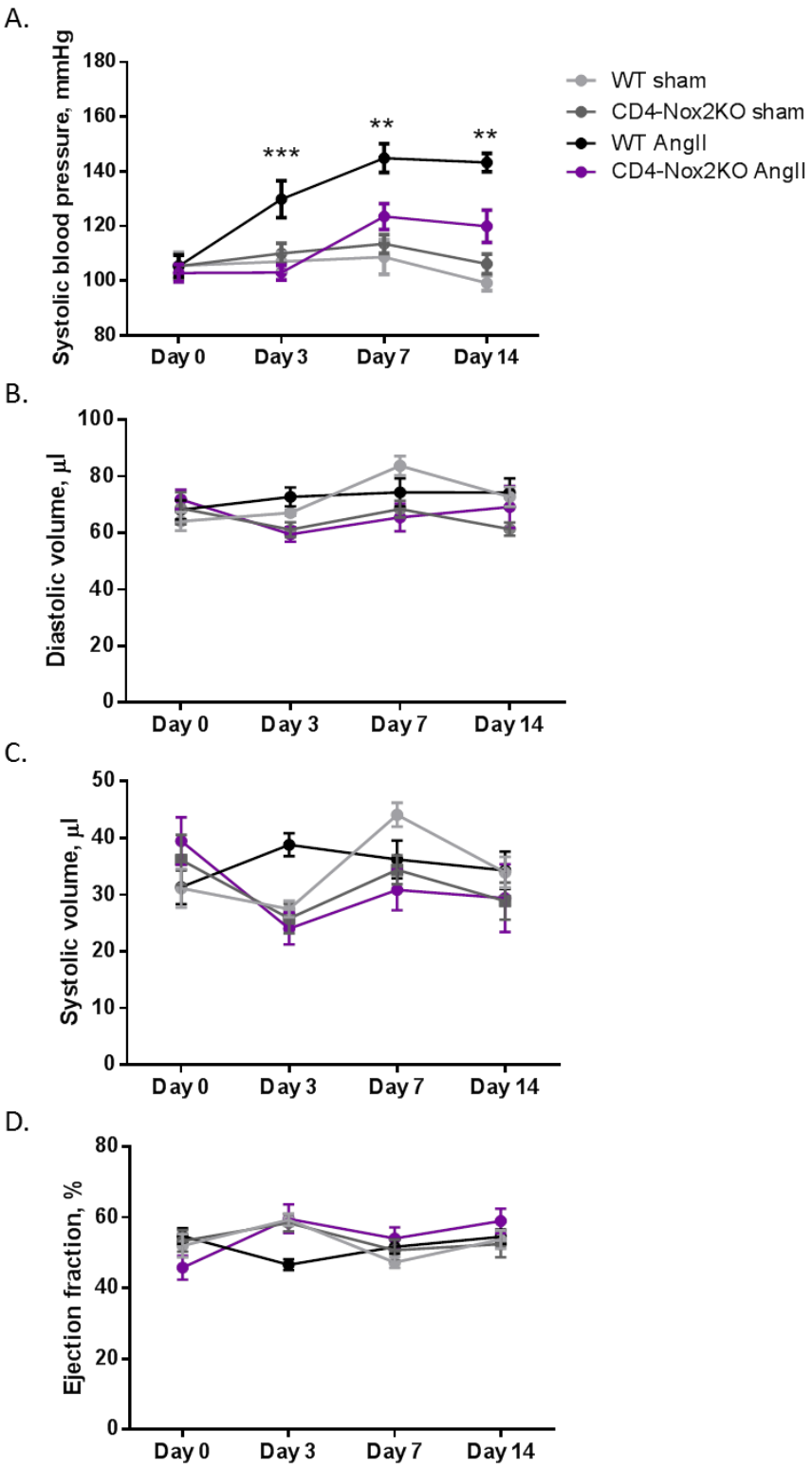

Figure 6-20: Blunted AngII-induced hypertension in CD4-Nox2KO animals. (A) *Systolic blood pressure, accompanied by stable* ***(B)*** *LV end-diastolic and* ***(C)*** *LV end-systolic volume and hence similar* ***(D)*** *ejection fraction. *WT AngII vs CD4-Nox2KO AngII. **p<0.01, ***p<0.001, N=6-8 per group.*

After the 14-day treatment period BW, HW and TL of all animals were recorded, *Figure 6-21*. HW/BW was significantly lower in sham CD4-Nox2KO animals (p=0.004) compared to WT littermates as observed in the baseline characterisation. This HW/BW ratio significantly increased after AngII treatment in CD4-Nox2KO animals (p=0.001) reaching 5.38±0.20mg/g, i.e. a similar level to WT littermates treated with AngII. No difference was identified between WT sham and WT AngII animals after 14-days. HW/TL ratios, a more accurate measure, showed a similar pattern but were statistically similar between all groups observed. In comparison the IVS thickness in WT littermates slowly increased over the 14-day treatment period with AngII, reaching significance at day 14 (p<0.001). However, CD4-Nox2KO animals did not develop an increase in IVS thickness throughout treatment, and had a 24% lower value than WT littermates after 14-days of AngII infusion (p<0.0001), as shown in *Figure 6-21*.

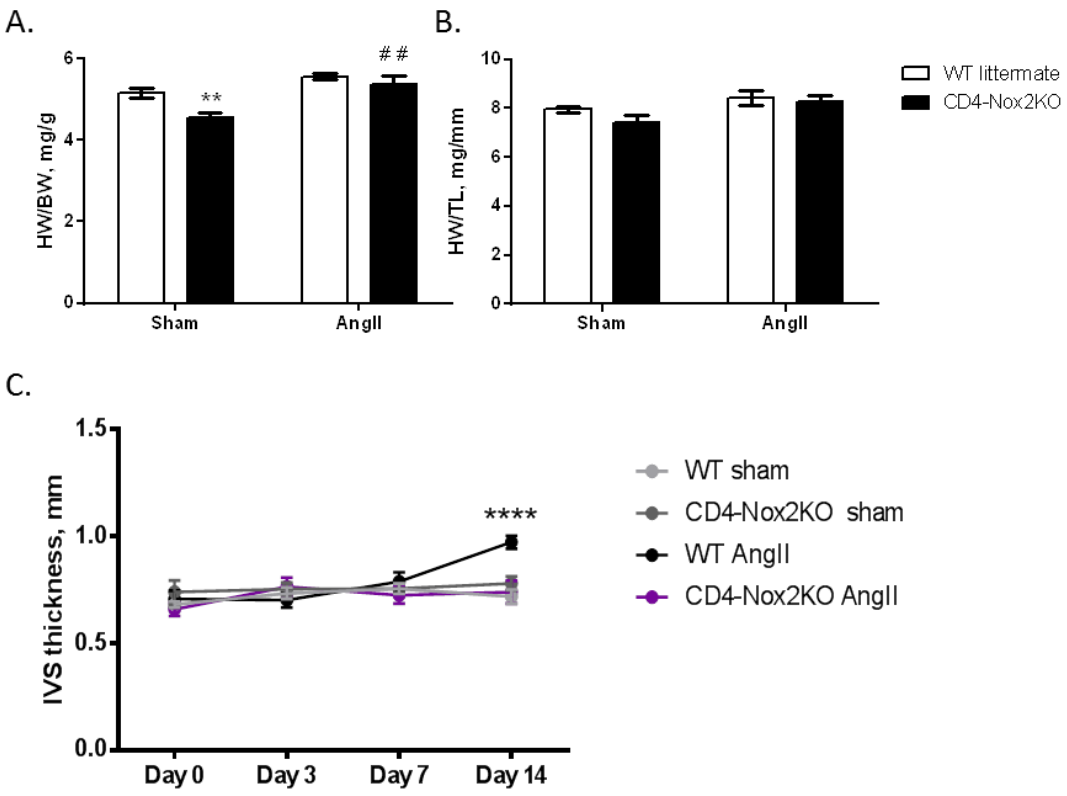

Figure 6-21: Attenuated AngII-induced cardiac hypertrophy in CD4-Nox2KO model. *Analysis of **(A)** Heart weight/body weight ratio (HW/BW), **(B)** Heart weight/tibia length ratio (HW/TL) and **(C)** interventricular septum thickness (IVS). *CD4-Nox2KO sham vs WT sham. # CD4-Nox2KO AngII vs CD4-Nox2KO sham. **p<0.01, ****p<0.0001, N=5-10 per group.*

Representative WGA staining images show an increase in cardiomyocyte size in AngII-treated WT animals as compared to WT sham ($p<0.001$), visualised in *Figure 6-22*. In comparison, CD4-Nox2KO animals showed a minimal increase in cardiomyocyte size with AngII. The cardiomyocyte cross-sectional area after AngII was 489±42µm^2 in WT littermate versus 311±16µm^2 in AngII-treated CD4-Nox2KO ($p=0.005$). 2-way ANOVA analysis confirmed a significant difference between CD4-Nox2KO and WT littermate groups ($p=0.0002$) and between sham and AngII treated groups ($p<0.0001$). This included a significant difference in interaction ($p=0.023$), showing the two genotypes respond differently to AngII.

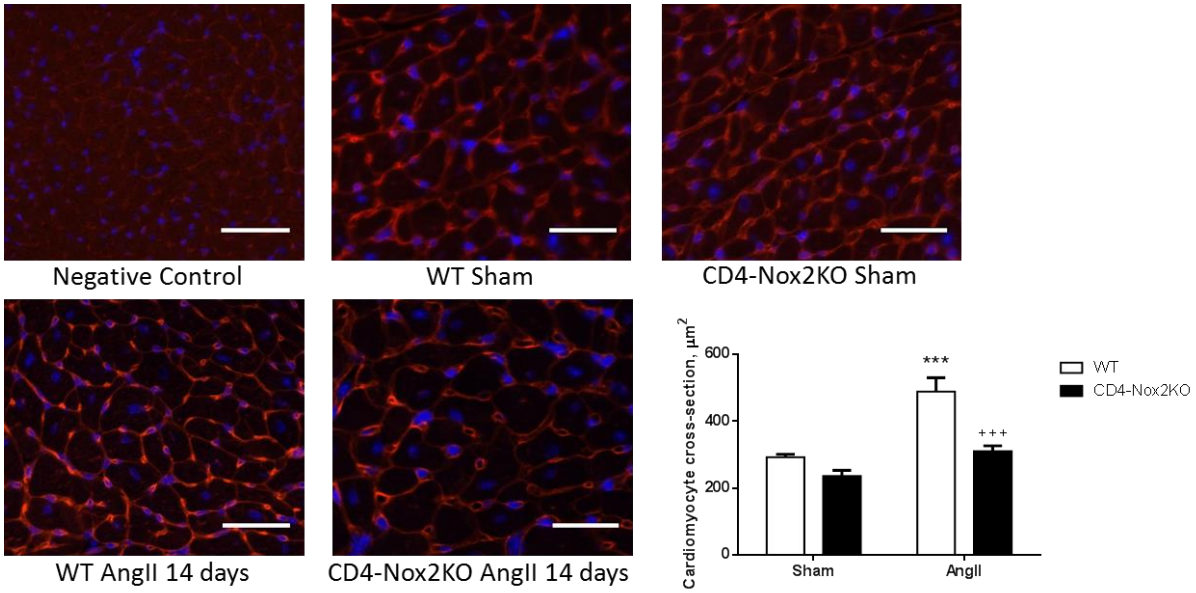

Figure 6-22: Attenuated AngII-induced cardiomyocyte hypertrophy in CD4-Nox2KO model. *Representative WGA images and analysis confirmed tissue-level hypertrophy, which was blunted in CD4-Nox2KO mice. *WT AngII vs WT sham. +CD4-Nox2KO AngII vs WT AngII. Scale bar=25µm; ***p<0.001; N=6 per group*

Paraffin sections were also stained with PSR to identify collagen within heart tissues, as illustrated in *Figure 6-23*. The characteristic increase in the percentage of collagen was observed in AngII treated WT littermate animals ($p<0.0001$) as previously shown. However, the CD4-Nox2KO group showed no increase in fibrosis after AngII treatments. After 14-days of AngII treatment CD4-Nox2KO animals had significantly lower levels of collagen compared to the WT littermates treated with AngII ($p<0.0001$).

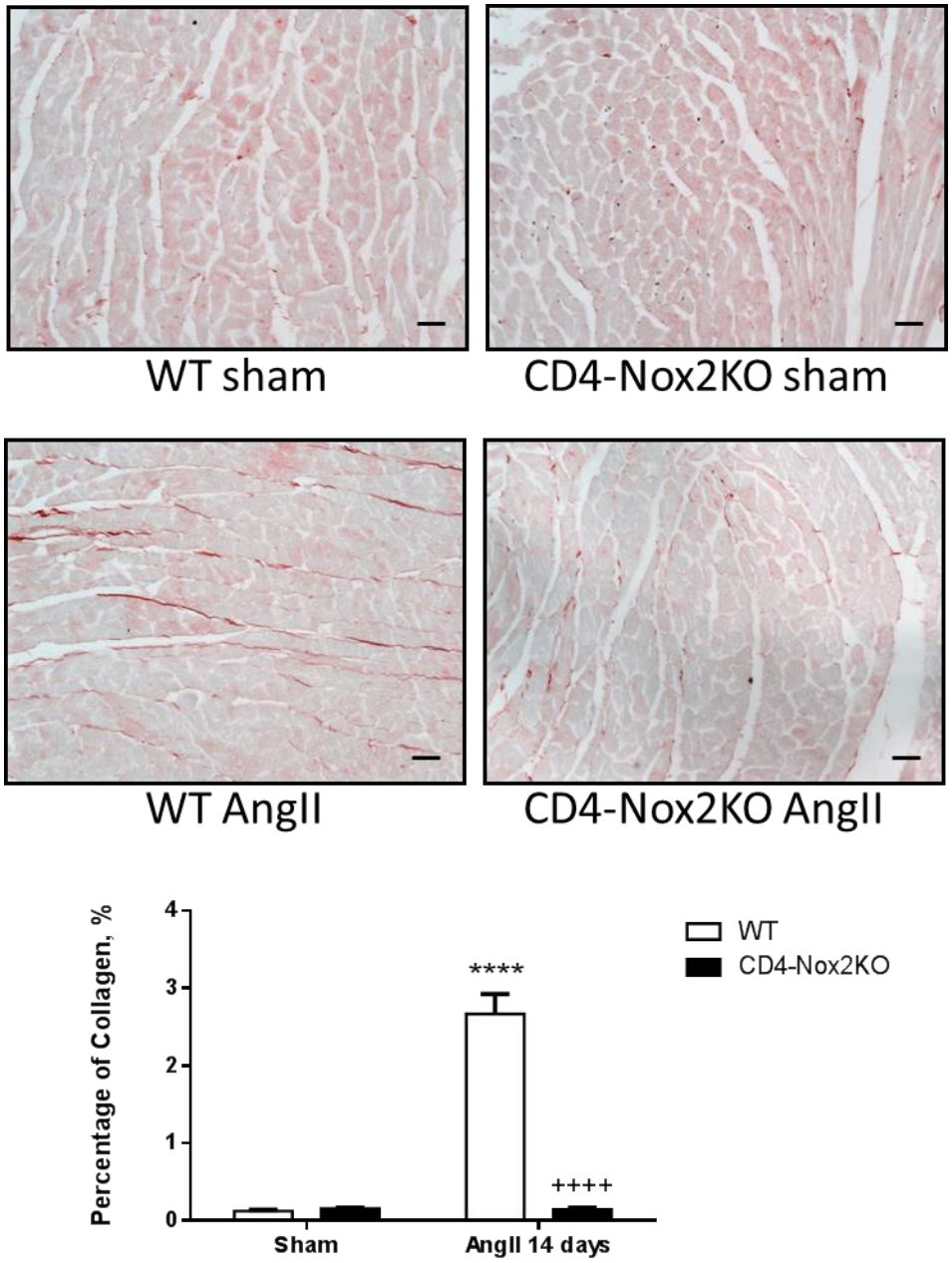

Figure 6-23: AngII-induced interstitial fibrosis is attenuated in CD4-Nox2KO animals. *Representative images of picrosirius red staining and analysis. *WT AngII vs WT sham. +CD4-Nox2KO AngII vs WT AngII. ****p<0.0001, Scale bar=25µm; N=6 per group.*

Supporting these findings, mRNA levels of col1α1 (p=0.048) and col3α1 (p=0.076) were lower in CD4-Nox2KO animals compared to WT littermates after AngII treatment (*Figure 6-24*). However, pro-fibrotic markers fibronectin, cTGF and TGFβ remained mRNA levels remained similar after 14-days of AngII treatment between both genotypes.

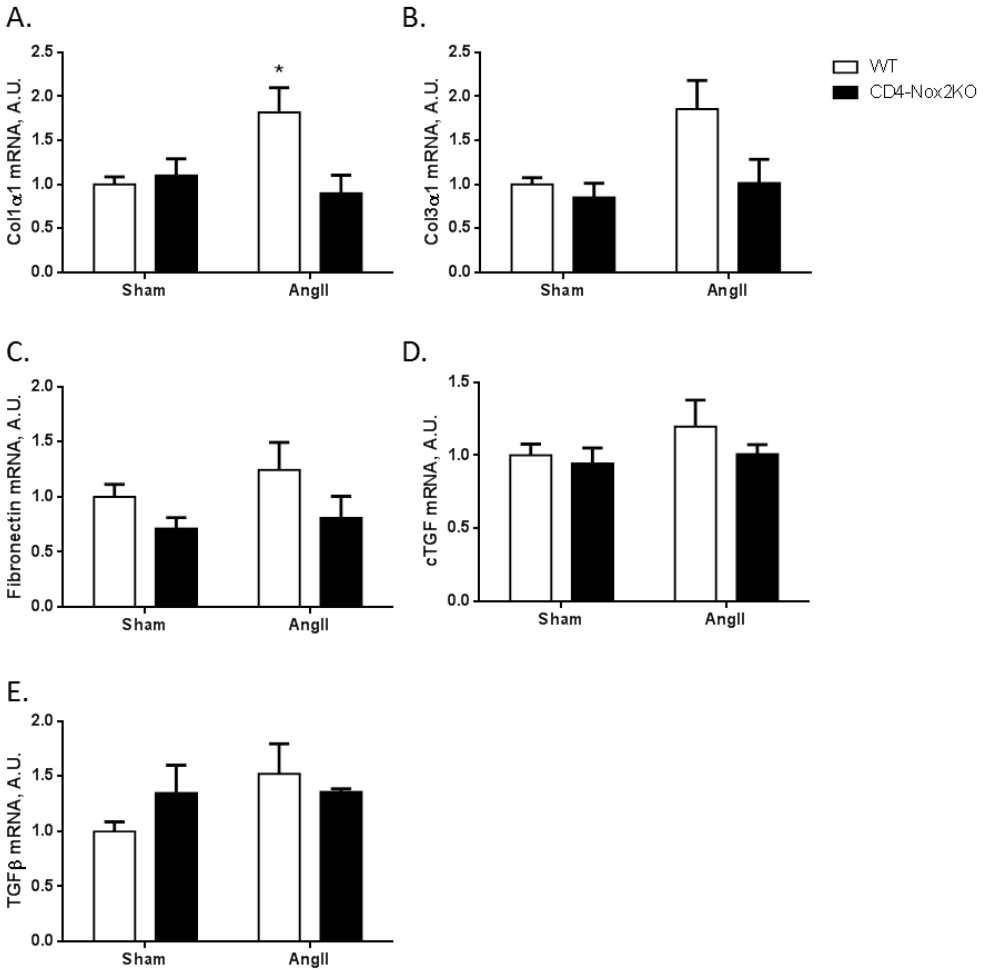

Figure 6-24: qPCR pro-fibrotic markers diminished in CD4-Nox2KO treated with AngII. *Fibrosis confirmed by quantification of* ***(A)*** *collagen1α1,* ***(B)*** *collagen3α1,* ***(C)*** *fibronectin,* ***(D)*** *CTGF and* ***(E)*** *TGFβ mRNA levels.*p<0.05, N=5-6 per group.*

The above results show that AngII induced hypertension, cardiomyocyte hypertrophy and interstitial fibrosis in WT littermate controls, similar to that observed in chapter 3. These responses to AngII were significantly attenuated in CD4-Nox2KO animals. This model gives us further insight into the development of AngII-induced cardiovascular responses and pinpoints $CD4^+$ T-cells as an important mediator of AngII-induced hypertension and cardiac remodelling.

6.4.5 Blunted cardiac infiltration of immune cells in CD4-Nox2KO mice

In order to quantify immune cell infiltration in the heart, aorta and spleen, single cell suspensions were prepared from animals treated with AngII for 3-days, or sham controls, and analysed using the CantoII™.

Flow cytometry dot plots, *Figure 6-25*, looking at total leukocytes ($CD45^+$ cells) and T-cells ($TCR\beta^+$ cells) showed a blunted infiltration of these immune cells in the CD4-Nox2KO heart compared to WT littermates when treated with AngII (*Figure 6-25*).

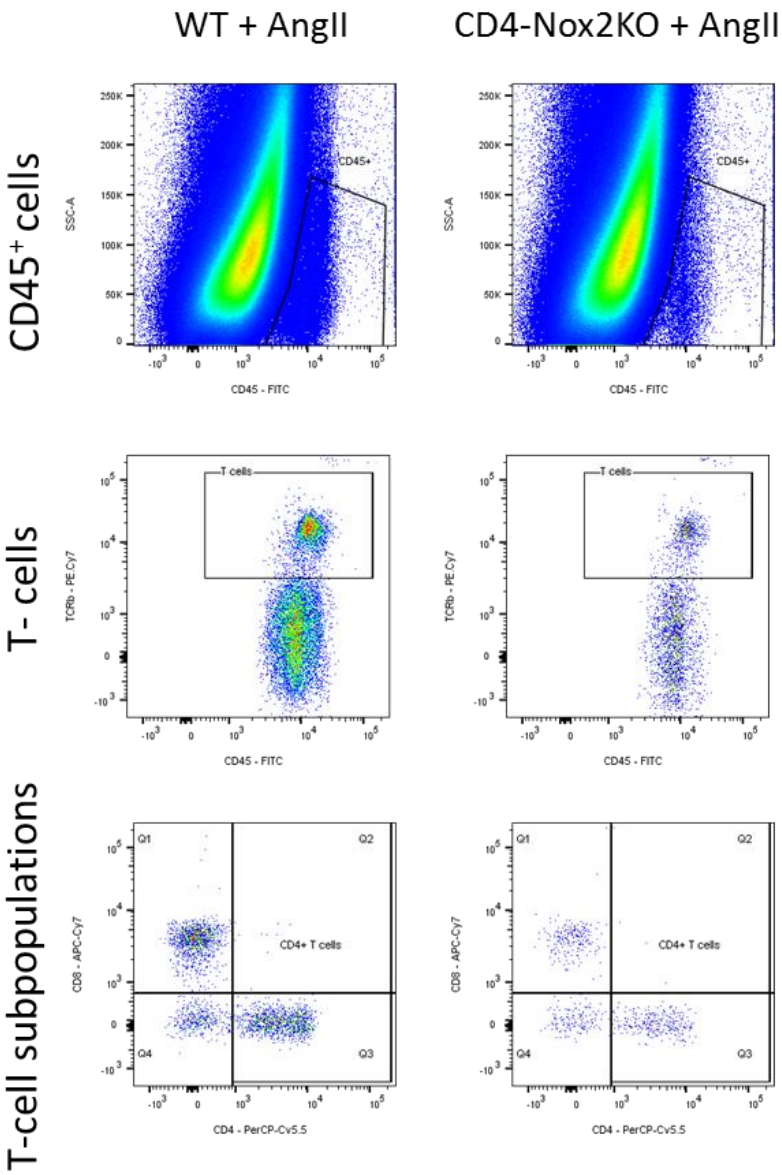

Figure 6-25: ***Representative flow cytometry dot plots showing reduced AngII-induced inflammation in hearts of CD4-Nox2KO animals.*** *Analysed on the BD FACS CantoII™.*

As observed previously, a significant cardiac infiltration of leukocytes occurs in WT littermate animals when treated with AngII (p=0.034), as shown in *Figure 6-26*. However, this increase is lost in CD4-Nox2KO mice (p=0.008) treated with AngII. Infiltration of T-cells behaves in an analogous manner, with a pronounced increase in WT littermates treated with AngII (p=0.007), which is blunted in AngII-treated CD4-Nox2KO animals (p=0.010). Each of the T-cell subpopulations follows a similar trend, with most prominent attenuation of $CD4^+$ T-cells (p=0.010) in CD4-Nox2KO compared to WT littermate controls. In comparison splenic immune cell levels, shown in *Figure 6-27*, are not influenced by the genotype or the treatment with AngII.

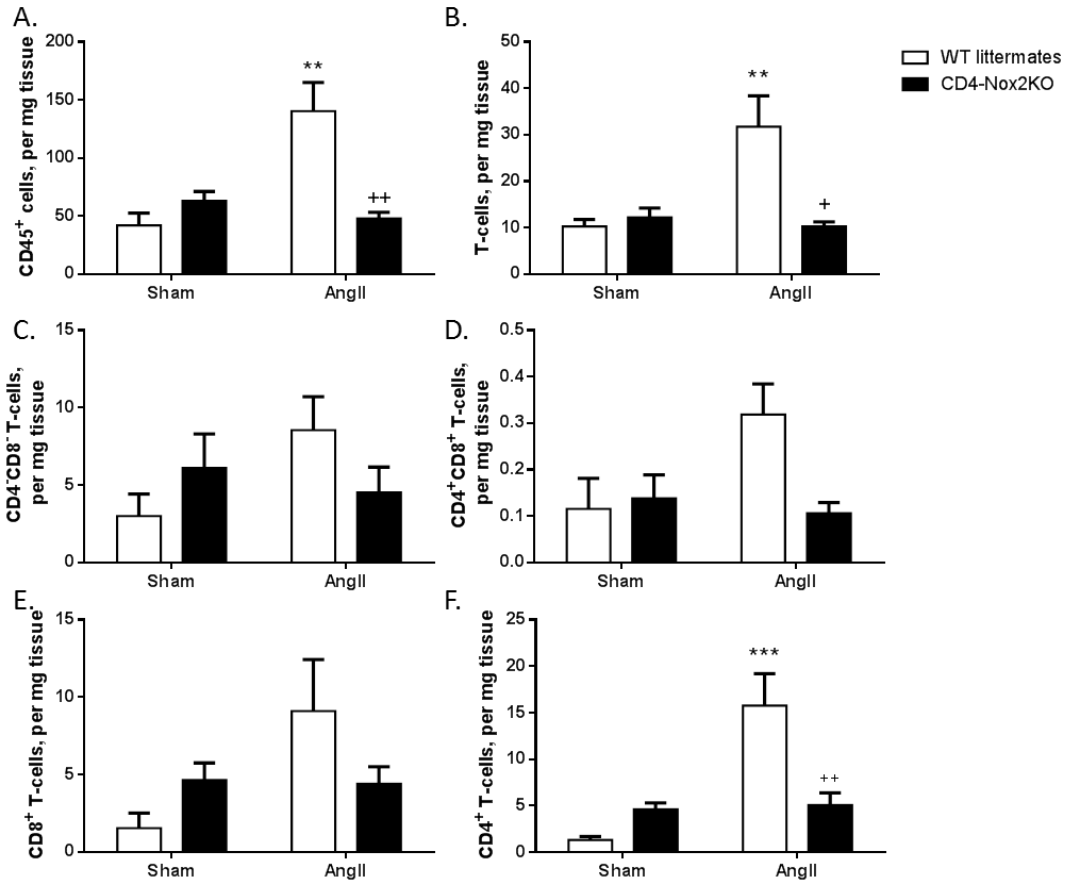

Figure 6-26: Reduced AngII-induced inflammation in CD4-Nox2KO animals. *The lack of CD4-Nox2 affects AngII-induced infiltration of* ***(A)*** *$CD45^+$ cells and* ***(B)*** *T-cells infiltration. Individual T-cell subpopulations, (****C****) $CD4^-CD8^-$, (****D****) $CD4^+CD8^+$, (****E****) $CD8^+$ and (****F****) $CD4^+$ T-cells. All data are represented as cells per mg of cardiac tissue acquired on the CantoII. *WT AngII vs WT sham. +CD4-Nox2KO AngII vs WT AngII.*p<0.05, **p<0.01, ***p<0.001, N=4 per group.*

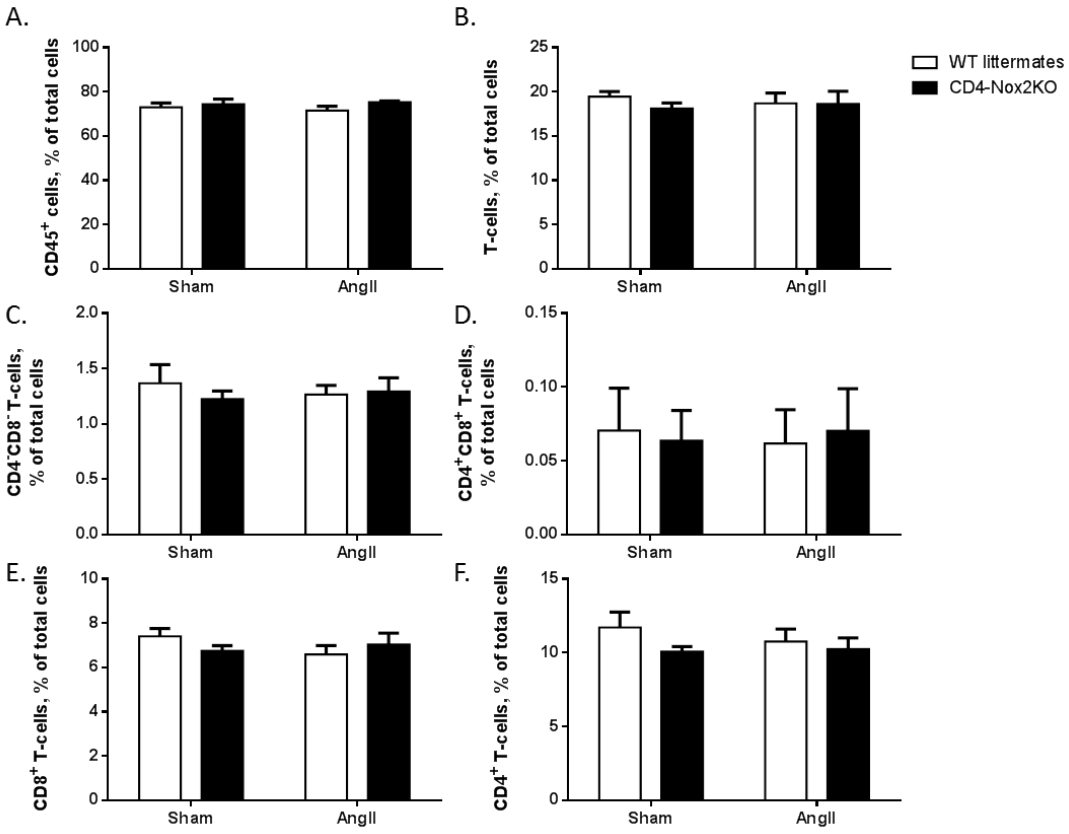

Figure 6-27: Lack of CD4-Nox2 does not alter splenic immune cell levels. *Spleen levels of* ***(A)*** *total leukocytes ($CD45^+$),* ***(B)*** *T-cells ($CD45^+TCR\beta^+$) and T-cell subpopulations* ***(C)*** *$CD4^-CD8^-$,* ***(D)*** *$CD4^+CD8^+$,* ***(E)*** *$CD8^+$ and* ***(F)*** *$CD4^+$ T-cells were analysed as a background control. All data are represented as a percentage of total cells, acquired on the CantoII™. N=4 per group.*

Of the $CD4^+$ T-cell population, Treg cardiac infiltration was also affected by the lack of CD4-Nox2, as shown in *Figure 6-28*. A significant increase in Tregs with AngII treatment was observed ($p_{CD4+CD25+}<0.001$; $p_{FoxP3+}=0.023$), as previously identified in chapter 3. $CD4^+CD25^+$ Tregs were 43% lower in AngII-treated CD4-Nox2KO mice compared to AngII-treated WT littermates however this was not significant. This pattern of response was also confirmed with FoxP3 staining, also showing a 43% difference between AngII-treated WT and CD4-Nox2KO, however this remained not statistically significant. The Treg composition within the spleen of the CD4-Nox2KO animals tended to be lower in sham animals compare to WT littermates but no significant differences were observed, especially after AngII treatment.

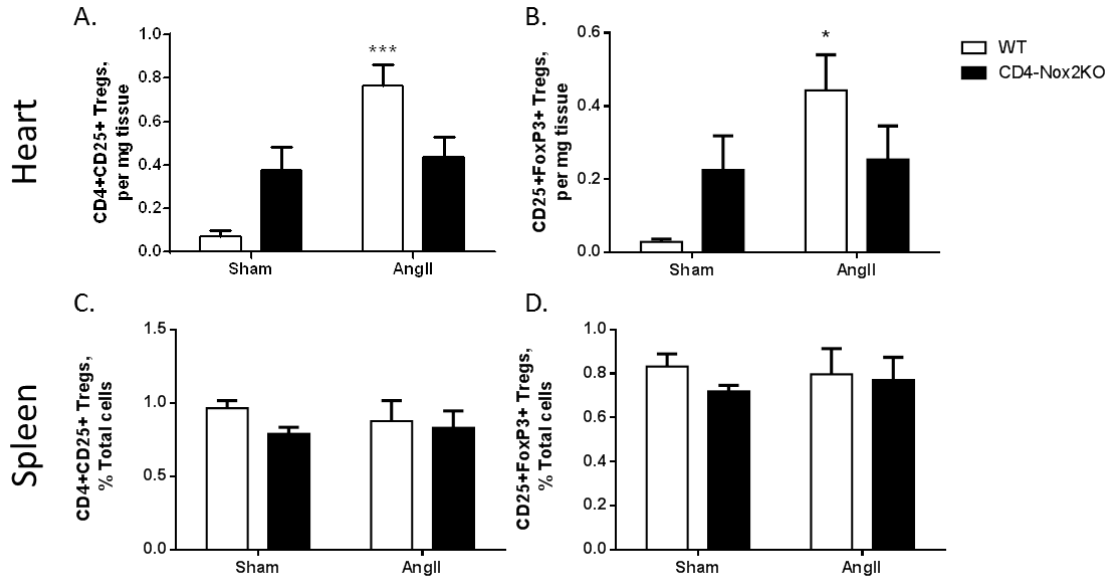

Figure 6-28: Cardiac Treg levels altered in CD4-Nox2KO treated with AngII compared to WT littermate controls. *Blunted AngII-induced cardiac Tregs observed by levels of* ***(A)*** *$CD4^+CD25^+$ Tregs and* ***(B)*** *$CD4^+CD25^+FoxP3^+$ Tregs.* ***(C&D)*** *Splenic levels of Tregs remain consistent in response to AngII. *WT AngII vs WT sham. *p<0.05, ***p<0.001. N=4 per group.*

The proportions of T-cells within the heart and spleen were also investigated to see if any T-cell ratios change between groups (*Figure 6-29*). T-cells as a percentage of $CD45^+$ cells, $CD4^+$ T-cells as a percentage of total T-cells and Tregs as a percentage of $CD4^+$ T-cells all remain consistent within the heart and spleen. However the sham-level of Tregs as a percentage of $CD4^+$ T-cells tends to be higher in CD4-Nox2KO compared to WT littermates, as previously identified in baseline measurements, however this was not significant using a 2-way ANOVA.

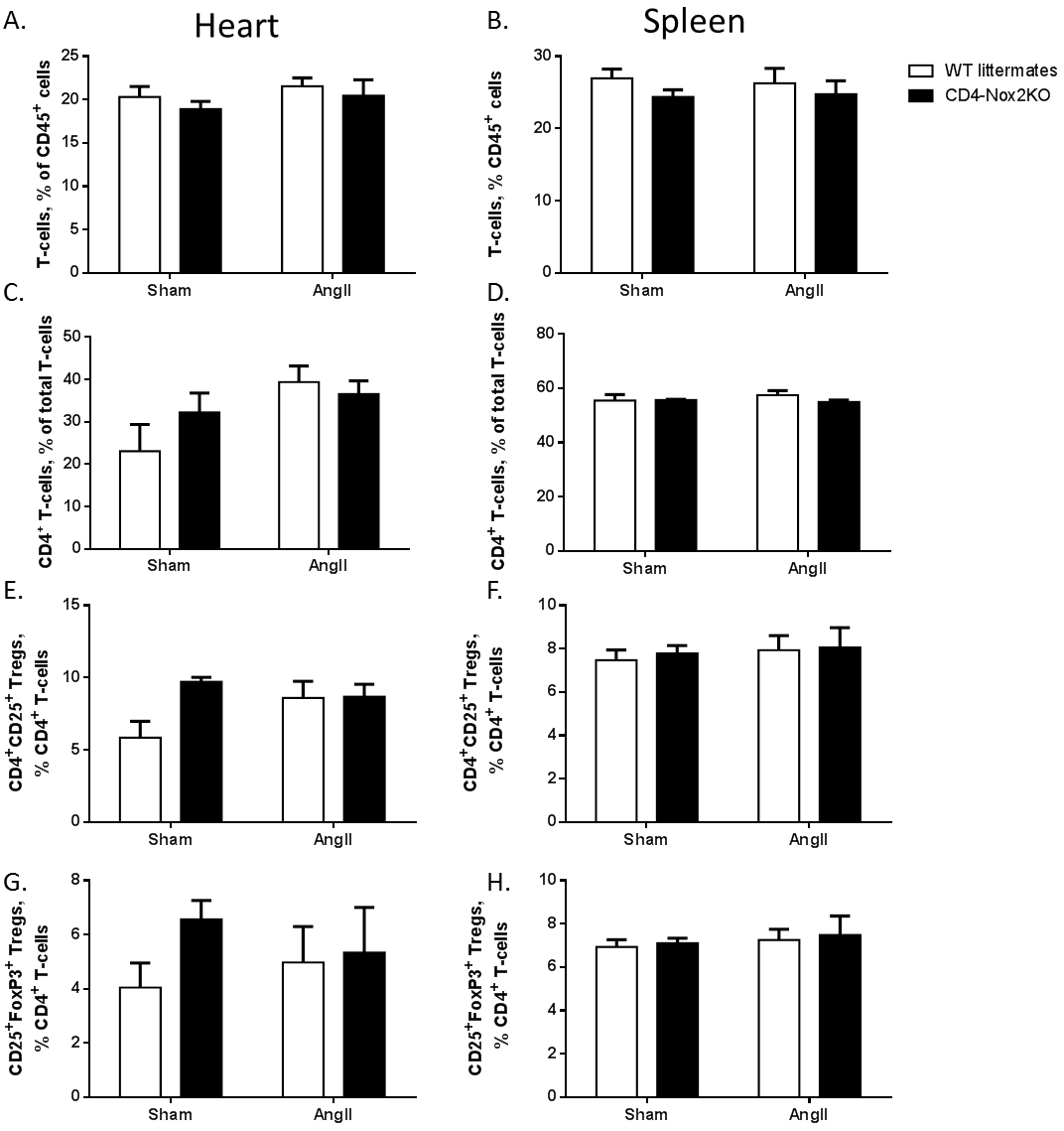

Figure 6-29: Impact of CD4-Nox2 deficiency on T-cell proportions during AngII treatment. *(**A&B**) T-cells as a percentage of $CD45^+$ cells, **(C&D)** $CD4^+$ T-cells as a percentage of total T-cells, **(E&F)** $CD4^+CD25^+$ Tregs as a percentage of $CD4^+$ T-cells and **(G&H)** $CD25^+FoxP3^+$ Tregs as a percentage of $CD4^+$ T-cells. N=4 per group, analysed on BD FACS CantoII™.*

Infiltration of immune cells into the aorta of these animals was also investigated in order to decipher the impact of CD4-Nox2KO on the vasculature, especially as there is an altered response to AngII in terms of systolic blood pressure. Within the aorta, equivalent immune cells were analysed and followed a similar trend to that within the heart, as shown in *Figure 6-30*, however these responses were not statistically significant probably due to low numbers of immune cells within the aorta. The aorta

reflected a similar immune cell response to the heart with AngII treatment, suggesting the response is cardiovascular-wide and not just restricted to the heart tissue.

Taken together, these results show that the CD4-specific Nox2KO has a protective phenotype against AngII-induced hypertension, cardiac remodelling and immune response. Within the CD4-Nox2KO at baseline, certain aspects may explain the protective responses observed with AngII. These include an altered immune composition and proportions, especially with Tregs in the heart, LNs and spleen. Overall this highlights the importance of CD4-specific Nox2 to the progression of AngII-induced inflammation and associated remodelling.

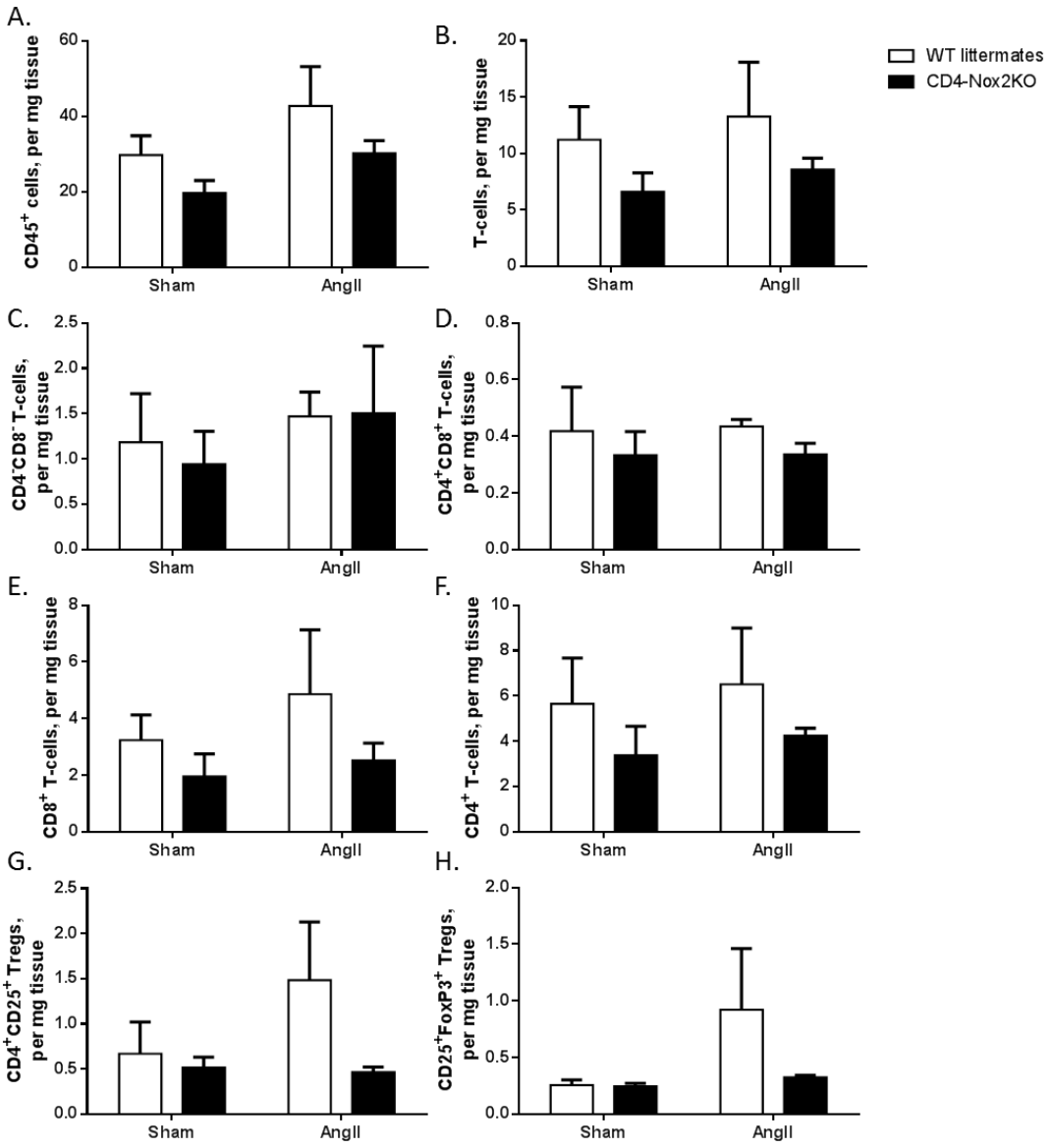

Figure 6-30: T-cell infiltration into the Aorta of CD4-Nox2KO and WT littermate animals after AngII treatment. ***(A)*** *Total leukocytes ($CD45^+$ cells),* ***(B)*** *T-Cells ($CD45^+TCR\beta^+$ cells) and each of the T-cell subpopulations:* ***(C)*** *$CD4^-CD8^-$,* ***(D)*** *$CD4^+CD8^+$,* ***(E)*** *$CD8^+$ and* ***(F)*** *$CD4^+$ T-cells all reflect that observed in the heart. This is also shown with* ***(G)*** *$CD4^+CD25^+$ Tregs and* ***(H)*** *$CD25^+FoxP3^+$ Tregs. N=4 per group.*

6.5 Discussion

Until now, there has been a lack of clear understanding of the effects of T-cell Nox2 in the cardiovascular response to AngII due to the presence of Nox2 in multiple cell types, where it may affect different functions. Generation of a CD4-Nox2KO model has enabled the investigation of the specific role of endogenous Nox2 within $CD4^+$ T-cells *in vivo*, and the impact this has in the setting of AngII-induced cardiovascular remodelling.

Firstly, the fidelity of the new murine model was confirmed by observing a significantly lower level of Nox2 specifically within $CD4^+$ T-cells isolated from CD4-Nox2KO mice compared to WT littermates. The CD4-Cre mice used to generate the CD4-Nox2KO used in this study, have previously been used by Pino-Lagos et al, to generate a mouse-line where $CD4^+$ T-cells express a double-negative retinoic acid (RA) receptor (dnRAR), thereby inhibiting downstream signalling[260]. However, as this was not a typical KO model, no results were shown to determine how effective this was under the CD4-Cre promoter. Other research groups utilised a similar CD4-Cre mouse model and demonstrated an 80-95% decrease with their floxed target genes[261-264].

Results presented here showed a smaller decrease in the target gene by qPCR; however there are a few aspects to bear in mind. During T-cell development (section 1.3.2.2) CD4-Cre is activated during later stages of DN cell development and is only fully expressed during the DP stage[265]. In addition, residual Nox2 mRNA may still remain after the initial DN stages of development, where CD4 is not yet expressed[265]. Therefore, in theory peripheral $CD4^+$ T-cells should be deficient in Nox2; however some may still express Nox2 mRNA, which could skew the results. Lack of Nox2 within $CD4^+$ T-cells may cause other cell types to compensate for this deficiency by increasing their expression of Nox2. Nox2 expression within all remaining immune cells was also examined, which was similar between the two genotypes, suggesting that the results were not confounded by compensatory changes in other cell types.

Interestingly, at baseline a number of differences between the CD4-Nox2KO and WT littermates were observed. The new mouse model displays thymus hyperplasia, whereas the LNs and spleen are a similar size to that of WT littermate controls. This may suggest an impact of the target gene on T-cell development, causing an

accumulation of cells or increased differentiation[265]. As observed previously, global Nox2KO mice also displayed enlarged lymphoid organs[199]. Therefore the lack of Nox2 specifically within $CD4^+$ T-cells, gives a similar response but directed towards the thymus, where T-cells develop.

Furthermore, the immune cell composition of MLNs and, more significantly, PLNs in the CD4-Nox2KO model was different compared to the WT littermate control. This included an increased level of T-cells, with an emphasis on $CD4^+$ T-cells in addition to Tregs. Interestingly, the Treg:T-cell ratio did not alter within the LNs, therefore both total T-cells and Tregs increased by the same amount. Lee et al, examined the LNs of global Nox2KO mice aged 15-18 weeks, in this setting they noticed increased levels of B-cells, macrophages and monocytes but a lower level of T-cells[199]. As this study was carried out in older animals, with a high incidence of arthritis, the T-cell composition of the LNs may be different. In addition, this study allows the novel investigation of Nox2 specifically in the $CD4^+$ T-cell subset, whereas previous experiments lack Nox2 within all cell types.

In comparison to this finding, immune cell levels in the spleen remained the same between both genotypes, except for a reduction in Tregs. Similar findings were observed with the global Nox2KO study. Here, this would suggest a potential change in the distribution of immune cells, potentially being recruited to the periphery in the CD4-Nox2KO mice.

An important and fascinating finding from this study was the observation of a smaller heart within the CD4-Nox2KO mice compared to WT littermates at baseline. This was confirmed by a smaller cardiomyocyte cross-section. It is interesting to postulate that the lack of Nox2 within cardiac-resident $CD4^+$ T-cells may influence cardiomyocyte development. One important aspect is that both cells of the cardiovascular system and immune cells are derived from the mesodermal layer during embryogenesis[266,267]; therefore early cellular signalling may affect cardiac development in CD4-Nox2KO mice. For instance, cardiac-resident $CD4^+$ T-cells that lack Nox2 may secrete modulators during development that affect cardiomyocyte growth. One such modulator may be RA, which has been implicated in $CD4^+$ T-cell differentiation and is also involved in cardiomyocyte development[260,268]. More RA may be utilised by CD4-

Nox2KO cells, reducing cytoplasmic levels, and hence slowing down cardiac development. However this would require further investigation. This difference observed in cardiomyocyte size, and overall heart size, was not substantial enough to affect heart rate, blood pressure or haemodynamic function. Moreover, collagen deposition, which is tightly linked to inflammation, remained the same between both genotypes.

Immune cell infiltration was highly affected by the lack of CD4-Nox2. AngII treatment of CD4-Nox2KO mice did not elicit the cardiac-infiltration of immune cells, previously observed with WT mice. Hence, compared to WT littermates, AngII-treated CD4-Nox2KO mice displayed significantly lower levels of total leukocytes and T-cells with an emphasis on $CD4^+$ T-cells and Tregs.

Within the CD4-Nox2KO mice at baseline, there is a higher ratio of cardiac-resident Tregs:T-cells, which may provide a protective response preventing further infiltration of immune cells with AngII treatment. Previous research where an adoptive transfer of Tregs has been used to increase basal levels of Tregs (as in the studies in chapter 5), has provided a beneficial response to AngII[190,191]. This was associated with lower immune cell infiltration and prevention of subsequent cardiac remodelling[190,191].

Analysis of AngII-induced immune cell infiltration within the aorta of CD4-Nox2KO mice followed a similar trend to that observed in the heart. However due to low numbers of immune-cells in the aorta, these data were not significant.

Intriguingly, in the heart at baseline there is an altered composition of T-cells with an enhanced level of $CD4^+$ T-cells and Tregs, in addition to an increased Treg:T-cell ratio. This increase in cardiac-resident Tregs, in combination with reduced splenic Treg levels, may suggest Treg recruitment to the heart. In-line with this, the global Nox2KO study also showed increases in $CD4^+$ T-cells and Tregs, however this was accompanied by increases in other T-cell subtypes. Therefore the CD4-Nox2KO model seems to possess similar basal characteristics to the global Nox2KO model, but with a specific effect on the $CD4^+$ T-cell compartment. This also falls in line with previous research suggesting increased inflammatory cells in the LNs of Nox2KO mice[199].

Furthermore, the lack of endogenous Nox2 in cardiac-resident $CD4^+$ T-cells may have a key role here in proliferation, maintenance or even migration of $CD4^+$ T-cells and/or Tregs, which would be interesting to investigate further. Nox2 has already been implicated in the setting of Th differentiation, where the absence of Nox2 leads to enhanced Th1 and Th17 differentiation[199,248-251]. This shows the capacity of Nox2 to augment $CD4^+$ T-cell responses. However, the direct ability of Nox2 to modulate T-cell apoptosis, cell maintenance and proliferation is not yet understood. One paper touching on this topic suggests that ROS are implicated in T-cell apoptosis via the costimulatory receptor programmed death-1 (PD-1)[269]. Nevertheless, this research mainly concentrated on mitochondrial-derived ROS instead of Nox-derived ROS; therefore conclusions cannot be drawn from this evidence. Hence, further investigation is required in this area.

As Nox2 has previously been shown to be involved in hypertension and cardiovascular remodelling, experiments were carried out using AngII to analyse the effect of CD4-Nox2 on cardiac hypertrophy and fibrosis. CD4-Nox2KO animals displayed a blunted hypertensive response to AngII, in addition to attenuated hypertrophy and fibrosis. Within this model, cardiomyocyte size is initially smaller but even taking this into account there was a minimal increase in size after AngII infusion. The differences between genotypes could be explained by the difference in blood pressure response although one cannot exclude a difference in the direct effects of AngII on the heart.

In terms of cardiac fibrosis, there is an important link between inflammation and fibroblasts, whereby inflammatory cells release pro-fibrotic stimuli and in turn fibroblasts can release pro-inflammatory mediators. $CD4^+$ T-cells have previously been identified to play a direct role in fibrosis by secretion of IFN-γ, TGFβ, IL-1 and IL-6, which all potentiate the development of fibrosis[115,122,123]. Cardiac fibroblasts also have been demonstrated to recruit $CD4^+$ Th17 cells to the myocardium during acute viral myocarditis[270]. Furthermore, direct molecular interactions between fibroblast-like cells and $CD4^+$ T-cells have been identified in other settings such as rheumatoid arthritis and chronic pulmonary disease[271-273]. Thereby, the CD4-Nox2KO model may display blunted fibrosis due to altered interactions between fibroblasts and $CD4^+$ T-cells in this setting. In addition, Tregs have the ability to modulate the phenotype and function of cardiac fibroblasts. Saxena et al identified that Treg depletion, using an anti-CD25

antibody (PC61), causes increased collagen deposition in an infarcted myocardium[241]. Furthermore, this group identified that, *in vitro*, Tregs displayed the ability to reduce α-SMA and MMP-3 mRNA expression by cardiac fibroblasts in addition to reducing their contractile ability, a process key to infarct healing[241]. Hence, it may be the Treg component of $CD4^+$ T-cells in the CD4-Nox2KO model that are important within this setting.

Previous research identified that the lack of $CD4^+$ T-cells provides a beneficial response to a pressure-overload model[184]. This research group clearly demonstrated that the lack of $CD4^+$ T-cells prevents fibrosis, collagen accumulation and cross-linking within the cardiac tissue after TAC[184]. In comparison, experiments in this chapter essentially pinpoint this response to a specific component of $CD4^+$ T-cells, Nox2, which is instigated in the response to pressure-overload, for example by AngII-treatment. In contrast to this, research by Hofmann et al identifies that the lack of $CD4^+$ T-cells provides an enhanced response to MI and hence implicates $CD4^+$ T-cells in the setting of cardiac wound healing[252]. By completely diminishing animals of $CD4^+$ T-cells, Tregs are also removed that have been shown to be beneficial during the cardiac response to stress[193,240]. Therefore a potential suggestion is that, it is the Tregs that have the ability to reduce $CD4^+$ T-cell levels, which are advantageous within this setting.

At baseline the CD4-Nox2KO mice displayed an increased cardiac-specific Treg:T-cell ratio, suggesting a regulatory phenotype that may provide a local protective mechanism. Hence, this balance between Tregs and Teff cells may determine the outcome to cardiac stressors such as AngII. Moreover, results show that Nox2 has the ability to impact Treg function[214]. In line with this, results presented here showed that Nox2KO-Tregs are more effective than their WT counterparts (chapter 5). This therefore suggests that the CD4-Nox2KO model may possess enhanced Treg abilities, which in turn could protect the heart from AngII-induced remodelling.

Furthermore, the lack of IL-17, a cytokine produced by the Th17 subset of $CD4^+$ T-cells, protects mice from AngII-induced cardiac remodelling[185]. This further confirms the involvement of Teff subsets of $CD4^+$ T-cells in this setting; hence an increased level of Tregs here may control Teff levels and could prove beneficial in the response to AngII.

Therefore one may suggest that the cardiac Teff:Treg ratio is pertinent to the cardiac outcome in response to stress.

Taken together, the results presented in this chapter show that CD4-Nox2KO mice have an increased level of cardiac-resident $CD4^+$ T-cells and Tregs at baseline with an augmented Treg:T-cell ratio. This in turn may provide a cardiac-specific protective mechanism due to the observed attenuated AngII response in terms of cardiac inflammation, hypertension and fibrosis. Therefore this study has identified a crucial role for CD4-Nox2 in the potentiation of AngII-induced hypertension and cardiac remodelling.

Chapter 7: General Discussion

7.1 General overview of findings

Nox2 is expressed in a variety of cell types including cardiomyocytes, fibroblasts, endothelial cells and immune cells. Nox2-derived ROS within T-cells may have the ability to mediate signalling pathways that can influence their differentiation, proliferation, migration and even maintenance. A handful of studies have identified a role for T-cells in cardiovascular remodelling. For instance a key paper by Guzik et al demonstrated that $RAG^{-/-}$ mice, lacking T- and B-cells, displayed a blunted response to AngII-induced hypertension. Furthermore, the adoptive transfer of T-, but not B-cells, back into these $RAG^{-/-}$ mice restored the expected pathophysiological response[134]. In addition to this, Nox2 is a major mediator of cardiovascular remodelling and has been implicated in the setting of cardiac hypertrophy, fibrosis and apoptosis. Such a role includes the potentiation of interstitial fibrosis in response to AngII, where in the absence of Nox2, this response fails to develop[108]. Convincing evidence has also placed T-cell Nox2 in the limelight. In the vasculature, Guzik et al also reconstituted $RAG^{-/-}$ mice with T-cells isolated from $p47^{phox-/-}$, lacking Nox2, and showed that this partially restored the expected hypertensive response to AngII[134].

Nox2 and inflammation have separately been identified in the potentiation of AngII-induced hypertension and fibrosis; however the specific, endogenous role of T-cell Nox2 within the cardiovascular setting requires further investigation. Therefore the aim of this thesis was to identify the function of T-cell Nox2 and its capacity to regulate cardiovascular remodelling in the setting of increased RAAS activation.

AngII is extensively used in mouse models to induced hypertension and cardiac fibrosis, both of these processes have previously been identified to be potentiated by inflammation and Nox2. Thereby AngII infusion was an ideal model for this investigation. Firstly, efficiency of AngII to induced hypertension and associated cardiac hypertrophy and fibrosis was confirmed, verifying the efficacy of the model, and characterised the precise pattern of inflammatory infiltration of the myocardium. Interestingly, cardiac inflammation with AngII occurred in a time-dependant manner, with a peak after 3-days of AngII. In addition a distinct spatial orientation of infiltrated immune cells was observed. AngII treatment also augmented the level of cardiac T-cells, specifically $CD4^{+}$ T-cells and Tregs. Furthermore, these results highlighted that

AngII treatment increased the level of cardiac-specific chemokines, which may suggest a direct impact of AngII on T-cells to encourage cardio-tropism. Therefore $CD4^+$ T-cells and Tregs potentially play a key role in the development of AngII-induced pathophysiology in a time-dependent manner.

To address how Nox2 within infiltrating immune cells may affect the cardiac-response to AngII, a global Nox2KO model was used. Initially, we confirmed that these mice show an attenuated response to AngII-treatment in terms of hypertension and cardiac hypertrophy. Until now, the effect of Nox2 on cardiac immune-cell infiltration in this setting was unknown. Global Nox2KO mice at baseline display larger lymphoid organs that suggest a potential altered inflammatory response. We identified that the lack of Nox2 augmented cardiac-resident T-cell compositions at baseline. Moreover, the ratio of Tregs:T-cells was markedly increased in global Nox2KO hearts prior to treatment. In line with the cardiac-response to AngII, global Nox2KO mice presented an attenuated infiltration of immune cells into the myocardium compared to WT littermate controls. These results suggested a potential protective, anti-inflammatory mechanism related to the altered Treg:T-cell ratio at baseline that may be important in the setting of AngII-induced cardiac remodelling.

Tregs have the ability to suppress inflammatory responses and have been identified previously to provide a protective response to cardiovascular stressors[189-192]. Here we highlighted that by increasing basal Treg-levels in mice via adoptive transfer, a protective phenotype can be achieved in response to AngII. Furthermore, this protective response was accompanied by an increased Treg:T-cell ratio, therefore the Treg ability to suppress $CD4^+$ Teff cells may prove beneficial. Moreover, Nox2KO-Tregs are more efficient at protecting the heart and along with *in vitro* data this shows that the lack of Nox2 in Tregs generates a greater suppressive function.

To fully appreciate the function of Nox2 in T-cells *in vivo*, it is vital to create a T-cell specific Nox2KO model. The previous global Nox2KO model gave us an essential insight into how Nox2 altered the cardiac inflammatory response, with a specific influence on T-cells. However, as all cell types were deficient in Nox2 it was difficult to ascertain which components are truly important during this setting. Furthermore, robust data from Laroumanie et al demonstrated that CD4KO, but not CD8KO, mice display protective responses to pressure overload, highlighting the importance of $CD4^+$ T-cells

here[184]. Therefore a novel in-house CD4-Nox2KO mouse was generated. This enabled further clarification of the involvement of endogenous Nox2 within $CD4^+$ T-cells. At baseline, these mice displayed an enlarged lymphoid organ, similar to global Nox2KO mice but with a specific impact on the thymus, where T-cells develop. CD4-Nox2KO mice also have an increased cardiac-specific ratio of Treg:T-cells, similar to that found in the global Nox2KO experiments, but without increases in other T-cell subsets. Additionally, these mice displayed a blunted response to AngII in terms of cardiac inflammation, hypertension and fibrosis. Overall the lack of Nox2 in $CD4^+$ T-cells is sufficient to protect mice from AngII-induced hypertension and remodelling. Therefore endogenous T-cell Nox2 may be essential to the progression of cardiovascular remodelling.

7.2 Implications of T-cell Nox2

During AngII-infusion, infiltration of T-cells into the WT mouse myocardium occurs with a peak after 3-days of treatment. However in both the global Nox2KO and CD4-Nox2KO mice this infiltration at 3-days is blunted. A potential explanation is that Nox2 in T-cells may modulate their migration to the heart and prevent upregulation of chemokines involved in cardio-tropism.

Fascinating results from Komarowska et al revealed that myocardial-produced hepatocyte growth factor (HGF) enters the heart-draining LN, where this cytokine can prime T-cells to express a unique and specific molecular signature, c-$Met^+CCR4^+CXCR3^+$, that allows cardio-tropism[183,274]. LNs allow drainage of fluid from circulating blood and local tissues, which enables the interaction of components from innate and adaptive immunity. Furthermore, the pharmacological blockade of c-Met during T-cell priming encouraged cardiac allograft survival, with an impaired ability of T-cells to localise to cardiac allografts[183].

In addition to this, AngII has been implicated in regulating cardiac-HGF levels. In SHR rats, that have naturally higher AngII levels, circulating HGF concentrations were higher whereas tissue-HGF within the heart, aorta and kidney were lower than controls[275]. Moreover, HGF within the heart has been linked to a reduction in myocardial injury in response to AngII, due to its anti-fibrotic mechanisms[276]. To my knowledge, no studies

have yet investigated the impact of AngII on HGF levels specifically within the LNs draining the heart. Hence, as AngII is associated with lower HGF levels in the myocardium, but increased levels within the heart-draining LNs, AngII may potentially encourage transportation of HGF to the LNs, or even upregulation of HGF within the LNs. Here, HGF primes T-cells to acquire vital cues that enable cardio-tropism potentially in response to AngII[183,275]. Primed T-cells can then elicit a cardiac-targeted immune response to resolve cardiac tissue homeostasis.

Data presented here have demonstrated that in the hearts of WT mice treated for 3-days of AngII, levels of cardiac-specific T-cell chemokines were upregulated, these included cMet, CCR4 and CXCR3. We were unable to study these levels in the KO models due to the lower level of T-cells infiltrating the heart after AngII treatment. Therefore, one interesting hypothesis is that Nox2 in T-cells may modulate upregulation of chemokines or adhesion molecules that are essential to T-cell recruitment to non-lymphoid tissues, such as the heart.

This hypothesis (*Figure 7-1*) is supported by the known implication of Nox2 in the HGF-c-Met signalling pathways within other cell types[277,278]. For instance Schroder et al showed that within endothelial progenitor cells (EPCs), HGF-induced mobilization of EPCs and the proangiogenic effects of HGF require Nox2, as in its absence these processes were inhibited[277]. The same research group also pinpointed Nox2-derived ROS signalling to the activation of JAK2 and JNK, which in turn activates the signal transducer and activator of transcription 3 (STAT3) transcription factors[277]. STAT3 has also been identified as a key component of HGF-induced chemokinesis within T-cells[183]. Therefore a similar process may occur in T-cell HGF priming, whereby the lack of Nox2 prevents STAT3 activation of cardiac-specific chemokine receptors.

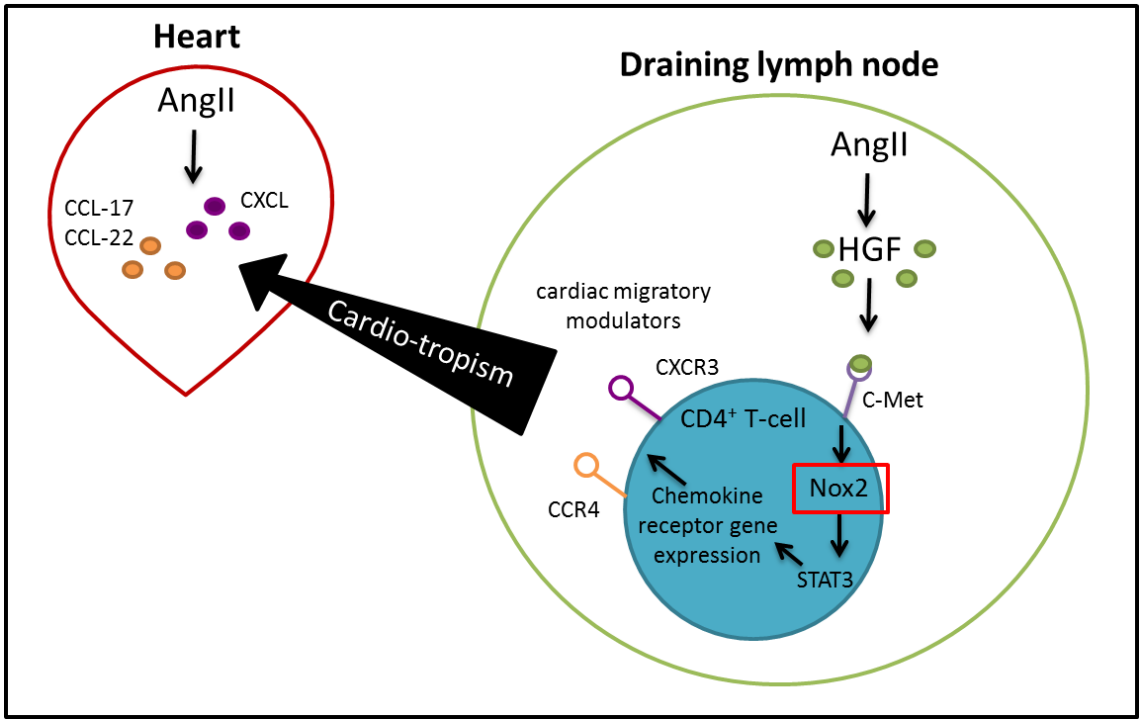

Figure 7-1: Proposed mechanism of AngII induced cardiac T-cell infiltration mediated by HGF.

A lower level of ROS within the local-environment has been found to influence the redox status of lymphocyte cell surface molecules, by an increased reduction of thiol groups (cysteine-SH)[279,280]. This in turn has been linked to a more reactive and proliferative cell type[279,280]. Further investigation by Gelderman et al identified that the endogenous capacity of T-cells to produce ROS, is also linked to an increased level of reduced thiol groups on the T-cell membrane surface[281]. Thereby, in the Nox2KO models, the lack of endogenous Nox2 in $CD4^+$ T-cells could cause an increased level of reduced thiols upon T-cell surface proteins, enhancing or reducing their function. This may then increase proliferation and function of all subsets of $CD4^+$ T-cells and hence may explain an increased basal level of $CD4^+$ T-cells observed in the Nox2KO hearts.

Further to this, downstream signalling from both TCR activation and AngII has the ability to activate Nox2 and subsequent ROS production[212]. In T-cells, Nox2-derived ROS could signal to activate certain transcription factors, such as NF-κB and STAT3. NF-κB activation is involved in chemotaxis of a variety of immune cells, potentially including T-cells. In macrophages, NF-κB is known to upregulate chemokines, such as MCP-1 and CCR2, which are vital in macrophage recruitment[2]. Moreover, the lack of

Nox2 prevents NF-κB mediated upregulation of these chemokines, inhibiting macrophage recruitment[201]. Hence a similar control mechanism may exist in T-cells. Similarly STAT3, as described above, may trigger transcription of chemokine receptors such as CCR4 and CXCR3, involved in T-cell migration during an inflammatory setting[282]. Hence, Nox2-derived ROS signalling downstream from AT_2R and TCR may regulate NF-κB-driven synthesis of cardiac-specific chemokine receptors. Therefore in the absence of Nox2, the lack of ROS may reduce the activation of NF-κB and impede chemokine upregulation. Furthermore NF-κB can activate synthesis of AngII within T-cells, which in turn would amplify the response. Lack of Nox2 would prevent this activation and further amplification, hence dampening down the AngII-response to a greater extent.

Overall, the lack of Nox2 in $CD4^+$ T-cells may inhibit signalling pathways required for the upregulation of molecules essential to their recruitment during AngII-induced cardiac stress. Consequently, the altered recruitment of $CD4^+$ T-cells observed here in the global and CD4-specific Nox2KO models, when treated with AngII, may provide the basis for their lack of response to the molecule. Published papers have identified the detrimental role of $CD4^+$ T-cells during the progression of cardiovascular remodelling[184]. Further to data already presented from Laroumanie et al, Koller et al also showed a similar link between $CD4^+$ T-cells and heart failure in a clinical setting[283]. A subset of circulating $CD4^+$ T-cells, $CD4^+CD28^{null}$, were associated with severity of chronic heart failure (CHF) in patients and may provide an indicator for mortality[283]. This subset of $CD4^+$ T-cells lacks the co-stimulatory CD28 molecule, and therefore is associated with repeated antigenic stimulation that may lead to CHF[283]. Further studies investigating this particular $CD4^+$ T-cell subset have also linked their adverse responses to autoimmune disease and coronary artery disease[284,285]. No reference has yet been made to this $CD4^+CD28^{null}$ subset in relation to the AngII-response; however this may comprise a detrimental component in the related cardiovascular remodelling process. Moreover, if the lack of Nox2 prevents infiltration of these cells into the heart, this may, in part, support the advantageous phenotype observed in the Nox2KO models. It is also possible that in the periphery these cells may accumulate in certain tissues and lead to autoimmune diseases such as arthritis, to which Nox2KO mice are susceptible[199]. Whereas, in the heart these cells are unable to accumulate or cause

damage in response to AngII, hence there is a local cardiac-specific protective mechanism in both the global Nox2KO and CD4-Nox2KO mice.

When studying $CD4^+$ T-cell effects one must take into account the various $CD4^+$ T-cell subtypes, which present different roles depending on the type of immune response required. A specific T-cell subset, Th17, has been implicated in AngII-induced cardiac inflammation. During AngII treatment, the level of a Th17-specific cytokine, IL-17, was found to significantly increase both *in vivo* within aorta and from T-cells isolated from treated mice and stimulated *ex vivo*[185]. Moreover, mice deficient in IL-17 displayed unstable hypertension, preserved vascular function and reduced vascular T-cell infiltration in response to AngII[185]. Therefore the Th17 subset of $CD4^+$ T-cells appears to be critical for the maintenance of AngII-induced hypertension in addition to subsequent cardiovascular remodelling. Furthermore, Nox2 has been implicated in Th differentiation pathways promoting Th2 responses, therefore in Nox2KO models the Th1 and Th17 responses may be enhanced.

In contrast, a few papers suggest a beneficial role of $CD4^+$ T-cells during cardiovascular remodelling, however these usually link to regulatory functions. For instance, a population of $CD4^+AT_2R^+$ T-cells identified by Skorska et al were found to be favourable during post-infarct remodelling[286]. This group also identified the ability of this $CD4^+$ subset to express FoxP3 and secrete IL-10, thereby taking on a regulatory function within this context[286]. The $CD4^+$ T-cell population includes subtypes that can orchestrate a variety of immune responses. Therefore, it is important to take this into account when trying to decipher the function of Nox2 within this population, as it may differ between subtypes.

The difficulty that arises with the model presented in this thesis is the lack of Nox2 within both Teff cells, such as Th17, and Tregs, which have opposing roles. The cardiac-inflammatory response to AngII treatment observed in the WT animals was accompanied by a transitory infiltration of Tregs, however the Treg:T-cell ratio remained consistent before and after treatment. Therefore this transitory Treg infiltration in the WT mice was insufficient to prevent further cardiac-inflammation and subsequent damage. In contrast, global Nox2KO and CD4-Nox2KO mice at baseline possess a higher cardiac-specific Treg:T-cell ratio. Tregs have the ability to suppress the immune response; hence they play an opposing role to other T-cell subsets. Therefore

one can postulate that it is this Treg:T-cell component that protects both global and CD4-sepcific Nox2 deficient mice from AngII-induced cardiac inflammation and subsequent remodelling. Data regarding the adoptive transfer of Tregs into WT mice treated with AngII, also shows that increasing the Treg:T-cell ratio in this manner can provide protection against cardiovascular remodelling. This has also been explored by a handful of studies, described previously, which demonstrates that an increase in basal Treg levels is beneficial during cardiovascular remodelling[190-192].

Results presented in this thesis also identified an increased suppressive function by Nox2KO-Tregs both *in vitro* and *in vivo*. This may involve a redox mechanism described by Yan et al, whereby DCs have the ability to increase extracellular cysteine levels that in turn provide a reduced environment for T-cell proliferation[287]. Tregs were shown to significantly lower extracellular cysteine levels, mediated by direct CTLA-4 interaction with DCs[288]. A fascinating concept is that the lack of Nox2 within Tregs may enhance this mechanism. Nox2 deficiency in T-cells has been linked to enhanced function, which may still be true in the Treg subset[279,280]. In addition, Tregs may also reduce cysteine levels by competitive uptake, which could in turn further enhance their function[288]. Data presented here support these ideas as a higher expression of CTLA-4, CD39 and CD73 was observed in the Nox2KO Tregs, thereby the lack of Nox2 may increase expression of these molecules and enhance their function. CTLA-4 expression upon Treg membranes enables interaction with APCs such as DCs, which express CD80/CD86, thereby preventing further inflammatory responses[229]. CD39 and CD73 degrade ATP, ADP and AMP to adenosine creating an adenosine-rich anti-inflammatory environment[176]. However, CD39 and CD73 can also regulate the function of APCs and encourage an anti-inflammatory phenotype[176]. Another possibility is that Nox2-derived ROS may signal within Tregs and regulate cytokine release, such as IL-10 or TGFβ. However, these indirect-mechanisms may not be involved here as previous papers identified a lower suppressive capacity of Nox2KO-Tregs, when analysed in the presence of anti-CD3/CD28 beads[214]. Tregs elicit a regulatory response by either secreting anti-inflammatory cytokines, directly interacting with Teff cells or by interacting with APCs to indirectly suppress Teff cells. The use of CD3/CD28 beads allows analysis of the first two suppressive mechanisms but not by interactions with APCs, suggesting that the enhanced suppressive capacity observed here is due to direct Treg interactions with APCs.

Numerous inflammatory diseases have been associated with an impaired Treg:Th17 ratio in a diverse range of tissues. These include human graft-versus-host disease in transplant patients[289], chronic hepatitis B driven liver disease progression[290], acute respiratory distress syndrome[291], chronic obstructive pulmonary disease[292] and rheumatoid arthritis[293]. Interestingly, an imbalance in the Treg:Th17 ratio has also been associated with cardiovascular pathophysiologies[294-296]. Chen et al observed a significant increase in Th17 cells, and a lower Treg:Th17 ratio, in uremic patients with cardiovascular complications compared to uremic patients without cardiovascular complications, both undergoing hemodialysis[294]. A similar imbalance was also identified in patients with acute coronary syndrome, with an increase in Th17 cells and its related cytokines (IL-17, IL-6 and IL-23)[295]. Furthermore, analysis of peripheral Th17 and Tregs from patients with chronic heart failure revealed a significant increase in the Th17 response and a blatant reduction in Tregs[296]. Thereby in the setting of chronic heart failure the peripheral Treg/Th17 balance is impaired[296].

These studies identify the importance of peripheral Treg:Th17 balance within a cardiovascular-related disease setting; however the specific cardiac-resident ratio has not yet been investigated. This Treg:Th17 balance controls inflammation and may therefore be crucial to the pathogenesis of AngII-induced cardiac remodelling. Furthermore, this may explain the protective response observed in the global Nox2KO and CD4-Nox2KO mice.

Due to these reports, an interesting concept to consider is the plasticity between $CD4^+$ T-cell subsets, specifically between Th17 cells and Tregs[62-64,70,254]. This plasticity is determined by the promiscuity of cytokine expression, phenotype and even the expression of master regulators between different subtypes[63]. There are a number of factors that link Tregs and Th17 cells. Firstly, both cell types require TGFβ for their differentiation and mice deficient in this cytokine lack both Tregs and Th17 cells[63,255]. Treatment of naïve $CD4^+$ T-cells with TGFβ *in vitro* can cause differentiation of both Tregs and Th17 cells in a concentration-dependent manner, leading to upregulation of either RORγt (at low concentrations) or FoxP3 (at high concentrations)[68]. Furthermore, $FoxP3^+RORγt^+$ cells, which express both master regulators indicative of Treg and Th17 lineages, have been identified in both mice and humans[64,68]. These transcription factors can interact with each other to alter T-cell phenotype and cytokine

production[63]. For instance a study from Voo et al demonstrated that these FoxP3$^+$RORγt$^+$ cells could produce IL-17 but still maintain a suppressive function[297]. Hence, these cells may reside as a transitory population that can give rise to either Treg or Th17 cells, and additional cytokines may determine the outcome[63,68,297].

In addition to this, Tregs can lose their FoxP3 expression and acquire the capacity to produce pro-inflammatory cytokines, such as IL-17. This could stipulate the trans-differentiation from Tregs to Th17 cells. For example a study by Komatsu et al, in the context of autoimmune arthritis, observed the conversion of Tregs into Th17 cells driven by synovial fibroblast-derived IL-6[298]. This involved the loss of Foxp3 expression and acquired capacity of Tregs to produce IL17. On the contrary, more recent literature has described the trans-differentiation of Th17 cells into Tregs. Gagliani et al carried out a series of *in vivo* and *ex vivo* experiments, using a sophisticated reporter mouse to study Th17 conversion[257]. This group discovered that Th17 cells could acquire an anti-inflammatory phenotype, expressing both IL-10 and FoxP3. Further *in vitro* experiments attributed this conversion to TGFβ signalling, which occurred in a dose-dependent manner. The downstream activation of Smad3 enables the reduction of RORγt activity, which in turn deters the Th17 phenotype[257]. A similar mechanism was also described in the setting of mesenchymal stem cell (MSC)-mediated allograft survival, where Tregs were derived from Th17 cells[256]. This group also indicated that the RA receptor gamma (RARγ) might play a role in Th17-Treg conversion in this setting. Further studies identify a role for RA in promoting Treg differentiation and expansion in addition to having the ability to prevent transition of T-cell into Th17 lineage[299,300].

An increased Treg:T-cell ratio was observed within both of the Nox2KO models, that demonstrate a better response to AngII, may suggest a role for Nox2 in the Treg/Th17 balance (*Figure 7-2*). There are two approaches that may explain how Nox2 could be involved here. Nox2-derived ROS signalling could either be involved in promoting the Th17 differentiation pathway or, ROS could signal to prevent the Treg differentiation. Ergo, in the Nox2KO models, the lack of CD4$^+$ T-cell Nox2 would promote an enhanced Treg:T-cell ratio. Furthermore, this could be specific to the heart due to a unique molecular component in the microenvironment, which is absent in peripheral lymphoid organs. For instance TGFβ or RA could be involved in this setting, as they are

both implicated in cardiac and Treg processes. ROS signalling mechanisms involved here could include the activation or inhibition of downstream signalling molecules or transcription factors, as described in the introduction. For instance, Nox2-derived ROS has been shown to activate the JAK2-STAT3 signalling cascade[301]. In turn, STAT3 is an important modulator of RORγt expression and may modulate Th17/Treg balance[302]. Furthermore, increased levels of STAT3 prevents STAT5 binding to FoxP3 promoter, hence reduce Treg levels[302]. Likewise, Nox2-derived ROS regulation of cell-surface receptors for cytokines that drive Th17-Treg trans-differentiation is also conceivable. This redox regulation of cell-surface molecules, as discussed earlier, suggests an increased function with the lack of Nox2 due to reduced cell surface thiols. Hence Nox2 may negatively regulate TGFβ receptors or RARs, which are involved in promoting Treg differentiation. Overall, the extent of plasticity between Tregs and Th17 cells is becoming more apparent and resultant effects may be context dependent, due to specific-tissue microenvironments. This could in part explain the differences observed between the Nox2KO models and WT littermates; however this would require further analysis of the Th17 population in this setting.

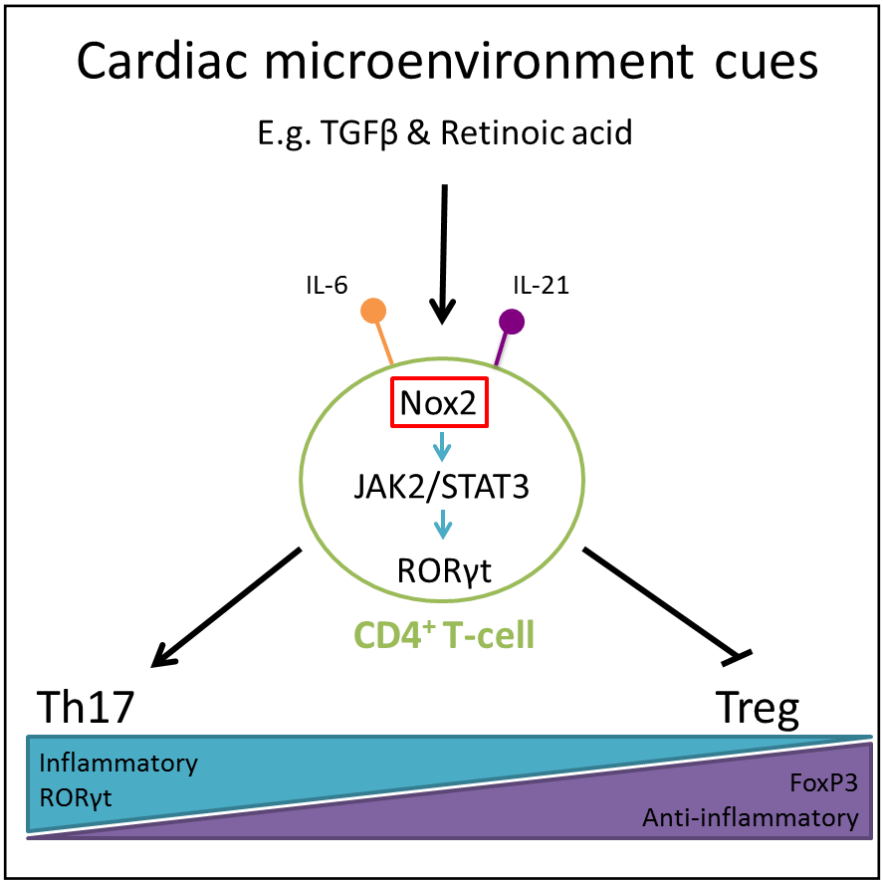

Figure 7-2: Proposed involvement of Nox2 in CD4$^+$ T-cell signalling. *Nox2-derived ROS activation of JAK2/STAT3 signalling pathway encourages RORγt expression and Th17 differentiation in turn preventing Treg development.*

Furthermore, TGFβ involved in Treg differentiation and suppression within the heart is also a pro-fibrotic modulator, which is related to AngII-induced fibrosis. In the Nox2KO models, a higher level of cardiac-resident Tregs was observed, hence when treated with AngII, extracellular TGFβ produced may be quenched by Nox2KO-Tregs and the resultant fibrotic response inhibited. Supporting this, the adoptive transfer of Nox2KO-Tregs, but not WT-Tregs, prevented AngII-induced cardiac fibrosis. One may hypothesise that Nox2KO-Tregs use a direct cell-cell mechanism for their enhanced suppression and hence may not secrete TGFβ as an anti-inflammatory cytokine. This could in turn reduce the level of fibrosis within this setting.

Taken together, both the detrimental role of CD4$^+$ Teff cells and the beneficial role of Tregs have been observed, and potentially determine the outcome of the cardiac-inflammatory response to AngII. Nox2 in CD4$^+$ Teff cells may be implicated in migratory mechanisms to the heart and regulate their function. Whereas, Nox2 in Tregs may

regulate redox-sensitive suppression mechanisms and control a location-specific Treg/Th17 balance. Hence, the lack of Nox2 in the global and CD4-specific models prevents $CD4^+$ T-cell infiltration with AngII treatment. In addition, the Nox2 alteration of the cardiac-resident Treg:T-cell ratio empowers Tregs to prevent incoming inflammatory cells and therefore protect the heart from subsequent damage. Data presented in this thesis suggests a double-mechanism allowing cardiac-specific protection in the absence of Nox2. However, difficulty arises in deciphering the relative contributions of both in this setting.

7.3 Clinical implications

In the UK more than a quarter of deaths (155,000 each year) result from CVD and an estimated 7 million people suffer from CVD (British Heart Foundation statistics, 2015). Therefore it is essential to fully understand the mechanisms that underline CVD in order to identify potential therapeutic targets. The inflammatory response observed in CVD can propagate disease development and ultimately lead to heart failure. Nox enzymes also are implicated in a wide variety of cardiovascular remodelling process, and also potentiate disease progression towards heart failure.

Targeting Nox enzymes to improve CVD outcomes has been suggested as a potential therapeutic approach[22,303]. However, this blanket approach does not take into account the specific actions of individual Nox isoforms. For instance, contrasting roles of Nox2 and Nox4 have been identified[304,305]. Pharmacologically, many Nox inhibitors do not allow specificity for a single Nox isoform[306]. The first technological advance towards the development of Nox2-specific inhibitors by Smith et al identified ebselen as a potential inhibitor[307]. By interrupting $p47^{phox}$ binding and interacting with $p22^{phox}$, ebselen prevents Nox2 assembly and subsequent activity. A recent study by Bosco et al have utilised an *in silico* screen to identify Phox-I1, an inhibitor of the interaction between Rac and $p67^{phox}$ [308]. Here, Phox-I1 binds to $p67^{phox}$, preventing Rac1 binding and therefore effectively inhibits Nox2-derived superoxide production in a dose-dependent manner[308]. Further Nox2-specific inhibitors are coming to light, such as bridged tetrahydroisoquinolines, which may serve as a platform for developing new therapeutic agents against Nox2[309].

Furthermore, Nox2 function can differ depending on its role in specific cell types, therefore in some cells Nox2 may be beneficial to CVD, whereas in other cells its role may propagate disease progression. Data in this thesis demonstrate that T-cell specific Nox2 is a major mediator of the inflammatory component observed prior to cardiovascular remodelling. In addition, eliminating Nox2 within $CD4^+$ T-cells is beneficial for disease outcome in mice. In light of this, a more specific therapeutic approach is necessary to target the main factors orchestrating a detrimental phenotype observed in CVD. This could include a direct cardiovascular target of $CD4^+$ T-cells. One method may involve delivering Nox2-specific therapeutic agents directly to cardiac tissue or to specific cell types, such as $CD4^+$ T-cells. This could involve using delivery materials such as lipid nanoparticles with targeting-ligands, enabling direct delivery of therapeutic agents[310]. Another technique may involve identifying downstream targets that are specific to Nox2 function within $CD4^+$ T-cells, or Tregs, a specific inhibitor could be generated. For instance, the proposed mechanism suggests JAK2/STAT3 pathway as an important modulator of Treg:Th17 balance downstream from Nox2. Therefore a specific JAK2 inhibitor, such as TG101348, or even siRNA mediated depletion of STAT3, could be delivered to cardiac $CD4^+$ T-cells to skew the Treg:Th17 towards an anti-inflammatory response[302].

Results presented in this thesis also highlight a beneficial role for Tregs within the setting of cardiovascular remodelling, specifically Nox2KO-Tregs. Additionally, published papers have suggested that the Treg/Th17 balance may dictate a patient's cardiovascular-outcome. Therefore a potential therapeutic approach may be Treg-therapy to provide CVD patients with an enhanced anti-inflammatory component promoting resolution of cardiovascular tissue homeostasis. Clinical trials are already in place using Treg therapy to aid allograft survival in transplant patients. For example a clinical trial called 'The ONE study' that Guy's and St Thomas' hospitals are part of, uses Tregs to aid kidney graft survival in end-stage renal failure patients[311-315]. Naturally occurring Tregs are isolated and purified from living-donor transplant recipients, amplified by sterile cell culture methods and re-infused into the transplant patient five days post-transplantation. A similar therapeutic method could be employed to enhance a patient's outcome to CVD. Isolated Tregs could also be depleted of Nox2 or important downstream signalling targets using siRNA[310], or other

silencing mechanisms, and these treated Tregs can be injected back into the patient to provide an enhanced cardiac-specific protective mechanism.

Further therapeutic approaches could involve exploiting the plasticity of Th17 cells to enhance a Treg:T-cell ratio within CVD patients. Therefore a more in depth understanding of the role Nox2 plays within this setting could provide a means to promote Treg differentiation and function specifically within cardiovascular tissues.

Therapeutic approaches to target cardiac fibrosis would also be beneficial to prevent subsequent cardiac arrhythmias and cardiac dysfunction. Currently there are no specific treatments for fibrosis; however ACE inhibitors, which prevent the conversion of AngI to AngII, may also have a beneficial effect on collagen deposition[316]. In addition, dual treatment with ARBs and ACE inhibitors could be an advantageous approach to fibrosis treatment[84,317]. However, the effects of these inhibitors are very general and more specific fibrosis-targeting therapeutics are required. Therefore results within this thesis may be relevant for identifying new therapeutic targets to prevent progression of fibrosis due to the close interaction between fibrosis and inflammation.

Findings within this thesis highlight a number of interesting therapeutic ideas; however one caveat is the difference between mice and humans, which must be taken into account when translating these data into potential clinical therapies.

7.4 Study limitations and future work

In this study a cardiac-infiltration of T-cells during AngII treatment was observed; however the mechanism that underlies T-cell migration to the heart and within the myocardium in this setting requires further clarification. To fully investigate this, a more detailed approach is required by analysing more time points during AngII treatment, to fully appreciate the individual stages in immune cell recruitment. In addition to this, identifying AngII-dependent upregulation of endothelial markers, such as VCAM-1, would provide insight into how immune cells are encouraged into the myocardium in the first place. Finally, investigations into which vessels are associated with the inflammatory recruitment, arterioles or venules, could help determine how

immune cells infiltrate the tissue. There are limited techniques available to analyse immune cell migration within the heart specifically. In recent years a research group were able to study neutrophil trafficking to the heart using two-photon intravital microscopy[318,319]. Optimisation of this method could allow detection of different immune cells, or even specific T-cell subtypes, using fluorescently labelled dyes to fully elucidate their response to AngII in real-time. Furthermore, one could directly inject AngII and analyse the immediate responses using this technique. This would help to clarify how the lack of Nox2 within these immune cells affects T-cell migration.

Flow cytometry data presented in this thesis are represented as cells per mg of cardiac tissue, or for lymphoid organs, as a percentage of total cells acquired. Another method for analysis would be to use counting beads (e.g. Invitrogen™Countbright™), which enables an accurate calculation of cell concentration. Counting beads are a calibrated suspension of fluorescent microspheres with a known concentration. Therefore a specific volume of counting beads can be added to a specific volume of sample so that a ratio of sample volume to microsphere volume is known. From this the volume of sample analysed can be calculated based on the number of microsphere events acquired. This would enable data to be accurately represented as cells per ml of sample. It could be interesting in another set of experiments to implement this method to further refine this quantification.

The lack of Nox2 in the CD4-Nox2KO line could be further verified by stimulating isolated $CD4^+$ T-cells with phorbol 12-myristate 13-acetate (PMA) to prompt ROS production. ROS can then be detected using dihydroethidium (DHE) by flow cytometry. This would be a good way of demonstrating lower ROS levels in the Nox2KO-$CD4^+$ T-cells. In addition to this, further confirmation could be achieved by western blot for Nox2 protein expression within a variety of tissues in addition to isolated $CD4^+$ T-cells. This would verify that Nox2 in other tissues is unaffected and demonstrate specificity for $CD4^+$ T-cells.

Further *in vitro* studies to analyse the role of Nox2 in naïve $CD4^+$ T-cell differentiation would also help to unravel the role that Nox2 plays in directing T-cell responses. Additionally, an important concept to study further is the mechanism that underlines the role of endogenous Nox2 in $CD4^+$ T-cells.

Herein, WT- and Nox2KO- Tregs isolated from LNs and spleens were characterised, which may portray a different phenotype to cardiac-resident T-cells. Currently, as baseline levels of $CD4^+$ T-cell subtypes, especially Tregs, are so low it is impossible to accurately analyse these cells. Accumulating data is identifying distinct phenotypes and roles for Tregs within non-lymphoid tissues. Therefore, as more sensitive methods for studying T-cells within the heart emerges, phenotyping cardiac-resident $CD4^+$ T-cell subsets fully would provide further understanding of their role, and the role of endogenous Nox2, within this setting.

In the adoptive transfer experiments, an increased Treg:T-cell ratio was identified, however flow cytometry was not sensitive enough to ascertain a change in cardiac Treg numbers. Further analysis here could involve an adoptive transfer using fluorescently labelled WT- or Nox2KO-Tregs, either from YFP animals or by staining isolated cells with CFSE. This would eliminate steps in the isolation protocol so that more cells survive for flow cytometry analysis. Additionally, cells would be easily identified in a range of tissues using fluorescence microscopy. Hence, organs that enable regulation of blood pressure could also be analysed, such as the kidney, aorta and brain. Alternatively, the intravital two-photon microscopy may also be useful for identifying Treg migration within this experiment. Pre-clinical *in vivo* imaging systems (IVIS) could also be used to identify Treg migration using a technology such as IVIS® Lumina (Perkin Elmer) using fluorescence markers. Furthermore, if operated in a clinical setting, MRI can be used as a non-invasive method to detect delivery and function of Tregs using a tracer molecule[320].

To further add to the understanding of Tregs within AngII-induced cardiac remodelling, a Treg depletion experiment could be undertaken using an anti-CD25 antibody (PC61) within both WT and the two Nox2KO models. The effect of this on blood pressure and cardiac remodelling in response to AngII could then be analysed to discern the impact of Tregs in this setting. Additionally, adoptive transfer of WT- or Nox2KO- $CD4^+$ Teff cells in similar settings could be beneficial to show their impact here.

The data showed, both *in vitro* and *in vivo*, that Nox2KO-Tregs display an increased suppressive phenotype. In addition to the suppression assays presented in this thesis, using thymidine uptake as a read out, a carboxyfluorescein succinimidyl ester (CFSE) suppression assay was also performed. This involves fluorescently labelling $CD4^+$ Teff

cells with CFSE, and co-culturing them with APCs, anti-CD3 antibody and either WT- or Nox2KO-Tregs for 3-days. The numbers of Teff cells can then be analysed by flow cytometry to indicate the level of proliferation. Data from this assay also suggest that Nox2KO-Tregs have a greater suppressive function; however this method needs further optimisation. Therefore repeating this protocol, which is more accurate, would be beneficial to confirm the thymidine suppression assay findings presented in this thesis. Furthermore, published papers have suggested opposing results when co-culturing Nox2KO-Tregs with Teff cells in the presence of anti-CD3/CD28 beads instead of isolated APC. This method allows analysis of Treg suppression by direct interaction with Teff cells or secretion of anti-inflammatory cytokines but not the indirect suppression via APC. Therefore, repeating these experiments using these conditions and evaluating the level of cytokines within the supernatant using an enzyme-linked immunosorbent assay (ELISA) may decipher the mechanisms used by Nox2KO-Tregs to suppress Teff cells. Further analysis of supernatants from these co-cultures could also determine whether secretion of anti-inflammatory cytokines differs between WT- and Nox2KO-Tregs.

Within this thesis, experiments concentrated on $CD4^+$ T-cells; however this population of cells encompasses a variety of subtypes. Further experiments would be required to understand the role of Nox2 specifically within these different subtypes, such as Th17 and Tregs. This could involve the generation of further specific-Nox2KO models such as Th17- or Treg-Nox2KOs. Initially, I planned to generate a Treg-specific Nox2KO model by crossing a FoxP3-Cre line with the novel Nox2 floxed line. However, both FoxP3 and Nox2 are X-linked therefore the generation of a FoxP3-Nox2KO mouse was near impossible. However, CD25 (IL2-R) is located on chromosome 15 and hence may be a better promoter to use for Nox2 deletion in Tregs[321,322]. Revisiting this idea and potentially generating a CD25-Nox2KO model may be beneficial for further understanding the depth of Treg involvement within the AngII-model.

Finally, limitations in the studies also arise when translating these findings to a clinical setting due to the use of mouse models. Differences in species, such as additional Nox enzymes within humans, the young age of mice studied, potential differences in immune and inflammatory responses between mice and humans, must be taken into account.

7.5 Conclusions

In conclusion, the work presented in this thesis demonstrates a clear role of endogenous Nox2 in $CD4^+$ T-cells within the setting of AngII-induced cardiovascular remodelling. Herein, the T-cell subtypes that are critical during the development of AngII-induced inflammation and cardiovascular remodelling have been deciphered. I have demonstrated two components in Nox2KO models that enable cardiac-specific protection: preventing migration of $CD4^+$ T-cells and a protective Treg response. The cardiac-infiltration of $CD4^+$ T-cells drives cardiovascular remodelling and Nox2 within these cells is an important orchestrator of the resultant pathophysiological responses. Although the detrimental effect of $CD4^+$ T-cells observed here plays the main role in disease progression, it is the Tregs that maintain the power to resolve cardiac-inflammation and tissue homeostasis. Moreover, I observed the intrinsic regulatory effect of Nox2-derived ROS within Tregs, controlling their suppressive function. Therefore by further understanding the Treg:Th17 balance, and the function of endogenous Nox2 within this setting, a potential therapeutic strategy could be developed.

Taken together, the results presented in this thesis provide further clarity to the role of T-cell Nox2 within AngII-induced hypertension and cardiovascular remodelling.

Chapter 8: References and Appendix

8.1 References

1. Devasagayam TP, Tilak JC, Boloor KK, Sane KS, Ghaskadbi SS, Lele RD. Free radicals and antioxidants in human health: current status and future prospects. The Journal of the Association of Physicians of India 2004; 52: 794-804.

2. Giordano FJ. Oxygen, oxidative stress, hypoxia, and heart failure. The Journal of Clinical Investigation 2005; 115(3): 500-8.

3. Al Ghouleh I, Khoo NK, Knaus UG, Griendling KK, Touyz RM, Thannickal VJ, Barchowsky A, Nauseef WM, Kelley MT, Bauer PM, Darley-Usmar V, Shiva S, Cifuentes-Pagano E, Freeman BA, Gladwin MT, Pagano PJ. Oxidases and peroxidases in cardiovascular and lung disease: new concepts in reactive oxygen species signaling. Free Radicical Biology and Medicine 2011; 51(7): 1271-88.

4. Burgoyne JR, Mongue-Din H, Eaton P, Shah AM. Redox Signaling in Cardiac Physiology and Pathology. Circulation research 2012; 111(8): 1091-106.

5. Jastroch M, Divakaruni AS, Mookerjee S, Treberg JR, Brand MD. Mitochondrial proton and electron leaks. Essays in Biochemistry 2010; 47: 53-67.

6. Zangar RC, Davydov DR, Verma S. Mechanisms that regulate production of reactive oxygen species by cytochrome P450. Toxicology and Applied Pharmacology 2004; 199(3): 316-31.

7. Roe ND, Ren J. Nitric oxide synthase uncoupling: a therapeutic target in cardiovascular diseases. Vascular Pharmacology 2012; 57(5-6): 168-72.

8. Dawson J, Walters M. Uric acid and xanthine oxidase: future therapeutic targets in the prevention of cardiovascular disease? British Journal of Clinical Pharmacology 2006; 62(6): 633-44.

9. Griendling KK, Sorescu D, Ushio-Fukai M. NAD(P)H oxidase: role in cardiovascular biology and disease. Circulation research 2000; 86(5): 494-501.

10. Kirkman HN, Gaetani GF. Catalase: a tetrameric enzyme with four tightly bound molecules of NADPH. Proceedings of the National Academy of Sciences USA 1984; 81(14): 4343-7.

11. Nordberg J, Arner ES. Reactive oxygen species, antioxidants, and the mammalian thioredoxin system. Free Radical Biololgy and Medicine 2001; 31(11): 1287-312.

12. Finkel T. Signal transduction by reactive oxygen species. The Journal of Cell Biology 2011; 194(1): 7-15.

13. Heo JS, Lee JC. Beta-catenin mediates cyclic strain-stimulated cardiomyogenesis in mouse embryonic stem cells through ROS-dependent and integrin-mediated PI3K/Akt pathways. The Journal of Cellular Biochemistry 2011; 112(7): 1880-9.

14. Sanchez G, Pedrozo Z, Domenech RJ, Hidalgo C, Donoso P. Tachycardia increases NADPH oxidase activity and RyR2 S-glutathionylation in ventricular muscle. The Journal of Molecular and Cellular Cardiology 2005; 39(6): 982-91.

15. Prysyazhna O, Rudyk O, Eaton P. Single atom substitution in mouse protein kinase G eliminates oxidant sensing to cause hypertension. Nature Medicine 2012; 18(2): 286-90.

16. Gul R, Shawl AI, Kim SH, Kim UH. Cooperative interaction between reactive oxygen species and Ca2+ signals contributes to angiotensin II-induced hypertrophy in adult rat cardiomyocytes. American Journal of Physiology: Heart and Circulation Physiology 2012; 302(4): H901-9.

17. Chen W, Frangogiannis NG. The role of inflammatory and fibrogenic pathways in heart failure associated with aging. Heart Failure Review 2010; 15(5): 415-22.

18. Kuster GM, Pimentel DR, Adachi T, et al. Alpha-adrenergic receptor-stimulated hypertrophy in adult rat ventricular myocytes is mediated via thioredoxin-1-sensitive oxidative modification of thiols on Ras. Circulation 2005; 111(9): 1192-8.

19. Higuchi Y, Otsu K, Nishida K, et al. The small GTP-binding protein Rac1 induces cardiac myocyte hypertrophy through the activation of apoptosis signal-regulating kinase 1 and nuclear factor-kappa B.The Journal of Biological Chemistry 2003; 278(23): 20770-7.

20. Barcellos-Hoff MH, Dix TA. Redox-mediated activation of latent transforming growth factor-beta 1. Molecular Endocrinology 1996; 10(9): 1077-83.

21. Park SK, Kim J, Seomun Y, Choi J, Kin DH, Han IO, Lee EH, Chung SK, Joo CK. Hydrogen peroxide is a novel inducer of connective tissue growth factor. Biochemical and Biophysical Research Communications 2001; 284(4): 966-71.

22. Altenhofer S, Kleikers PW, Radermacher KA, Scheurer P, Rob Hermans JJ, Schriffers P, Ho H, Wingler K, Schmidt HH. The NOX toolbox: validating the role of NADPH oxidases in physiology and disease. Cellular and Molecular Life Sciences 2012; 69(14): 2327-43.

23. El-Benna J, Dang PM, Gougerot-Pocidalo MA, Elbim C. Phagocyte NADPH oxidase: a multicomponent enzyme essential for host defenses. Archivum Immunologiae et Therapiae Experimentalis 2005; 53(3): 199-206.

24. Cui XL, Brockman D, Campos B, Myatt L. Expression of NADPH oxidase isoform 1 (Nox1) in human placenta: involvement in preeclampsia. Placenta 2006; 27(4-5): 422-31.

25. Hilenski LL, Clempus RE, Quinn MT, Lambeth JD, Griendling KK. Distinct subcellular localizations of Nox1 and Nox4 in vascular smooth muscle cells. Arteriosclerosis, Thrombosis and Vascular Biology 2004; 24(4): 677-83.

26. Suh YA, Arnold RS, Lassegue B, et al. Cell transformation by the superoxide-generating oxidase Mox1. Nature 1999; 401(6748): 79-82.

27. Szanto I, Rubbia-Brandt L, Kiss P, et al. Expression of NOX1, a superoxide-generating NADPH oxidase, in colon cancer and inflammatory bowel disease. The Journal of Pathology 2005; 207(2): 164-76.

28. Quinn MT, Ammons MC, Deleo FR. The expanding role of NADPH oxidases in health and disease: no longer just agents of death and destruction. Clinical Science 2006; 111(1): 1-20.

29. Bedard K, Krause KH. The NOX family of ROS-generating NADPH oxidases: physiology and pathophysiology. Physiological Reviews 2007; 87(1): 245-313.

30. Jones SA, O'Donnell VB, Wood JD, Broughton JP, Hughes EJ, Jones OT. Expression of phagocyte NADPH oxidase components in human endothelial cells. American Journal of Physiology 1996; 271(4 Pt 2): H1626-34.

31. Gorlach A, Brandes RP, Nguyen K, Amidi M, Dehghani F, Busse R. A gp91phox containing NADPH oxidase selectively expressed in endothelial cells is a major source of oxygen radical generation in the arterial wall. Circulation research 2000; 87(1): 26-32.

32. Banfi B, Malgrange B, Knisz J, Steger K, Dubois-Dauphin M, Krause KH. NOX3, a superoxide-generating NADPH oxidase of the inner ear. The Journal of Biological Chemistry 2004; 279(44): 46065-72.

33. Geiszt M, Kopp JB, Varnai P, Leto TL. Identification of renox, an NAD(P)H oxidase in kidney. Proceedings of the National Academy of Sciences USA 2000; 97(14): 8010-4.

34. Petry A, Djordjevic T, Weitnauer M, Kietzmann T, Hess J, Gorlach A. NOX2 and NOX4 mediate proliferative response in endothelial cells. Antioxidants and Redox Signaling 2006; 8(9-10): 1473-84.

35. Yang S, Madyastha P, Bingel S, Ries W, Key L. A new superoxide-generating oxidase in murine osteoclasts. The Journal of Biological Chemistry 2001; 276(8): 5452-8.

36. Cucoranu I, Clempus R, Dikalova A, Phelan PJ, Ariyan S, Dikalov S, Sorescu D. NAD(P)H oxidase 4 mediates transforming growth factor-beta1-induced differentiation of cardiac fibroblasts into myofibroblasts. Circulation research 2005; 97(9): 900-7.

37. Cheng G, Cao Z, Xu X, van Meir EG, Lambeth JD. Homologs of gp91phox: cloning and tissue expression of Nox3, Nox4, and Nox5. Gene 2001; 269(1-2): 131-40.

38. Banfi B, Molnar G, Maturana A, Steger K, Hededus B, Demaurex N, Krause KH. A Ca(2+)-activated NADPH oxidase in testis, spleen, and lymph nodes. The Journal of Biological Chemistry 2001; 276(40): 37594-601.

39. De Deken X, Wang D, Many MC, Costagliola S, Libert F, Vassart G, Dumont JE, Miot F. Cloning of two human thyroid cDNAs encoding new members of the NADPH oxidase family. The Journal of Biological Chemistry 2000; 275(30): 23227-33.

40. Sumimoto H, Ueno N, Yamasaki T, Taura M, Takeya R. Molecular mechanism underlying activation of superoxide-producing NADPH oxidases: roles for their regulatory proteins. Japanese Journal of Infectious Diseases 2004; 57(5): S24-5.

41. Ago T, Kuribayashi F, Hiroaki H, Takeya R, Ito T, Kohda D, Sumimoto H. Phosphorylation of p47phox directs phox homology domain from SH3 domain toward phosphoinositides, leading to phagocyte NADPH oxidase activation. Proceedings of the National Academy of Sciences USA 2003; 100(8): 4474-9.

42. Nabeebaccus A, Zhang M, Shah AM. NADPH oxidases and cardiac remodelling. Heart Failure Review 2011; 16(1): 5-12.

43. Ackermann M, Liebhaber S, Klusmann JH, Lachmann N. Lost in translation: pluripotent stem cell-derived hematopoiesis. The European Molecular Biology Organisation: Molecular Medicine 2015.

44. Vivier E, Raulet DH, Moretta A, Caligiuri MA, Zitvogel L, Lanier LL, Yokoyama WM, Ugolini S. Innate or adaptive immunity? The example of natural killer cells. Science 2011; 331(6013): 44-9.

45. Sacks SH, Zhou W. The role of complement in the early immune response to transplantation. Nature Review Immunology 2012; 12(6): 431-42.

46. Segal AW. How neutrophils kill microbes. Annual Review of Immunology 2005; 23: 197-223.

47. Shortman K, Liu YJ. Mouse and human dendritic cell subtypes. Nature Review Immunology 2002; 2(3): 151-61.

48. Murray PJ, Wynn TA. Protective and pathogenic functions of macrophage subsets. Nature Review Immunology 2011; 11(11): 723-37.

49. Kraaij MD, Koekkoek KM, van der Kooij SW, Gelderman KA, van Kooten C. Subsets of human type 2 macrophages show differential capacity to produce reactive oxygen species. Cellular Immunology 2013; 284(1-2): 1-8.

50. Steinman RM. The dendritic cell system and its role in immunogenicity. Annual Review of Immunology 1991; 9: 271-96.

51. Leliefeld PH, Koenderman L, Pillay J. How Neutrophils Shape Adaptive Immune Responses. Frontiers in Immunology 2015; 6: 471.

52. Kalyan S, Kabelitz D. When neutrophils meet T cells: beginnings of a tumultuous relationship with underappreciated potential. European Journal of Immunology 2014; 44(3): 627-33.

53. Scapini P, Cassatella MA. Social networking of human neutrophils within the immune system. Blood 2014; 124(5): 710-9.

54. Melchers F. Checkpoints that control B cell development. Journal of Clinical Investigation 2015; 125(6): 2203-10.

55. LeBien TW, Tedder TF. B lymphocytes: how they develop and function. Blood 2008; 112(5): 1570-80.

56. Berthelot JM, Jamin C, Amrouche K, Le Goff B, Maugars Y, Youinou P. Regulatory B cells play a key role in immune system balance. Joint Bone Spine 2013; 80(1): 18-22.

57. Rosser EC, Mauri C. Regulatory B cells: origin, phenotype, and function. Immunity 2015; 42(4): 607-12.

58. Mauri C, Bosma A. Immune regulatory function of B cells. Annual Review of Immunology 2012; 30: 221-41.

59. Ding T, Yan F, Cao S, Ren X. Regulatory B cell: New member of immunosuppressive cell club. Human Immunology 2015.

60. D'Acquisto F, Crompton T. CD3+CD4-CD8- (double negative) T cells: saviours or villains of the immune response? Biochemical Pharmacology 2011; 82(4): 333-40.

61. Broere F, Apasov SG, Sitkovsky MV, Eden WV. T cell subsets and T cell-mediated immunity. Principles of Immunopharmacology. 3rd edition ed: Springer Basel A. G. ; 2011.

62. O'Shea JJ, Paul WE. Mechanisms underlying lineage commitment and plasticity of helper CD4+ T cells. Science 2010; 327(5969): 1098-102.

63. Zhou L, Chong MM, Littman DR. Plasticity of CD4+ T cell lineage differentiation. Immunity 2009; 30(5): 646-55.

64. Nakayamada S, Takahashi H, Kanno Y, O'Shea JJ. Helper T cell diversity and plasticity. Current Opinion in Immunology 2012; 24(3): 297-302.

65. Wang C, Collins M, Kuchroo VK. Effector T cell differentiation: are master regulators of effector T cells still the masters? Current Opinion in Immunology 2015; 37: 6-10.

66. Li MO, Sanjabi S, Flavell RA. Transforming growth factor-beta controls development, homeostasis, and tolerance of T cells by regulatory T cell-dependent and -independent mechanisms. Immunity 2006; 25(3): 455-71.

67. Veldhoen M, Hocking RJ, Flavell RA, Stockinger B. Signals mediated by transforming growth factor-beta initiate autoimmune encephalomyelitis, but chronic inflammation is needed to sustain disease. Nature Immunology 2006; 7(11): 1151-6.

68. Zhou L, Lopes JE, Chong MM, Ivanov II, Min R, Victoria GD, Shen Y, Du J, Rubtsov YP, Rudensky AY, Ziegler SF, Littman DR. TGF-beta-induced Foxp3 inhibits T(H)17 cell differentiation by antagonizing RORgammat function. Nature 2008; 453(7192): 236-40.

69. Zhou L, Littman DR. Transcriptional regulatory networks in Th17 cell differentiation. Current Opinion in Immunology 2009; 21(2): 146-52.

70. Geginat J, Paroni M, Maglie S, Alfen JS, Kastirr I, Gruarin P, De Simone M, Pagani M, Abrignani S. Plasticity of human CD4 T cell subsets. Frontiers in Immunology 2014; 5: 630.

71. O'Garra A, Vieira P. T(H)1 cells control themselves by producing interleukin-10. Nature Review Immunology 2007; 7(6): 425-8.

72. Carretero OA, Oparil S. Essential hypertension. Part I: definition and etiology. Circulation 2000; 101(3): 329-35.

73. Atlas SA. The renin-angiotensin aldosterone system: pathophysiological role and pharmacologic inhibition. The Journal of Managed Care Pharmacy 2007; 13(8 Suppl B): 9-20.

74. Lanfranchi PA, Somers VK. Arterial baroreflex function and cardiovascular variability: interactions and implications. The American Journal of Physiology: Regulative, Integrative and Comparative Physiology 2002; 283(4): R815-26.

75. Cohn JN, Ferrari R, Sharpe N. Cardiac remodeling--concepts and clinical implications: a consensus paper from an international forum on cardiac remodeling. Behalf of an International Forum on Cardiac Remodeling. Journal of the American College of Cardiology 2000; 35(3): 569-82.

76. Wollert KC, Drexler H. The renin-angiotensin system and experimental heart failure. Cardiovascular research 1999; 43(4): 838-49.

77. Morgan L, Broughton Pipkin F, Kalsheker N. Angiotensinogen: molecular biology, biochemistry and physiology. The International Journal of Biochemistry and Cell Biology 1996; 28(11): 1211-22.

78. Te Riet L, van Esch JH, Roks AJ, van den Meiracker AH, Danser AH. Hypertension: renin-angiotensin-aldosterone system alterations. Circulation research 2015; 116(6): 960-75.

79. Mehta PK, Griendling KK. Angiotensin II cell signaling: physiological and pathological effects in the cardiovascular system. The American journal of physiology: Cell physiology 2007; 292(1): C82-97.

80. Romero CA, Orias M, Weir MR. Novel RAAS agonists and antagonists: clinical applications and controversies. Nature Reviews Endocrinology 2015; 11(4): 242-52.

81. Reudelhuber TL. The renin-angiotensin system: peptides and enzymes beyond angiotensin II. Current Opinion in Nephrology and Hypertension 2005; 14(2): 155-9.

82. Nguyen G, Delarue F, Burckle C, Bouzhir L, Giller T, Sraer JD. Pivotal role of the renin/prorenin receptor in angiotensin II production and cellular responses to renin. Journal of Clinical Investigation 2002; 109(11): 1417-27.

83. Kim S, Iwao H. Molecular and cellular mechanisms of angiotensin II-mediated cardiovascular and renal diseases. Pharmacology Review 2000; 52(1): 11-34.

84. Funabiki K, Onishi K, Dohi K, Koji T, Imanaka-Yoshida K, Ito M, Wada H, Isaka N, Nobori T, Nakano T. Combined angiotensin receptor blocker and ACE inhibitor on myocardial fibrosis and left ventricular stiffness in dogs with heart failure. American Journal of Physiology: Heart and Circulation Physiology 2004; 287(6): H2487-92.

85. Kehat I, Molkentin JD. Molecular pathways underlying cardiac remodeling during pathophysiological stimulation. Circulation 2010; 122(25): 2727-35.

86. Drazner MH. The progression of hypertensive heart disease. Circulation 2011; 123(3): 327-34.

87. Santos CX, Anilkumar N, Zhang M, Brewer AC, Shah AM. Redox signaling in cardiac myocytes. Free Radical Biology and Medicine 2011; 50(7): 777-93.

88. Nadruz W. Myocardial remodeling in hypertension. Journal of Human Hypertension 2015; 29(1): 1-6.

89. Tardiff JC. Cardiac hypertrophy: stressing out the heart. Journal of Clinical Investigation 2006; 116(6): 1467-70.

90. Bernardo BC, Weeks KL, Pretorius L, McMullen JR. Molecular distinction between physiological and pathological cardiac hypertrophy: Experimental findings and therapeutic strategies. Pharmacology Therapeutics 2010; 128(1): 191-227.

91. Grossman W, Jones D, McLaurin LP. Wall stress and patterns of hypertrophy in the human left ventricle. Journal of Clinical Investigation 1975; 56(1): 56-64.

92. Weber KT. Fibrosis and hypertensive heart disease. Current Opinion in Cardiology 2000; 15(4): 264-72.

93. Van Empel VP, De Windt LJ. Myocyte hypertrophy and apoptosis: a balancing act. Cardiovascular research 2004; 63(3): 487-99.

94. Liu Y, Huang H, Zhang Y, et al. Regulator of G protein signaling 3 protects against cardiac hypertrophy in mice. Journal of Cellular Biochemistry 2014; 115(5): 977-86.

95. Krenning G, Zeisberg EM, Kalluri R. The Origin of Fibroblasts and Mechanism of Cardiac Fibrosis. Journal of Cellular Physiology 2010; 225(3): 631-7.

96. Leask A. Getting to the Heart of the Matter New Insights Into Cardiac Fibrosis. Circulation research 2015; 116(7): 1269-76.

97. Zeisberg EM, Tarnavski O, Zeisberg M, Dorfman AL, McMullen JR, Gustafsson E, Chandraker A, Yuan X, Pu WT, Roberts AB, Neilson EG, Sayegh MH, Izumo S, Kalluri R. Endothelial-to-mesenchymal transition contributes to cardiac fibrosis. Nature Medicine 2007; 13(8): 952-61.

98. Leask A, Abraham DJ. TGF-beta signaling and the fibrotic response. The Journal of the Federation of American Societies for Experimental Biology 2004; 18(7): 816-27.

99. Souders CA, Bowers SLK, Baudino TA. Cardiac Fibroblast The Renaissance Cell. Circulation research 2009; 105(12): 1164-76.

100. Dobaczewski M, Chen W, Frangogiannis NG. Transforming growth factor (TGF)-beta signaling in cardiac remodeling. The Journal of Molecular and Cellular Cardiology 2011; 51(4): 600-6.

101. Bujak M, Frangogiannis NG. The role of TGF-beta signaling in myocardial infarction and cardiac remodeling. Cardiovascular research 2007; 74(2): 184-95.

102. Fontes MS, Kessler EL, van Stuijvenberg L, et al. CTGF knockout does not affect cardiac hypertrophy and fibrosis formation upon chronic pressure overload. The Journal of Molecular and Cellular Cardiology 2015; 88: 82-90.

103. Kai H, Mori T, Tokuda K, Takayama N, Tahara N, Takemiya K, Kudo H, Sugi Y, Fukui D, Yasukawa H, Kuwahara F, Imaizumi T. Pressure overload-induced transient oxidative stress mediates perivascular inflammation and cardiac fibrosis through angiotensin II. Hypertension Research 2006; 29(9): 711-8.

104. Olivetti G, Abbi R, Quaini F, Kajstura J, Cheng W, Nitahara JA, Quaini E, Di Loreto C, Beltrami CA, Krajewski S, Reed JC, Anversa P. Apoptosis in the failing human heart. The New England journal of medicine 1997; 336(16): 1131-41.

105. Kostin S. Types of cardiomyocyte death and clinical outcomes in patients with heart failure. The Journal of the American College of Cardiology 2011; 57(14): 1532-4.

106. Crow MT, Mani K, Nam YJ, Kitsis RN. The mitochondrial death pathway and cardiac myocyte apoptosis. Circulation research 2004; 95(10): 957-70.

107. Regula KM, Kirshenbaum LA. Apoptosis of ventricular myocytes: a means to an end. The Journal of Molecular and Cellular Cardiology 2005; 38(1): 3-13.

108. Bendall JK, Cave AC, Heymes C, Gall N, Shah AM. Pivotal role of a gp91(phox)-containing NADPH oxidase in angiotensin II-induced cardiac hypertrophy in mice. Circulation 2002; 105(3): 293-6.

109. Bodiga S, Zhong JC, Wang W, Basu R, Lo J, Liu GC, Guo D, Holland SM, Scholey JW, Penninger JM, Kassiri Z, Oudit Gy. Enhanced susceptibility to biomechanical stress in ACE2 null mice is prevented by loss of the p47(phox) NADPH oxidase subunit. Cardiovascular research 2011; 91(1): 151-61.

110. Satoh M, Ogita H, Takeshita K, Mukai Y, Kwiatkowski DJ, Liao JK. Requirement of Rac1 in the development of cardiac hypertrophy. Proceedings of the National Academy of Sciences USA 2006; 103(19): 7432-7.

111. Nakamura T, Kataoka K, Fukuda M, Nako H, Tokutomi Y, Dong YF, Ichijo H, Oqawa H, Kim-Mitsuyama S. Critical role of apoptosis signal-regulating kinase 1 in aldosterone/salt-induced cardiac inflammation and fibrosis. Hypertension 2009; 54(3): 544-51.

112. Mann DL. Innate immunity and the failing heart: the cytokine hypothesis revisited. Circulation research 2015; 116(7): 1254-68.

113. Kalra D, Sivasubramanian N, Mann DL. Angiotensin II induces tumor necrosis factor biosynthesis in the adult mammalian heart through a protein kinase C-dependent pathway. Circulation 2002; 105(18): 2198-205.

114. Mann DL. The emerging role of innate immunity in the heart and vascular system: for whom the cell tolls. Circulation research 2011; 108(9): 1133-45.

115. Frieler RA, Mortensen RM. Immune cell and other noncardiomyocyte regulation of cardiac hypertrophy and remodeling. Circulation 2015; 131(11): 1019-30.

116. Testa M, Yeh M, Lee P, et al. Circulating levels of cytokines and their endogenous modulators in patients with mild to severe congestive heart failure due to coronary artery disease or hypertension. The Journal of the American College of Cardiology 1996; 28(4): 964-71.

117. Rosenkranz S, Flesch M, Amann K, et al. Alterations of beta-adrenergic signaling and cardiac hypertrophy in transgenic mice overexpressing TGF-beta(1). The American Journal of Physiology: Heart and Circulation Physiology 2002; 283(3): H1253-62.

118. Kuwahara F, Kai H, Tokuda K, et al. Transforming growth factor-beta function blocking prevents myocardial fibrosis and diastolic dysfunction in pressure-overloaded rats. Circulation 2002; 106(1): 130-5.

119. Sakata Y, Chancey AL, Divakaran VG, Sekiguchi K, Sivasubramanian N, Mann DL. Transforming growth factor-beta receptor antagonism attenuates myocardial fibrosis in mice with cardiac-restricted overexpression of tumor necrosis factor. Basic Research in Cardiology 2008; 103(1): 60-8.

120. Sun M, Chen M, Dawood F, et al. Tumor necrosis factor-alpha mediates cardiac remodeling and ventricular dysfunction after pressure overload state. Circulation 2007; 115(11): 1398-407.

121. Bozkurt B, Kribbs SB, Clubb FJ, Jr., et al. Pathophysiologically relevant concentrations of tumor necrosis factor-alpha promote progressive left ventricular dysfunction and remodeling in rats. Circulation 1998; 97(14): 1382-91.

122. Kubota T, McTiernan CF, Frye CS, et al. Dilated cardiomyopathy in transgenic mice with cardiac-specific overexpression of tumor necrosis factor-alpha. Circulation research 1997; 81(4): 627-35.

123. Honsho S, Nishikawa S, Amano K, et al. Pressure-mediated hypertrophy and mechanical stretch induces IL-1 release and subsequent IGF-1 generation to maintain compensative hypertrophy by affecting Akt and JNK pathways. Circulation research 2009; 105(11): 1149-58.

124. Van Tassell BW, Arena RA, Toldo S, et al. Enhanced interleukin-1 activity contributes to exercise intolerance in patients with systolic heart failure. PloS one 2012; 7(3): e33438.

125. Ikonomidis I, Lekakis JP, Nikolaou M, et al. Inhibition of interleukin-1 by anakinra improves vascular and left ventricular function in patients with rheumatoid arthritis. Circulation 2008; 117(20): 2662-9.

126. Abbate A, Van Tassell BW, Biondi-Zoccai G, et al. Effects of interleukin-1 blockade with anakinra on adverse cardiac remodeling and heart failure after acute myocardial

infarction [from the Virginia Commonwealth University-Anakinra Remodeling Trial (2) (VCU-ART2) pilot study]. The American Journal of Cardiology 2013; 111(10): 1394-400.

127. Melendez GC, McLarty JL, Levick SP, Du Y, Janicki JS, Brower GL. Interleukin 6 mediates myocardial fibrosis, concentric hypertrophy, and diastolic dysfunction in rats. Hypertension 2010; 56(2): 225-31.

128. Coles B, Fielding CA, Rose-John S, Scheller J, Jones SA, O'Donnell VB. Classic interleukin-6 receptor signaling and interleukin-6 trans-signaling differentially control angiotensin II-dependent hypertension, cardiac signal transducer and activator of transcription-3 activation, and vascular hypertrophy in vivo. The American Journal of Pathology 2007; 171(1): 315-25.

129. Ma F, Li Y, Jia L, et al. Macrophage-stimulated cardiac fibroblast production of IL-6 is essential for TGF beta/Smad activation and cardiac fibrosis induced by angiotensin II. PloS one 2012; 7(5): e35144.

130. Schiffrin EL. The immune system: role in hypertension. The Canadian journal of Cardiology 2013; 29(5): 543-8.

131. Harrison DG, Guzik TJ, Lob HE, et al. Inflammation, immunity, and hypertension. Hypertension 2011; 57(2): 132-40.

132. Savoia C, Schiffrin EL. Inflammation in hypertension. Current Opinion in Nephrology and Hypertension 2006; 15(2): 152-8.

133. Jackson SH, Devadas S, Kwon J, Pinto LA, Williams MS. T cells express a phagocyte-type NADPH oxidase that is activated after T cell receptor stimulation. Nature Immunology 2004; 5(8): 818-27.

134. Guzik TJ, Hoch NE, Brown KA, et al. Role of the T cell in the genesis of angiotensin II induced hypertension and vascular dysfunction. The Journal of Experimental Medicine 2007; 204(10): 2449-60.

135. Lob HE, Schultz D, Marvar PJ, Davisson RL, Harrison DG. Role of the NADPH oxidases in the subfornical organ in angiotensin II-induced hypertension. Hypertension 2013; 61(2): 382-7.

136. Murdoch CE, Alom-Ruiz SP, Wang M, et al. Role of endothelial Nox2 NADPH oxidase in angiotensin II-induced hypertension and vasomotor dysfunction. Basic Research in Cardiology 2011; 106(4): 527-38.

137. Brown M, Wittwer C. Flow cytometry: principles and clinical applications in hematology. Clinical Chemistry 2000; 46(8 Pt 2): 1221-9.

138. Roederer M. Compensation in flow cytometry. Current protocols in cytometry 2002; 1:1.14.

139. Baumgarth N, Roederer M. A practical approach to multicolor flow cytometry for immunophenotyping. The Journal of Immunological Methods 2000; 243(1-2): 77-97.

140. Langeveld M, Gamadia LE, ten Berge IJ. T-lymphocyte subset distribution in human spleen. The European Journal of Clinical Investigation 2006; 36(4): 250-6.

141. Myrick C, DiGuisto R, DeWolfe J, et al. Linkage analysis of variations in CD4:CD8 T cell subsets between C57BL/6 and DBA/2. Genes and Immunology 2002; 3(3): 144-50.

142. Chazotte B. Labeling membrane glycoproteins or glycolipids with fluorescent wheat germ agglutinin. Cold Spring Harbor Protocols 2011; 2011(5): 5623.

143. Lattouf R, Younes R, Lutomski D, et al. Picrosirius red staining: a useful tool to appraise collagen networks in normal and pathological tissues. Journal of Histochemistry and Cytochemistry 2014; 62(10): 751-8.

144. Wang Y, Seto SW, Golledge J. Angiotensin II, sympathetic nerve activity and chronic heart failure. Heart Failure Review 2014; 19(2): 187-98.

145. Griendling KK, UshioFukai M, Lassegue B, Alexander RW. Angiotensin II signaling in vascular smooth muscle - New concepts. Hypertension 1997; 29(1): 366-73.

146. Benigni A, Cassis P, Remuzzi G. Angiotensin II revisited: new roles in inflammation, immunology and aging. The European Molecular Biology Organisation: Molecular Medicine 2010; 2(7): 247-57.

147. Suzuki Y, Ruiz-Ortega M, Egido J. Angiotensin II: a double-edged sword in inflammation. The Journal of Nephrology 2000; 13(3): S101-10.

148. Suzuki Y, Ruiz-Ortega M, Lorenzo O, Ruperez M, Esteban V, Egido J. Inflammation and angiotensin II. The International Journal of Biochemistry and Cell Biology 2003; 35(6): 881-900.

149. Kranzhofer R, Schmidt J, Pfeiffer CA, Hagl S, Libby P, Kubler W. Angiotensin induces inflammatory activation of human vascular smooth muscle cells. Arteriosclerosis, Thrombosis and Vascular Biology 1999; 19(7): 1623-9.

150. Wolf G, Wenzel U, Burns KD, Harris RC, Stahl RA, Thaiss F. Angiotensin II activates nuclear transcription factor-kappaB through AT1 and AT2 receptors. Kidney International 2002; 61(6): 1986-95.

151. Luft FC, Mervaala E, Muller DN, et al. Hypertension-induced end-organ damage : A new transgenic approach to an old problem. Hypertension 1999; 33(1 Pt 2): 212-8.

152. Mervaala EM, Muller DN, Park JK, et al. Monocyte infiltration and adhesion molecules in a rat model of high human renin hypertension. Hypertension 1999; 33(1 Pt 2): 389-95.

153. Muller DN, Dechend R, Mervaala EM, et al. NF-kappaB inhibition ameliorates angiotensin II-induced inflammatory damage in rats. Hypertension 2000; 35(1 Pt 2): 193-201.

154. Tian N, Gu JW, Jordan S, Rose RA, Hughson MD, Manning RD, Jr. Immune suppression prevents renal damage and dysfunction and reduces arterial pressure in salt-sensitive

hypertension. The American Journal of Physiology: Heart and Circulation Physiology 2007; 292(2): H1018-25.

155. Karin M. How NF-kappaB is activated: the role of the IkappaB kinase (IKK) complex. Oncogene 1999; 18(49): 6867-74.

156. Zhang L, Ma Y, Zhang J, Cheng J, Du J. A new cellular signaling mechanism for angiotensin II activation of NF-kappaB: An IkappaB-independent, RSK-mediated phosphorylation of p65. Arteriosclerosis, Thrombosis and Vascular Biology 2005; 25(6): 1148-53.

157. Jurewicz M, McDermott DH, Sechler JM, et al. Human T and natural killer cells possess a functional renin-angiotensin system: further mechanisms of angiotensin II-induced inflammation. Journal of the American Society of Nephrology 2007; 18(4): 1093-102.

158. Dai Q, Xu M, Yao M, Sun B. Angiotensin AT1 receptor antagonists exert anti-inflammatory effects in spontaneously hypertensive rats. British Journal of Pharmacology 2007; 152(7): 1042-8.

159. Gunther J, Kill A, Becker MO, et al. Angiotensin receptor type 1 and endothelin receptor type A on immune cells mediate migration and the expression of IL-8 and CCL18 when stimulated by autoantibodies from systemic sclerosis patients. Arthritis Research and Therapy 2014; 16(2): R65.

160. Capers Qt, Alexander RW, Lou P, et al. Monocyte chemoattractant protein-1 expression in aortic tissues of hypertensive rats. Hypertension 1997; 30(6): 1397-402.

161. Gilbert KC, Brown NJ. Aldosterone and inflammation. Current Opinion in Endocrinology, Diabetes and Obesity 2010; 17(3): 199-204.

162. Rocha R, Rudolph AE, Frierdich GE, et al. Aldosterone induces a vascular inflammatory phenotype in the rat heart. The American Journal of Physiology: Heart and Circulation Physiology 2002; 283(5): H1802-10.

163. Blasi ER, Rocha R, Rudolph AE, Blomme EA, Polly ML, McMahon EG. Aldosterone/salt induces renal inflammation and fibrosis in hypertensive rats. Kidney International 2003; 63(5): 1791-800.

164. Kintscher U, Wakino S, Kim S, Fleck E, Hsueh WA, Law RE. Angiotensin II induces migration and Pyk2/paxillin phosphorylation of human monocytes. Hypertension 2001; 37(2 Pt 2): 587-93.

165. Ruiz-Ortega M, Lorenzo O, Ruperez M, Konig S, Wittig B, Egido J. Angiotensin II activates nuclear transcription factor kappaB through AT(1) and AT(2) in vascular smooth muscle cells: molecular mechanisms. Circulation research 2000; 86(12): 1266-72.

166. Brown NJ. Contribution of aldosterone to cardiovascular and renal inflammation and fibrosis. Nature Reviews Nephrology 2013; 9(8): 459-69.

167. Bush E, Maeda N, Kuziel WA, et al. CC chemokine receptor 2 is required for macrophage infiltration and vascular hypertrophy in angiotensin II-induced hypertension. Hypertension 2000; 36(3): 360-3.

168. Soejima H, Ogawa H, Yasue H, et al. Angiotensin-converting enzyme inhibition reduces monocyte chemoattractant protein-1 and tissue factor levels in patients with myocardial infarction. The Journal of the American College of Cardiology 1999; 34(4): 983-8.

169. Kirabo A, Fontana V, de Faria AP, et al. DC isoketal-modified proteins activate T cells and promote hypertension. The Journal of Clinical Investigation 2014; 124(10): 4642-56.

170. Wu K, Zhou T, Sun G, et al. Valsartan inhibited the accumulation of dendritic cells in rat fibrotic renal tissue. Cellular and Molecular Immunology 2006; 3(3): 213-20.

171. Lapteva N, Ide K, Nieda M, et al. Activation and suppression of renin-angiotensin system in human dendritic cells. Biochemical and Biophysical Research Communications 2002; 296(1): 194-200.

172. Vinh A, Chen W, Blinder Y, et al. Inhibition and genetic ablation of the B7/CD28 T-cell costimulation axis prevents experimental hypertension. Circulation 2010; 122(24): 2529-37.

173. Muller DN, Shagdarsuren E, Park JK, et al. Immunosuppressive treatment protects against angiotensin II-induced renal damage. The American Journal of Pathology 2002; 161(5): 1679-93.

174. Rodriguez-Iturbe B, Quiroz Y, Nava M, et al. Reduction of renal immune cell infiltration results in blood pressure control in genetically hypertensive rats. The American Journal of Physiology 2002; 282(2): F191-201.

175. Johar S, Cave AC, Narayanapanicker A, Grieve DJ, Shah AM. Aldosterone mediates angiotensin II-induced interstitial cardiac fibrosis via a Nox2-containing NADPH oxidase. The Journal of the Federation of American Societies for Experimental Biology 2006; 20(9): 1546-8.

176. Antonioli L, Pacher P, Vizi ES, Hasko G. CD39 and CD73 in immunity and inflammation. Trends in Molecular Medicine 2013; 19(6): 355-67.

177. Wing K, Onishi Y, Prieto-Martin P, et al. CTLA-4 control over Foxp3+ regulatory T cell function. Science 2008; 322(5899): 271-5.

178. Rothstein DM, Camirand G. New insights into the mechanisms of Treg function. Current opinion in organ transplantation 2015; 20(4): 376-84.

179. Yadav M, Louvet C, Davini D, et al. Neuropilin-1 distinguishes natural and inducible regulatory T cells among regulatory T cell subsets in vivo. The Journal of Experimental Medicine 2012; 209(10): 1713-22, S1-19.

180. Weiss JM, Bilate AM, Gobert M, et al. Neuropilin 1 is expressed on thymus-derived natural regulatory T cells, but not mucosa-generated induced Foxp3+ T reg cells. The Journal of Experimental Medicine 2012; 209(10): 1723-42, S1.

181. Iellem A, Mariani M, Lang R, et al. Unique chemotactic response profile and specific expression of chemokine receptors CCR4 and CCR8 by CD4(+)CD25(+) regulatory T cells. The Journal of Experimental Medicine 2001; 194(6): 847-53.

182. Lee I, Wang L, Wells AD, Dorf ME, Ozkaynak E, Hancock WW. Recruitment of Foxp3+ T regulatory cells mediating allograft tolerance depends on the CCR4 chemokine receptor. The Journal of Experimental Medicine 2005; 201(7): 1037-44.

183. Komarowska I, Coe D, Wang G, et al. Hepatocyte Growth Factor Receptor c-Met Instructs T Cell Cardiotropism and Promotes T Cell Migration to the Heart via Autocrine Chemokine Release. Immunity 2015; 42(6): 1087-99.

184. Laroumanie F, Douin-Echinard V, Pozzo J, et al. CD4+ T cells promote the transition from hypertrophy to heart failure during chronic pressure overload. Circulation 2014; 129(21): 2111-24.

185. Madhur MS, Lob HE, McCann LA, et al. Interleukin 17 promotes angiotensin II-induced hypertension and vascular dysfunction. Hypertension 2010; 55(2): 500-7.

186. Marko L, Kvakan H, Park JK, et al. Interferon-gamma Signaling Inhibition Ameliorates Angiotensin II-Induced Cardiac Damage. Hypertension 2012; 60(6): 1430-U154.

187. Duerrschmid C, Crawford JR, Reineke E, et al. TNF receptor 1 signaling is critically involved in mediating angiotensin-II-induced cardiac fibrosis. Journal of Molecular and Cellular Cardiology 2013; 57: 59-67.

188. Duerrschmid C, Trial J, Wang Y, Entman ML, Haudek SB. Tumor necrosis factor: a mechanistic link between angiotensin-II-induced cardiac inflammation and fibrosis. Circulation: Heart Failure 2015; 8(2): 352-61.

189. Kanellakis P, Dinh TN, Agrotis A, Bobik A. CD4(+)CD25(+)Foxp3(+) regulatory T cells suppress cardiac fibrosis in the hypertensive heart. The Journal of Hypertension 2011; 29(9): 1820-8.

190. Barhoumi T, Kasal DA, Li MW, et al. T regulatory lymphocytes prevent angiotensin II-induced hypertension and vascular injury. Hypertension 2011; 57(3): 469-76.

191. Kvakan H, Kleinewietfeld M, Qadri F, et al. Regulatory T cells ameliorate angiotensin II-induced cardiac damage. Circulation 2009; 119(22): 2904-12.

192. Kasal DA, Barhoumi T, Li MW, et al. T regulatory lymphocytes prevent aldosterone-induced vascular injury. Hypertension 2012; 59(2): 324-30.

193. Tang TT, Yuan J, Zhu ZF, et al. Regulatory T cells ameliorate cardiac remodeling after myocardial infarction. Basic Research in Cardiology 2012; 107(1): 232.

194. Lam GY, Huang J, Brumell JH. The many roles of NOX2 NADPH oxidase-derived ROS in immunity. Seminars in Immunopathology 2010; 32(4): 415-30.

195. Segal BH, Veys P, Malech H, Cowan MJ. Chronic granulomatous disease: lessons from a rare disorder. Biology of Blood and Marrow Transplantation 2011; 17(1 Suppl): S123-31.

196. Kobayashi SD, Voyich JM, Braughton KR, et al. Gene expression profiling provides insight into the pathophysiology of chronic granulomatous disease. Journal of immunology 2004; 172(1): 636-43.

197. Matsue H, Edelbaum D, Shalhevet D, et al. Generation and function of reactive oxygen species in dendritic cells during antigen presentation. Journal of immunology 2003; 171(6): 3010-8.

198. Gelderman KA, Hultqvist M, Pizzolla A, et al. Macrophages suppress T cell responses and arthritis development in mice by producing reactive oxygen species. The Journal of Clinical Investigation 2007; 117(10): 3020-8.

199. Lee K, Won HY, Bae MA, Hong JH, Hwang ES. Spontaneous and aging-dependent development of arthritis in NADPH oxidase 2 deficiency through altered differentiation of CD11b+ and Th/Treg cells. Proceedings of the National Academy of Sciences USA 2011; 108(23): 9548-53.

200. Rada B, Leto TL. Oxidative innate immune defenses by Nox/Duox family NADPH oxidases. Contributions to Microbiology 2008; 15: 164-87.

201. Forman HJ, Torres M. Redox signaling in macrophages. Molecular Aspects of Medicine 2001; 22(4-5): 189-216.

202. Zhang Y, Choksi S, Chen K, Pobezinskaya Y, Linnoila I, Liu ZG. ROS play a critical role in the differentiation of alternatively activated macrophages and the occurrence of tumor-associated macrophages. Cell Research 2013; 23(7): 898-914.

203. Chaubey S, Jones GE, Shah AM, Cave AC, Wells CM. Nox2 is required for macrophage chemotaxis towards CSF-1. PloS one 2013; 8(2): e54869.

204. Mantegazza AR, Savina A, Vermeulen M, et al. NADPH oxidase controls phagosomal pH and antigen cross-presentation in human dendritic cells. Blood 2008; 112(12): 4712-22.

205. Savina A, Jancic C, Hugues S, et al. NOX2 controls phagosomal pH to regulate antigen processing during crosspresentation by dendritic cells. Cell 2006; 126(1): 205-18.

206. Kotsias F, Hoffmann E, Amigorena S, Savina A. Reactive oxygen species production in the phagosome: impact on antigen presentation in dendritic cells. Antioxidants and Redox Signaling 2013; 18(6): 714-29.

207. George-Chandy A, Nordstrom I, Nygren E, et al. Th17 development and autoimmune arthritis in the absence of reactive oxygen species. The European Journal of Immunology 2008; 38(4): 1118-26.

208. Wheeler ML, Defranco AL. Prolonged production of reactive oxygen species in response to B cell receptor stimulation promotes B cell activation and proliferation. Journal of immunology 2012; 189(9): 4405-16.

209. Pollock JD, Williams DA, Gifford MA, et al. Mouse model of X-linked chronic granulomatous disease, an inherited defect in phagocyte superoxide production. Nature genetics 1995; 9(2): 202-9.

210. Bendall JK, Heymes C, Cave AC, Gall NP, Shah AM. Attenuation of angiotensin II-induced cardiac hypertrophy in GP91(phox)-deficient mice. Circulation 2001; 104(17): 307-.

211. Nam SJ, Oh IS, Yoon YH, et al. Apocynin regulates cytokine production of CD8 T cells. Clinical and Experimental Medicine 2013.

212. Bai A, Moss A, Rothweiler S, et al. NADH oxidase-dependent CD39 expression by CD8(+) T cells modulates interferon gamma responses via generation of adenosine. Nature communications 2015; 6: 8819.

213. Nam SJ, Oh IS, Yoon YH, et al. Apocynin regulates cytokine production of CD8(+) T cells. Clinical and Experimental Medicine 2014; 14(3): 261-8.

214. Efimova O, Szankasi P, Kelley TW. Ncf1 (p47phox) is essential for direct regulatory T cell mediated suppression of CD4+ effector T cells. PloS one 2011; 6(1): e16013.

215. Kraaij MD, Savage NDL, van der Kooij SW, et al. Induction of regulatory T cells by macrophages is dependent on production of reactive oxygen species. Proceedings of the National Academy of Sciences USA 2010; 107(41): 17686-91.

216. Kraaij MD, van der Kooij SW, Reinders ME, et al. Dexamethasone increases ROS production and T cell suppressive capacity by anti-inflammatory macrophages. Molecular Immunology 2011; 49(3): 549-57.

217. Ouyang W, Beckett O, Ma Q, Li MO. Transforming growth factor-beta signaling curbs thymic negative selection promoting regulatory T cell development. Immunity 2010; 32(5): 642-53.

218. Vignali DA, Collison LW, Workman CJ. How regulatory T cells work. Nature Review Immunology 2008; 8(7): 523-32.

219. Corthay A. How do regulatory T cells work? Scandinavian Journal of Immunology 2009; 70(4): 326-36.

220. Campbell DJ. Control of Regulatory T Cell Migration, Function, and Homeostasis. Journal of immunology 2015; 195(6): 2507-13.

221. Sakaguchi S, Wing K, Onishi Y, Prieto-Martin P, Yamaguchi T. Regulatory T cells: how do they suppress immune responses? International Immunology 2009; 21(10): 1105-11.

222. Grossman WJ, Verbsky JW, Tollefsen BL, Kemper C, Atkinson JP, Ley TJ. Differential expression of granzymes A and B in human cytotoxic lymphocyte subsets and T regulatory cells. Blood 2004; 104(9): 2840-8.

223. Gondek DC, Lu LF, Quezada SA, Sakaguchi S, Noelle RJ. Cutting edge: contact-mediated suppression by CD4+CD25+ regulatory cells involves a granzyme B-dependent, perforin-independent mechanism. Journal of immunology 2005; 174(4): 1783-6.

224. Cao X, Cai SF, Fehniger TA, et al. Granzyme B and perforin are important for regulatory T cell-mediated suppression of tumor clearance. Immunity 2007; 27(4): 635-46.

225. Pandiyan P, Zheng L, Ishihara S, Reed J, Lenardo MJ. CD4+CD25+Foxp3+ regulatory T cells induce cytokine deprivation-mediated apoptosis of effector CD4+ T cells. Nature Immunology 2007; 8(12): 1353-62.

226. Thornton AM, Shevach EM. CD4+CD25+ immunoregulatory T cells suppress polyclonal T cell activation in vitro by inhibiting interleukin 2 production. The Journal of Experimental Medicine 1998; 188(2): 287-96.

227. Burchill MA, Yang J, Vogtenhuber C, Blazar BR, Farrar MA. IL-2 receptor beta-dependent STAT5 activation is required for the development of Foxp3+ regulatory T cells. Journal of immunology 2007; 178(1): 280-90.

228. Zarek PE, Huang CT, Lutz ER, et al. A2A receptor signaling promotes peripheral tolerance by inducing T-cell anergy and the generation of adaptive regulatory T cells. Blood 2008; 111(1): 251-9.

229. Qureshi OS, Zheng Y, Nakamura K, et al. Trans-endocytosis of CD80 and CD86: a molecular basis for the cell-extrinsic function of CTLA-4. Science 2011; 332(6029): 600-3.

230. Shevach EM. Mechanisms of foxp3+ T regulatory cell-mediated suppression. Immunity 2009; 30(5): 636-45.

231. Burzyn D, Benoist C, Mathis D. Regulatory T cells in nonlymphoid tissues. Nature Immunology 2013; 14(10): 1007-13.

232. Tang TT, Song Y, Ding YJ, et al. Atorvastatin upregulates regulatory T cells and reduces clinical disease activity in patients with rheumatoid arthritis. The Journal of Lipid Research 2011; 52(5): 1023-32.

233. Cipolletta D, Feuerer M, Li A, et al. PPAR-gamma is a major driver of the accumulation and phenotype of adipose tissue Treg cells. Nature 2012; 486(7404): 549-53.

234. Burzyn D, Kuswanto W, Kolodin D, et al. A special population of regulatory T cells potentiates muscle repair. Cell 2013; 155(6): 1282-95.

235. Sather BD, Treuting P, Perdue N, et al. Altering the distribution of Foxp3(+) regulatory T cells results in tissue-specific inflammatory disease. The Journal of Experimental Medicine 2007; 204(6): 1335-47.

236. Dobaczewski M, Xia Y, Bujak M, Gonzalez-Quesada C, Frangogiannis NG. CCR5 signaling suppresses inflammation and reduces adverse remodeling of the infarcted heart, mediating recruitment of regulatory T cells. The American Journal of Pathology 2010; 176(5): 2177-87.

237. Ait-Oufella H, Salomon BL, Potteaux S, et al. Natural regulatory T cells control the development of atherosclerosis in mice. Nature Medicine 2006; 12(2): 178-80.

238. Mallat Z, Ait-Oufella H, Tedgui A. Regulatory T Cell Responses: potential role in the control of atherosclerosis. Currrent Opinions in Lipidology 2005; 16(5): 518-24.

239. Nahrendorf M, Swirski FK. Regulating repair: regulatory T cells in myocardial infarction. Circulation research 2014; 115(1): 7-9.

240. Weirather J, Hofmann UD, Beyersdorf N, et al. Foxp3+ CD4+ T cells improve healing after myocardial infarction by modulating monocyte/macrophage differentiation. Circulation research 2014; 115(1): 55-67.

241. Saxena A, Dobaczewski M, Rai V, et al. Regulatory T cells are recruited in the infarcted mouse myocardium and may modulate fibroblast phenotype and function. The American Journal of Physiology: Heart and Circulation Physiology 2014; 307(8): H1233-42.

242. Ait-Oufella H, Wang Y, Herbin O, et al. Natural regulatory T cells limit angiotensin II-induced aneurysm formation and rupture in mice. Arteriosclerosis, Thrombosis and Vascular Biology 2013; 33(10): 2374-9.

243. Zhou Y, Wu W, Lindholt JS, et al. Regulatory T cells in human and angiotensin II-induced mouse abdominal aortic aneurysms. Cardiovascular research 2015; 107(1): 98-107.

244. Meng X, Yang J, Zhang K, et al. Regulatory T cells prevent angiotensin II-induced abdominal aortic aneurysm in apolipoprotein E knockout mice. Hypertension 2014; 64(4): 875-82.

245. Crowley SD, Gurley SB, Herrera MJ, et al. Angiotensin II causes hypertension and cardiac hypertrophy through its receptors in the kidney. Proceedings of the National Academy of Sciences USA 2006; 103(47): 17985-90.

246. Li JM, Wheatcroft S, Fan LM, Kearney MT, Shah AM. Opposing roles of p47phox in basal versus angiotensin II-stimulated alterations in vascular O2- production, vascular tone, and mitogen-activated protein kinase activation. Circulation 2004; 109(10): 1307-13.

247. Schaper M, Leib SL, Meli DN, Brandes RP, Tauber MG, Christen S. Differential effect of p47phox and gp91phox deficiency on the course of Pneumococcal Meningitis. Infection and Immunity 2003; 71(7): 4087-92.

248. Snelgrove RJ, Edwards L, Williams AE, Rae AJ, Hussell T. In the absence of reactive oxygen species, T cells default to a Th1 phenotype and mediate protection against pulmonary Cryptococcus neoformans infection. Journal of immunology 2006; 177(8): 5509-16.

249. Shatynski KE, Chen H, Kwon J, Williams MS. Decreased STAT5 phosphorylation and GATA-3 expression in NOX2-deficient T cells: role in T helper development. European Journal of Immunology 2012; 42(12): 3202-11.

250. Hoffmann FW, Hashimoto AC, Shafer LA, Dow S, Berry MJ, Hoffmann PR. Dietary selenium modulates activation and differentiation of CD4+ T cells in mice through a mechanism involving cellular free thiols. Journal of Nutrition 2010; 140(6): 1155-61.

251. King MR, Ismail AS, Davis LS, Karp DR. Oxidative stress promotes polarization of human T cell differentiation toward a T helper 2 phenotype. Journal of immunology 2006; 176(5): 2765-72.

252. Hofmann U, Beyersdorf N, Weirather J, et al. Activation of CD4+ T lymphocytes improves wound healing and survival after experimental myocardial infarction in mice. Circulation 2012; 125(13): 1652-63.

253. Taleb S, Tedgui A, Mallat Z. IL-17 and Th17 cells in atherosclerosis: subtle and contextual roles. Arteriosclerosis, Thrombosis and Vascular Biology 2015; 35(2): 258-64.

254. Kleinewietfeld M, Hafler DA. The plasticity of human Treg and Th17 cells and its role in autoimmunity. Seminars in Immunology 2013; 25(4): 305-12.

255. Muranski P, Restifo NP. Essentials of Th17 cell commitment and plasticity. Blood 2013; 121(13): 2402-14.

256. Obermajer N, Popp FC, Soeder Y, et al. Conversion of Th17 into IL-17A(neg) regulatory T cells: a novel mechanism in prolonged allograft survival promoted by mesenchymal stem cell-supported minimized immunosuppressive therapy. Journal of immunology 2014; 193(10): 4988-99.

257. Gagliani N, Vesely MC, Iseppon A, et al. Th17 cells transdifferentiate into regulatory T cells during resolution of inflammation. Nature 2015; 523(7559): 221-5.

258. Mucida D, Park Y, Kim G, et al. Reciprocal TH17 and regulatory T cell differentiation mediated by retinoic acid. Science 2007; 317(5835): 256-60.

259. Weissmann N, Sydykov A, Kalwa H, et al. Activation of TRPC6 channels is essential for lung ischaemia-reperfusion induced oedema in mice. Nature communications 2012; 3: 649.

260. Pino-Lagos K, Guo Y, Brown C, et al. A retinoic acid-dependent checkpoint in the development of CD4+ T cell-mediated immunity. The Journal of Experimental Medicine 2011; 208(9): 1767-75.

261. Rutz S, Kayagaki N, Phung QT, et al. Deubiquitinase DUBA is a post-translational brake on interleukin-17 production in T cells. Nature 2015; 518(7539): 417-21.

262. Liao FH, Shui JW, Hsing EW, et al. Protein phosphatase 4 is an essential positive regulator for Treg development, function, and protective gut immunity. Cell and Bioscience 2014; 4: 25.

263. Phee H, Au-Yeung BB, Pryshchep O, et al. Pak2 is required for actin cytoskeleton remodeling, TCR signaling, and normal thymocyte development and maturation. Elife Sciences 2014; 3: 2270.

264. Steinke FC, Yu S, Zhou X, et al. TCF-1 and LEF-1 act upstream of Th-POK to promote the CD4(+) T cell fate and interact with Runx3 to silence Cd4 in CD8(+) T cells. Nature Immunology 2014; 15(7): 646-56.

265. Sharma S, Zhu J. Immunologic applications of conditional gene modification technology in the mouse. Current Protocols in Immunology 2014; 105:10.34.1-10.34.13

266. Paige SL, Plonowska K, Xu A, Wu SM. Molecular regulation of cardiomyocyte differentiation. Circulation research 2015; 116(2): 341-53.

267. Inoue-Yokoo T, Tani K, Sugiyama D. Mesodermal and hematopoietic differentiation from ES and iPS cells. Stem Cell Review 2013; 9(4): 422-34.

268. Wobus AM, Kaomei G, Shan J, et al. Retinoic acid accelerates embryonic stem cell-derived cardiac differentiation and enhances development of ventricular cardiomyocytes. The Journal of Molecular and Cellular Cardiology 1997; 29(6): 1525-39.

269. Tkachev V, Goodell S, Opipari AW, et al. Programmed death-1 controls T cell survival by regulating oxidative metabolism. Journal of immunology 2015; 194(12): 5789-800.

270. Yu M, Hu J, Zhu MX, et al. Cardiac fibroblasts recruit Th17 cells infiltration into myocardium by secreting CCL20 in CVB3-induced acute viral myocarditis. Cellular Physiology and Biochemistry 2013; 32(5): 1437-50.

271. Tran CN, Lundy SK, White PT, et al. Molecular interactions between T cells and fibroblast-like synoviocytes: role of membrane tumor necrosis factor-alpha on cytokine-activated T cells. The American Journal of Pathology 2007; 171(5): 1588-98.

272. Vancheri C, Mastruzzo C, Trovato-Salinaro E, et al. Interaction between human lung fibroblasts and T-lymphocytes prevents activation of CD4+ cells. Respiration Research 2005; 6: 103.

273. Loubaki L, Hadj-Salem I, Fakhfakh R, et al. Co-culture of human bronchial fibroblasts and CD4+ T cells increases Th17 cytokine signature. PloS one 2013; 8(12): e81983.

274. Wolf D, Li J, Ley K. HGF Guides T Cells into the Heart. Immunity 2015; 42(6): 979-81.

275. Nakano N, Moriguchi A, Morishita R, et al. Role of angiotensin II in the regulation of a novel vascular modulator, hepatocyte growth factor (HGF), in experimental hypertensive rats. Hypertension 1997; 30(6): 1448-54.

276. Taniyama Y, Morishita R, Nakagami H, et al. Potential contribution of a novel antifibrotic factor, hepatocyte growth factor, to prevention of myocardial fibrosis by angiotensin II blockade in cardiomyopathic hamsters. Circulation 2000; 102(2): 246-52.

277. Schroder K, Schutz S, Schloffel I, et al. Hepatocyte growth factor induces a proangiogenic phenotype and mobilizes endothelial progenitor cells by activating Nox2. Antioxidants and Redox Signaling 2011; 15(4): 915-23.

278. Clavijo-Cornejo D, Enriquez-Cortina C, Lopez-Reyes A, et al. Biphasic regulation of the NADPH oxidase by HGF/c-Met signaling pathway in primary mouse hepatocytes. Biochimie 2013; 95(6): 1177-84.

279. Sahaf B, Heydari K, Herzenberg LA, Herzenberg LA. Lymphocyte surface thiol levels. Proceedings of the National Academy of Sciences USA 2003; 100(7): 4001-5.

280. Angelini G, Gardella S, Ardy M, et al. Antigen-presenting dendritic cells provide the reducing extracellular microenvironment required for T lymphocyte activation. Proceedings of the National Academy of Sciences USA 2002; 99(3): 1491-6.

281. Gelderman KA, Hultqvist M, Holmberg J, Olofsson P, Holmdahl R. T cell surface redox levels determine T cell reactivity and arthritis susceptibility. Proceedings of the National Academy of Sciences USA 2006; 103(34): 12831-6.

282. McLoughlin RM, Jenkins BJ, Grail D, et al. IL-6 trans-signaling via STAT3 directs T cell infiltration in acute inflammation. Proceedings of the National Academy of Sciences USA 2005; 102(27): 9589-94.

283. Koller L, Richter B, Goliasch G, et al. CD4+ CD28(null) cells are an independent predictor of mortality in patients with heart failure. Atherosclerosis 2013; 230(2): 414-6.

284. Schmidt D, Goronzy JJ, Weyand CM. CD4+ CD7- CD28- T cells are expanded in rheumatoid arthritis and are characterized by autoreactivity. The Journal of Clinical Investigation 1996; 97(9): 2027-37.

285. Liuzzo G, Goronzy JJ, Yang H, et al. Monoclonal T-cell proliferation and plaque instability in acute coronary syndromes. Circulation 2000; 101(25): 2883-8.

286. Skorska A, von Haehling S, Ludwig M, et al. The CD4(+) AT2R(+) T cell subpopulation improves post-infarction remodelling and restores cardiac function. Journal of Cellular and Molecular Medicine 2015; 19(8): 1975-85.

287. Yan Z, Garg SK, Kipnis J, Banerjee R. Extracellular redox modulation by regulatory T cells. Nature Chemical Biology 2009; 5(10): 721-3.

288. Yan Z, Garg SK, Banerjee R. Regulatory T cells interfere with glutathione metabolism in dendritic cells and T cells. The Journal of Biological Chemistry 2010; 285(53): 41525-32.

289. Ratajczak P, Janin A, Peffault de Latour R, et al. Th17/Treg ratio in human graft-versus-host disease. Blood 2010; 116(7): 1165-71.

290. Geng X, Zhang B, Zhou W, Liang J, Wang L, Wang S. The significance of Th17/Treg ratio in peripheral blood of patients with chronic hepatitis B. Xi Bao Yu Fen Zi Mian Yi Xue Za Zhi 2014; 30(12): 1304-6.

291. Yu ZX, Ji MS, Yan J, et al. The ratio of Th17/Treg cells as a risk indicator in early acute respiratory distress syndrome. The Journal of Critical Care 2015; 19: 82.

292. Li H, Liu Q, Jiang Y, Zhang Y, Zhang Y, Xiao W. Disruption of th17/treg balance in the sputum of patients with chronic obstructive pulmonary disease. The American Journal of Medical Science 2015; 349(5): 392-7.

293. Niu Q, Cai B, Huang ZC, Shi YY, Wang LL. Disturbed Th17/Treg balance in patients with rheumatoid arthritis. Rheumatology International 2012; 32(9): 2731-6.

294. Chen D, Huang X, Lu S, Gan H, Tang W, Liu K. Treg/Th17 imbalance is associated with cardiovascular complications in uremic patients undergoing maintenance hemodialysis. Biomedical Reports 2013; 1(3): 413-9.

295. Cheng X, Yu X, Ding YJ, et al. The Th17/Treg imbalance in patients with acute coronary syndrome. Clinical immunology 2008; 127(1): 89-97.

296. Li N, Bian H, Zhang J, Li X, Ji X, Zhang Y. The Th17/Treg imbalance exists in patients with heart failure with normal ejection fraction and heart failure with reduced ejection fraction. Clinica Chimica Acta 2010; 411(23-24): 1963-8.

297. Voo KS, Wang YH, Santori FR, et al. Identification of IL-17-producing FOXP3+ regulatory T cells in humans. Proceedings of the National Academy of Sciences USA 2009; 106(12): 4793-8.

298. Komatsu N, Okamoto K, Sawa S, et al. Pathogenic conversion of Foxp3+ T cells into TH17 cells in autoimmune arthritis. Nature Medicine 2014; 20(1): 62-8.

299. Benson MJ, Pino-Lagos K, Rosemblatt M, Noelle RJ. All-trans retinoic acid mediates enhanced T reg cell growth, differentiation, and gut homing in the face of high levels of co-stimulation. The Journal of Experimental Medicine 2007; 204(8): 1765-74.

300. Brown CC, Esterhazy D, Sarde A, et al. Retinoic acid is essential for Th1 cell lineage stability and prevents transition to a Th17 cell program. Immunity 2015; 42(3): 499-511.

301. Yoon S, Woo SU, Kang JH, et al. STAT3 transcriptional factor activated by reactive oxygen species induces IL6 in starvation-induced autophagy of cancer cells. Autophagy 2010; 6(8): 1125-38.

302. Zheng Y, Wang Z, Deng L, et al. Modulation of STAT3 and STAT5 activity rectifies the imbalance of Th17 and Treg cells in patients with acute coronary syndrome. Clinical immunology 2015; 157(1): 65-77.

303. Octavia Y, Brunner-La Rocca HP, Moens AL. NADPH oxidase-dependent oxidative stress in the failing heart: From pathogenic roles to therapeutic approach. Free Radical Biology and Medicine 2012; 52(2): 291-7.

304. Byrne JA, Grieve DJ, Bendall JK, et al. Contrasting roles of NADPH oxidase isoforms in pressure-overload versus angiotensin II-induced cardiac hypertrophy. Circulation research 2003; 93(9): 802-5.

305. Zhang M, Brewer AC, Schroder K, et al. NADPH oxidase-4 mediates protection against chronic load-induced stress in mouse hearts by enhancing angiogenesis. Proceedings of the National Academy of Sciences USA 2010; 107(42): 18121-6.

306. Cifuentes-Pagano E, Meijles DN, Pagano PJ. The quest for selective nox inhibitors and therapeutics: challenges, triumphs and pitfalls. Antioxidants and Redox Signaling 2014; 20(17): 2741-54.

307. Smith SM, Min J, Ganesh T, et al. Ebselen and congeners inhibit NADPH oxidase 2-dependent superoxide generation by interrupting the binding of regulatory subunits. Chemical Biology 2012; 19(6): 752-63.

308. Bosco EE, Kumar S, Marchioni F, et al. Rational design of small molecule inhibitors targeting the Rac GTPase-p67(phox) signaling axis in inflammation. Chemical Biology 2012; 19(2): 228-42.

309. Cifuentes-Pagano E, Saha J, Csanyi G, et al. Bridged tetrahydroisoquinolines as selective NADPH oxidase 2 (Nox2) inhibitors. Medicinal chemical communications 2013; 4(7): 1085-92.

310. Kanasty R, Dorkin JR, Vegas A, Anderson D. Delivery materials for siRNA therapeutics. Nature Materials 2013; 12(11): 967-77.

311. ClinicalTrials.gov. The ONE Study UK Treg Trial (ONETreg1). 2014. https://clinicaltrials.gov/ct2/show/NCT02129881 (accessed 26 November 2015).

312. Lee K, Nguyen V, Lee KM, Kang SM, Tang Q. Attenuation of donor-reactive T cells allows effective control of allograft rejection using regulatory T cell therapy. American journal of transplantation: official journal of the American Society of Transplantation and the American Society of Transplant Surgeons 2014; 14(1): 27-38.

313. Hutchinson JA, Ahrens N, Riquelme P, et al. Clinical management of patients receiving cell-based immunoregulatory therapy. Transfusion 2014; 54(9): 2336-43.

314. Edozie FC, Nova-Lamperti EA, Povoleri GA, et al. Regulatory T-cell therapy in the induction of transplant tolerance: the issue of subpopulations. Transplantation 2014; 98(4): 370-9.

315. Safinia N, Scotta C, Vaikunthanathan T, Lechler RI, Lombardi G. Regulatory T Cells: Serious Contenders in the Promise for Immunological Tolerance in Transplantation. Frontiers in Immunology 2015; 6: 438.

316. Budinger GR. Angiotensin II and pulmonary fibrosis, a new twist on an old story. American Journal of Physiology: Lung Cellular and Molecular Physiology 2011; 301(3): L267-8.

317. Yamamoto K, Mano T, Yoshida J, et al. ACE inhibitor and angiotensin II type 1 receptor blocker differently regulate ventricular fibrosis in hypertensive diastolic heart failure. Journal of Hypertension 2005; 23(2): 393-400.

318. Li W, Goldstein DR, Kreisel D. Intravital 2-photon imaging, leukocyte trafficking, and the beating heart. Trends in Cardiovascular Medicine 2013; 23(8): 287-93.

319. Li W, Nava RG, Bribriesco AC, et al. Intravital 2-photon imaging of leukocyte trafficking in beating heart. Journal of Clinical Investigation 2012; 122(7): 2499-508.

320. Ahrens ET, Helfer BM, O'Hanlon CF, Schirda C. Clinical cell therapy imaging using a perfluorocarbon tracer and fluorine-19 MRI. Magnetic Resonance in Medicine 2014; 72(6): 1696-701.

321. Suzuki H, Duncan GS, Takimoto H, Mak TW. Abnormal development of intestinal intraepithelial lymphocytes and peripheral natural killer cells in mice lacking the IL-2 receptor beta chain. The Journal of Experimental Medicine 1997; 185(3): 499-505.

322. Malek TR, Vincek V, Gatalica B, Bucan M. The IL-2 receptor beta chain gene (Il-2rb) is closely linked to the Pdgfb locus on mouse chromosome 15. Immunogenetics 1993; 38(2): 154-6.

8.2 Appendix

Appendix 1:

Client : Debbi Young, BSU, James Black Centre, Denmark Hill, KCL
Lab No. : 13/7671-7672
Sample Details : 2 Female CD1 Mice from Room 037

Mouse Report	Test Frequency	Current Test Date	Current Test Results	Testing Laboratory	Test Method	Results Since September 2013
Serology						
Minute Virus of Mice	3 months	4 Sep 2013	0/2	SDL	MFIA	0/2
Mouse Hepatitis Virus	3 months	4 Sep 2013	0/2	SDL	MFIA	0/2
Pneumonia Virus of Mice	3 months	4 Sep 2013	0/2	SDL	MFIA	0/2
Reovirus Type III	3 months	4 Sep 2013	0/2	SDL	MFIA	0/2
Mouse Encephalomyelitis Virus	3 months	4 Sep 2013	0/2	SDL	MFIA	0/2
Sendai Virus	3 months	4 Sep 2013	0/2	SDL	MFIA	0/2
Epizootic Diarrhoea of Infant Mice	3 months	4 Sep 2013	0/2	SDL	MFIA	0/2
Mouse Parvovirus	3 months	4 Sep 2013	0/2	SDL	MFIA	0/2
Mouse Norovirus	3 months	4 Sep 2013	0/2	SDL	MFIA	0/2
Clostridium piliforme	3 months	4 Sep 2013	0/2	SDL	MFIA	0/2
Mycoplasma pulmonis	3 months	4 Sep 2013	0/2	SDL	MFIA	0/2
Lymphocytic Choriomeningitis Virus	12 months			SDL	MFIA	
Hantaan Virus	12 months			SDL	MFIA	
Ectromelia Virus	12 months			SDL	MFIA	
Mouse Cytomegalovirus	12 months			SDL	MFIA	
Mouse Adenovirus 1	12 months			SDL	MFIA	
Mouse Adenovirus 2	12 months			SDL	MFIA	
Polyoma Virus	12 months			SDL	MFIA	
K Virus	12 months			SDL	MFIA	
Parasitology						
INTESTINAL PROTOZOA	3 months	4 Sep 2013	0/2	SDL	MIC	0/2
FAECAL OVA	3 months	4 Sep 2013	0/2	AB/SDL	FLOT/MIC	0/2
HELMINTHS	3 months	4 Sep 2013	0/2	SDL	MIC	0/2
ATHROPODS	3 months	4 Sep 2013	0/2	SDL	MIC	0/2
Bacteriology						
Bordetella bronchiseptica	3 months	4 Sep 2013	0/2	SDL	CULT	0/2
Citrobacter rodentium	3 months	4 Sep 2013	0/2	SDL	CULT	0/2
Corynebacterium kutscheri	3 months	4 Sep 2013	0/2	SDL	CULT	0/2
Helicobacter species	On Request			SDL	PCR	
Helicobacter hepaticus	On Request			SDL	PCR	
Helicobacter bilis	On Request			SDL	PCR	
Klebsiella species	3 months	4 Sep 2013	0/2	SDL	CULT	0/2
Pasteurellaceae	3 months	4 Sep 2013	0/2	SDL	CULT	0/2
Pseudomonas aeruginosa	3 months	4 Sep 2013	0/2	SDL	CULT	0/2
Salmonella species	3 months	4 Sep 2013	0/2	SDL	CULT	0/2
Staphylococci species	3 months	4 Sep 2013	0/2	SDL	CULT	0/2
Streptobacillus moniliformis	3 months	4 Sep 2013	0/2	SDL	CULT	0/2
Streptococcus pneumoniae	3 months	4 Sep 2013	0/2	SDL	CULT	0/2
B-haemolytic Streptococci	3 months	4 Sep 2013	0/2	SDL	CULT	0/2
Yersinia species	3 months	4 Sep 2013	0/2	SDL	CULT	0/2
Necropsy						
External Lesions/Abnormalities	3 months	4 Sep 2013	0/2	SDL	MIC	0/2
Internal Lesions/Abnormalities	3 months	4 Sep 2013	0/2	SDL	MIC	0/2

Bacteriology & Parasitology Notes:

MFIA = Multiplexed Immuno-Fluorescent Assay, PCR = Polymerase Chain Reaction, CULT = Culture, MIC = Microscopy, FLOT = Faecal Flotation
SDL = Surrey Diagnostics Ltd, AB = Abbey Veterinary Services, BD = Bio-Doc

Appendix 2:

harlan®

Final Health Monitoring Report

Test Date	Species	Submitter	Area	Profile
04 December 13	Mouse	Kings College London	41	51M

Viruses	Positive/Tested	Test Method
Minute virus of mice	0/2	Bead
Mouse hepatitis virus	0/2	Bead
Mouse parvovirus	0/2	Bead
Mouse rotavirus (EDIM)	0/2	Bead
Pneumonia virus of mice	0/2	Bead
Sendai virus	0/2	Bead
Theiler's murine encephalomyelitis virus	0/2	Bead

Bacteria, Mycoplasma and Fungi	Positive/Tested	Test Method
Citrobacter rodentium	0/2	Culture
Clostridium piliforme	0/2	Bead
Corynebacterium kutscheri	0/2	Culture
Mycoplasma spp	0/2	Bead
Pasteurella spp	0/2	Culture
Salmonella sp	0/2	Culture
Streptococci Beta-haemolytic (not group D)	0/2	Culture
Streptococcus pneumoniae	0/2	Culture

Parasites	Positive/Tested	Test Method
Ectoparasites	0/2	Microscopy
Endoparasites	0/2	Microscopy

Pathological Lesions	Positive/Tested	Test Method
External	0/2	Pathology
Necropsy	0/2	Pathology